ON THE STRUCTURE OF FLOW IN AN INCLINED SETTLING COLUMN

A DISSERTATION

SUBMITTED TO

DEPARTMENNT OF CIVIL ENGINEERING

PUBLIC HEALTH ENGINEERING SECTION

OF

UNIVERSITY OF STRATHCLYDE

IN PARTIAL FULFILLMENT OF THE REQUIREMENTS

FOR THE DEGREE OF

DOCTOR OF PHILOSOPHY

By

Fatimeh Jaara

Glasgow, 1988

To my mother

ACKNOWLEGEMENTS

I would like to express my gratitude to Dr. D. H. Bache, whose sound guidance, continuous encouragement and interest have contributed greatly to this work.

This research has been supported by grants from University of Aleppo.

SUMMARY

Although there have been useful developments in the theory of solid-liquid separation in inclined tubes, many assumptions and concepts have not been tested. In the present study the principal objective was to gain a clearer understanding of the settling mechanism through observation of the flow fields within a particle-free fluid layer which exists at the upper face of the bulk suspension and within the bulk suspension itself.

Experimental investigations were carried out using glass beads in an aqueous glycerol solution.

Preliminary tests in a vertical column showed that the relationship between the settling velocity V_c and the solids concentration C could be described by

$$V_c = A\ (\ 1 - C\ )^n \qquad \text{when} \qquad n = 4.66$$

In the subsequent work in an inclined column the flow field in the clear fluid channel and within the suspension core was studied for suspension under the concentration conditions $C_o = 0.1$ and $C_o = 0.2$.

Characteristics features (width, velocity and average flow) of the clear-fluid layer were measured and compared with existing theory. Generally it was shown that there is a fairly good agreement between theory and experiments especially at early stages of settling and away from the top interface. Particular attention was paid to mode of infiltration from the bulk suspension into the clear-fluid channel.

Measurements of the concentration distribution along the settling column were carried out using an electro-conductivity technique from suspension. Fluid velocity was measured by a dye-tracer. From the data, it was seen that the fluid velocities within the suspension were exceedingly high, being roughly 10 times the bulk settling velocity of the suspension .

All the characteristics of the flow field within the clear-fluid channel indicate a change in behaviour between the upper and lower parts of the settling column and take place as if there was a form of rotation above and below a horizontal axis at the middle of the tube.

Existing theory (PNK) was modified to take account of the height of the sediment layer at the bottom of the tube. This provided good agreement with experimental data over the range of conditions studied, apart from the final stages of settlement.

TABLE OF CONTENTS

Contents cont. Page No.

Contents cont. Page No.

Content cont. Page NO.

LIST OF ILLUSTRATIONS

LIST OF ILLUSTRATIONS cont.

LIST OF ILLUSTRATIONS cont.

figure Page No.

LIST OF ILLUSTRATIONS cont.

figure Page No.

List of tables

CHAPTER ONE

INTRODUCTION

CHAPTER ONE

INTRODUCTION

1.1 The settling convection phenomenon

Sedimentation is widely used in chemical engineering as a means of separating particles from the fluid in which they are suspended, as well as a way of separating particles with different settling speeds from each other. The sedimentation process in a convection settler is often very slow especially when particles are small. Hence there is an advantage to be gained from any simple device that permits solid-liquid separation to be carried out more rapidly. One such device is known (commercially) as the " lamella settler " or " high rate settler ", in which the retention times can be reduced by an order of magnitude or more below those in corresponding vertical settlers. These settlers may be composed either of narrow tubes or a channel inclined from the vertical or of a large tank containing several closely spaced tilted plates such as shown in figure (1.1)

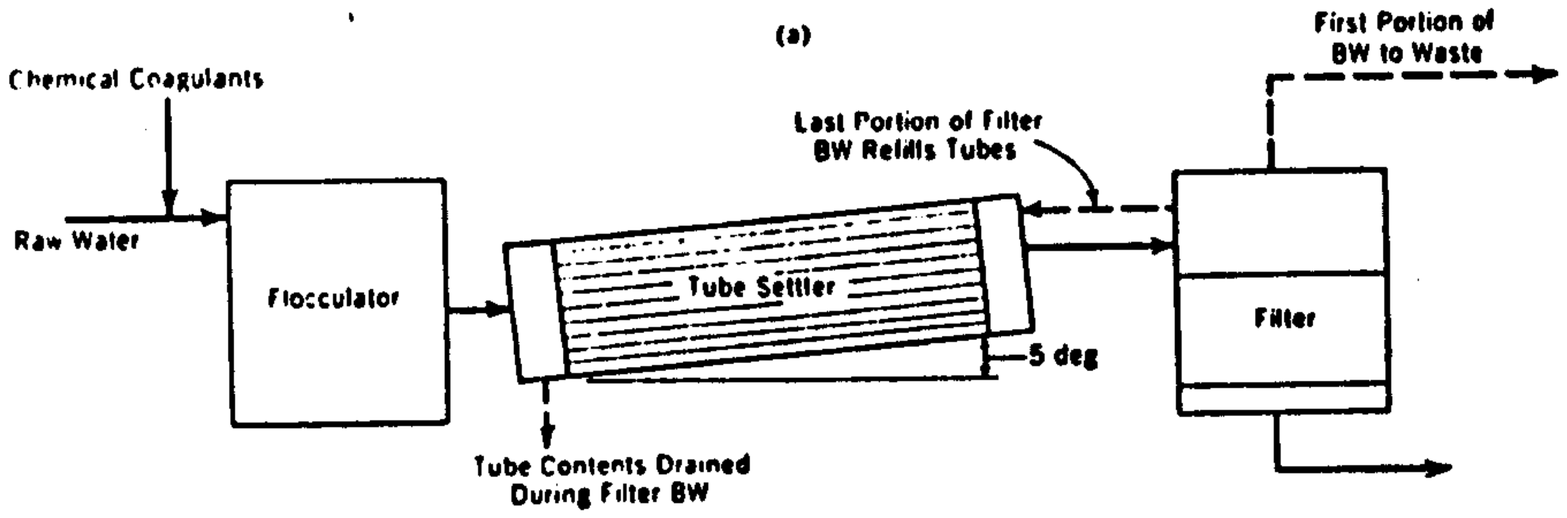

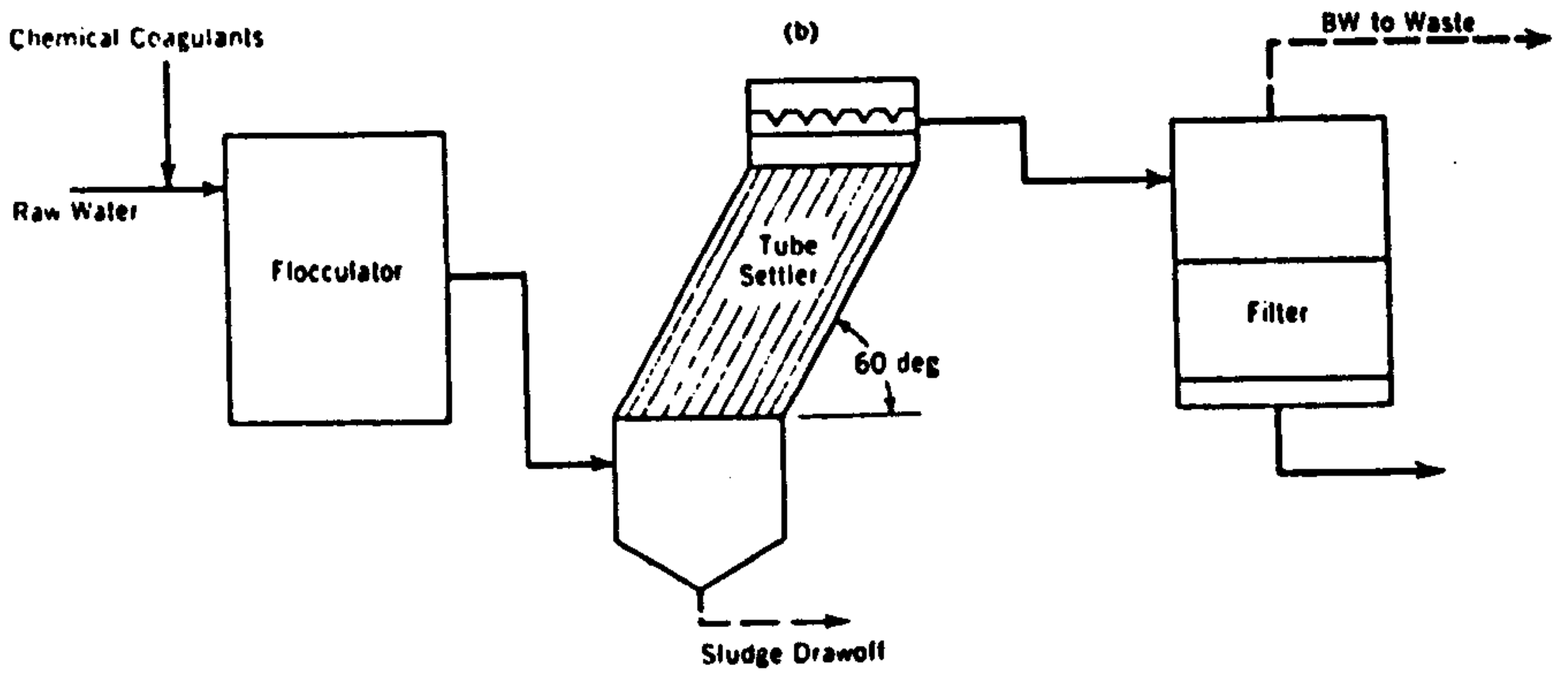

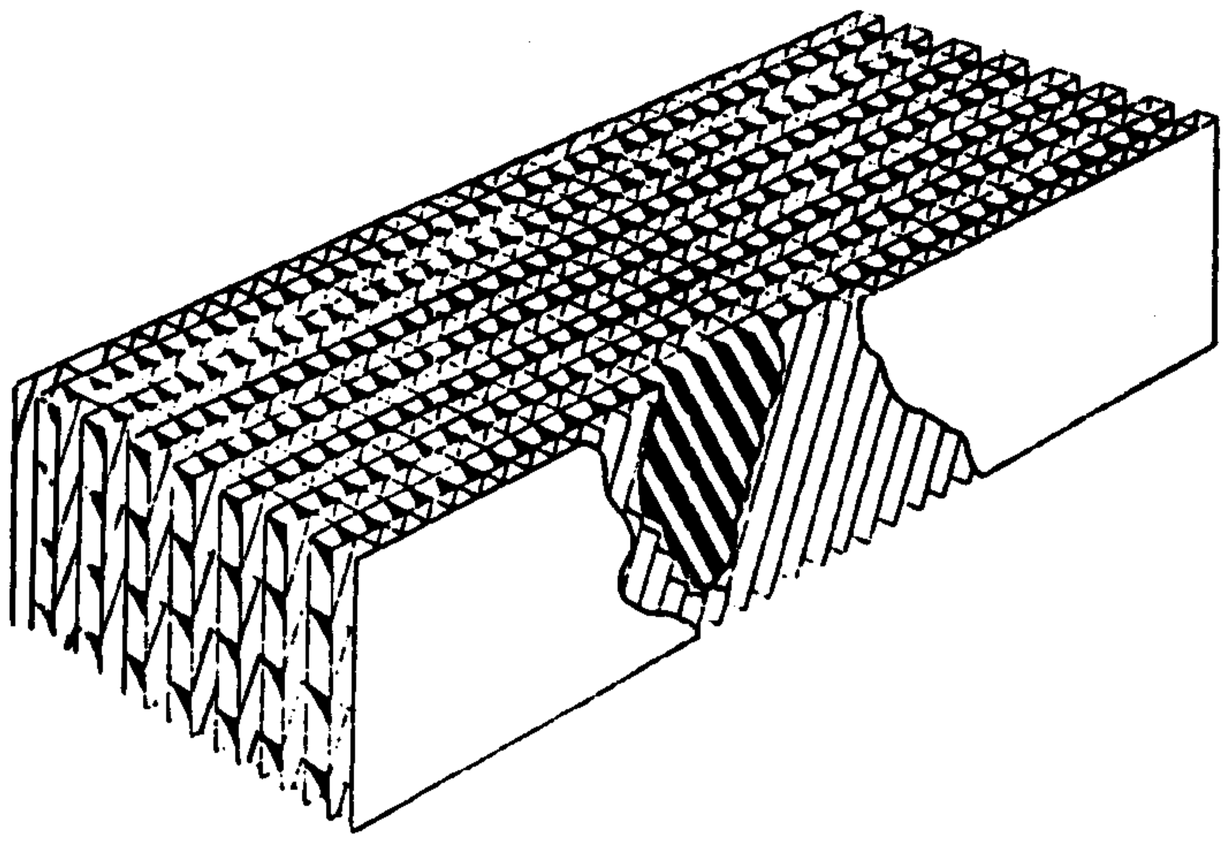

Figure (1.1): Lamella settler

The phenomenon of enhanced sedimentation in inclined channels has a long history stemming from Boycott (1920), who observed that when blood is put to stand in narrow tubes, the corpuscles sediment a good deal faster if the tube is inclined than when it is vertical. Studied by Ponred (1925) and Nakamura and Kuroda (1937) who established the first quantitative model (PNK theory), and more recently studies by Hill (1974) and Acrivos et al (1979), who provided an explanation to the phenomenon in term of theoretical continuum mechanics.

1.2 Scope of the study

Although there have been useful developments in theory, many assumptions and concepts have not been tested and this forms the basis of the present study

The principal objective of the study was to gain a clearer understanding of the settling mechanism on the basis of experiment, focussing on:

1- The clear-fluid layer characteristics (upward velocity , width and flow changes with time),

2- The flow field within the bulk suspension ,

3- The concentration changes with time and along the settling column, and

4- on the effects of inclination on the solids concentration distribution .

5- The adequacy of current theory

The structure of this study is outlined below:

Chapter two surveys the background literature and focuses on the general aspects of settling convection phenomena. Particular attention is paid to the effects of solids concentration on the settling process and what the relationships governing these effects were.

In chapter three a description is provided of enhanced sedimentation phenomena. Attention was paid to the theories behind the enhancement and to the possible modification of these theories.

Chapter four concentrates on the experimental tests on the interfacial behaviour, in settling in vertical and inclined tubes. Preliminary checks were made on materials and methods to be employed in subsequent analysis, and for convenience this was confined to vertical tubes. Preliminary checks were also carried out on the PNK theory. Glass beads were used to examine the effect of initial concentration on the initial settling velocity, in an inclined tube.

Chapter five was primarily concerned with the characteristics of the clear-fluid layer under the downward facing surface, whereas chapter six dwells on the flow field within the bulk suspension. Data from both chapters five and six were analysed to gain a clear understanding of the way the fluid is released into the clear-fluid layer.

CHAPTER TWO

LITERATURE SURVEY ON THE VERTICAL SETTLING

CHAPTER TWO

LITERATURE SURVEyON THE VERTICAL SETTLING

2.1 Settling of discrete spherical particles

Stokes, (1851), was the first to study theoretically the force acting on a rigid single particle falling in an infinite viscous fluid. The resistance force (F) to the motion of a single spherical particle is given as

$$F=3\pi\mu Vd \qquad \ldots.(2.1)$$

where V is the relative velocity of the falling sphere, μ is the dynamic viscosity of the fluid and, d is the particle diameter.
The falling sphere reaches its constant terminal velocity V_o when the viscous drag force given by equation (2.1) equals the effective gravitational force ie

$$3\pi\mu V_o d = \frac{\pi d^3(\rho_s-\rho)g}{6} \qquad \ldots.(2.2)$$

$$V_o = \frac{d^2(\rho_s-\rho)g}{18\mu} \qquad \ldots.(2.3)$$

Equation (2.3), is only valid in the following conditions

i- when $Re<0.1$ (Flemmer et al, 1986) where $Re = Vd\rho/\mu$, ie laminer creeping flow.

ii- A single particle is not affected by the presence of any other

particles ie. free settling.

iii- the wall effect should be eliminated by using a very large container: It has been found that vessel walls significantly modify the settling behaviour of a single particle, when the ratio of tube diameter to particle diameter, is less than 50 to 100

2.2 Sedimentation of monodisperse suspension in vertical containers

2.2.1 Introduction

If a homogeneous mixture of solid particles and fluid is allowed to stand in a container with vertical walls, then after a short period of time, four zones are usually formed (Coe and Clevenger, (1916). Referring to figure (2.1)

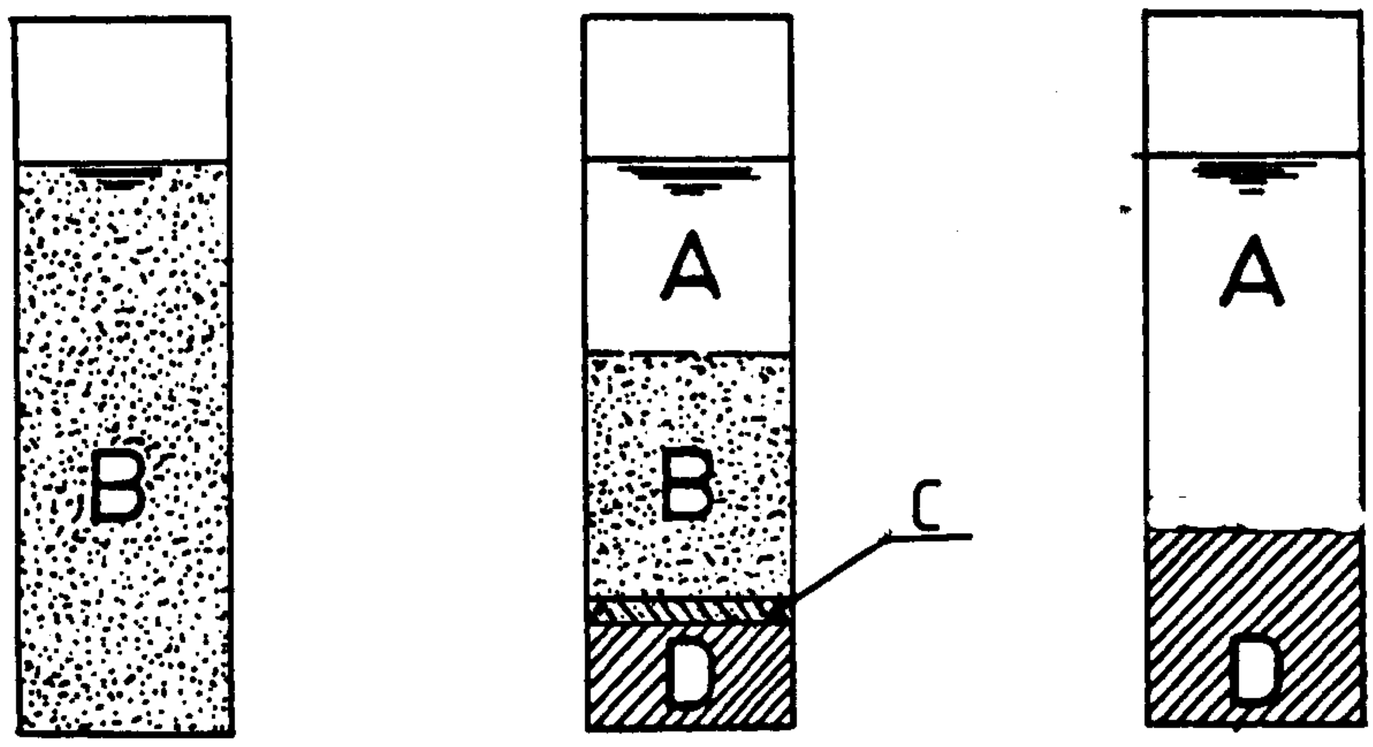

(a) (b) (c)

Figure (2.1) settling column at a (begining of settling process), b(after time t), and ,c(at the end of settling process).

These zones may be labelled A, B, C and D and refer to clear liquid zone, the initial-concentration zone, the graded-concentration zone and the sediment zone, respectively. In zone B, if the initial concentration is under a critical limit, the flocs (or "particles" if the material is not flocculated) do not exert direct forces on each other, it is referred to as the "free settling zone". In this zone, Coe and Clevenger(1916), assumed that the settling velocity of flocs (or particles), is a function only of the solids concentration.

At the bottom of the container where the particles can not settle any further, they deposit on each other , and exert forces on each other forming a compression zone (zone D). Depending on the structure of the settling particles, Kynch (1952), predicted the formation of a graded-concentration zone, (zone C), between the

initial-concentration and compression zones. Dixon (1977), considered that the graded-concentration zone can only form within the compression zone, and that when the solids are rigid particles, they deposit on each other at their maximum concentration, to form an incompressible sediment layer.

According to Shannon et al (1963), the maximum concentration is likely to be 0.64 (vol. ratio). In this case the graded-concentration layer does not exist, because there is no compression zone, Dixon, (1977).

The velocity of the interface separating zones A and B depends on the solids concentration of the suspension in zone B, and is constant for a suspension of rigid spheres of uniform initial concentration. As time progresses, zone D increases in depth and its upper boundary ascends at a rate which depends on the difference in concentration above and below the interface, (Kynch, 1952). Thus when the material is incompressible, the concentration below the interface corresponds to the maximum concentration, and the concentration above refers to the initial concentration in zone B, and leads to a build-up rate (of the sediment layer), which is a constant with time. Figure (2.2) illustrates these features for both compressible and incompressible suspensions

incompressible suspensions

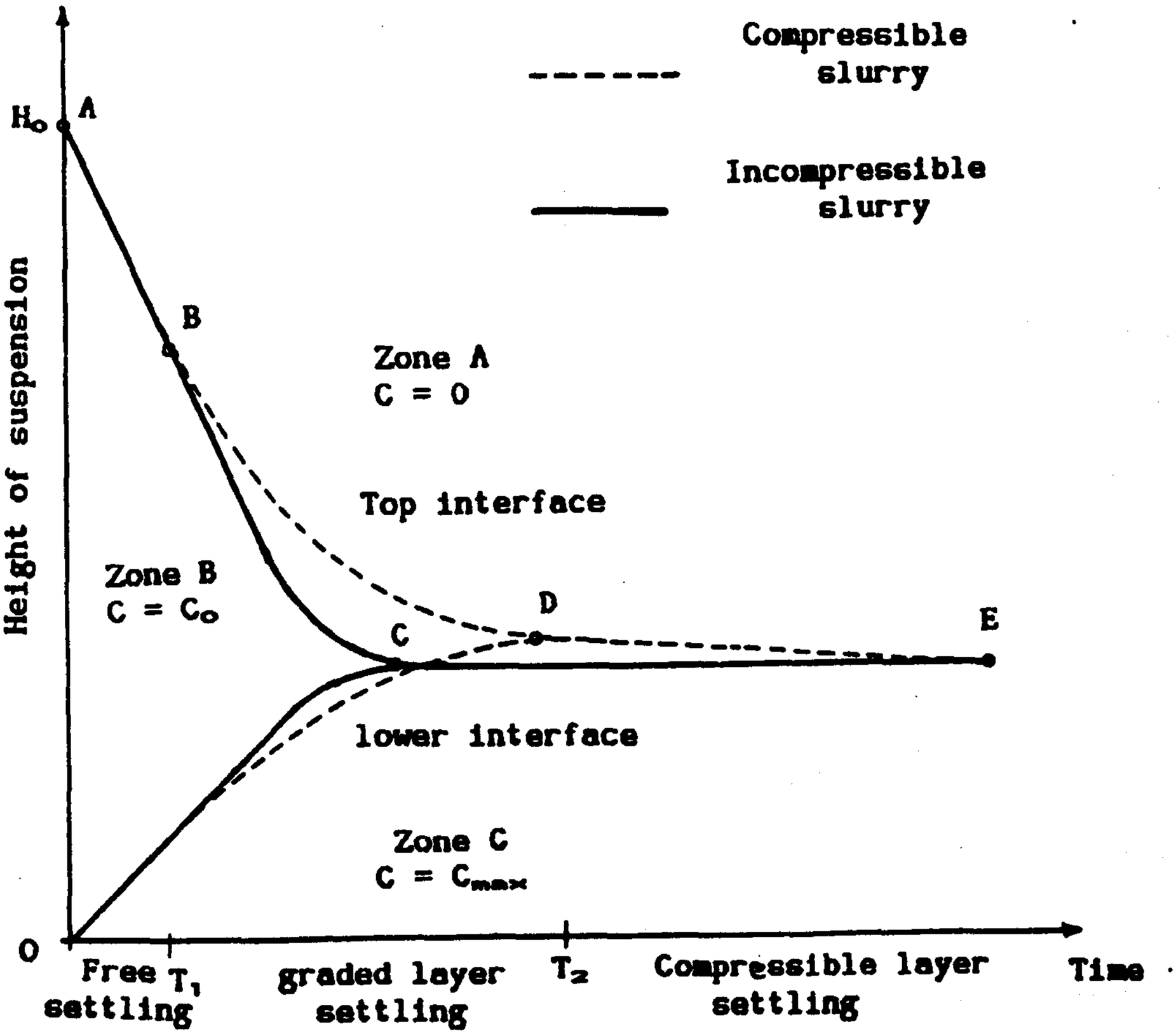

Figur 2.2: Settling curves for compressible and incompressible suspensions

The less compressible the flocs are the nearerthe plot is to a straight line.

2.2.2 Settling velocity-concentration relationships in the free settling zone

The idea of the dependency of local settling velocity in the free settling zone, on solids concentration, is acceptable to all observers of the settling phenomenon. For an ideal suspension, where the flocculation and attrition can be neglected, the presence of other particles affects the terminal velocity in different ways, as stated below

i -the presence of other particles causes reduction of the voidage within the suspension, which reduces the free area available for the liquid to pass through the particles, and causes higher interparticle velocity of fluid.

ii -the presence of other particles can modify the flow pattern around a particle (Davies et al, 1976), and affects the velocity field and the fluid drag

iii -the particles will tend to carry some of the fluid with them as static volume, thus magnifying the displacement effect, and increasing the interparticle upward flow velocity.

Many investigators of the settling of suspension have focused on the constant rate settling period. In order to eliminate the effects of size and shape of particles, most observers have used identical rigid spheres of such a small size that the Reynolds number of the settling particles is small and inertial forces can be neglected.

The primary task of the majority of the workers has been to determine the relationship between the settling rate of the suspension, the individual settling rate of the constituent particles, and the particle concentration.

Davies et al (1976) reported that when two sphere of equal radii, are placed axisymmetrically in a steady Stokes stream, separation of the flow from the spheres occurs if the distance between their centres, is less than approximately 3.57 times the sphere radius. This means that the flow pattern of the fluid around the settling particles differs in the dilute suspensions, from that in the concentrated ones. With this difference in the flow pattern in view, many investigators have restricted their studies to dilute suspension, using the assumption of the unit cell arrangement of the particles within the fluid. The cell technique has been employed to show schematically (and in a highly idealized form), the nature of the flow pattern involved in the basic types of motion around the settling particles.

A number of particles are assumed to be settling with equal velocity under the influence of gravity through a fluid. Attention has been paid to one particle which is surrounded by a fluid envelope. The dimension of the envelope is established by assuming that the cell contains the same volumetric proportion of solid to fluid, as exists in the entire assemblage. Some investigators (eg Famularo. 1962), have assumed the fluid envelope to be of a regular

geometrical pattern such as a cubical array, with the length scale of the array being of the order $rC^{-1/3}$, or a spherical cell with radius $rC^{-1/3}$, where r is the raduis of the rigid sphere (in spherical array, the particle is considered to exist in the centre of a sphere of fluid. The radii of the sphere is chosen to have the same solids concentration of the settled suspension).

All these calculations with a cell radius proportional to $C^{-1/3}$, gave a fractional reduction in the fall speed which is proportional to $C^{-1/3}$. For C << 1 , the results of Famularo's investigations are summarized in the equations (2-4), (2-5) and (2-6).

Cubic $$\frac{U}{U_o} = \frac{1}{1+1.91\ C^{1/3}} \qquad \ldots.(2.4)$$

Rhombohedral suspension $$\frac{U}{U_o} = \frac{1}{1+1.79\ C^{1/3}} \qquad \ldots.(2.5)$$

Random suspension $$\frac{U}{U_o} = \frac{1}{1+1.3\ C^{1/3}} \qquad \ldots.(2.6)$$

where U is the settling velocity of particles within suspension of concentration C

and U_o is the settling velocity of discrete particles

The unit cell technique was modified by Feuillebois (1984), in order to investigate the sedimentation of monodisperese spheres in dilute suspension, that is homogeneous in any horizontal plane, but in which a vertical concentration profile is prescribed.

Barnea & Mizrahi (1973) proposed that the semiempirical formula,

$$f(C) = \frac{(1-C)^2}{(1+C^{1/3})\exp(5C/3(1-C))} \qquad \ldots.(2.7)$$

equation (2.7), was considered to provide the best fit in the case of a very small particle Reynolds number, which transforms to $f(C) \simeq 1 - C^{1/3}$ at the dilute limit.

Where investigators have used statistical analytical methods in attempts to determine the hindered settling rate of a random distribution of spheres, (eg Burgers (1942), and Pyun and Fixman 1964), they have found that the reduced settling velocity U/U_o, is proportional to the concentration of the first degree. Indeed, using a statistical analysis, Batchelor (1972) showed that

$$U = U_o\ (1-6.55C) \qquad \text{when } C \ll 1 \qquad \ldots.(2.8)$$

In a concentrated suspension, the fluid follows a different flow pattern around the settling particles, but the reduced settling velocity U/U_o, remains as a function of the solids concentration. The unit cell technique was used also to predict the settling behaviour in the concentrated suspension. McNown et al (Proc. 7th Int. cong. Apply. Mech. London 1948), considered the settling particle to be situated in the centre of a hexagon of fluid, as indicated in figure (2.3) Hawksley (1950), also considered the particles to be arranged in adjacent horizontal layers, so as to

offer the minimum resistance to the motion of a fluid, flowing through the system..

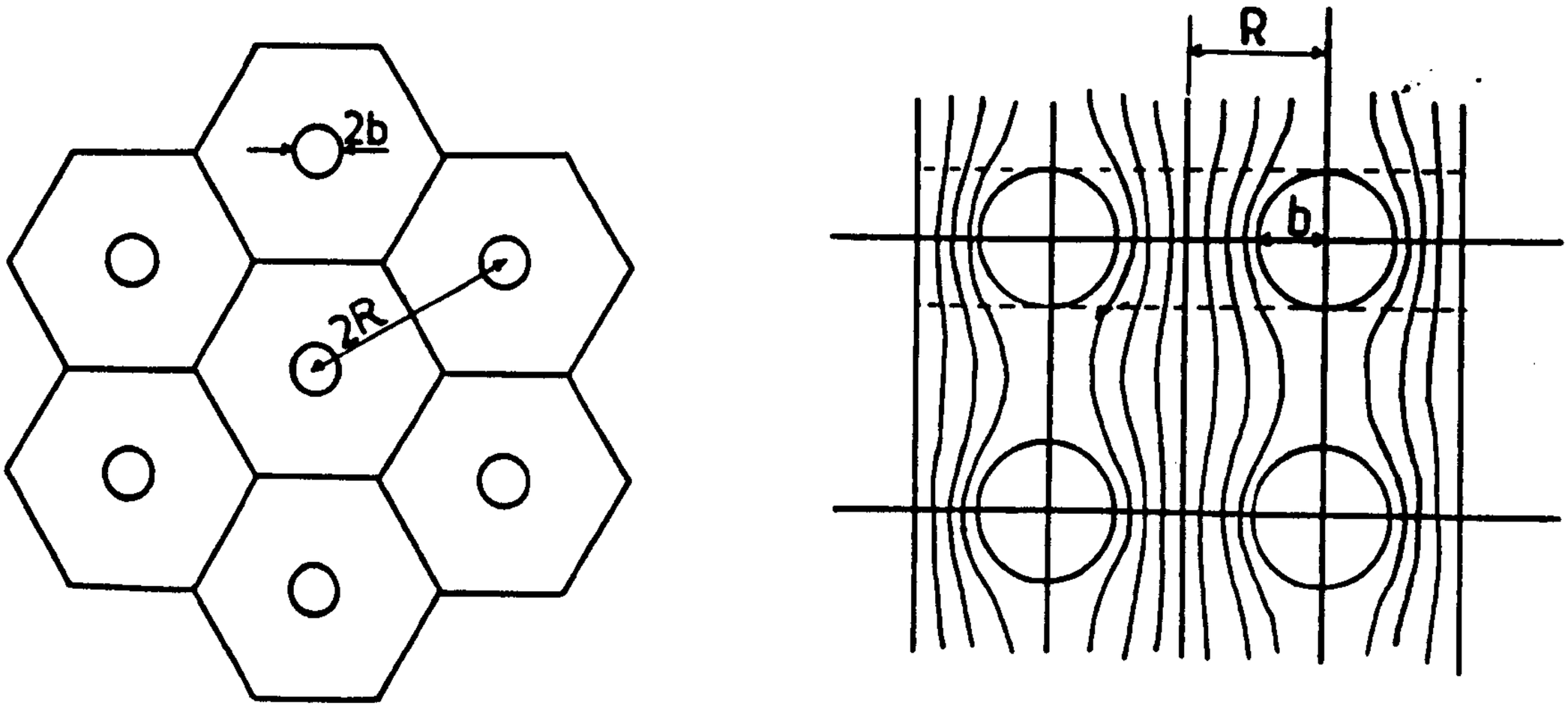

Figure (2.3): Hexagonal arrangement of settling particles

Depending on the shearing force balance of the fluid around the settling particle, Richardson and Zaki (1954-b), adopting the unit cell arrangement of McNown et al, derived a correction factor to Stokes' law for multiparticle systems which is in the form

$$\beta_r = (1-C)^{-4.65} \qquad \ldots.(2.9)$$

Their model was in agreement with their experimental work for C > 0.05.

When C < 0.01, $(1-C)^{4.65}$ can be stated as 1 - 4.65C, which means that the velocity is proportional to C. This agrees with

Batchelor's equation, but with different values of the proportionally constant.

A very similar result was found by Moud and Whitmore (1958), when they derived a theoretical relationship between c and V_c of a non-flocculated suspension of particles, regardless of the particles arrangement and the flow pattern around the settling particles and using the force balance on the settling particles, neglecting inertial forces. They deduced the equation

$$U_c = U_o\ (1-C)^{\alpha} \qquad \ldots.(2.10)$$

where $1 < \alpha < 8$

with $\alpha \simeq 5$ as the best representation, this being very close to the value 4.65 in Richardson and Zaki

Since 1954, the Richardson and Zaki equation has been the most commonly used empirical correlation . According to Garside and AL-Dibouni (1977) a value of n = 5.1, most accurately represents their data for small Reynolds number. Richardson and Zaki, (1954), using dimensional analysis, argued that the terminal settling velocity of particles, is a function only of the voidage ε (and the dimension of containing vessel in the dilute suspensions). Due to its importance, the analysis of Richardson and Zaki (1954) is reproduced overleaf.

The resistance to the motion of a single sphere in a fluid, when both skin friction and form drag are significant, depends on μ, ρ, and V ie

$$R = f_1(\mu,\ \rho,\ d,\ V). \qquad \ldots.(2.11)$$

Where R = resistance force per unit cross-sectional area of particle,

μ = viscosity of the fluid,

ρ = density of the fluid,

d = diameter of sphere,

V = velocity of fluid relative to the particle.

If the sphere forms part of a uniform suspension, the resistance force also depends on the presence of the other particles, since they affect the flow pattern. The restriction of the flow spaces between the particles, with increase in concentration, results in steeper velocity gradients in the fluid, and consequently greater shearing stresses. Hence the flow pattern is a function of the ratio of the diameter of particle (d), to the distance between the particles (s). For a uniformly dispersed suspension, d/s is a function of the porosity (ε) only. Thus we can write:

$$R_c = f_2(\mu,\ \rho,\ d,\ V,\ \varepsilon). \qquad \ldots.(2.12)$$

Where R_c = resistance force to a constituent particle, per unit cross-sectional area of particle.

In order to consider the effect of the ratio of particle diameter to tube diameter, equations (2.11) and (2.12) can be modified as follows:

$$R = f_3(\mu,\ \rho,\ d,\ V,\ d/D) \qquad \ldots.(2.13)$$

and
$$R_c = f_4(\mu,\ \rho,\ d,\ V,\ \varepsilon,\ d/D) \qquad \ldots.(2.14)$$

When the particles are settling at a uniform rate under the action of gravity, the resistance to motion per unit area of particle (R_t) is defined by

$$R_t = (2/3)\ d\ (\rho_s-\rho)\ g$$

ie (the effective weight divided by the projected area).

For a single particle under these conditions,

$$R_t = f_5(\mu,\ \rho,\ d,\ V_o,\ d/D) \qquad \ldots.(2.15)$$

and for a constituent particle of a suspension,

$$R_t = f_6(\mu,\ \rho,\ d,\ V_s,\ \varepsilon,\ d/D) \qquad \ldots.(2.16)$$

Where V_o is the terminal falling velocity of a single particle,

and V_s is the settling velocity of the particles in a suspension, relative to the fluid.

In both cases, the resistance force acting on an individual particle $R_t \cdot \pi d^2/4$, is equal to its weight, but the settling velocity of a suspension, is less than that of an isolated particle.

The actual settling velocity of a particle relative to the fluid, can be expressed in terms of the apparent rate of settling by,

$$V_s = \frac{V_c}{\varepsilon} \qquad \ldots\ldots (2.17)$$

and therefore it has been found from equation (2.16) that

$$R_t = f_7(\mu,\ \rho,\ d,\ V_c,\ \varepsilon,\ d/D) \qquad \ldots\ldots (2.18)$$

Rearranging equations (2.15) and (2.18),

$$V_o = f_8(\mu,\ \rho,\ d,\ R_t,\ d/D) \qquad \ldots\ldots (2.19)$$

$$V_c = f_9(\mu,\ \rho,\ d,\ R_t,\ \varepsilon,\ d/D) \qquad \ldots\ldots (2.20)$$

Dividing equation (2.20) by equation (2.19),

$$\frac{V_c}{V_o} = f_{10}(\mu,\ \rho,\ R_t,\ \varepsilon,\ d/D) \qquad \ldots\ldots (2.21)$$

The only possible dimensionless combination of the variables, μ, ρ, d, R_t is

$$\frac{R_t \rho d^2}{\mu^2}$$

and therefore $$\frac{V_c}{V_o} = f_{11}\left(\frac{R_t \rho d^2}{\mu^2},\ \frac{d}{D},\ \varepsilon\right) \qquad \ldots\ldots (2.22)$$

The group $$\frac{R_t \rho d^2}{\mu}$$

is equal to $\left(\frac{R_t}{\rho V_o^2}\right) \cdot \left(\frac{V_o d R}{\mu}\right)^2$,

where $\frac{R_t}{(\rho V_o)^2}$ is a resistance coefficient,

and $\frac{V_o d\rho}{\mu}$ is the Reynolds Group with respect to the particle.

For a particle of a given shape, $\frac{R}{\rho V_o^2}$

is a unique function of $\frac{V_o d\rho}{\mu}$,

and therefore equation (2.22) can be rewritten as

$$\frac{V_c}{V_o} = f_{12}\left(\frac{V_o d\rho}{\mu}, \frac{d}{D}, \varepsilon\right) \qquad \ldots\ldots (2.23)$$

In this derivation, no assumption have been made concerning the nature of the flow past the particles.

In the case of viscous conditions, (Re <0.1), Stokes' equation is based on the assumption that relative velocity is sufficiently low for inertial effects to be negligible, so that the whole resistance may be attributed to skin friction. Under these conditions,

$$F = R \cdot \frac{\pi d^2}{4} = 3 \pi \mu V d$$

where F= is viscous drag

R being independent of ρ, the density of the fluid. Equation (2.21) then becomes

$$\frac{V_c}{V_o} = f_{13} \left(\mu, d, R_t, \varepsilon, \frac{d}{D}\right) \quad \ldots\ldots (2.24)$$

Now, μ, d, R_t cannot be arranged in a dimensionless group. Therefore $\frac{V_c}{V_o}$ must be independent of these variables under conditions of streamline flow, so that

$$\frac{V_c}{V_o} = f_{14}\left(\varepsilon, \frac{d}{D}\right) \quad \ldots\ldots (2.25)$$

Through their experimental work on sedimentation, Richardson and Zaki (1954-a) found that,

$$V_c = V_o (1-C)^n \quad \ldots\ldots (2.26)$$

Where n depends on Reynolds number, (Re), and the ratio d/D, where d is the particle's diameter, and D is the settling column dimension. For small Reynold number and sedimentation of small particles they found agreement with experiments that had been carried out by other

workers (Lewis et al 1949 , and Steinour 1944), (see figures 2.4 and 2.5).

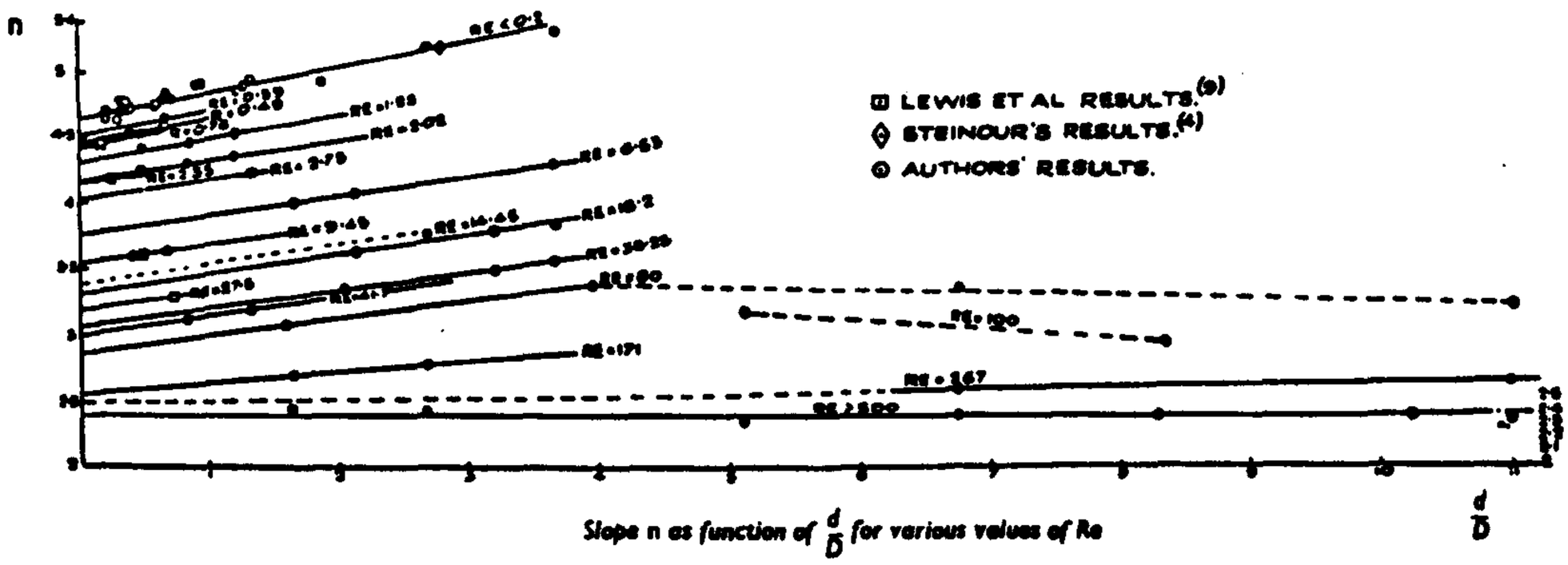

Slope n as function of $\frac{d}{D}$ for various values of Re

Figure 2.4: Slope n as a function of d/D for various values of Re

(Figure 18 in Richardson and Zaki (1954-a)

2.2.3 Kynch's theory and zone settling

Kynch's theory of sedimentation was based on Coe and Clevenger's assumption that at any point in a column of suspension, the settling velocity is a function only of the concentration of that point. Predicting the behaviour of the suspension, Kynch, (1952), showed that the relationship between settling velocity and concentration, can be deduced from the observation of a batch settling curve eg Figure (2.5).

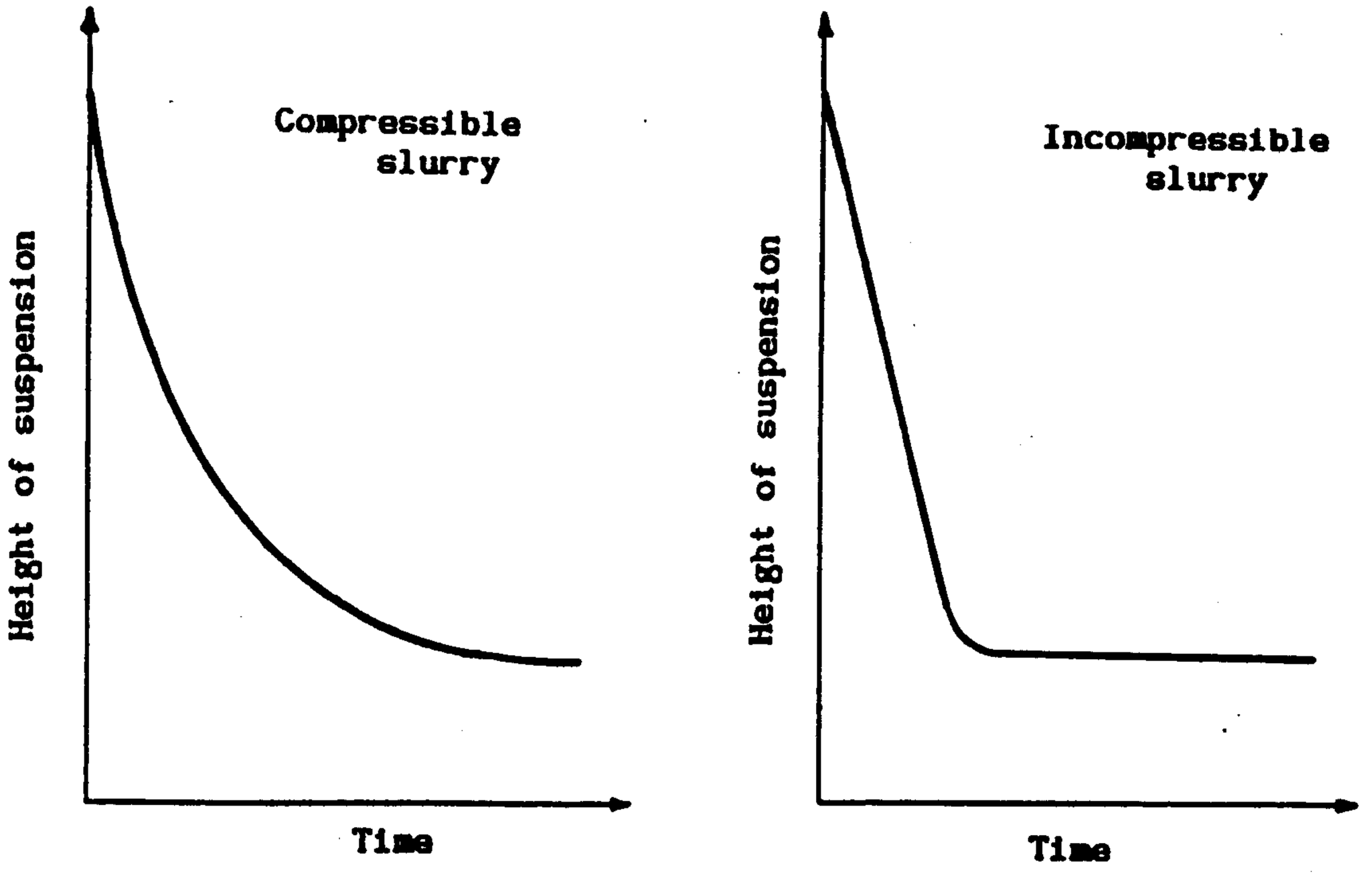

Figure (2.5): Batch settling curves for compressible and incompressible slurries

Assuming that the particles have the same size and shape, and that the concentration is the same across any horizontal layer, the particle flux S at any level, is determined by the solids concentration.

$$S = C\,V \qquad \ldots\ldots (2.27)$$

where C is the volume fraction of solids concentration, and V is the settling velocity of the suspension.

For a suspension of uniform concentration, the solids will settle at a velocity corresponding to the initial concentration, everywhere except at the bottom, where zero velocity is obtained. At this position the concentration is at its maximum value, and the flux is zero. Hence , there is a discontinuity between the position of the maximum concentration, and the initial concentration. This discontinuity does not stay at the bottom, but propagates upwards as it receives more solids from the suspension above, (see figure 2.6).

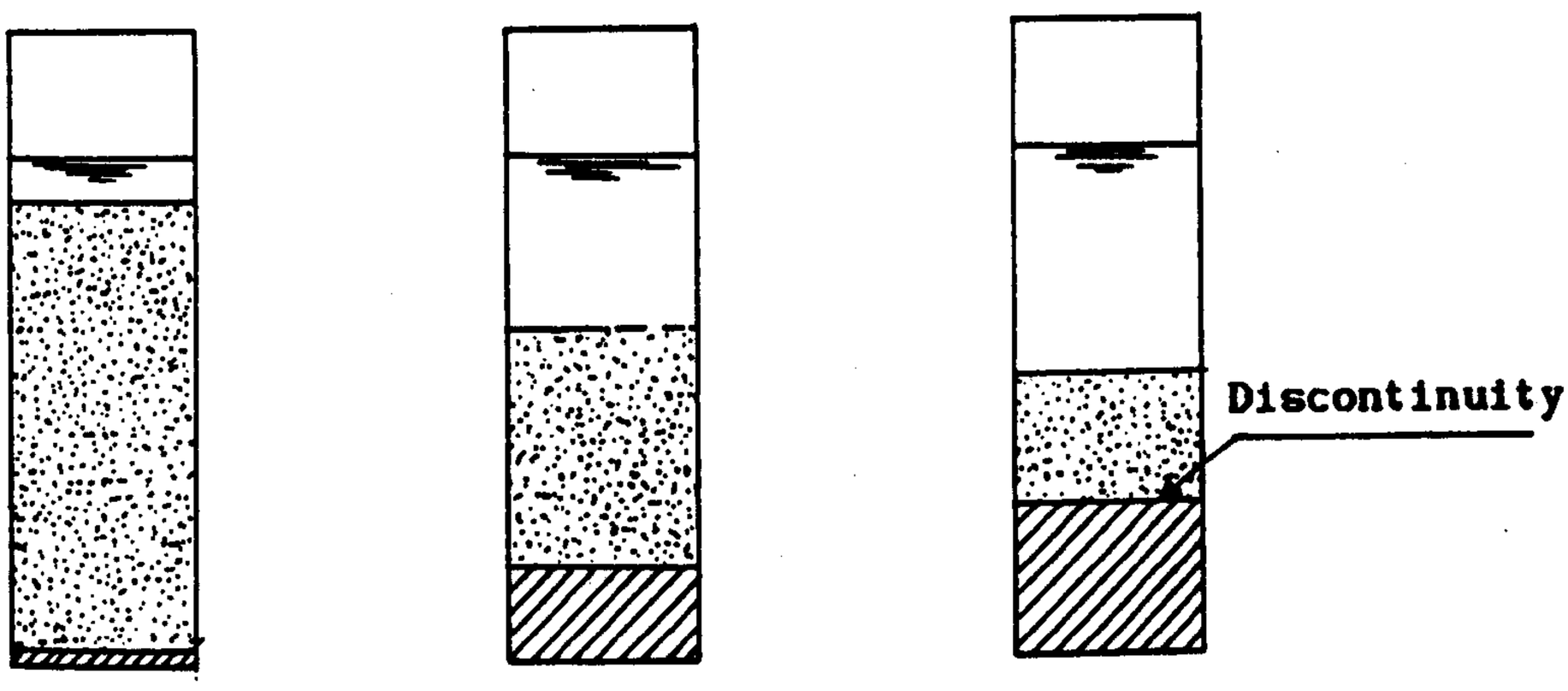

Figure (2.6): Propagation of discontinuity with the progress of settling

The propagation at velocity U is relative to the container wall. Since the discontinuity is considered as a horizontal plane, and there is no solid accumulation within this plane, the material balance through the discontinuity can be written as,

Solids flux into the plane from above = Solids flux out of the plane to below ....(2.28)

If the suffix 1 denotes the layer above the discontinuity and the suffix 2 the layer below, and U is the upwards velocity of the discontinuity

$$C_1 (V_1 + U) = C_2 (V_2 + U) \quad \ldots.(2.29)$$

$$C_1 V_1 - C_2 V_2 = U (C_2 - C_1) \quad \ldots.(2.30)$$

As $S = C V$

$$S_1 - S_2 = U (C_1 - C_2) \quad \ldots.(2.31)$$

$$U = - \frac{S_1 - S_2}{C_1 - C_2} \quad \ldots.(2.32)$$

On an S against C diagram, the speed U is the negative value of the slope of the chord, between the points (C_1, S_1) and (C_2 , S_2) respectively, representing conditions immediately above and below the discontinuity, see figure (2.7).

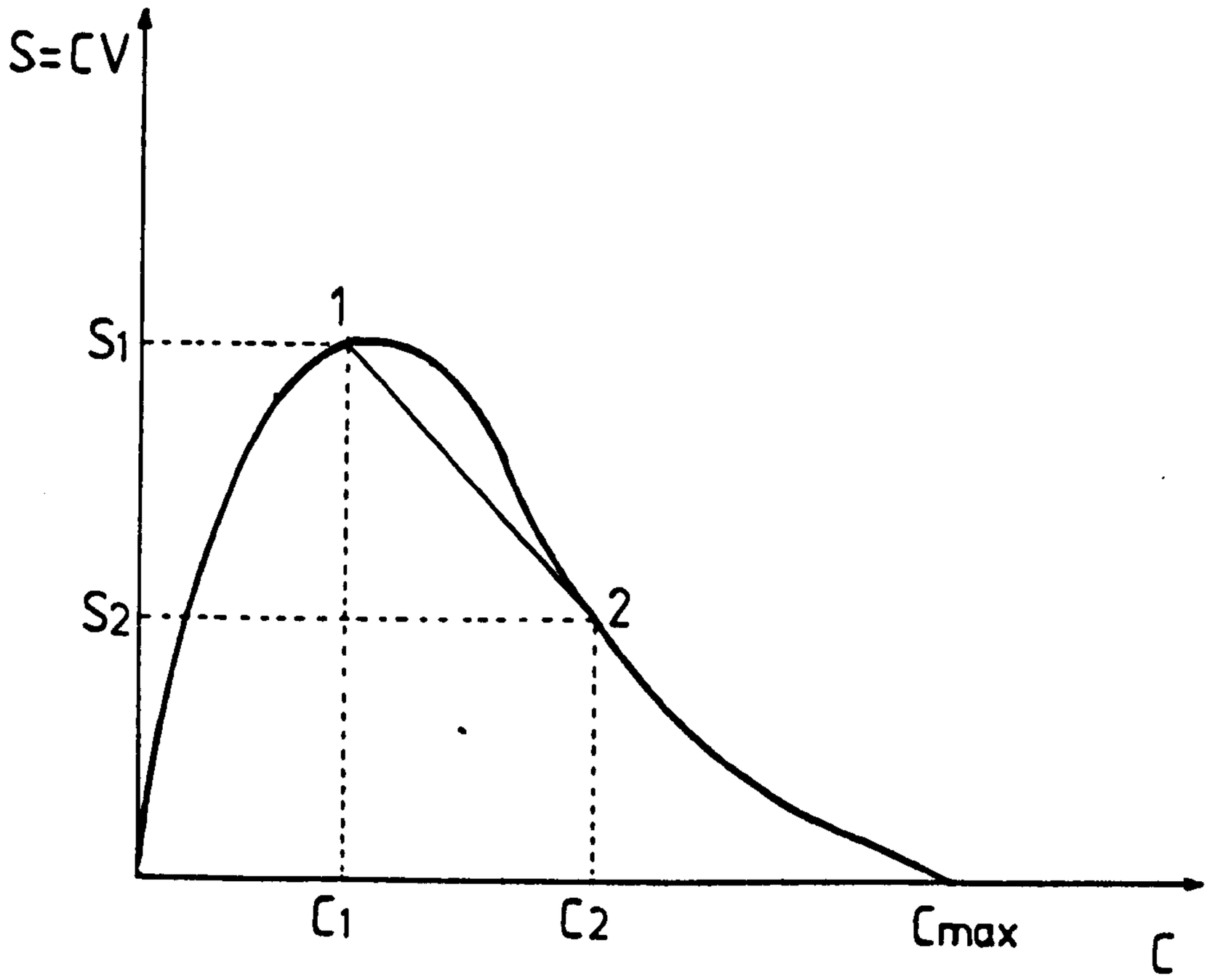

Figure (2.7): the flux plot

If the concentration changes gradually with depth, the locus of C_2 will propagate with a velocity determined by the slope of the plot at 2.

Kynch argued that the initial concentration discontinuity at the bottom of the settling column, could be considered to contain all concentrations between the initial and the maximum values. For an incompressible slurry of rigid spheres, the maximum concentration was found to be 0.64, Shannon et al (1963). This means that in the flux plot at C = 0.64, S = 0. Hence the discontinuity created at the bottom between the maximum concentration and the initial one, will propagate upwards at a velocity determined by the slope of the chord between these two concentrations, on the flux plot figure (2.8).

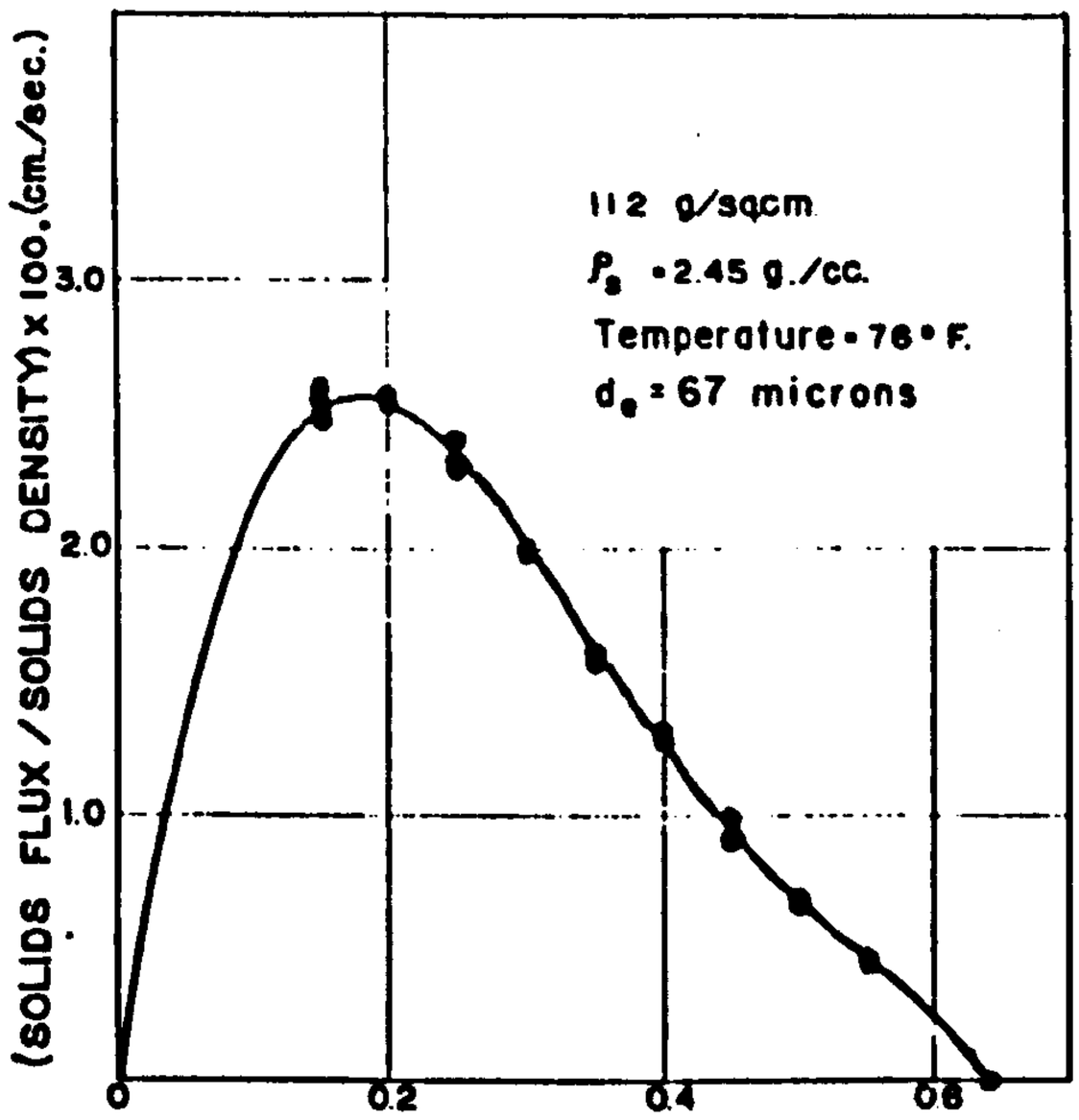

figure(2.8): Flux plot for rigid spheres according to Shannon et al (1963)

Utilizing the flux plot in figure (2.7), Kynch, (1952) demonstrated the conditions at which the initial discontinuity would change into an expanding zone of graded concentration. The settling velocity could be represented by

$$V = V_o\, f(C) \qquad \ldots\ldots (2.33)$$

from which the reduced velocity is defined as $V/V_o = f(C)$ and the reduced solids flux is represented by $S = C\, f(C)$. Since f(C) differs between the workers, the flux curve differs as well. While the flux plot is singly concave for most of the equations

$S = C\,f(C)$, Shannon et al (1963) found the plot for an incompressible slurry to be doubly concave. From their experimental data on glass spheres Shannon et al (1964), suggested that the reduced velocity could be represented by a power series of the form

$$f(c) = 0.338433 - 1.37672(1-\varepsilon) + 1.62275(1-\varepsilon)^2 + 0.11264(1-\varepsilon)^3 - 0.902235(1-\varepsilon)^4 \quad \ldots\ldots (2.34)$$

$$S' = \frac{dS}{dC} = f(C) + Cf'(C) \quad \ldots\ldots (2.35)$$

The plot has a maximum value when $S' = 0$

ie
$$C = \frac{f(C)}{f'(C)} \quad \ldots\ldots (2.36)$$

Since the flux is a power series from the fourth degree of the concentration, the flux plot has two inflection points, which make it doubly concave . This plot can be divided into four zones according to the initial solids concentration, as shown in figure (2.9)

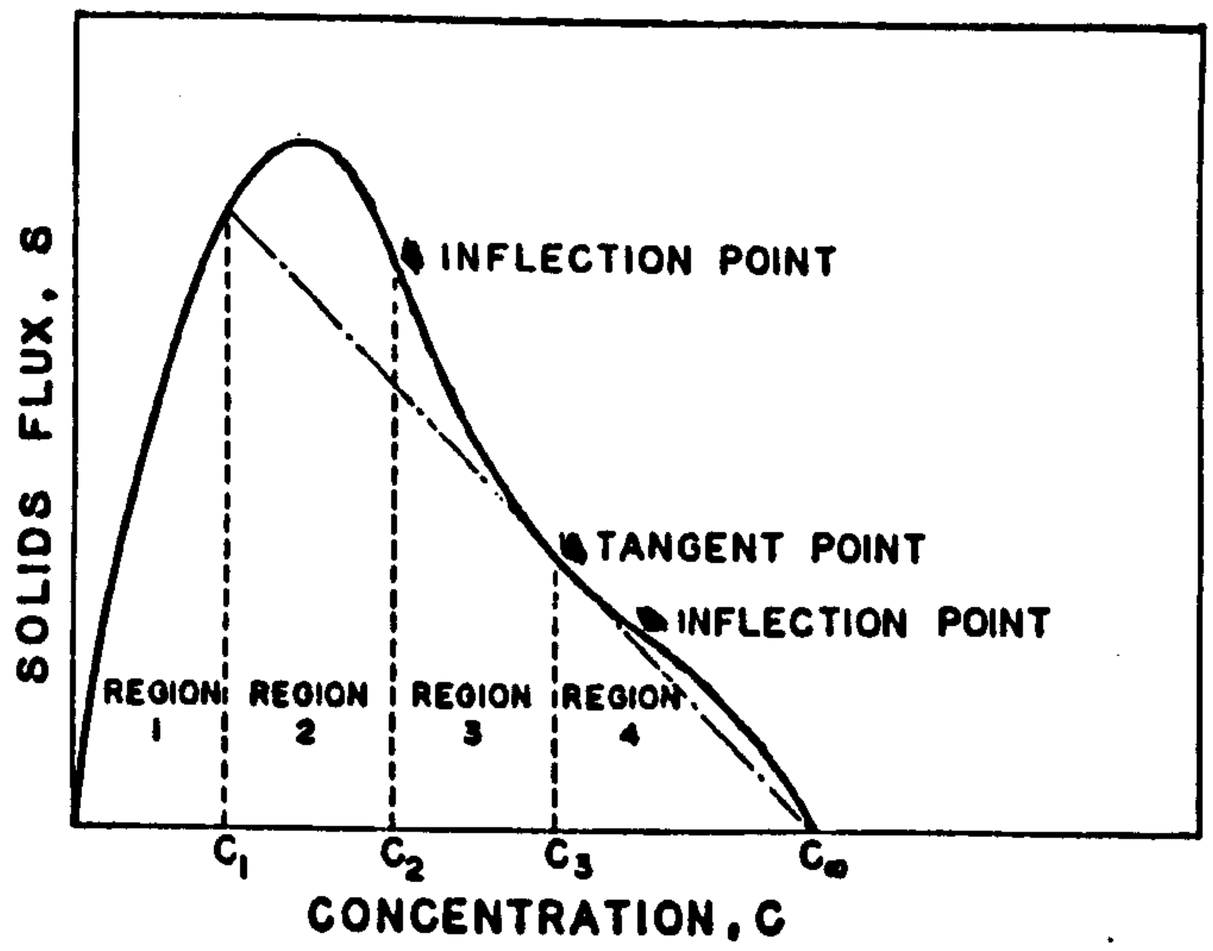

Figure (2.9): The four zones in flux plot for rigid spheres

(Shannon et al 1964)

When the initial concentration lies within the regions 2 or 3 , where C ≈ 0.15 to 0.45 respectively, Shannon et al, 1964, noticed an upper and lower interfaces, between which an expanding layer of graded concentration was reported.

The rate of rise of the fixed bed portion shown in figure (2.10), was measured by Shannon et al (1963).

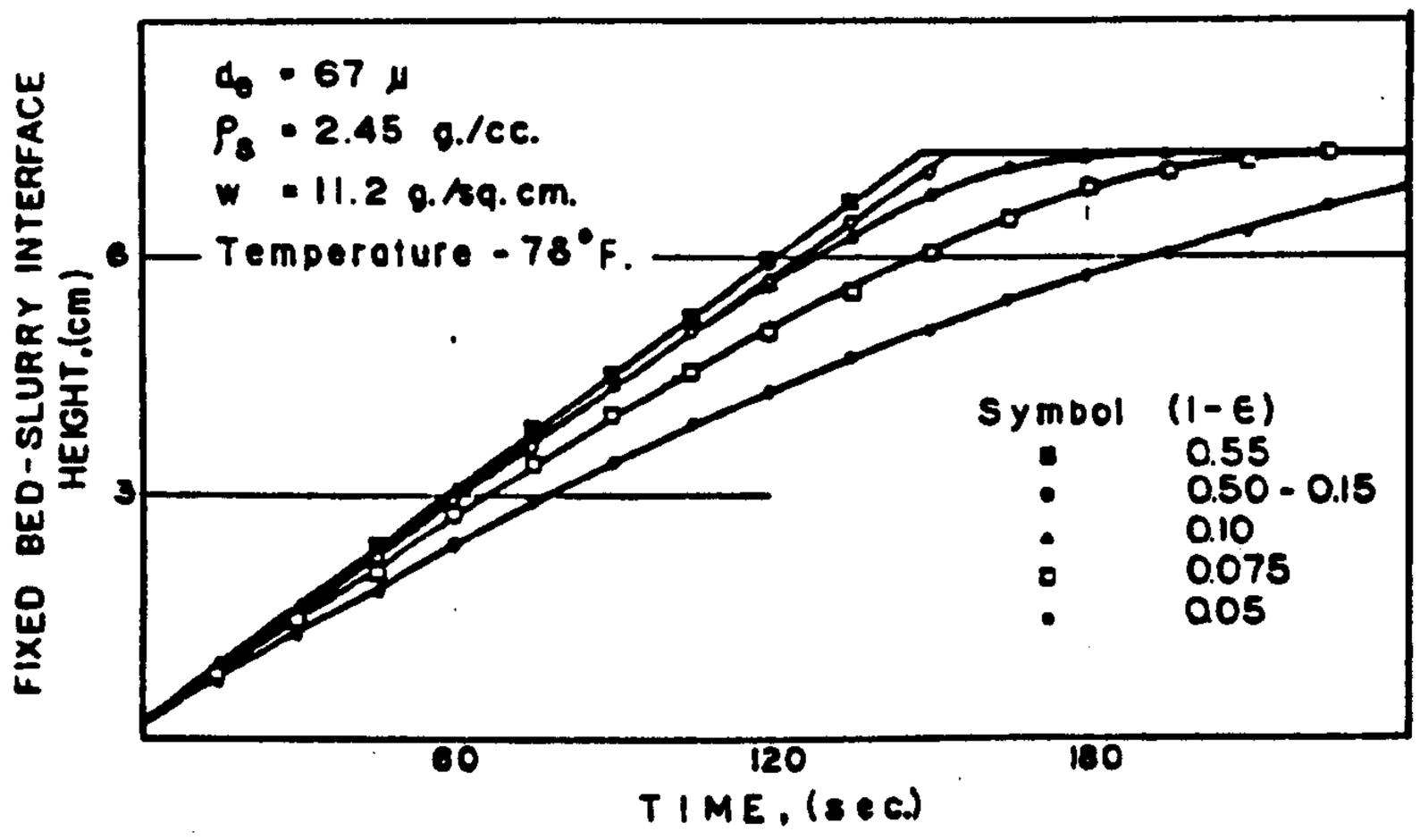

Figure (2.10): Rise of fixed bed during batch settling of 67μ spherical glass beads in water (Shannon et al 1963)

They found it was constant with time for initial concentrations in the range 0.15 - 0.5, but was non linear for C < 0.15. The latter behaviour was attributed to two reasons:

1- particle size segregation

2 - at low initial concentrations a uniform distribution cannot be achieved; this means that a higher concentration existing at the bottom of the vessel, causes the fixed bed portion to grow faster than predicted.

Whilst these workers have tried to modify Kynch's theory to suit the characteristics of a compressible industrial slurry, Dixon et al , (1976) ; Dixon, (1977), and Wakeman, (1981), all state that

Kynch's theory should never be used to predict the propagation of discontinuity , because it does not take into account the inertial forces between the particles in the graded concentration layer.

Dixon et al, (1976), used a simple model of an incompressible slurry and made a numerical test of the effect of neglecting inertial effects, in sedimentation. They showed that when the inertia was included , the interface layer in no cases continued to expand. Instead, the interface rapidly approached a constant thickness. And when inertia was neglected, they found a good agreement with Kynch's analysis. Using the momentum-balance relationship for the solids in the system, Dixon, (1977), concluded that the graded-concentration zone which developed during the process, must lie in the compression concentration range, because the retarding forces-which are necessary to produce increases in concentration, are not present in the free settling zone. Also considering the case of an incompressible slurry , Shannon et al (1964), proposed that a graded-concentration layer results from the increase of propagating discontinuities, for initial concentration range 0.15 to 0.45, which are completely in the free settling region.

Dixon (1977), showed that an incompressible slurry forms a sediment layer which is so strong, that the lower layers show no evidence of compression due to the weight of the layers above. As noted previously when particles come into contact, they are at the critical concentration ie the maximum concentration, and in an incompressible slurry the particles never achieve a higher

concentration, because the application of a compressible stress due to build-up. More sediment above, causes no further increase in concentration. Dixon concluded that a concentration-graded layer can not propagate upward from the sediment into settling zone, because there is no retardation until the sediment is reached, and no increase in the concentration within the settling zone. He also tried to explain Shannon et al's results by considering that the short graded-concentration zone, could be due to compressive effects, resulting from the rearrangement of the spheres into a more closely packed system. In cubical packing , the concentration obtained with identical spheres is 0.524, whereas for tetragonal packing it is 0.741; in the random packing it lies between these values. Dixon also considered that it is possible for spheres to come into sliding contact before they reach their concentration, and that a compressive effect could exist even in the incompressible sediment case.

CHAPTER THREE

ENHANCED SEDIMENTATION IN VESSELS HAVING INCLINED WALL

CHAPTER THREE

ENHANCED SEDIMENTATION IN VESSELS HAVING INCLINED WALLS

3.1 Introduction

If a settling column is set in an inclined position, within a few seconds four regions can be distinguished in the suspension, as shown in figure (3.1) these can be labelled as A, B, C and D

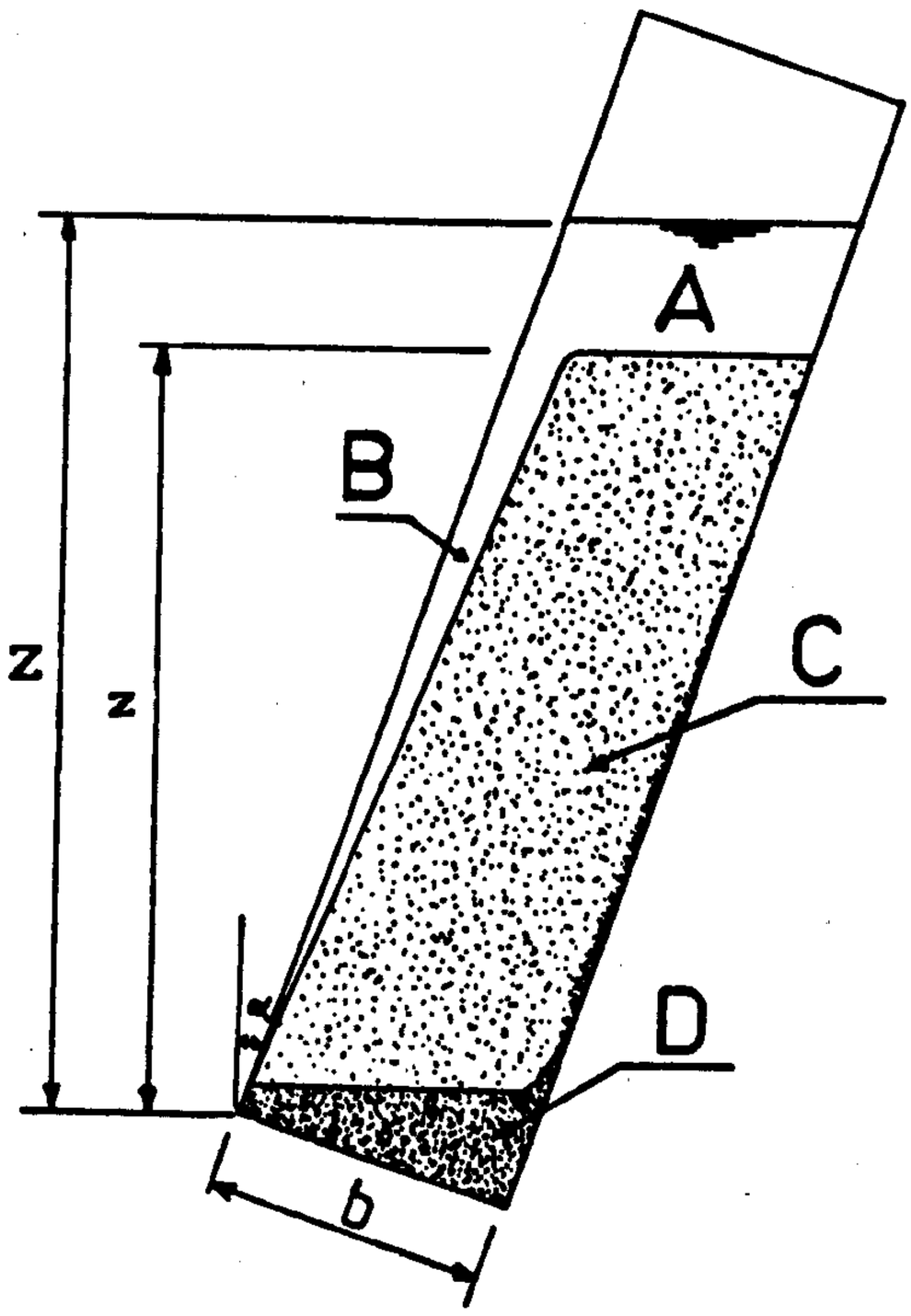

Figure (3.1): The four regions shown in suspension within tilted tube of rectangular section

Region A is a clear fluid layer whose depth increases with time. Region B is a very thin clear fluid layer. The fluid within this layer moves upward at a velocity, which is high compared to the settling velocity of the suspension

Region C is a core of suspension. The concentration in this layer is said to be uniform, and equal to the initial concentration. D is the sediment layer. The interface between regions A and C is horizontal, and moves downward in a settling velocity several times faster, than the settling velocity of the same suspension in a vertical tube ,Boycott (1920). The inclined interface position seems to be a steady state condition at a distance below the top interface, and is independent of time. Below this interface there exists a very thin layer of suspension, whose particles are moving upward by the action of the up-flow within the layer B. At the upward facing surface there exists a very thin layer of concentrated suspension moving downward in a high velocity, to join bulk of the sediment layer D.

3.2 The development of enhanced sedimentation theory

The enhancement in the sedimentation in inclined tubes has a long history, Boycott (1920), being the first to note that when blood is put to stand in narrow tubes, the corpuscles sediment a good deal faster if the tube is inclined, than when it is vertical. Boycott reported that settling rate increases as inclination increases, and as the tube diameter decreases. At the time, Boycott thought the phenomenon was caused by Brownian movement of the lower corpuscles in

the settling blood column. The enhancement phenomenon has attracted considerable intrest to discover its cause and properties. Berczeller and Wastl (1924), Lungren (1927), Ponder(1925) and Nakamura and kuroda (1937), each examined the phenomenon using blood.

Berczeller and Wastl (1924), observed the corpuscles falling along the upward-facing wall and rising along the downward-facing wall, and thought that the friction between the rising and falling groups of blood corpuscles diminished, as the angle of tilt tube increases.

Lungren (1927), noticed a stream of plasma flowing upward under the downward-facing surface (region B), and concluded that this layer was responsible for the increase in the settling rate, since rising fluid in region B results in a reduction of the hydrodynamic resistance to sedimentation.

Ponder (1925) considered that the inclination increases the horizontal area which is needed for settling, as the settling always happens in a vertical direction . Ponder expressed this verbally.

However Nakamura and Kuroda (1937) were the first to present a quantitative theoretical model. Their formula was based on two conditions.

a - Only the downward-facing surface accelerates sedimentation

b - The concentration in the suspension is constant, and equals the initial concentration.

They argued that since the thickness of the liquid layer (region B) under the downward-facing surface is typically observed to be small and independent of time, the portion of clarified fluid formed under this surface can be added instantaneously to the clear fluid above the horizontal interface. Thus the settling rate is enhanced by adding the fluid due to the settling of the inclined interface. With reference to Figure (3.2) the PNK theory is sketched out below.

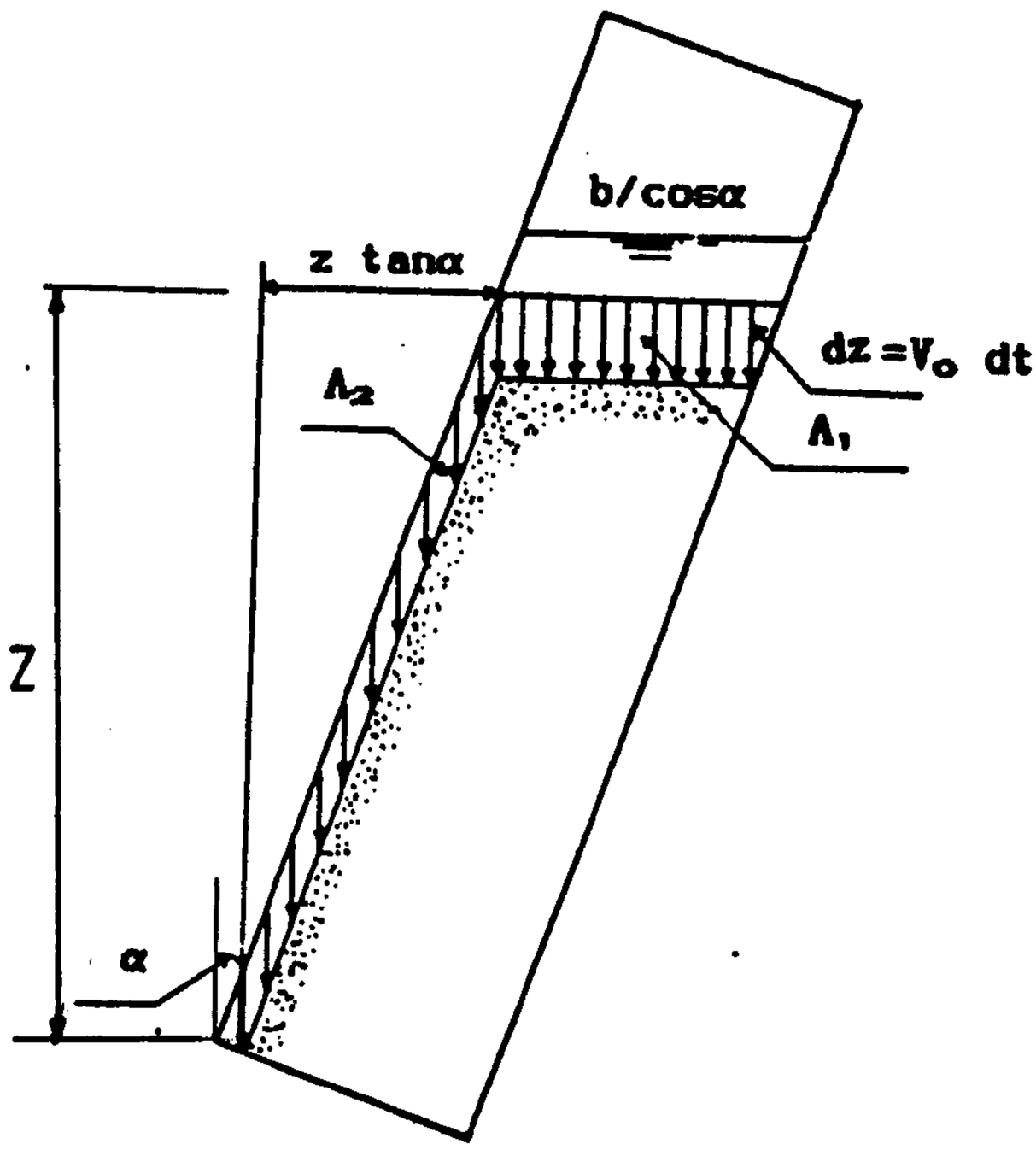

Figure (3.2): Settling in an inclined tube

The volume of clear fluid ΔS, accumulated over the top horizontal interface in time dt, equals the settling velocity of the same

suspension in a vertical tube, times the projected area of the interfaces (horizontal + inclined), on to a horizontal plane.

$$\Delta S = V_o\ (A_1 + A_2).\ \Delta t \qquad \ldots.(3.1)$$

$$A_1 = (b / \cos\alpha)\ e$$

$$A_2 = z \tan\alpha\ e$$

where e dimension of the tube in the third direction

b width of the tube

V_o settling velocity of the same suspension in a vertical tube

α angle of inclination from the vertical

$$\Delta S = V_o\ .\ e\ .\ ((b/\cos\alpha) + (z \tan\alpha)) .\ \Delta t$$

$$\frac{\Delta z}{\Delta t} = \frac{\Delta S}{(b/\cos\alpha)\ \Delta t\ e} \qquad \ldots.(3.2)$$

$$\frac{\Delta z}{\Delta t} = V_o \left(1 + \frac{z}{b} \sin\alpha \right) \qquad \ldots.(3.3)$$

Taking the limits as $\Delta S \to 0$, and integrating the resultant differential equation gives

$$Z - z = \frac{b + Z \sin\alpha}{\sin\alpha} \left[1 - \exp\left(\frac{- Vt}{b} \sin\alpha \right) \right] \qquad \ldots.(3.4)$$

According to PNK equation, the enhancement in settling velocity in an inclined tube, is proportional to the aspect ratio Z/b, and the angle of inclination α. This was predicted by Boycott (1920).

Since 1937, the vast majority of the workers concerned with this phenomenon have concentrated on testing the validity of PNK theory

for different types of suspensions, and different shapes of tube settlers.

Kinosita (1949), Inouye et al (1954), Graham and Lama (1963) and Pearce (1962), all of them tested PNK theory using flocculated materials like blood corpuscles, smoke in air, emery powder in water, magnesium hydroxide in sea water and calcium carbonate in tap water. Kinosita (1949) (using rabbit's blood) initially and smoke in air and emery powder in water in the later study, noticed that the high velocity of the upward flow under the downward-facing surface, was a hundred times the settling velocity of the core suspension. The smoke at first settled more slowly and then more faster than predicted by PNK theory.

Kinosita attributed this variation in settling velocity to the coagulation, which he considered to be more pronounced in tilted tube.

Inouye et al (1954) used human blood, carbon in ethyl alcohol and zinc oxide in water. Of these blood was the only medium which showed agreement with the PNK equation, whereas with the other materials the suspension settled more slowly, and sometimes more quickly.

Using magnesium hydroxide in sea water and calcium carbonate in tap water, Pearce (1962), observed that both settled more slowly. From this it was concluded that the nature of the suspension itself must have a complex effect on the settling process. For the

non-flocculated material, it was anticipated that the actual settling rate would be less than the theoretical. The deviation will increase with settling rate because the faster the settling process, the more vigorous is the circulation in the vessel. A greater proportion of the potential energy of the suspension is consumed in shearing itself and overcoming the hindrance of the vessel walls.

Also using a calcium carbonate suspension, Graham and Lama (1963), tried to correlate their results with the PNK formula by multiplying the predicted settling velocity by a factor F ie

$$\frac{dz}{dt} = F\ V\ \left(1 + \frac{z}{b}\ \sin\alpha \right) \qquad \ldots\ldots (3.5)$$

F was found to be in the range 0.4-0.8.

Oliver and Jenson (1964) noticed that the ascending clear fluid under the downward-facing surface, forms a triangular channel. Through their experimental work they showed that this fluid does not transfer instantaneously, as predicted by Nakamura and Kuroda (1937). Instead it formed a roughly wedge shaped channel along the upper inclined face of the tube, as illustrated in figure (3.1)
They considered that the force causing the transfer of fluid, arises from the differences in hydrostatic head between a column of suspension and a column of clear liquid, and the retarding force consists of friction at the side of the tubes. They proposed a model which is based on counter current steady state flow of two liquids,

of similar densities, between parallel plates of equal flux, and considered that the concentration of the settling suspension affects both the width of the channel, and the shape of the settling curve. They found that the initial settling rate is equal to that observed in a vertical position. Only fair agreement was obtained between their theory and their experimental data.

Using clay in water with the solid concentration in the range 2-20%, Zahavi and Rubin (1975), considered that the settling rate (V_{in}), results from the addition of clear liquid originating from the flow under the inclined interface (V_p), to the clear liquid originating from the settling of solids at the liquid-suspension horizontal interface, at the upper part of the vessel (V_v).

$$V_{in} = V_p + V_v \qquad \ldots\ldots (3.6)$$

where V_p results from two effects

a - settling of particles at the inclined interface in the vertical direction

b - filtration of the liquid from suspension of concentration C to clear liquid by the action of the forces exerted by suspension because of the difference in pressure between suspension and clear fluid.

They stated that V_v depends on the suspension concentration while V_p (in the initial position), is independent of suspension concentration, This is because increases in the initial suspension

concentration result in decreases in the settling effect, and increases in the filtration effects. They assumed the net result to be fairly constant.

By observing a dye tracer injected into the core of the suspension, they stated (what they considered to be a contradiction of the PNK theory's assumption), that most of the clear liquid layer originated from the suspension itself, and not from the settling solids under the inclined plane.

They defined an improvement factor as the ratio between initial settling velocity in a vessel with an inclined plane, and a vertical vessel under the same initial conditions.

$$\left(\frac{V_{In}}{V_v}\right)_o = \frac{(V_p)_o + (V_v)_o}{(V_v)_o} = 1 + \left(\frac{(V_p)}{V_v}\right)_o \quad \ldots\ldots (3.7)$$

Zahavi and Rubin involved the affect of the upward-facing surface in the settling operation, and considered that the thin layer of the solids sliding along the lower wall of the settling tube becomes out of the settling game, reducing the suspension concentration in the parallelogram vessel, which they used in their settling tests.

3.3 Hydrodynamic studies on enhanced sedimentation

3.3.1 Introduction

All the above mentioned models were based on observations and did not rationally proceed from the basic equations of fluid mechanics. Hill (1974) were the first to study the phenomenon theoretically. He obtained a numerical solution of the two-phase flow equations, limiting his investigations to a very diluted suspension of solids spheres under conditions of negligible Reynolds number. In this case V_o can be given by Stokes' Law

$$V_o = \frac{2}{9} a^2(\rho_s - \rho_f)g/\mu \qquad \ldots.(3.8)$$

where a is the radius of the spheres, ρ_s is their density, ρ_f is the density of the fluid, μ is the viscosity of the fluid, and g is the gravitational constant.

Aside from the geometric factors such as the shape of the container and the angle of inclination, Hill (1974)proposed that the process is governed by two dimensionless groups; R, a sedimentation Reynolds number, and the ratio of a sedimentation Grashof number to Reynolds number Γ,

$$R = l\rho_f V_o/\mu = f(C)\ \frac{2}{9}\ l\ a^2\ \rho_f\ (\rho_s - \rho_f)g/\mu^2 \qquad \ldots.(3.9)$$

$$\Gamma = l^2 g\ (\rho_s - \rho_f)\ C_o\ /V_o\mu = \frac{9}{2\ f(C)}\ (\frac{1}{a})^2\ C_o \qquad \ldots.(3.10)$$

where l a characteristic length of the macroscale motion was taken as the initial height of suspension, and C_o is the initial volume fraction of solids which was assumed to be initially uniform. Hill et al (1977) determined the sedimentation rates in various upward-pointing cones, and preformed experiments whose results compared successfully with their theoretical predictions

The range of parameters covered by Hill et al (1977) was

Theory	experiments
$0.8 < R < 6.5$	$0.8 < R < 1.5$
$250 < \Gamma < 2500$	$2800 < \Gamma < 2900$
$30° < \alpha < 43°$	$30° < \alpha < 43°$

$$2 . 10^{-7} < C_o < 2 . 10^{-3}$$

These authors concluded that the PNK theory gave the correct expression for the settling rate in the limits $\Gamma \to \infty$, and $R \to 0$, and this was confirmed by Acrivos et al (1979) when they studied the phenomenon theoretically using analytical techniques. As with Hill et al (1977), Acrivos et al limited their study to a suspension of identical spheres of neglegibly small Reynold's number, and restricted their analysis to the following conditions

$$\Gamma >> 1 \quad \text{and} \quad R\Gamma^{-1/3} < O(1)$$

Since Hill et al (1977), work has tended to concentrate on studying the phenomenon theoretically and more attention has focused on the flow pattern in the clear fluid layer and in the bulk suspension . Efforts have been made to predict the dimensions of the

clear fluid layer from the mathmatical analysis to the phenomenon, but restricted to conditions of those of PNK theory

3-3-2 Settling rate of the top interface

Using continum mechanics, Acrivos et al (1979) developed a theory describing qualitatively the sedimentation of small particles in the vessel having inclined wall. The settling rate S was shown to depend upon the two dimensionless groups R and Γ (as mentioned before).

They treated the suspension as an effective fluid and expressed the ensemble-average fluid and particles velocity in terms of the bulk average velocity U, and the average slip velocity U_s defined as

$$U = (1-C)\, U_f + C\, U_p \qquad \ldots.(3.11)$$

$$U_s = U_p - U$$

where C is the local volume solids concentration.

In order to express the equations in the coming analysis in the dimensionless form; the concentration was divided by the initial value C_o, the velocities were divided by V_o the (settling velocity of the particles in the suspension of concentration C_o), all length were divided by length scale, l and the time by l/V_o.

For an incompressible slurry the continuity equations gives

$$\nabla . U = 0 \qquad \ldots.(3.12)$$

and

$$\frac{\partial \emptyset}{\partial t} + U_p . \nabla . \emptyset = - \emptyset \nabla . U_s \qquad \ldots.(3.13)$$

where $\emptyset$ is the dimensionless local concentration $\emptyset = C/C_o$

When R is very small R < O(1) ie for small sizes or highly viscous conditions, the interaction between the fluid and particles appears only in the drag, which must be balanced by the gravitational force on the particles, due to their excess weight. Hence Acrivos et al (1979) assumed that effects of particle-particle interactions depends only on the local solids concentration. For R << 1 They considered $\emptyset$ = 1 ie constant throughout the duration of settling process and everywhere in the bulk suspension except at the bottom and near the upward-facing surface, where $\emptyset$ rises from 1 to $\emptyset_m$, where $\emptyset_m$ is the maximum concentration in the sediment layer

When $\Gamma \to \infty$ and for a given geometry, the settling rate S was concluded to be predicted from PNK theory, provided that

a- the suspension is monodisperse,

b- the particles Reynolds number is small ie $R \to 0$,

c- the initial concentration distribution is uniform,

d- Γ is large and

e- the interface between the clear fluid layer and suspension remains stable.

3.3.3 Details of the flow field.

Acrivos et al deduced expressions for the velocity field, both within the clear-fluid layer underneath the downward-facing surface, and in the bulk of the suspension.

Since R is assumed to be small, the inertial effects were neglected. It was assumed that the suspension behaves like a Newtonian fluid with an effective viscosity, depending only on the local volume

fraction of particles.

Under these conditions, the ensemble-averaged momentum equations for a uniform particle concentration become,

$$R\rho(\emptyset)\ DU/D_t = -\nabla.P - \Gamma(1-\emptyset)e + \mu(\emptyset)\ \nabla^2 U \quad ....(3.14)$$

where e is the unit vector in the direction of gravity,

$$\rho(\emptyset) \equiv 1 + C_o\ \emptyset(\ \rho_s/\rho_f - 1\ ),$$

$$\mu(\emptyset) = \mu(c)/\mu(0),$$

$$V_o = u_o f(c_o)$$

$$P = \frac{p}{\mu v_o}$$ dimensionless pressure head due to the suspension concentration

$$\nabla.P = \nabla.p - \frac{gl}{\mu v_o}\ (\ C_o\rho_s + (\ 1-C_o\ )\rho_f\ )e \quad .... (3.15)$$

$$= \nabla.p - \Gamma[\ 1 + \frac{1}{C_o}\ \frac{\rho_f}{\rho_s - \rho_f}\ ]e$$

Due to this definition for p, the body force on the suspension appears as a buoyancy term $-\Gamma(1-\emptyset)\ e$, which tends to induce an upward motion in the suspension wherever the concentration is less than C_o, ($\emptyset < 1$), or conversely a downward flow, wherever $\emptyset > 1$.
The thickness of the particle-free layer was found to be vanishengly small as $\Gamma \to \infty$.

Defining the boundary-layer co-ordinates, (h, y), with h denoting the co-ordinate along the downward-facing surface, and y the co-ordinate normal to it, the corresponding velocity components are u and v (see fig. 3.3)

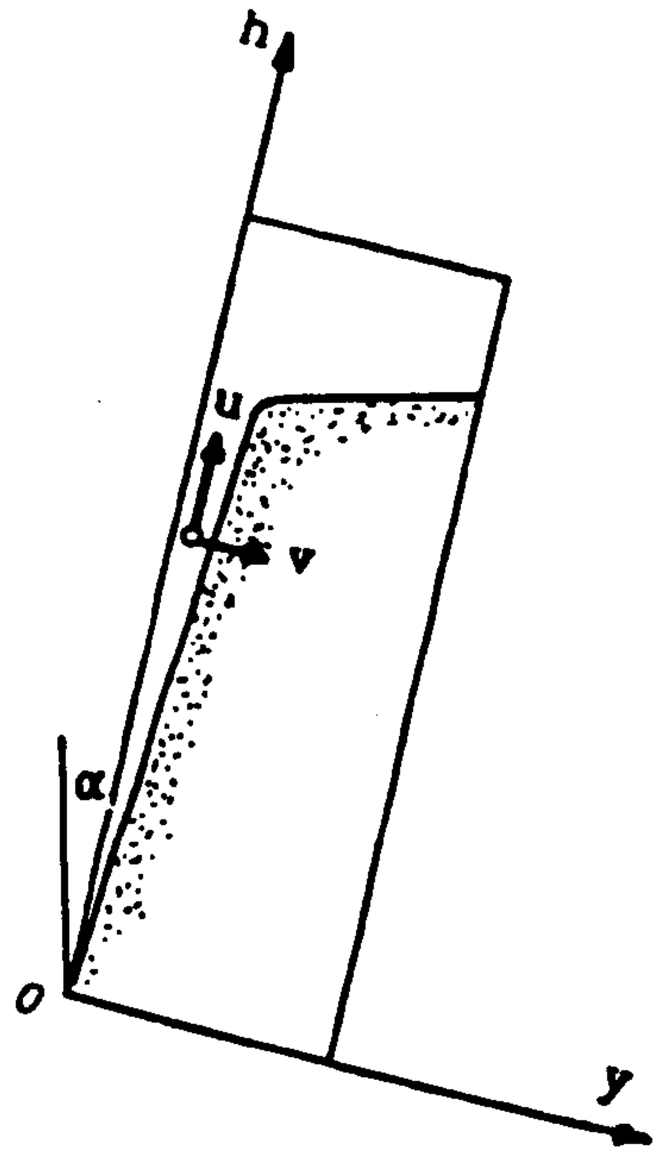

Figure (3.3): The boundary layer coordinates

v was deduced to be O(1) along the interface between the suspension and the particle-free fluid, and hence it is O(1) within the clear-fluid layer. This implies that the longitudinal velocity u, is inversely proportional to the thickness of this layer (δ).

Since the viscous force must balance the buoyancy term in this region, it follows that $u = O(\Gamma^{1/3})$ and that the thickness of the layer is $O(\Gamma^{-1/3})$. The shape of the channel was given by

$$\delta(h) = \Gamma^{-1/3} \left[\frac{3}{\cos\alpha(h)} \int_0^h \sin\alpha(h)\, dh \right]^{1/3} + O(1) \qquad \ldots\ldots (3.16)$$

If α(h) is considered constant along the inclined interface

$$\int_0^h \sin\alpha(h)\, dh = \sin\alpha$$

and the equation (3.16) becomes

$$\delta(h) = \Gamma^{-1/3}(3\ h\ \tan\alpha\ )^{1/3} \qquad \ldots.(3.16')$$

The above solution does not apply near the leading edge where h = 0. At this region the channel width is given by

$$\delta = \Gamma^{-1/3}\left(\frac{C}{\cos\alpha} + \frac{3}{\cos\alpha}\int_0^h \sin\alpha\ dh \right)^{1/3} + O(1) \qquad \ldots.(3.17)$$

C depends on the surface geometry. Near h = 0, $C = O(\Gamma^{-1/2})$ if α is

$O(1)$ as $h \to 0$, or $C = O(\Gamma^{-2})$ if $\alpha = O(h)$ as $h \to 0$

For a fixed h, δ was reported to increase linearly with time until it reaches its steady-state value for that h. Hence at any given h, δ reaches its steady state (3.16')when

$$t = \Gamma^{-1/3}\ (3h\tan\alpha)^{1/3}/\sin\alpha \qquad \ldots.(3.18)$$

At the top interface, the width of the particles-free layer is given approximately by

$$\delta_m = \frac{3\Gamma^{-1}}{\cos\alpha(h)}\int_0^h \sin\alpha\ dh \qquad \ldots.(3.19)$$

The PNK theory applies for predicting the instantaneous height of the suspension, only if δ_m is much less than the length of the effectively horizontal portion of the length of the suspension-clear fluid interface.

The buoyancy-induced motion in the particle-free region imparts a longitudinal velocity at the interface equal to

$$U = 1/2\ \Gamma^{1/3}\delta^2\ \cos\alpha(h), \qquad \ldots.(3.20)$$

where δ is given by equation (3.16).

In the region where $\emptyset = 1$, the buoyancy term is absent. The longitudinal velocity is $O(\Gamma^{1/3})$, at least close to the interface between the suspension and the particle-free layer underneath the downward-facing surface. Hence the inertia term in equation (3.15) must be balanced by the viscous term.

When $\emptyset \equiv 1$ the characteristic Reynolds number is $R\Gamma^{1/3}$, rather than $\bar{R}$ where $\bar{R} = R\rho(1)/\mu(1)$.

Within the bulk suspension, the value of $(\bar{R}\Gamma^{-1/3})^{1/2}$ governs the settling system instead of $\bar{R}$.

For $(\bar{R}\Gamma^{-1/3})^{1/2} = O(1)$, when $H >> (\bar{R}\Gamma^{-1/3})^{1/2}$ in the core suspension, u and v must be of comparable order, $O(\bar{R}^{-1/2}\Gamma^{1/6})$. The momentum and continuity equations become respectively,

$$\bar{u}\ \frac{\partial\bar{u}}{\partial h} + \bar{v}\ \frac{\partial\bar{u}}{\partial\bar{y}} = \frac{\partial^2\bar{U}}{\partial\bar{y}^2} - \frac{1}{\bar{R}\Gamma^{2/3}}\ \frac{\partial p}{\partial h} \qquad \ldots.(3.21)$$

$$+ O(\Gamma^{-1/3}) + O(\bar{R}\Gamma^{1/3}) - 1,$$

$$\partial P/\partial\bar{y} = O(\Gamma^{1/3}), \qquad \ldots.(3.21a)$$

$$\partial\bar{u}/\partial h + \partial\bar{v}/\partial\bar{y} = 0 \qquad \ldots.(3.21b)$$

the stretched variable $\bar{u}$, $\bar{y}$ and $\bar{v}$ are defined as

$$\bar{u} = \Gamma^{-1/3}\, u \ , \quad \bar{y} = (\bar{R}^{1/3})^{1/2} y \ , \quad \bar{v} = \Gamma^{-1/3}(\bar{R}\Gamma^{1/3})^{1/2})v \quad \ldots (3.22)$$

These differential equations which needed a numerical solution can apply everywhere within the suspension, (except within singular regions near the top and bottom) but the boundary condition at the upward-facing surface. must be replaced with

$$\bar{v} = 0 \quad \bar{u} = - U_m(h) \text{ at } \quad \bar{y} = (\bar{R}\Gamma^{1/3})^{1/2}\, b(h)/Z \quad \ldots . (3.23)$$

In the region where $\emptyset > 1$, the large buoyancy term in equation (3.14), tends to induce a downward motion. Acrivos et al (1979) stated that the flow here is analogous to that in the clear fluid layer. In the sediment layer, the buoyancy term can be balanced only in a thin viscous layer, immediately adjacent to the upward-facing wall whereas in the clear-fluid layer, the interface is self-sharpening, so that the concentration distribution is known. In the sediment layer the concentration varies continuously, and must be determined as part of the solution.

Acrivos et al carried out their settling tests for typically ideal glass spheres under the following set of conditions:

$$2 < Z_o < 8 \ ; \qquad 0^\circ < \alpha < 50^\circ \ ; \qquad 0.76 < R_o < 3.04$$

$$4.8 \times 10^{5} < \Gamma < 1.5 \times 10^{7} \ ; \qquad 0.01 < C_o < 0.10$$

Typical experimental results for the height of suspension as a function of time, were plotted together with the corresponding prediction of the PNK theory for $C_o = 0.1$, $Z_o/b = 8$

Acrivos et al stated that an account should be taken for the existence of the concentrated sediment region at the bottom of the vessel. They said that Z should be replaced by $Z - Z_s$, where Z_s refers to the height above the interface, between the bottom sediment layer and the suspension.

Acrivos et al calculated the maximum concentration Cs in the sediment layer at the bottom of the settling tube, directly from measurements of the suspension height Z and the height of the sediment layer Z_s. The calculation was carried out by neglecting the clear-fluid layer and the thin sediment layer at the upward-facing surface, and the concentration in the suspension and sediment were assumed to be uniform with values of $C_{\hat{o}}$ and C_s respectively. C_s was found to increase with time during a given experiment, the typical range being C_s = 0.43 to 0.53, whereas the concentration in the maximum packing for incompressible materials was about 0.64 (Shannon et al (1964)

The variation in C_s with time in a given experiment was explained by Acrivos et al (1979), by the fact that the average concentration in the sediment layer on the upward-facing surface is relatively low, and that after it flows off the wall, this sediment can slowly compact, while remaining at the bottom of the vessel.

Acrivos et al (1979), did not carry out any quantitative measurements about the velocity fields in the clear fluid layer, or within the bulk suspension, and did not measure the time at which the clear fluid layer reaches its steady state. But they measured the

dimensions of the clear fluid slit in its steady state and gave qualitative descriptions of the phenomenon which are described below.

i - the boundary of the particle-free layer forms immediately after mixing has ceased

ii the flow in this region reaches a steady state after a few seconds.

iii- the shape of the clear fluid slit is very thin at the beginning along the tube, but turns sharply (to become horizontal), on the top interface. After a short time, the 'sharp turn' broadens gradually at a distance of about 2cm below the horizontal interface.

After a short time the thickness of this layer at a given point on the downward-facing surface should be independent of both time and the instantaneous height of the suspension. This was found to be the case everywhere except near the top of the suspension, where the width of the slit at a given point increased with time as the top of the suspension approached. see figure (3.4).

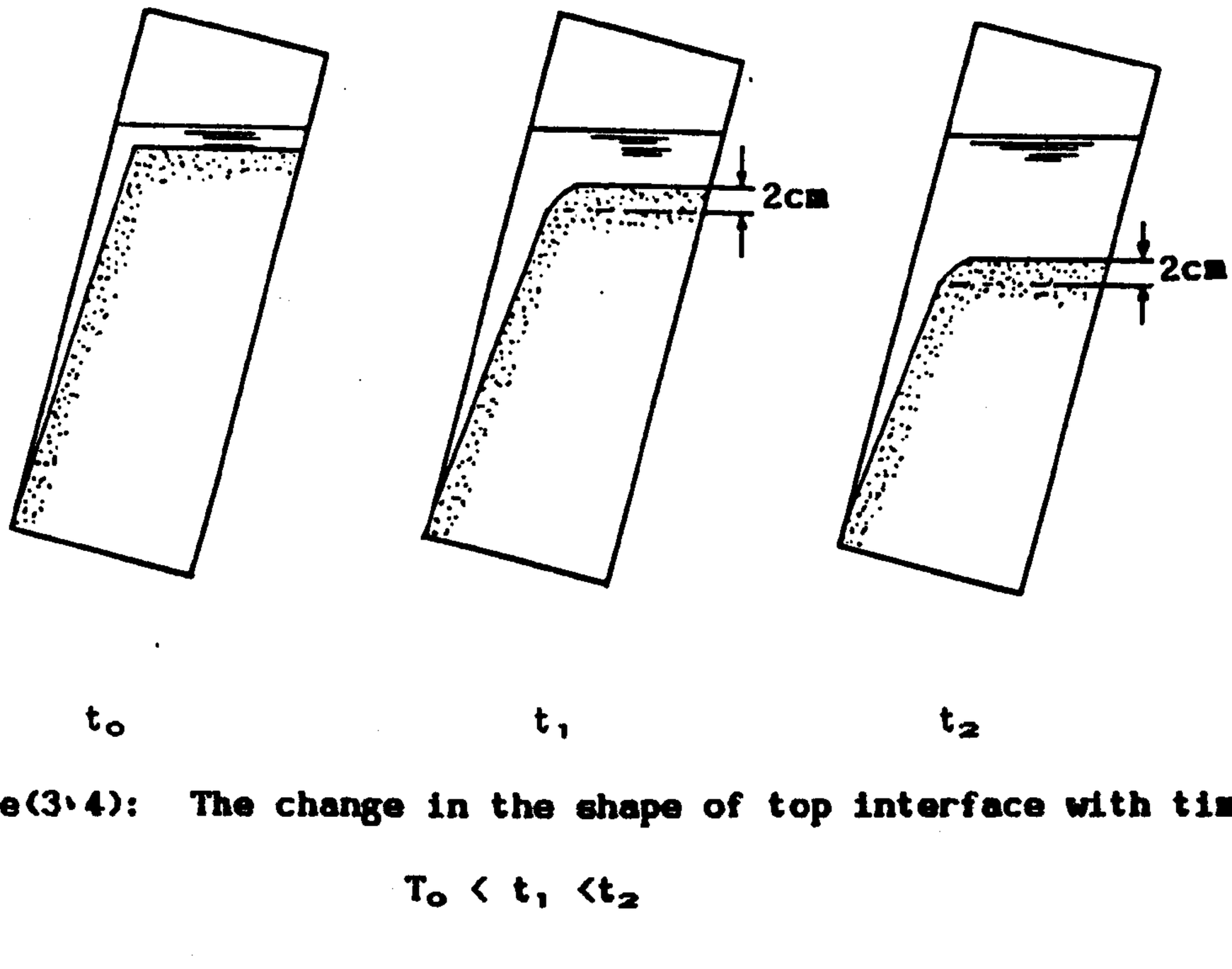

figure(3.4): The change in the shape of top interface with time

$T_o < t_1 < t_2$

iv - By visually observing the motion of the particles, large velocities were found near the interface between the clear-fluid layer underneath the downward-facing surface, and the suspension. This velocity was directed along the interface and its magnitude increased from essentially zero at the bottom of the vessel, to a maximum value near the top of the suspension. This was roughly one or two order of magnitudes greater than the vertical settling velocity.

v - In the core of the suspension, the motion was relatively slow everywhere, except in a thin layer adjacent to the clear-fluid slit, beneath the downward-facing surface. The thickness of this layer was approximately five times that of the clear-fluid layer. The particles close to the clear-fluid layer were observed to rise rapidly, come to an abrupt stop at the top of

the suspension, and then descend rapidly in a thin layer immediately adjacent to that where the particles were rising. The primary flow in the core was much slower, with the particles moving primarily down the vessel.

Near the top of the suspension, a thin stream of rapidly moving suspension was observed to break away from the main flow and to descend rapidly into the bulk of the suspension, where it seemed to die down in the vessel. This behaviour has not yet been explained.

Using Acrivos et al's assumptions, Shiba 1985), solved equations (3.12) and (3.13) taking into account the inertia effects within the clear-fluid layer. They deduced an expression for the thickness of the clear-fluid slit as;

$$\delta = \left(\Gamma^{-1} \frac{3h \sin\alpha}{\cos\alpha - I_h} \right)^{1/3} \quad \ldots\ldots (3.25)$$

where I_h is the inertia term, in integration of equation (3.13).

If $R\Gamma^{-1/3}$ and $R\Gamma^{-2/3}$ are less than 0.1, I_h can be neglected and the width of the clear fluid slit can be represented by equation (3.19).

The case studied above is valid when the spacing between the plates (b), is much larger than the thickness of the particle-free layers.

If the spacing is decreased, the large velocity at the clear-fluid interface, may set the bulk of the suspension into rapid circulating motion, similar to that observed in closed cavities with one moving wall.

For very large values of $R\Gamma^{1/3}$ (the effective Reynolds number for the flow in the suspension.), the motion was said to resemble the Batchelor (1956) model of high Reynolds number steady flow, with closed streamline ie a constant vorticity inviscid core surrounded by a thin boundary layer. The velocity in the bulk of the suspension will be $O(\Gamma^{1/3})$, and the flow will be inviscid. When Z/b is large, the streamlines of the inviscide constant vorticity flow in the core, are effectively parallel to the inclined walls of the container, with longitudinal velocity given by

$$v = \omega b \ (1/2 - y\ Z/b\ ) \qquad \ldots.(3.26)$$

where ω, a dimensionless uniform vorticity in the core is given by

$$\frac{\omega b}{2} = \Gamma^{1/3} \left[\frac{3^{7/3}}{56} \cos - {}^{5/3}\alpha \sin^{4/3}\alpha \right]^{1/2} \qquad \ldots.(3.27)$$

This core is separated from the interface between the particle-free region, underneath the downward-facing step. This was confirmed by Schneider (1982), who studied the particular case in detail.

Schneider (1982) was concerned with the case

$$R^{-1}\Gamma \to \infty \text{ while } R^{-3}\Gamma \to \infty \ .$$

He based his analysis on the continuity equations for the particulate phase and the incompressible mixture. Respectively supplemented by a drift-flux relation describing the relative motion of the particles and the liquid in terms of the particle concentration. As the inertial terms are neglected in the bulk flow, the particle concentration was considered to be constant in planes perpendicular to the body forces ie in horizontal planes. Hence it

followed that there were horizontal kinematic-wave fronts whose vertical motion depends on the two-dimensional, or three-dimensional total volume flux.

Schneider did not consider the particle concentration to be constant in the whole suspension, as did Acrivos et al (1979). Schneider also predicted sedimentation processes with centred waves which emerge from the bottom of the initial concentration, in such a way that a simple concentration jump from the suspension to the sediment is not possible. ie $\emptyset_s < \emptyset_o < \emptyset_t$

Using the kinematic-wave theory Schneider (1982), considered the flow in the bulk of the suspension could be determined without any knowledge of the details of the flow in the boundary layer. and that the boundary layer can be subdivided into an inviscide main part, a viscous sublayer at the wall, and a free shear layer at the interface between the clear liquid and the suspension.

CHAPTER FOUR

EXPERIMENTAL OBSERVATION OF THE INTERFACIAL BEHAVIOUR

CHAPTER FOUR

EXPERIMENTAL OBSERVATION OF THE INTERFACIAL BEHAVIOUR

4.1 Introduction

This chapter focuses on the interfacial behaviour of a settling suspension. According to theory (see section 2.2.2, equation 2.26), vertical tube settling is described by the Richardson and Zaki's equation

$$V = V_o\ (1-C)^n \qquad \ldots.(4.1)$$

with V_o identified by Stoke's equation for a discrete particle

$$V_o = d^2\ (\rho_s - \rho_f)\ g/18\mu \qquad \ldots.(4.2)$$

Though it is evident that equation (4.1) must be true when $C \Rightarrow 1$, the author is unaware of experimental work (apart from Richardson and Zaki) which confirms the theoretical identity when $C < 1$

Preliminary experiments were carried out in a vertical tube to check the sensitivity of the functions $V/(1-C)^n$ to changes in diameter and viscosity. This is intended to provide a check on the accuracy of the experimental procedures and to provide necessary data for testing the PNK theory and its modifications which are considered in section (4.4.2).

4.2 Experimental set-up

4.2.1 Preparation of solids

The solid material which was used for all the research experimental work was white glass beads supplied by Jencons (Scientific ltd), from grades 15, 13 and 11, which cover the size range from 55 to 250 μm. The material was first of all sieved into size ranges between the sizes; 0, 63, 75, 90, 106, 125, 150, 180, 200 and 250 μm.

Each size glass was washed with water and then subjected to differential settlement in a 90% glycerol solution to help detach small spheres stuck to the large ones. To achieve this the solids and glycerol were added to a 500 ml measuring cylinder and the suspension was stirred and left to settle for 2 minutes. The supernatant (which was initially cloudy due to the presence of the very small particles) was withdrawn by a pippette. This process was repeated until a clear supernatant appears on the top of the suspension. After this, glycerol was removed by washing with tap water

For the chemical wash, the materials were soaked initially in an alkaline liquid (soap) for 24 hours for the acidic impurities to be dissolved, and thereafter for six hours in an acidic solution of 0.1N of HCL. Following this, the material were washed further with non-ionised water to remove chemical traces. The beads were then dried in an oven with temperature 105° in preparation for the tests. The glass

beads were re-useable, and after any test were washed chemically and dried as mentioned above.

The diameters of fifty glass spheres were measured under a microscope, and the mean diameter was considered to be the representative of the particular size glass. Using a specific gravity bottle the density of the beads was found to be ρ_s = 2.849 g/cm^3

4.2.2 The fluid

The suspending fluid used in the series of experiments was a mixture of distilled water and glycerol in a different weight ratio to give different values of fluid viscosity as part of the confirmatory studies concerning the effect of viscosity on the settling process.

Table (4.1) gives density and viscosity of the fluid mixture at different values of mixing ratio at a temperature 21 ± 0.5°C. These were obtained using a tube viscometer. In table (4.1) the term G/W refers to the ratio of glycerol solution (98% pure glycerol) to water; ρ_f is specific density of the mixture and μ is the dynamic viscosity of the mixture

Table (4.1): Composition, density and dynamic viscosity of aqueous glycerol used as the suspension fluid

G/W %	ρ_f g/cm³	μ poise
65	1.153	0.145
70	1.169	0.200
75	1.180	0.305
80	1.198	0.480
85	1.215	0.87
90	1.228	1.530

4.2.3 Settling column system.

Two square tubes (termed Tube 1 and Tube 2) were made of perspex with the cross sections of area 4.62 cm² and 3.79 cm² respectively and with a height 30 cm were used in the experiments (see figure 4.1). A scaled tape was fixed to one side of the tube. To create a homogeneous suspension at the beginning of an experimental run a stirrer unit was constructed from a square plate (side is 1.8 cm) with a 3 mm hole in each corner to facilitate mixing by raising and plunging (see figure 4.1).

Since the fluid viscosity is sensitive to temperature and can have a significant effect on the experiments, the column was immersed in a water bath. The temperature was maintained at 21 ± 0.5°C.

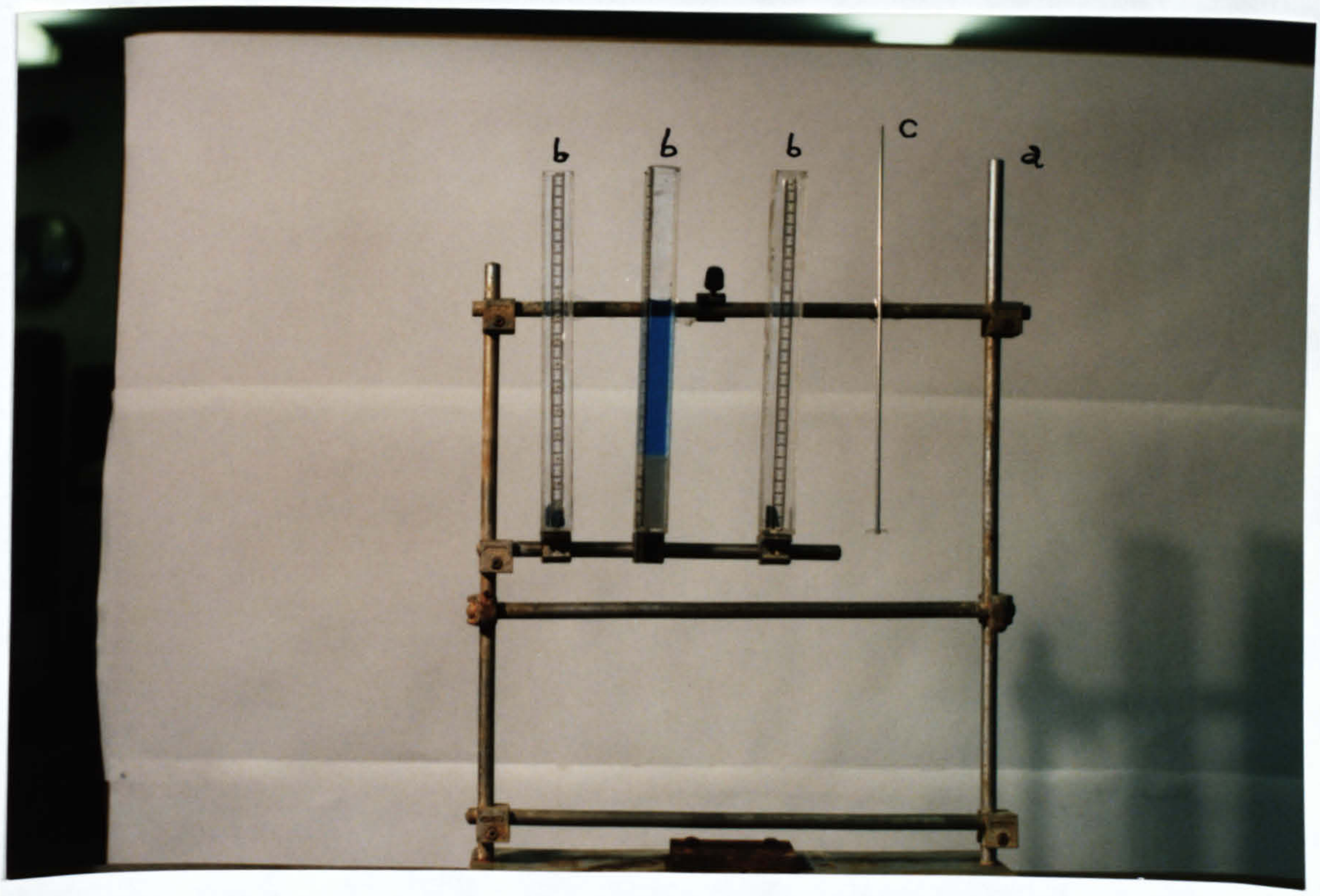

Figure (4.1) a- the frame carrying the settling tube.

b- the settling tube.

c- the plate stirrer

4.2.4 Dye solution

Dye solution was used in the experimental study for two reasons: (i) , in batch settling tests to give colour to the settling suspension, this helps to distiguish the existence of interfaces easily, because the more dense the suspension is the lighter is the colour of the suspension. (ii), the dye solution was used as tracer to measure the fluid velocity within the clear fluid channel in an inclined tube and within the suspension core.

Blue dye was dessolved in the fluid mixture described in section (4.2.2). G/W = 0.8. The quantity of the added dye powder was not measured, it was just enough to give a dark solution. However, few drops of this solution was needed to colour the suspension, so that its effect on the fluid density is negligible

When the dye solution was used as a tracer (see chapter six), the density effect of the dye solution was tested by injecting it into pure fluid. The dye drops stayed within the fluid at the injecting points and did not have velocity components in any direction.

4.2.5 Suspension preparation

The procedure described below were used for the preparation of the suspension.

- the test tube was set at the required inclination and placed in a constant temperature tank.
- glycerol solution was poured carefully into the test tube to avoid the intrusion of bubbles.
- the required quantity of the glass beads were added very slowly, and carefully so that a thin layer of glass beads was set on the top of the fluid. No further beads were added until this layer was wet and sank into the fluid by its wet weight. This helps to avoid the ingress of air bubbles.
- after adding the required quantity of glass beads additional glycerol solution was poured to bring the suspension to the selected height.
- the column was left for an hour for thermal equilibrium to be attained.
- the suspension in the tube was stirred until the uniform concentration distribution was reached. Timing was commenced from the moment at which stirring ceased.

4.3 Experimental procedure in vertical tubes

4.3.1 Initial height and settling velocity

Preliminary experiments were carried out to check the effect of the initial suspension height on the interfacial velocity. In these experiments beads with d = 100 μm and a suspension characterised by viscosity μ = 0.48 poise and concentration C_o = 0.202 was used.

The suspension was prepared in the way described in section (4.2.5) and the height of top interface measured from the tube bottom was recorded with time. The initial height ranged from 9 to 19 cm and led to the data shown in figure (4.3). Inspection of figure (4.3) indicates that interfacial velocity

is $V = 0.39 \pm 0.014$ cm/min.

Errors refer to the 95% confidence interval, and it is seen that V is essentially independent of the release height h except for the height H = 9 cm where the settling velocity seems to be higher. This is probably caused by experimental error, but the reasons are unclear.

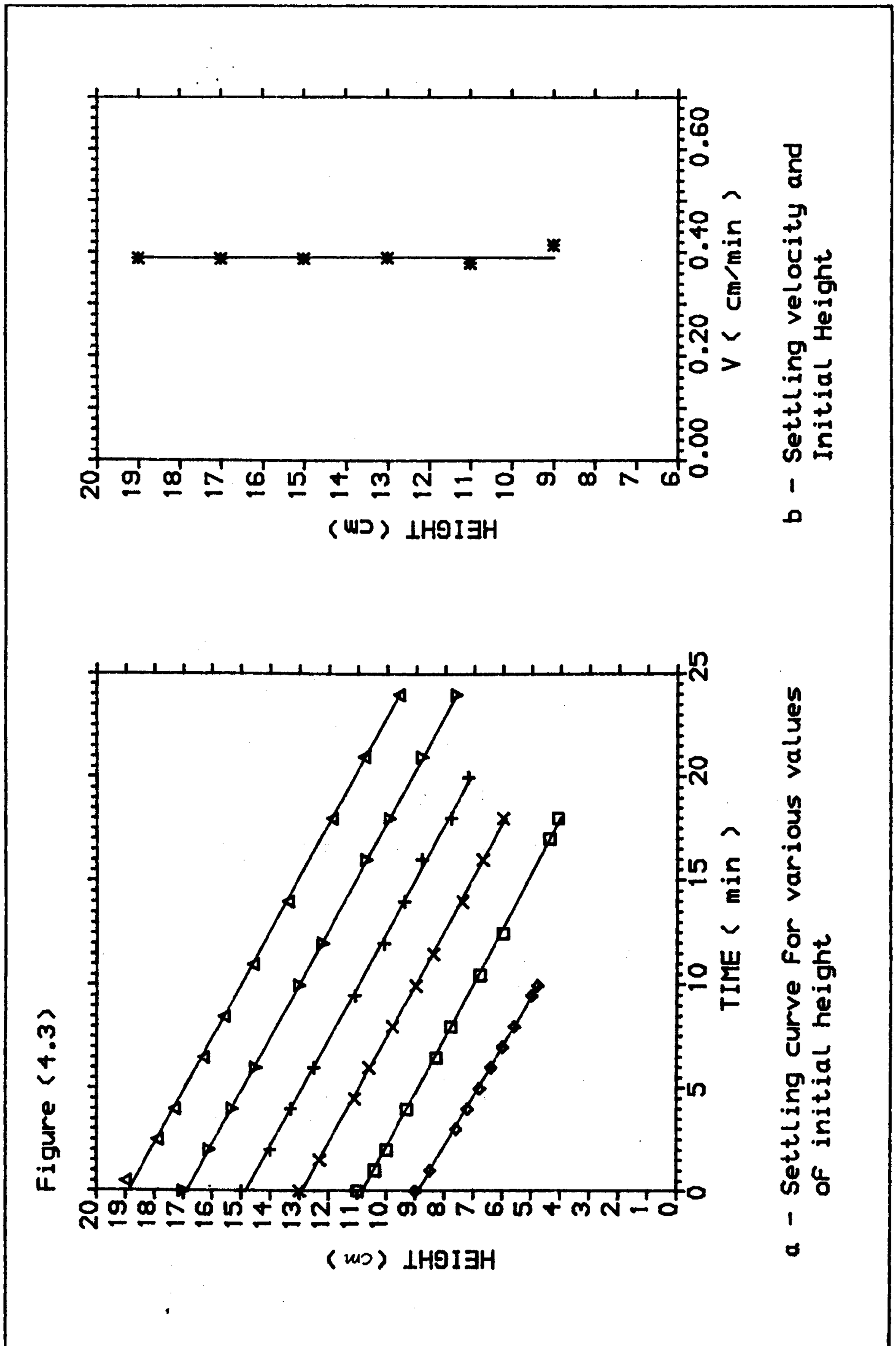
HEIGHT (cm)
20
19
18
17
16
15
14
13
12
11
10
9
8
7
6
0.00
0.20
0.40
0.60
V (cm/min)
b - Settling velocity and
Initial Height
HEIGHT (cm)
25
20
15
10
5
0
TIME (min)
a - Settling curve for various values
of initial height

Figure (4.3)

Overall, the results of this test justifies the procedures of controlling the concentration in settling tube by using fixed amounts of solids and varying the associated volume of the glycerol solution.

4.3.2 The relationships $V - C_o$

In literature, as it was mentioned in section (2.2.2), there are many forms of the relationships which predict the settling velocity as a function of the initial concentration in the form

$$V_c = V_o \, f(C)$$

where V_c is the settling velocity of suspension of solids concentration C and, V_o is the settling velocity of discrete particles in the same settling media, predicted by Stockes' equation (2.3)

Barnea and Mezrahi (1973) predicted f(C) according to equation (2.7)

$$f(C) = \frac{(1 - C)^2}{(1 + C^{1/3}) \exp(5C/ 3(1 - C))}$$

Batchelor (1972) according to equation (2.8)

$$f(C) = 1 - 6.55C \quad \text{for } C \ll 1$$

and, Richardson and Zaki (1954-b) according to equation (2.9)

$$f(C) = (1-C)^{4.65}$$

To check the validity of the equations above to the existed experimental data, the effect of concentration on settling velocity was studied.

Particles of diameter d = 0.0135 cm was used. The fluid mentioned in section 4-2-2 was used with a viscosity μ = 0.48 poise. The suspension was prepared in the way described in section (4.2.4) and, the concentration was in the range C_o = 0.147 to 0.29.

For different values of concentration batch settling tests were carried out. As in section (4.3.1) the position of the interface was recorded at different times and the velocity was deduced. The mean settling velocity was deduced by plotting the settling curve which is a straight line (the same way followed in figure 4.3).

The relationship between initial concentration and velocity ratio V_c/V_o is plotted in figure (4.4) along with the theoretical relationships (2.7), (2.8) and (2.9).

Figure (4.4) is an evidence that the existed experimental data are very close to the curve representing Richadson and Zaki's equation (2.9). Therefore it is justified to represent the settling velocity as a function of initial concentration of the form

$$V_c = V_o \ (\ 1-C)^n$$

n is to be discussed in section (4.3.5)

Figure (4.4)

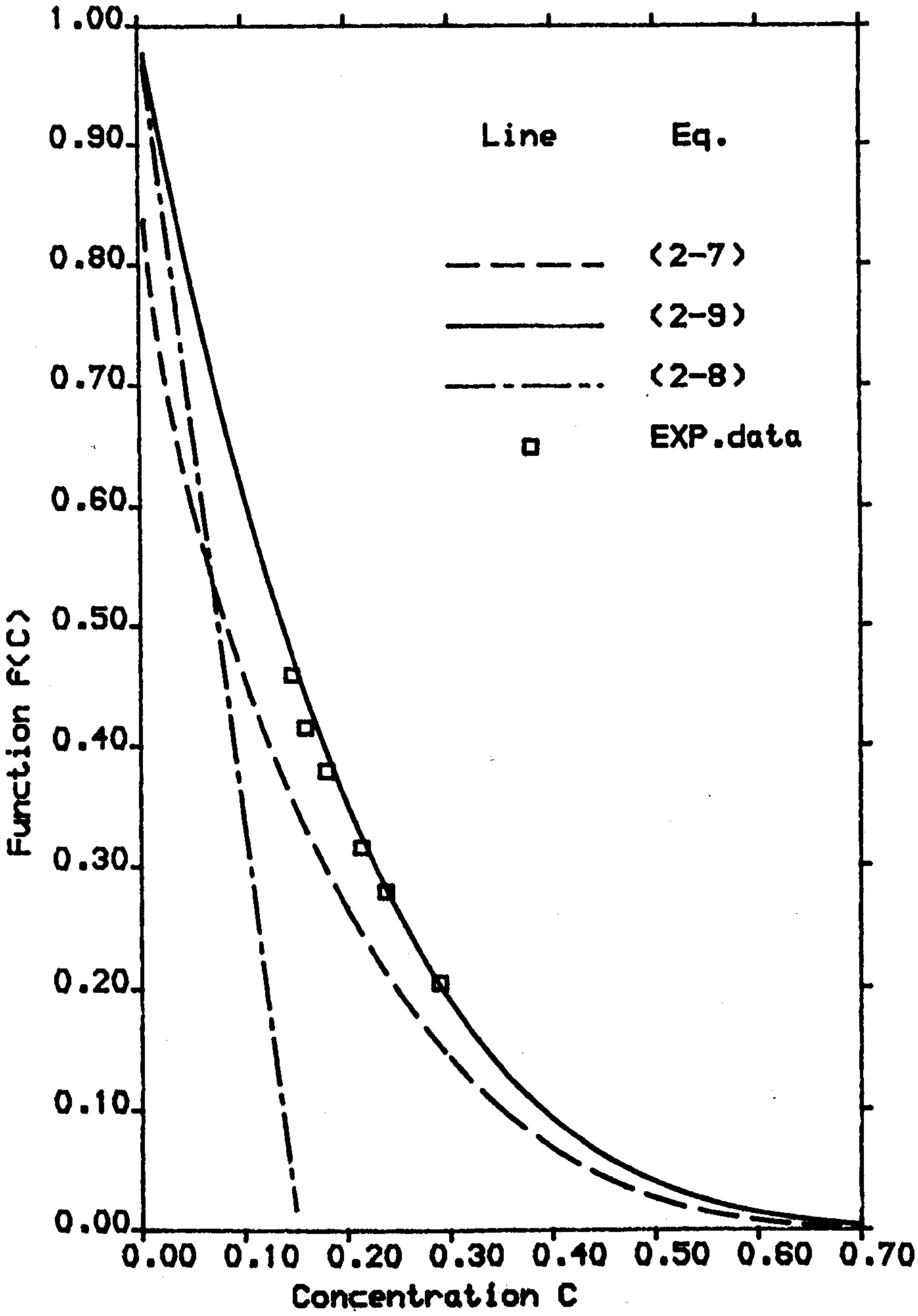

Comparison between theories For F(C)

4.3.3 Viscosity and settling velocity

The object of this set of tests was to test that the term $V_o = V / (1-C)^n$ in Richardson and Zaki's equation is inversely proportional to the fluid viscosity (see equations 4.1 and 4.2)

In these experiments beads with d = 117 μm were used; C_o was in the range 0.15 to 0.24 and the initial suspension height set between 13.5 to 21.7 cm. The viscosity was varied from 0.145 to 1.53 poise. As in section (4.3.1) the position of the interface was recorded at different times and the velocity was deduced.

For every value of fluid viscosity μ, data was fitted by equation (4.1) rewritten as $V = A (1 - C)^n$ which is equivalent to:

$$\ln V = \ln A + n \ln(1-C) \qquad \ldots\ldots (4.3)$$

Data was compared with (4.3) and the coefficients A and n were found by a least square fit.

Table (4.2) summarizes the results showing Coefficients A and n for different values of fluid absolute viscosity

Also shown in table (4.2) is the Stokes' velocity V_o based on equation (2.3).

Tables (A2 to A7) in appendix A summarise the raw data for this set of experiments.

Table (4.2): A summary of the effect of viscosity on settling velocity.
In col. 3 ,5 errors refer to the 95% confidence interval.

μ poise	ρ_f g/cm^3	ln(A)	A cm/min	n	V_o cm/min	Re X 10^3
0.145	1.153	1.61 ± 0.093	5.00	4.65 ± 0.47	5.23	8
0.200	1.169	1.18 ± 0.085	3.26	4.75 ± 0.40	3.76	4
0.305	1.180	0.74 ± 0.018	2.10	4.48 ± 0.08	2.25	1.8
0.480	1.198	0.36 ± 0.030	1.44	4.83 ± 0.15	1.53	0.7
0.870	1.215	-0.42 ± 0.022	0.65	4.53 ± 0.10	0.84	0.2
1.530	1.228	-0.69 ± 0.040	0.50	4.76 ± 0.17	0.47	0.1

In theory
$$A \equiv \frac{d^2 (\rho_s - \rho_f) g}{18 \mu} \qquad \ldots\ldots (4.4)$$

Since the fluid viscosity was altered by using different ratio of glycerol to water mixture, the specific gravity of the fluid consequently was altered. This implies that $(\rho_s - \rho_f)$ was not constant . Hence Equation (4.4) was re-cast in the form

$$\frac{A}{\rho_s - \rho_f} = K \frac{1}{\mu} \qquad \ldots\ldots (4.5)$$

with K as a constant if the dependency on μ^{-1} is maintained. Figure (4.5) shows the experimental relationship between $A/(\rho_s - \rho_f)$ and $1/\mu$

Figure (4.5-a) confirms that the slope is constant and by implication K is constant, confirming that $A/(\rho_s - \rho_f) \alpha 1/\mu$

Figure (4.5-b) shows a comparison between the experimental value of A and V_o defined by Stokes' equation .

Also shown in figure (4.5-b) is the comparison between A and V_o and confirms the identity

$$A \equiv V_o$$

shown by the trend line. The parameter n shows no significant dependency on viscosity and has average value

$$n = 4.66 \pm 0.11$$

(error limits refer to 95% confidence interval)

Figure (4.5)

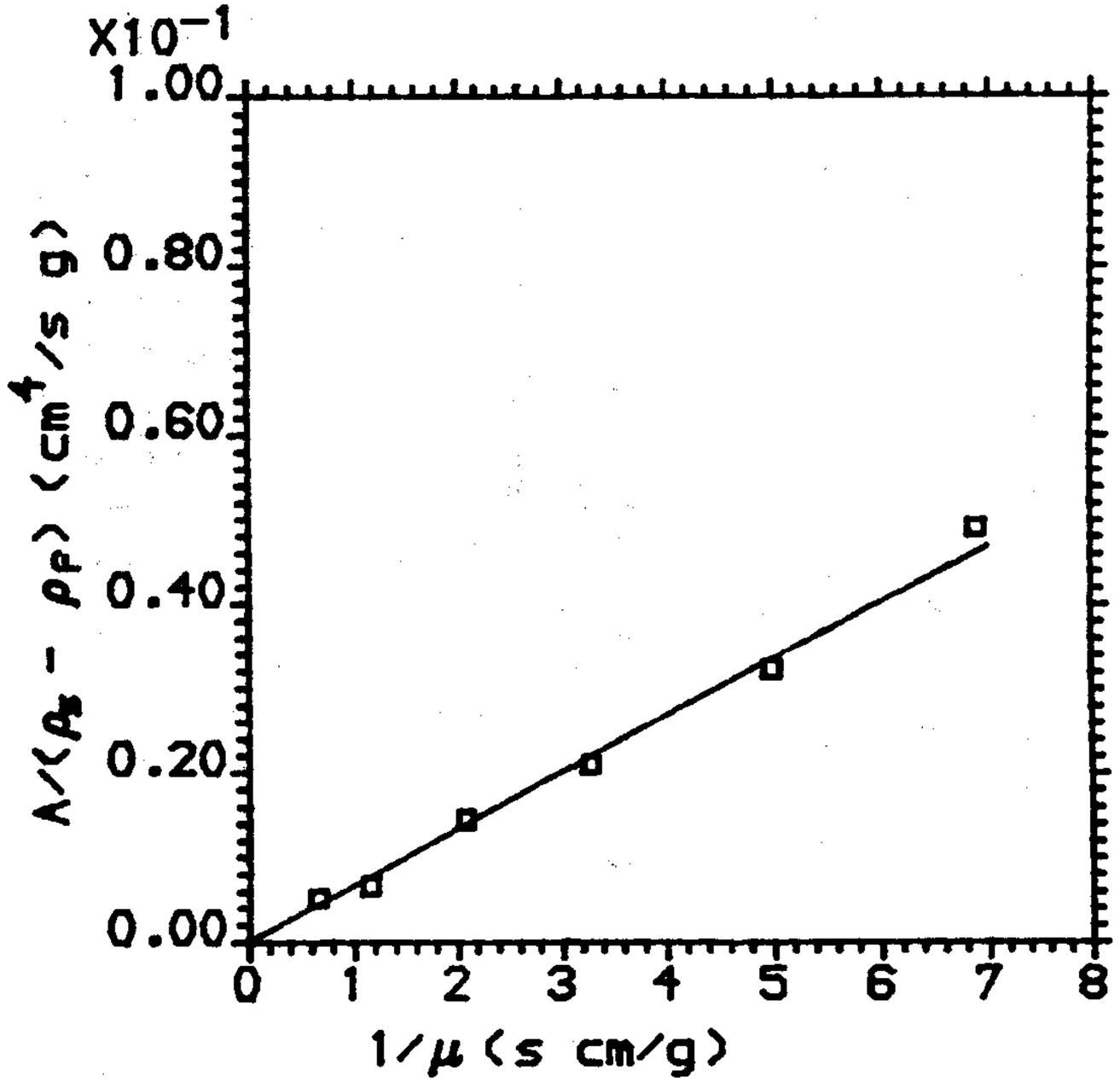

a - Influence of viscosity on Factor A in equation(4.5)

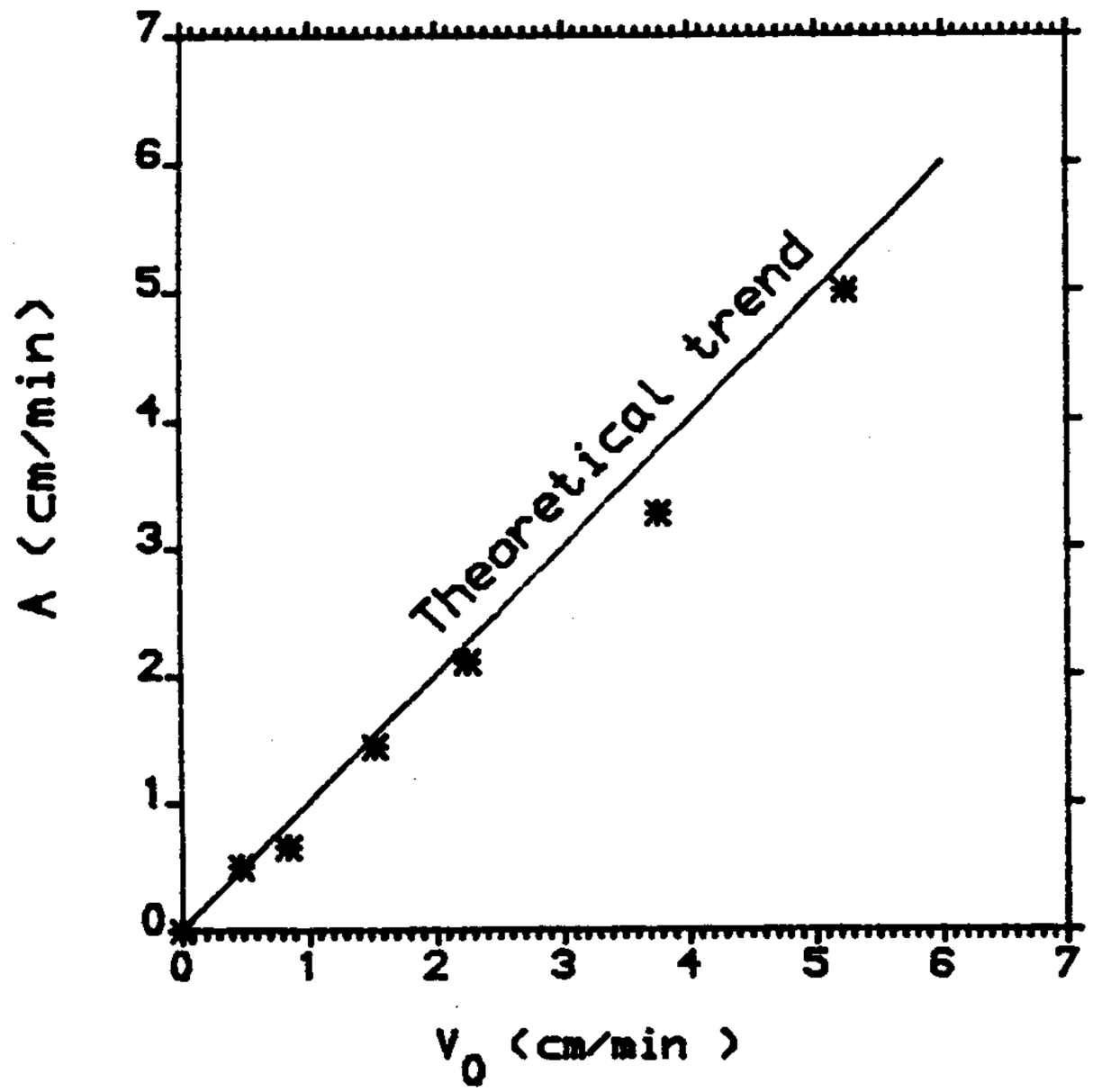

b - Comparison between V_0 and A

4.3.4 Size of particles and settling velocity

The object of this set of tests was to confirm experimentally that the term V_o in equation (4.1) is proportional to d^2 where d is the settling particle's diameter where

$$V_o \equiv V/(1-C)^n \quad \ldots\ldots (4.6)$$

In these experiments, μ = 0.48 poise; C_o was in the range 0.14 to 0. 29; the initial height was in the range 11 to 21.7 cm and particle diameter d was in the range 117 to 217 μm.

As in section (4.3.1) the position of the interface was recorded at different times and the velocity was deduced.
For each d, data was again fitted by equation (4.1) in the form of equation (4.3) in which coefficients A and n were found by least square fit. Table (4.3) summarizes the results showing coefficients A and n for values of particle's diameter . Also shown in table (4.3) is the stokes' velocity V_o based on equation (4.2).

Table (4.3): A summary of data on the effect of particle diameter on settling velocity. In col. 3, 5 errors refer to 95% confidence interval.

d/D X 10^2	d μm	ln A	A cm/min	n	V_o cm/min	Re X 10^3
0.58	117	0.36 ± 0.022	1.44	4.85 ± 0.11	1.54	0.75
0,66	132	0.55 ± 0.025	1.73	4.40 ± 0.11	1.96	1.08
0.84	168	0.98 ± 0.042	2.65	4.97 ± 0.18	3.17	2.20
1.00	200	1.47 ± 0.048	4.32	5.47 ± 0.21	4.50	3.7
1.08	217	1.57 ± 0.062	4.82	5.41 ± 0.26	5.30	4.7

Figure (4.6)

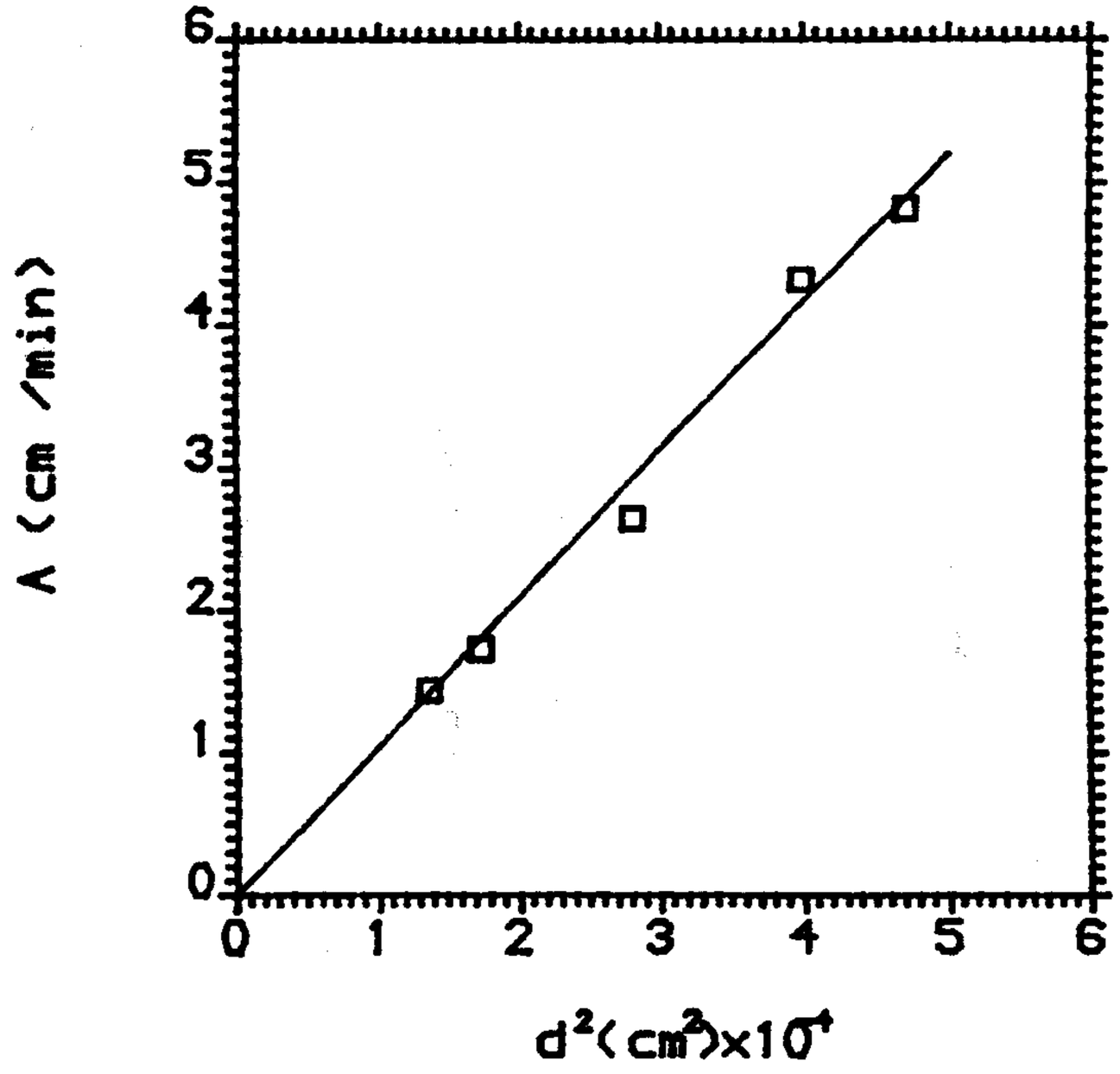

a - Diameter effect on velocity

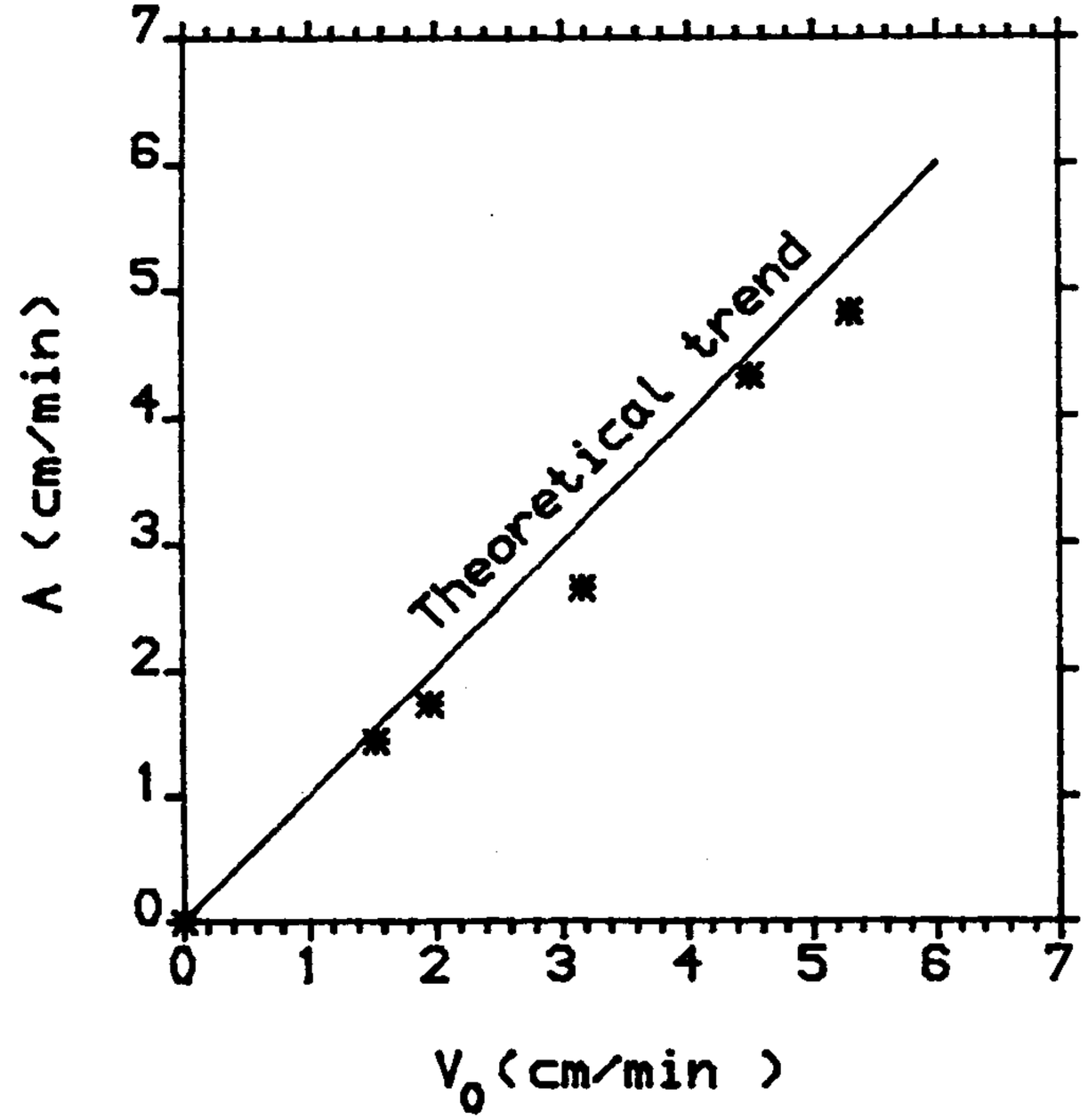

b - Comparison between V_0 and A

Tables (A8 to A12) in appendix A contains the raw data (h, t) for this set of experiments.

In theory $$A \equiv \frac{d^2\ (\rho_s - \rho_f) g}{18 \qquad \mu} \qquad \ldots\ldots (4.7)$$

which can be set in the form

$$A = K\ \ d^2 \qquad \ldots\ldots (4.8)$$

with K as constant if the dependence on d^2 is maintained.

Figure (4.6-a) shows that the slope, and by implication K, is constant confirming $A \alpha d^2$. Also shown in figure (4.6-b) is the comparison between A and V_o and confirms the identity $A \equiv V_o$ shown by the trend line. From data in table (4.3) n increases as d increases (see figure 4.7).

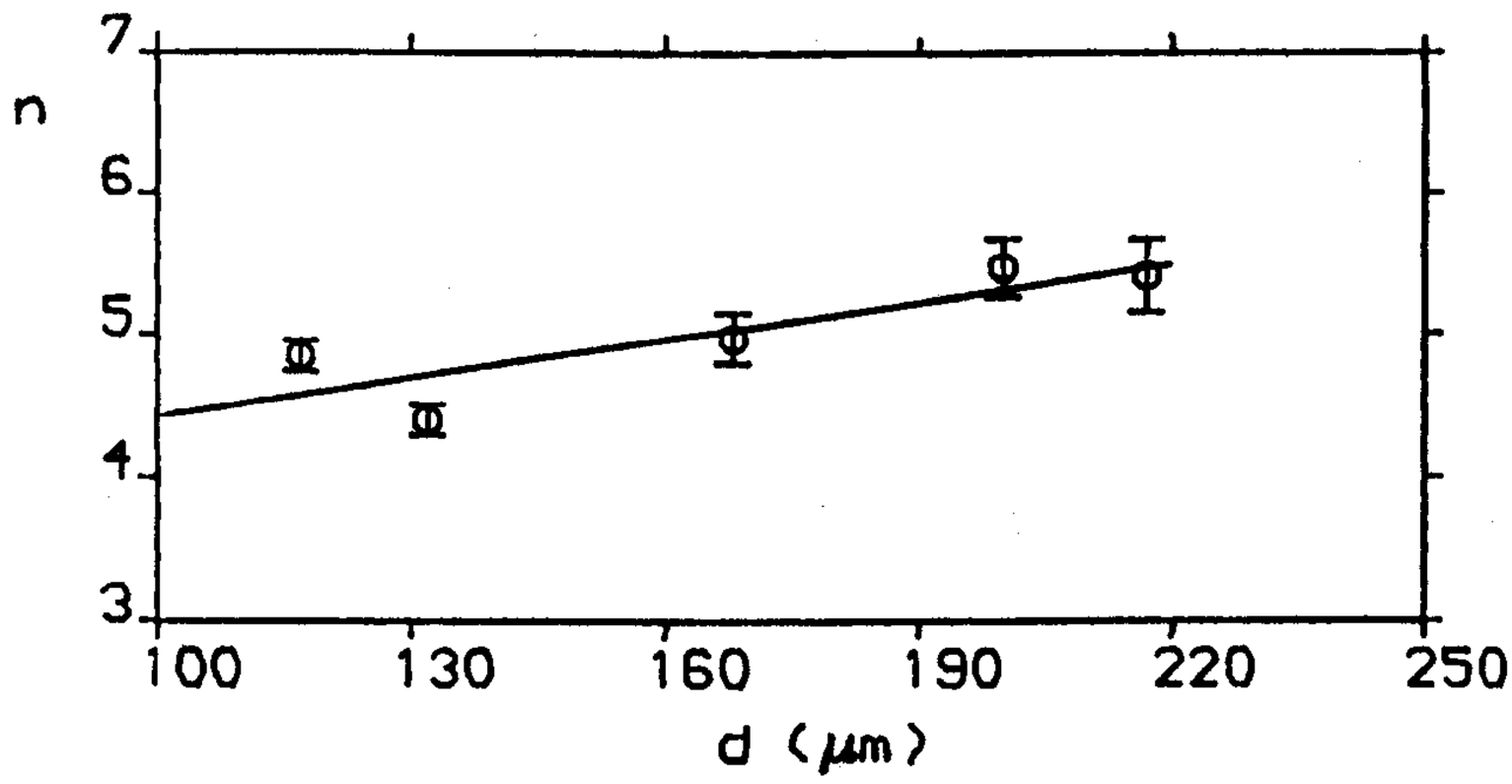

Figure (4.7): Coefficient n as a function of d

Using the data in table (4.3) the relationship between n and d is of the form

$$n = 3.55 + 0.00882\ d \qquad \ldots\ldots (4.9)$$

where the unit of d is μm

4.3.5 Comment

Figure (4.4) confirms that in the existed experimental data, V - C relationship follows the form

$$V_c = V_o \, (\, 1-C \,)^n \, .$$

Tests also confirm that term A defined in equation (4.3) was proportional to μ^{-1} and d^2 provided term n in $(1-C)^n$ is not considered to be a constant. A direct comparison with A and V_o defined by Stokes' equation shows $A \equiv V_o$. For influence of C_o, in the case of μ varying

$$n = 4.66 \pm 0.11$$

whereas for changing d, n increased. In Richardson and Zaki's analysis they demonstrated the effect of the ratio d/D (D being the dimension of the settling tube) on the value of the coefficient n. For Re < 0.2 this was given in the form

$$n = 4.65 + 19.5 \, d/D$$

Considering D ≃ 2 cm the side length of the settling tube, equation (4.9) can be rewritten in the form

$$n = 3.55 + 189 \, d/D \qquad \ldots . (4.10)$$

Since in the present work the highest value of Re is 0.008 < 0.2 equation (4.10) can be compared with the experimental value in figure (2.4). Figure (4.8) shows fitting of the data in figure (4.7) to previous experimental data taken from figure (2.4) for Re < 0.2 .

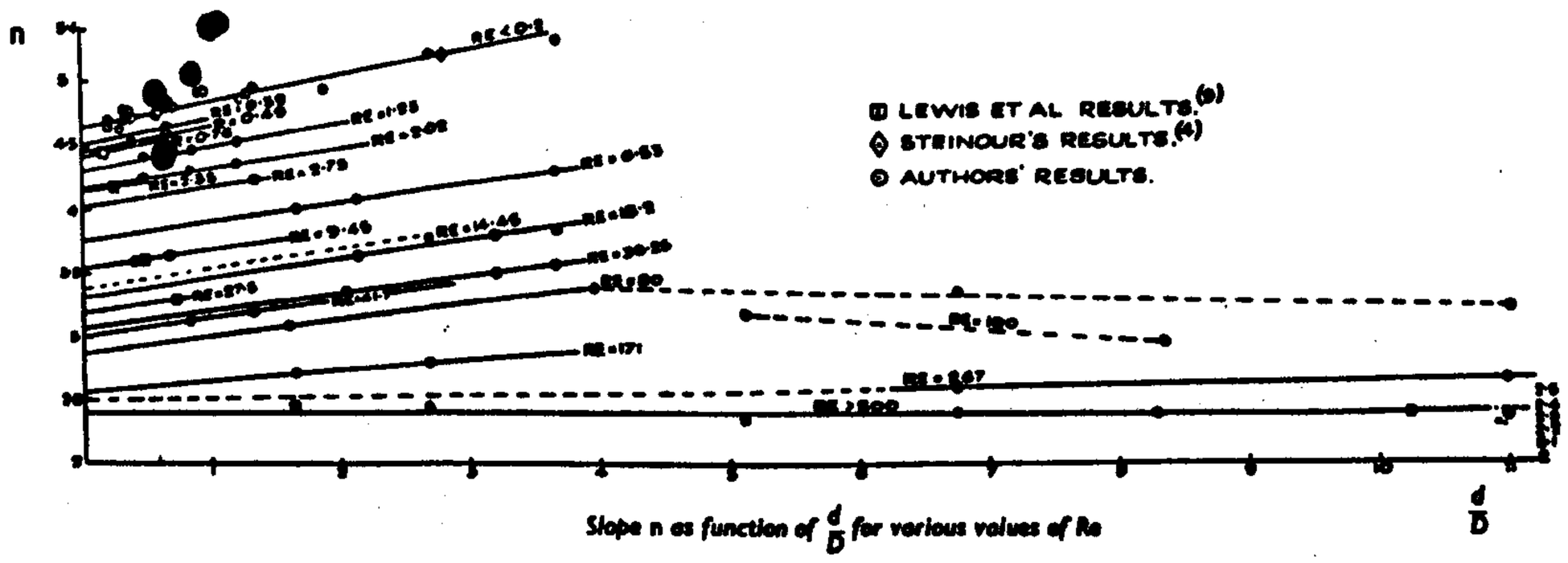

Slope n as function of $\frac{d}{D}$ for various values of Re

Figure (4.8): Slope n as a function of d/D,

figure (2.4) plus experimental data of exsisted study

● Experimental data

4.4 Experimental procedure in sloping tubes

4.4.1 Control of concentration and angle of inclination

The original aim was to undertake sedimentation tests for a particular solids suspension at 5% increments in porosity . This would provide a series of tests at 95%; 90%; 85% etc. down to initial porosity at which a suspension would no longer mix to a uniform distribution in the column. Thus the settled solids from a previous test could be reused. The initial porosity was adjusted by decanting supernatant and adding fresh solids. The initial suspension height was remained at 20 cm which is equivalent to a volume 75.8 cm^3 within the column . Thus a 5% increment in volume of solids represents a removal of 3.79 cm^3 supernatant and a consequent addition of 3.79 cm^3 of solids. 3.79 cm^3 of solids is equivalent to 10.797 g. In practice the weight increment was actually 10.78 g. This gives an error to the highest concentration value, about 1.2% which is acceptable and was not considered to be significant.

For each value of initial concentration, the test was repeated at different angle of inclination measured from the vertical with α in the range 0 - 30° at 5° intervals. The entire procedure was carried out for particles with d = 67 μm and d = 133 μm; the ratio of glycerol solution to water was w/g = 80% and the absolute viscosity of the fluid was 0.48 poise at temperature 21° (see table 4.1)

Data in tables A13 to A17 was analysed to study the effect of solids concentration on initial settling velocity in an inclined tube; Analysis focused on (a) PNK theory (b) modified PNK theory to take account of sediment layer and (c) the Zahavi and Rubin interpretation of PNK theory.

4.4.2 Test of PNK theory and its developments

The data contained in Appendix A, was used to test the PNK equation, which was discussed in section (3.3). The integrated form of PNK equation is,

$$Z - z = \frac{b + Z \sin\alpha}{\sin\alpha} \left[1 - \exp \left(\frac{- V_o\, t}{b} \sin\alpha \right) \right] \quad \ldots\ldots (4.13)$$

The plots shown in Figures (4-10) and (4-11) show that equation (4.13) under-estimates the height variation shown in the data, particularly at longer times.

One feature which was not taken into account in the original PNK theory is the possible influence of the sediment layer, this affecting the magnitude of the term z. This is discussed bellow.

4.4.3 Modifications to PNK theory

From section (3.2) the modified form of PNK equation is (see equation 3.3)

$$\frac{dz}{dt} = V_o \left(1 + \frac{z}{b} \sin\alpha \right) \qquad \ldots\ldots (4.14)$$

When the sediment layer builds up with time the interface length of the clear fluid channel is scaled by the term.

$$z_1 = z - z_m \, . \qquad \ldots\ldots (4.15)$$

This can be substituted into the right hand side of equation (4.14). Two possibilities exist to define the left hand side. The first case (case I) is that this term remains unaltered dz/dt simply models of interface.

The second case (case II) is that dz/dt term models interface length

$$\frac{dz_1}{dt} = \frac{dz}{dt} - \frac{dz_m}{dt} \qquad \ldots\ldots (4.16)$$

Since dz/dt and dz_m/dt are in opposite directions, this is equivalent to

$$\left| \frac{dz_1}{dt} \right| = \left| \frac{dz}{dt} \right| + \left| \frac{dz_m}{dt} \right| \qquad \ldots\ldots (4.17)$$

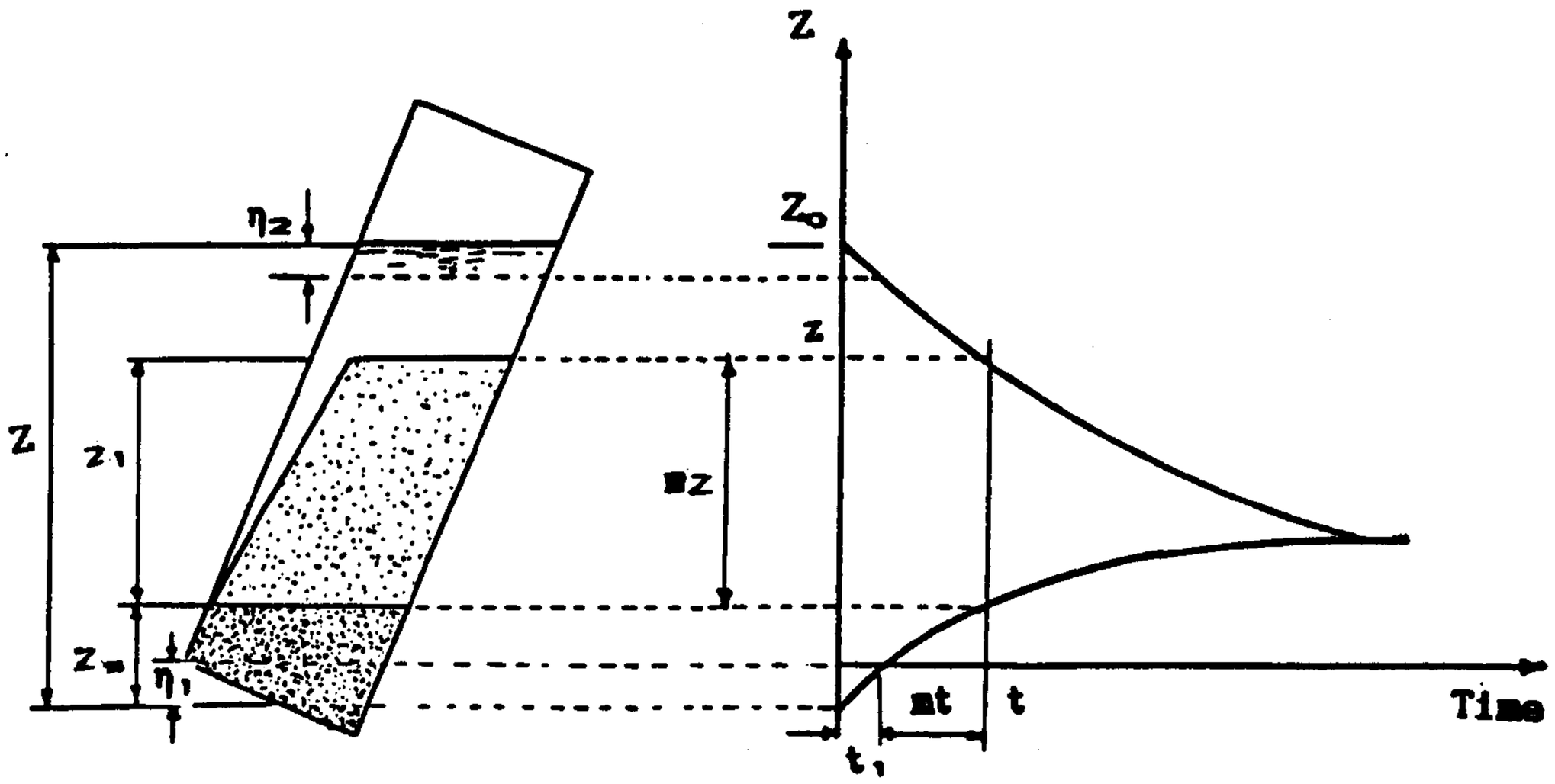

Figure (4.9): settling curve in an inclined tube

Applying conservation of mass in settling column gives,

$$(z - z_m)C_o + z_m C_m = Z C_o \qquad \ldots\ldots (4.18)$$

where z, z_m and Z are defined as shown in figure (4.9) C_o the initial solids concentration in the suspension and C_m the concentration of the sediment layer at the bottom of the settling column.

$$z_m = (Z-z)\ C_o\ /\ (C_m - C_o) \qquad \ldots\ldots (4.19)$$

$$z_1 = z - z_m \qquad \ldots\ldots (4.20)$$

$$z_1 = z - (Z-z)\ C_o\ /\ (C_m - C_o) \qquad \ldots\ldots (4.21)$$

Defining the factor $\beta = C_o\ /\ (C_m - C_o)$ $\ldots\ldots (4.22)$

equation (4.9) becomes,

$$z_1 = z\ (1+\beta) - \beta Z \qquad \ldots\ldots (4.23)$$

Replacing z by z_1 to the right hand side of equation (4.14) and assuming that the left hand side is unaltered (case I) leads to

$$\frac{dz}{dt} = V_o \left(\xi + \frac{(1+\beta)z}{b} \sin\alpha \right) \qquad \ldots\ (4.24)$$

where $$\xi = 1 - \beta Z \sin\alpha / b \qquad \ldots\ (4.25)$$

$$\int_Z^z \frac{dz}{\xi + (1+\beta)\sin\alpha\, z / b} = - V_o \int_0^t dt \qquad \ldots\ (4.26)$$

Taking $\lambda = \xi + (1+\beta)\sin\alpha\, z / b$ equation (4.26) becomes

$$\frac{b}{(1+\beta)\sin\alpha} \int_{\lambda_1}^{\lambda_2} \frac{d\lambda}{\lambda} = - V_o \int_0^t dt \qquad \ldots\ (4.27)$$

where $$\lambda_1 = \xi + (1+\beta)\sin\alpha\, Z/b \qquad \ldots\ (4.28)$$

and $$\lambda_2 = \xi + (1+\beta)\sin\alpha\, z/b \qquad \ldots\ (4.29)$$

Integrating equation (4.27) and compensating λ_1 , λ_2 and ξ by their values from (4.28), (4.29) and (4.25) gives the modified PNK equation as

$$\boxed{Z - z = \frac{b + Z \sin\alpha}{(1+\beta)\sin\alpha} \left[1 - \exp\left(\frac{-V_o\, t}{b} \sin\alpha\, (1+\beta) \right) \right]} \qquad \ldots(4.30)$$

Experiments described in section (4.4) and the data in tables A13 to A17 in appendix A were used as settling tests in inclined tube. Figures (4.11) and (4.12) show a comparison between the experimental settling curves, the theoretical curves deduced from the origin PNK equation (4.13) and the modified equation (4.30).

V_o in equations (4.13) and (4.30) was taken directly from experiment

on the same suspension settling in a vertical position

To calculate $1+\beta = \frac{C_m}{C_m - C_o}$, C_m was taken equals to 0.55 which is less than the maximum concentration for glass beads in vertical settling (this is discussed later in section 5.3.4.3).

Inspection of figures (4.10) and (4.11) shows that equation (4.30) represents an improvement on the PNK prediction .

4.4.4 Implication of sediment height on dz/dt term (case II)

For the case when dz_1/dt follows the equation (4.17) it can be deduced that

$$dz_1/dt = (1+\beta)\, dz/dt \qquad \ldots.(4.31)$$

Equation (4.24) becomes

$$(1+\beta)\ \frac{dz}{dt} = V_o \left(\xi + \frac{(1+\beta)z}{b} \sin\alpha \right) \qquad \ldots. (4.32)$$

Integrating equation (4.32) leads to the modified PNK equation in this case to be of the form .

$$\boxed{Z - z = \frac{b + Z \sin\alpha}{(1+\beta)\sin\alpha}\left[1 - \exp\left(\frac{-V_o\, t}{b}\sin\alpha\right)\right]} \quad \ldots\ldots (4.33)$$

when this was tested it was found that the theoretical prediction was above the experimental points. Thus it is deduced that dz/dt on left hand side of equation (4.14) models the interface speed rather than the clear fluid channel length.

4.4.5 Effect of the shape of tube bottom

In the derivation of equation (4.15) the influence of storage in the dip was ignored. If we consider its potential influence, the time t_1 needed to fill the dip must be taken into account. t_1 can be deduced from equation (4.13) as

$$t_1 = \frac{-b}{V_o \sin\alpha} \ln\left[1 - \frac{\eta_1 \sin\alpha}{b + Z_2 \sin\alpha}\right] \quad \ldots\ldots (4.34)$$

where $\eta_1 = b \tan\alpha/2$

and $Z_2 = Z - \eta_1$

To compare experimental data with the theory, the co-ordinate (z, t) in the equation (4.30) to be shifted by the t_1 and $\eta_1 + \eta_2$. The new co-ordinate s become.

$\eta_2 = 1/2\ b \sin\alpha\ C_m/C_o$

$mt = t - t_1$, t_1 is given by equation (4.34)

and $\quad mZ = Z - \eta_1 - \eta_2 \qquad \ldots\ldots (4.35)$

Figure (4.10)

$C_0 = 0.2$

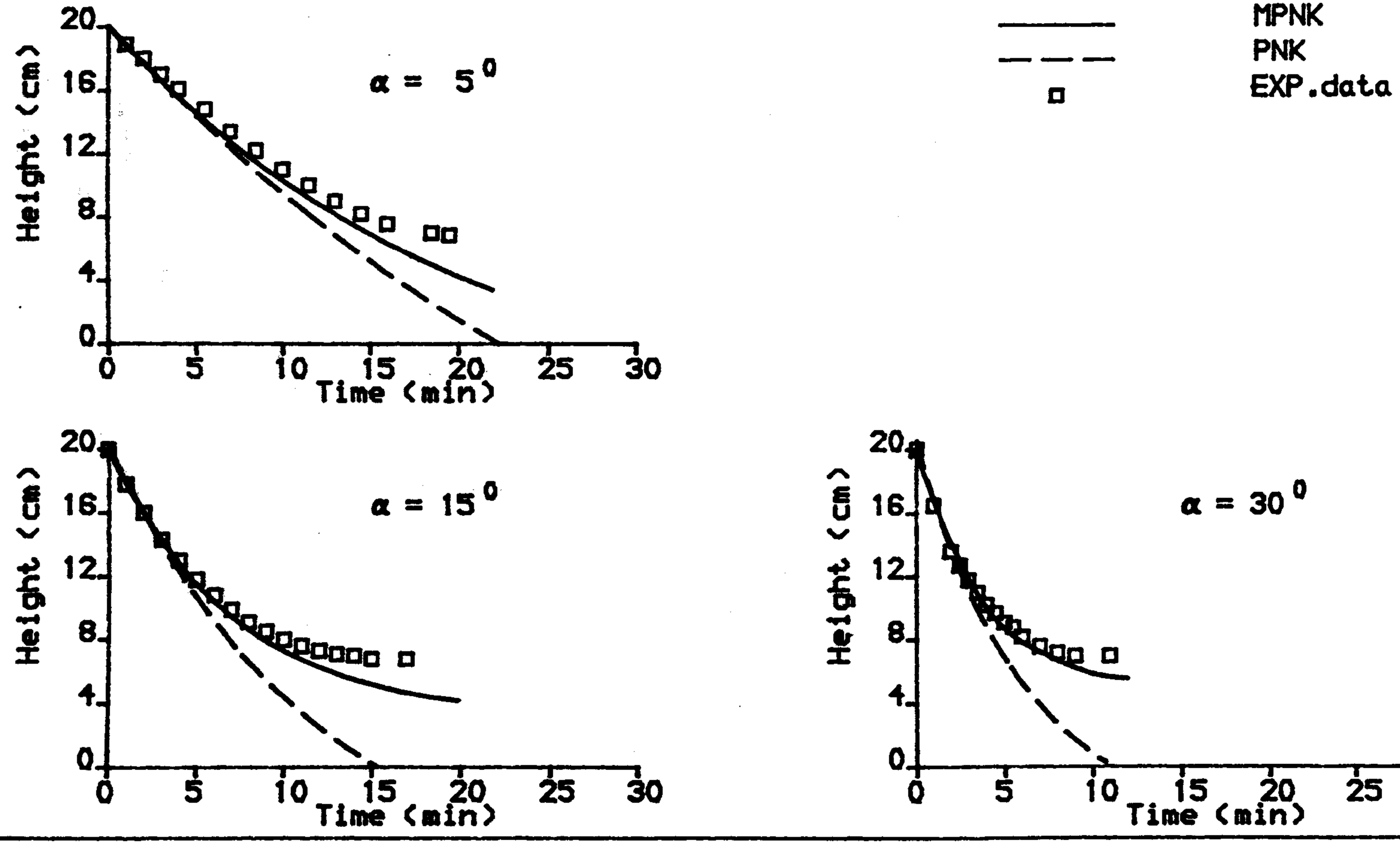

Comparison between PNK theory modified, Originl and experimental data

Figure (4.11) $\alpha = 30^0$

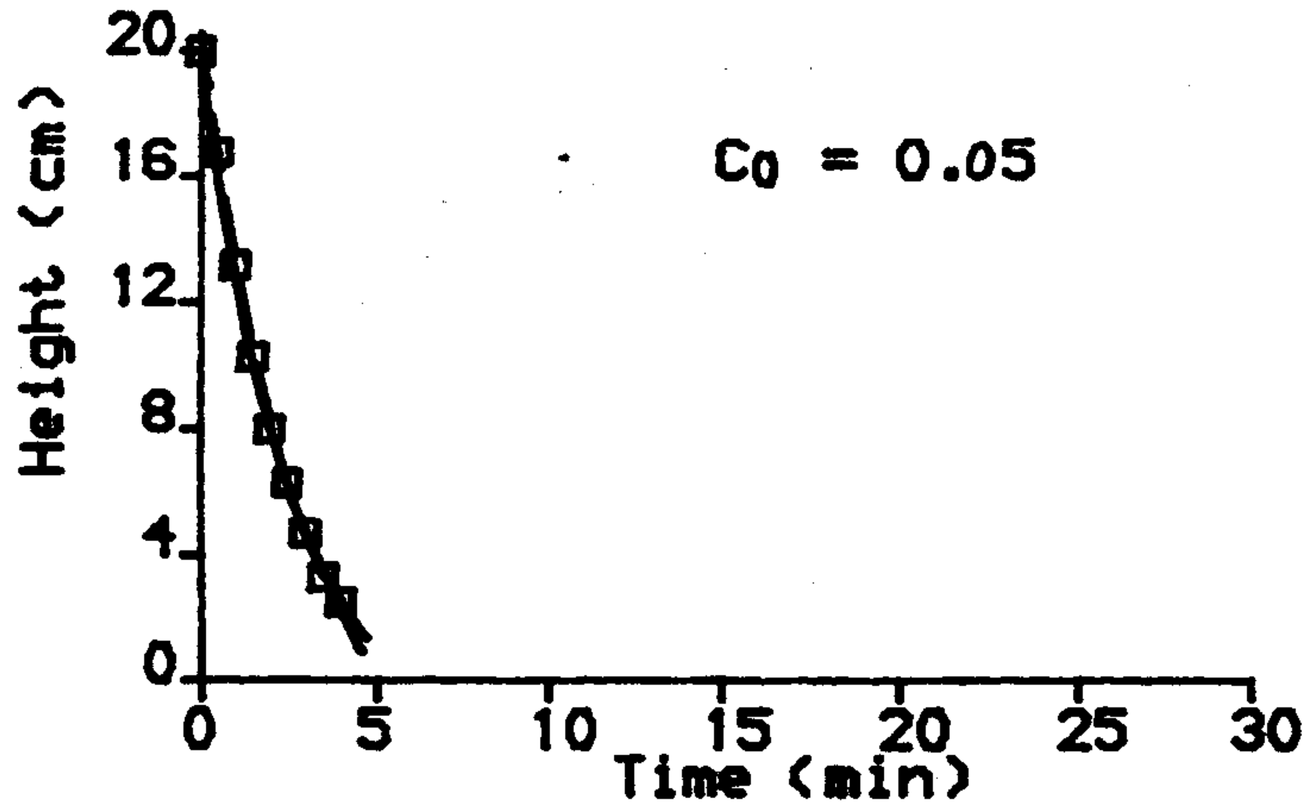

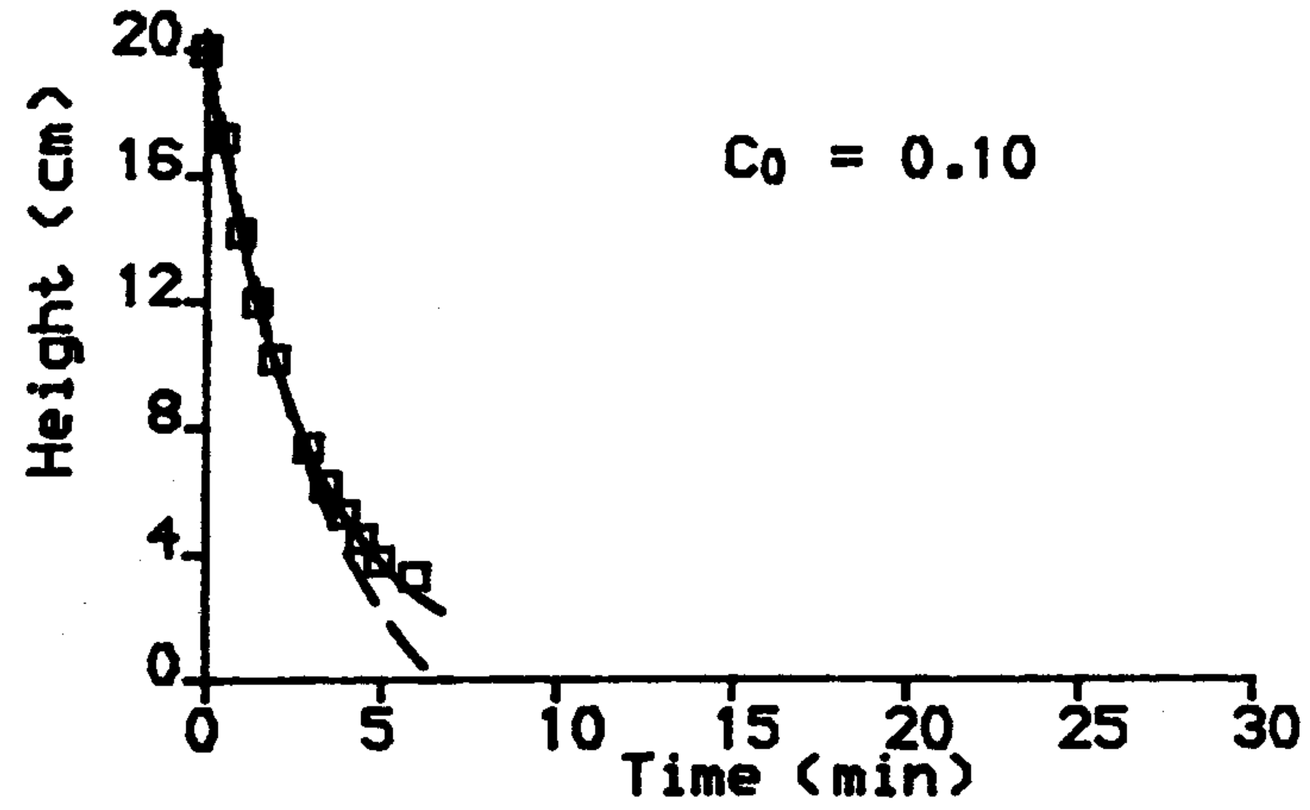

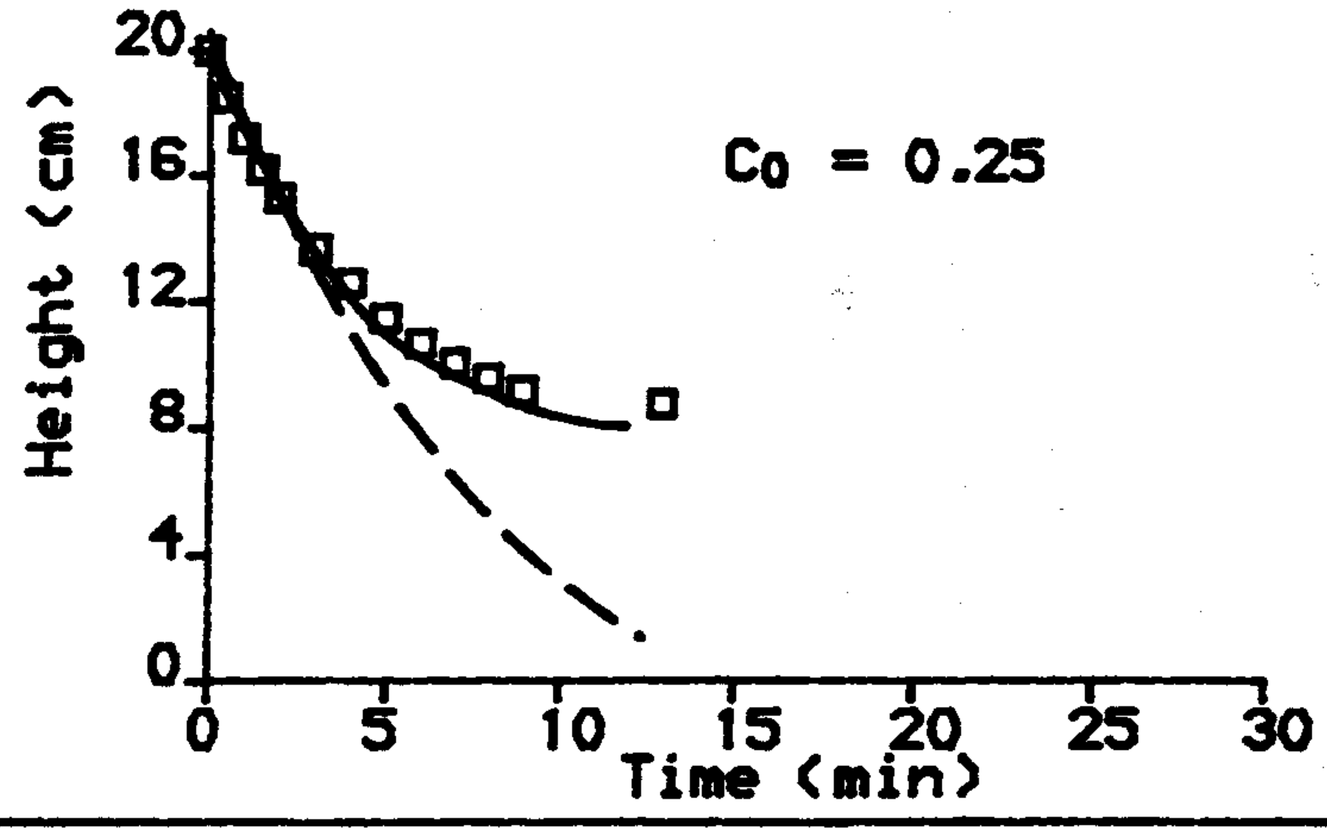

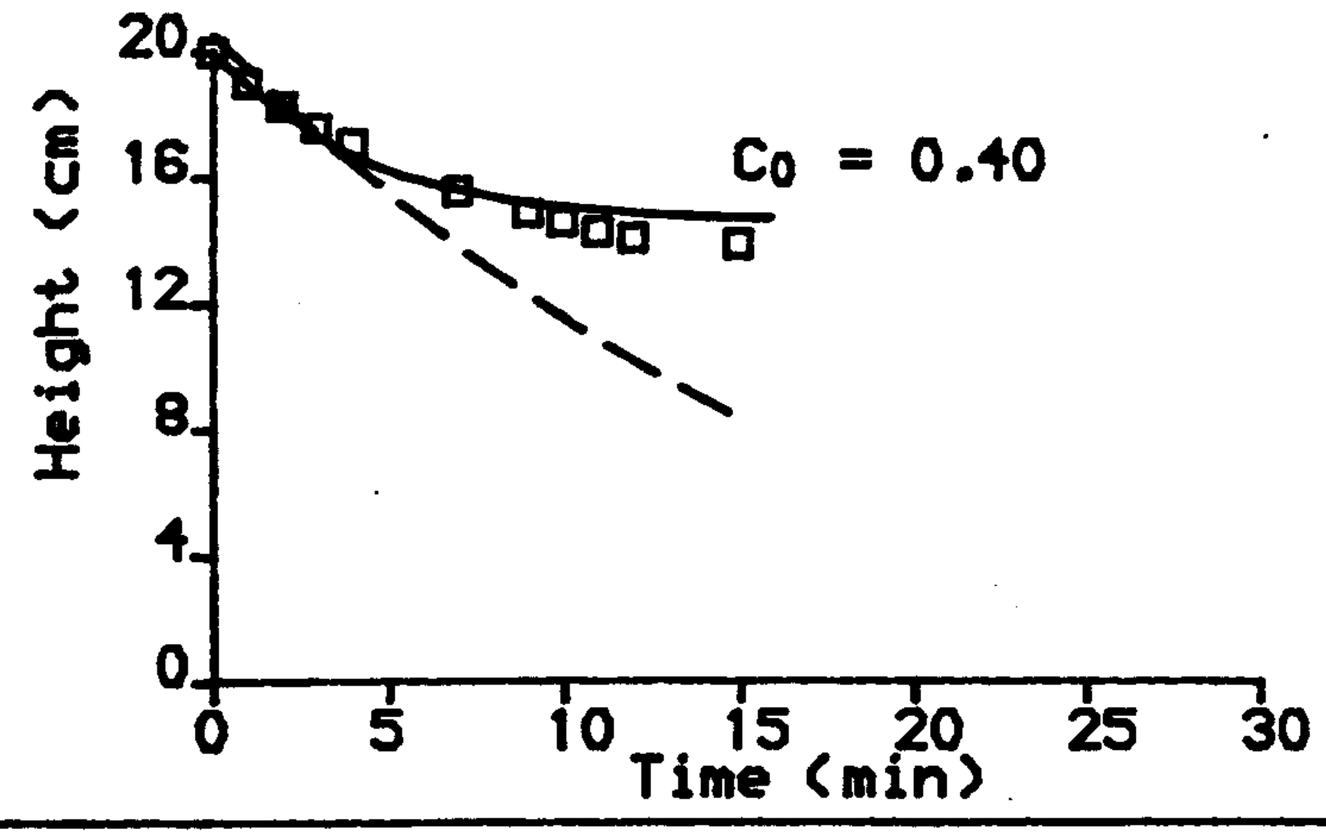

Comparison between PNK theory modified, Originl and experimental data

4.4.6 Test of Zahavi and Rubin.

In section (3.2) Zahavi and Rubin (1975) considered that the settling velocity of top interface in an inclined tube follows equation (3.6)

$$V_{in} = V_v + V_p \qquad \ldots.(4.36)$$

where V_{in} is the total settling velocity for angle of inclination α V_v is the settling velocity of the same suspension in a vertical tube ($\alpha = 0$) V_p is the contribution of the inclined interface to the settling process, They assumed that V_p in the initial position is independent of initial solids concentration. To check the above assumption, the experimental data of section (4.4.1) and data in tables A13 to A17 were used for the value d = 133 μm. Data are summarized in tables (4.4) and (4.5). Figures (4.12-a) and (4.13-a) show plots of

$$V_p = V_{in} - V_v.$$

These show that V_p depends strongly on C_o. The dependence of V_p on C_o increases as the inclination increases. However V_p/V_v shown in figures (4.12-b) and (4.13-b) is essentially independent of C_o for the range considered.

table (4.4) Initial settling velocity V_{in}
d = 67 μm

C_o	α= 0°	α= 5°	α=10°	α=15°	α=20°	α=30°
5	0.38	0.60	0.83	0.98	1.22	1.49
10	0.31	0.45	0.60	0.82	0.94	1.30
15	0.25	0.34	0.52	0.68	0.84	1.04
20	0.18	0.29	0.40	0.48	0.66	0.76
25	0.12	0.18	0.30	0.39	0.40	0.49
30	0.10	0.14	0.19	0.23	0.28	0.35
35	0.07	0.11	****	0.20	****	0.28

table (4.5) Initial settling velocity V_{in}
d = 133 μm

C_o	α= 0°	α= 5°	α=10°	α=15°	α=20°	α=30°
5	1.38	2.06	3.05	4.06	4.80	6.28
10	1.10	1.59	2.22	3.48	3.95	5.33
15	0.85	1.26	1.84	2.61	3.05	4.02
20	0.64	1.00	1.48	2.08	2.44	3.03
25	0.44	0.75	1.05	1.59	1.88	2.42
30	0.30	0.50	0.84	0.97	1.17	1.40
35	0.22	0.35	0.44	0.60	0.86	1.08
40	0.15	0.30	0.34	0.39	0.58	0.74

Figure (4.12)

d = 0.0067 cm

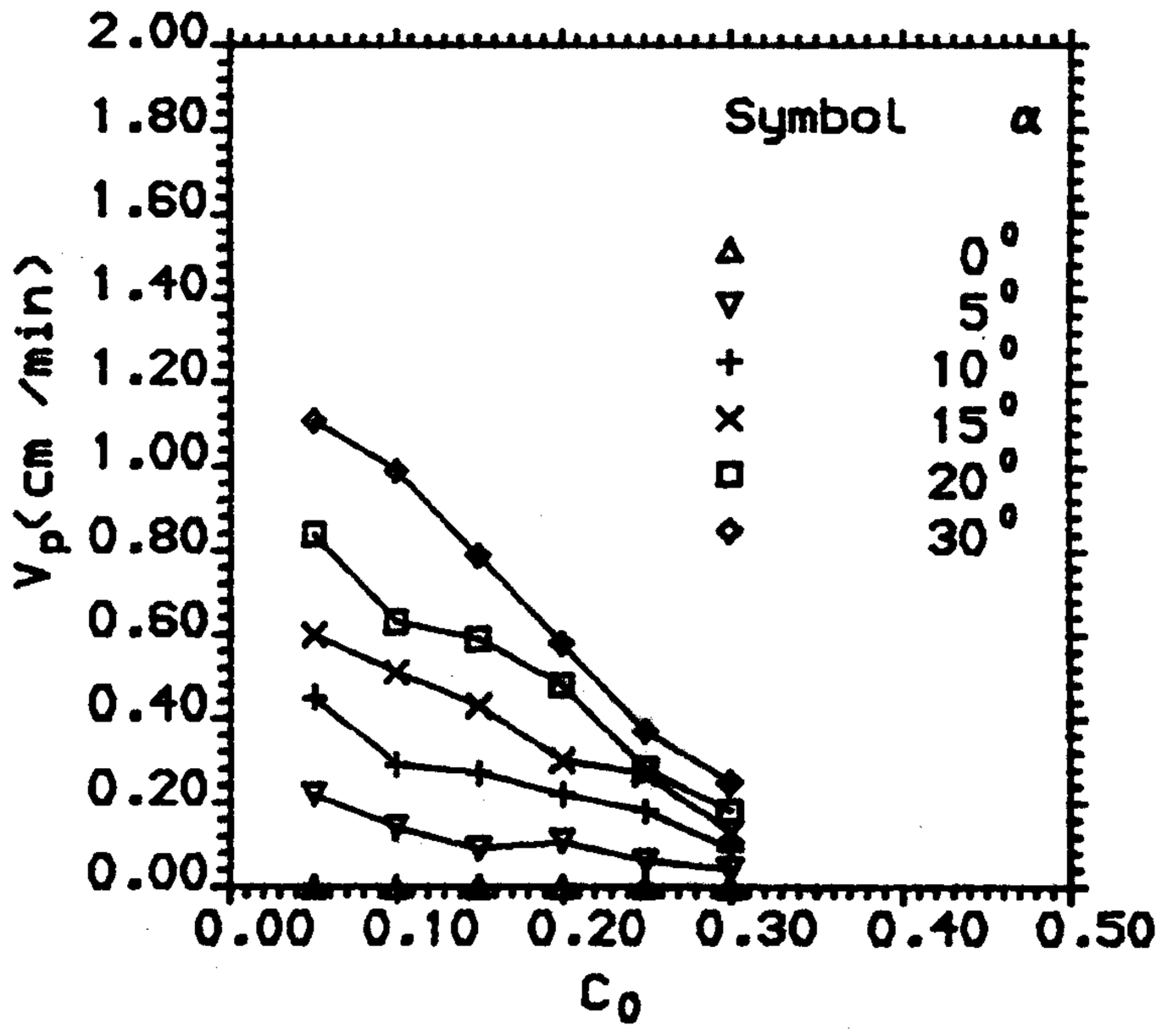

a - Effect of concentration on V_p

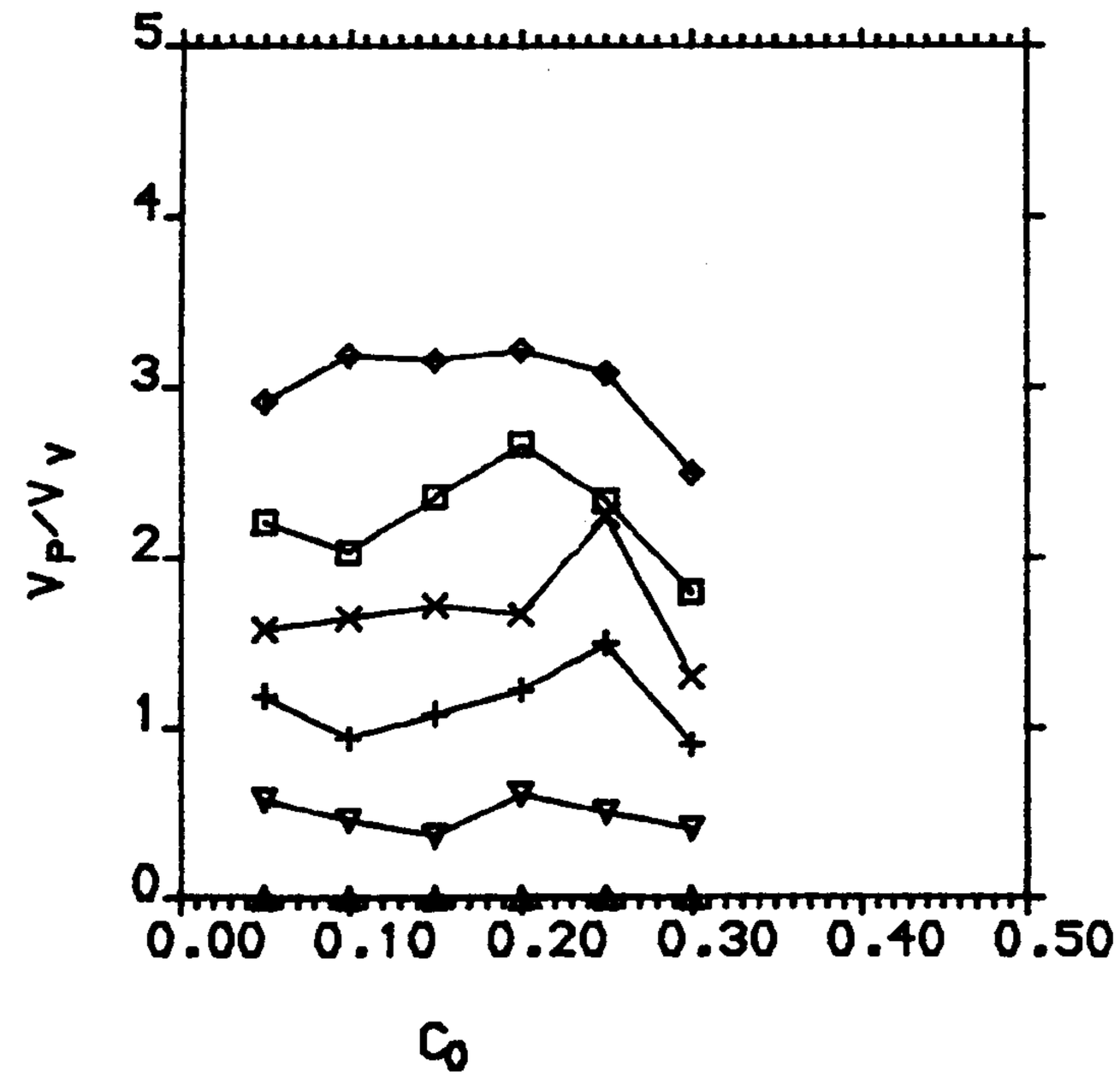

b - Effect of concentration on V_P/V_V

Figure (4.13)

d = 0.0133 cm

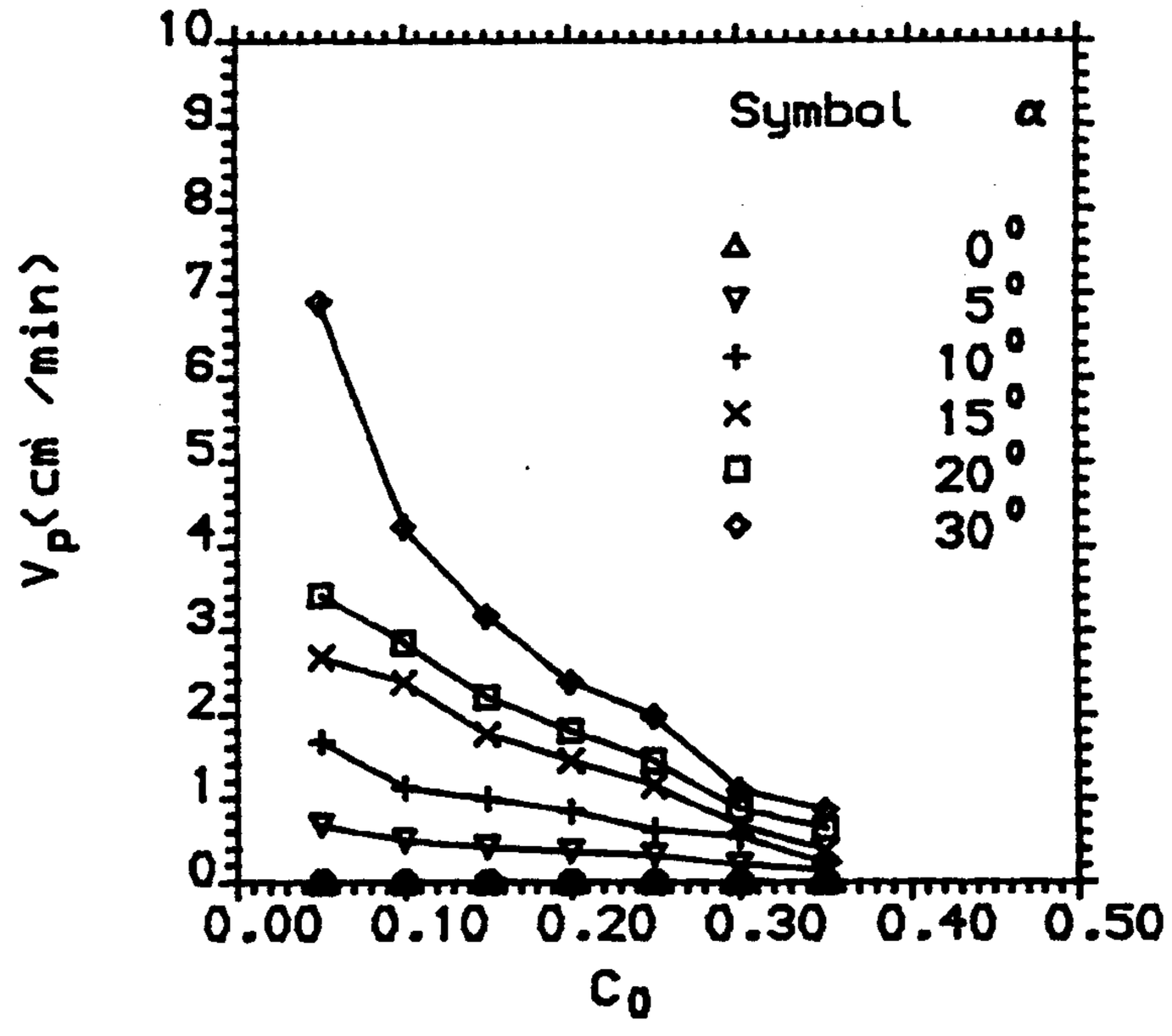

a - Effect of concentration on V_p

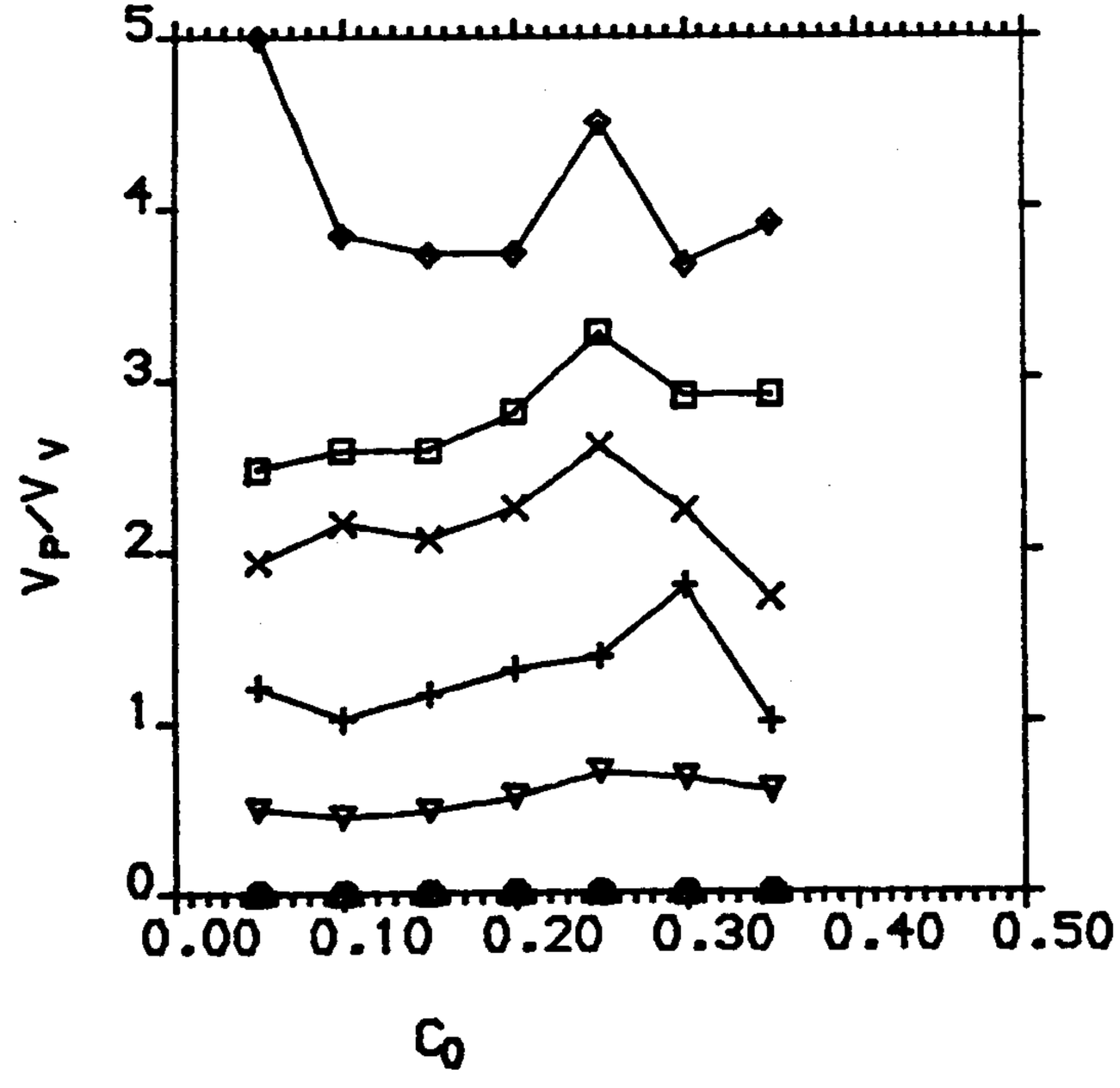

b - Effect of concentration on V_p/V_v

CHAPTER FIVE

CHARACTERISTICS OF THE CLEAR FLUID LAYER

CHAPTER FIVE

CHARACTERISTICS OF THE CLEAR FLUID LAYER

5.1 Introduction

In this chapter the characteristics of the clear fluid layer were studied experimentally. The experimental results are compared with a theory was predicted by Acrivos et al (1979) and a clearer idea is deduced about the flow within the clear fluid layer and about the concentration distribution along the settling column in both cases of vertical and inclined settling.

Sections (5.2) and (5.3) contain a description of the experimental set-up and the methods used to measure the dimensions of the clear fluid layer, the velocity of the flow within this layer and the concentration distribution within the settling column.

In section (5.4) the measured data is compared with the theory by Acrivos et al (1979). Tests were carried out for two values of initial concentration, $C_o = 0.2$ and $C_o = 0.1$.

In section (5.5) an analysis focusses on the contribution of flow through the inclined interface to the overall settling process.

5.2 Experimental set-up

For this sequence of experiments the apparatus, suspension and suspending fluid are as described in section (4.2)

5.2.1 Audio visual equipment

The audio visual equipment consisted of a colour video camera, a video recorder and a 14" portable colour monitor. The colour video-camera had the advantage of recording the time with an accuracy of 0.01 second. By attaching a lens unit to the camera a magnification of 15 times could be achieved. This magnification allows the observation of the movement of particles of diameter as small as 0.133 mm and to measure the dimension of clear fluid channel ( ) 0.1 mm).

5.2.2 Measurements of suspension concentration

The experimental equipment for measuring solids concentration based on the electrical conductivity of the suspension is shown schematically in figure (5.1). It consists of:

- a digital universal resistance bridge excited by a 1000 Hz A.C. signals was used to measure the resistance a across a pair of electrodes.
- a sedimentation column forms one arm of the universal bridge in a

settling tube of approximately the same dimensions of the tube No.2 described in section (4.2.3). The tube has a cross sectional area of 3.84 cm^2. A scaled tape was fixed to one face of the tube. In the wall of the sedimentation volume resistace pins were set at 2cm intervals starting from 1.5 cm height until 19.5 cm on opposite face of the tube. The resistance pins were made of platinum wire of diameter 0.87 mm and long enough to fix into the tube wall, project 3 mm into the tube and hold the electrodes from the switching unit

- switching unit has the capacity to join 10 pairs of electrode .

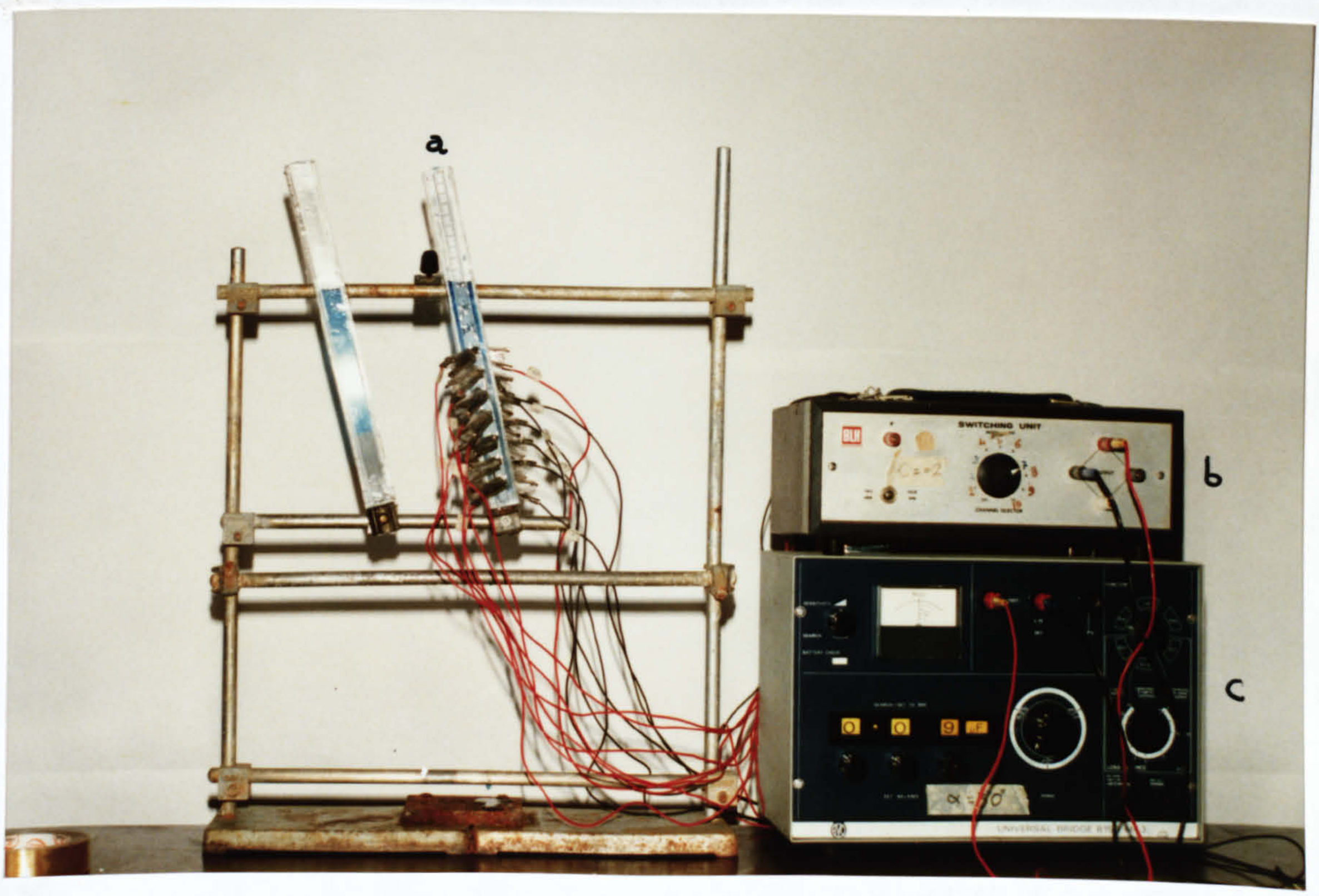

Figure (5.1): Electro-conductivity Equipment

a- settling tube with the resistance pins b-switching unit and

c-universal bridge

The principle of the measurements is that, the settling column forms an arm in a bridge circuit as shown in figure (5-1'), in order to measure the electrical resistance of the suspension at specific height.

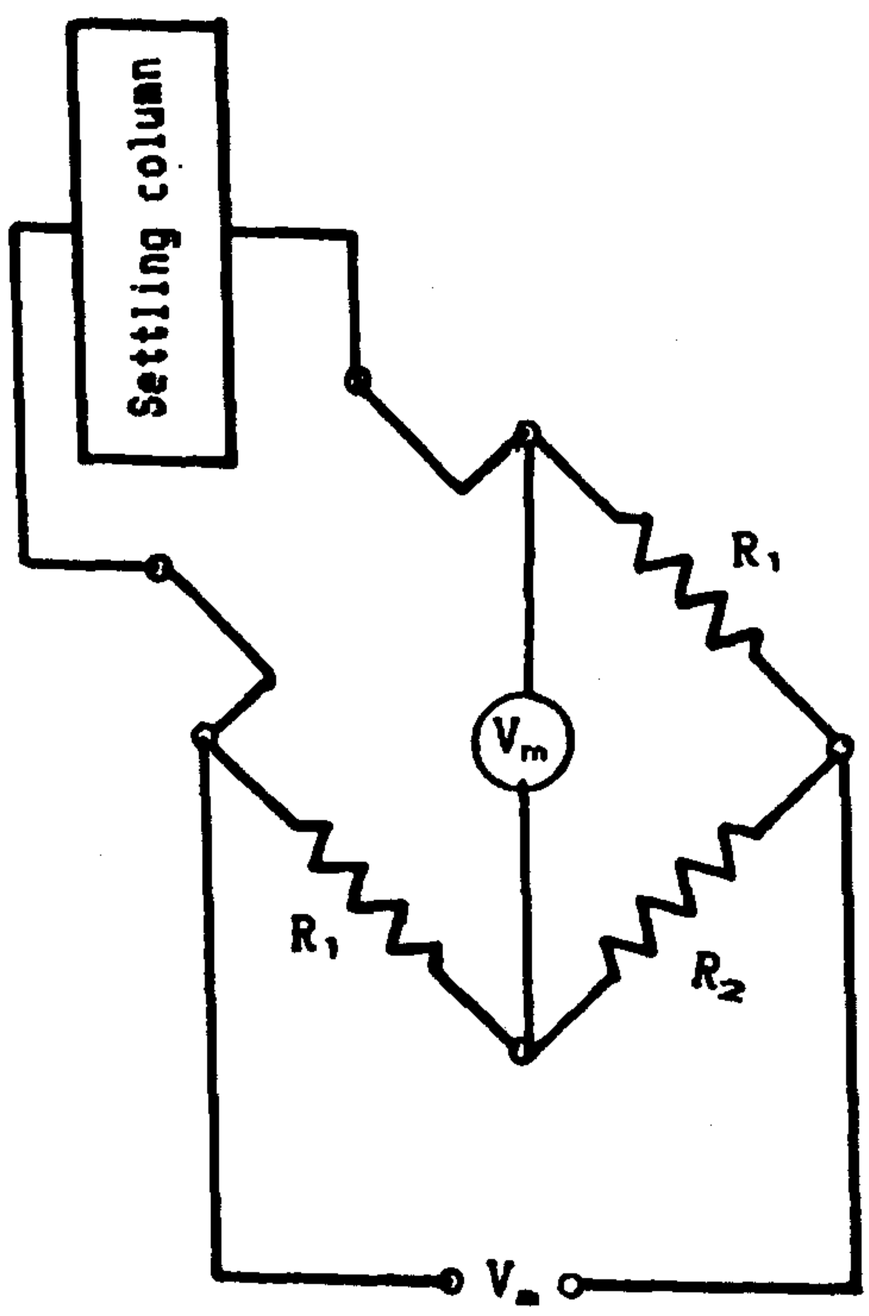

Figure (5.1') Sedimentation column as an arm of a bridge circuit

Measurements required bringing the bridge into balance and to scan all pairs of resistance pins as quickly as possible. To facilitate this process and to avoid the necessity of writing down results the audio visual equipment was used to record all the essential data during the manipulation of the instrumentation while the experiment was in progress.

5.3 Experimental procedure

5.3.1 upward velocity of the clear-fluid layer

This part of experimental program was designed to measure the velocity of the clear fluid layer with a view to calculating the overall flow. The velocity was assessed by monitoring the progress of particles and by dye injection.

5.3.1.1 Observation of particles

As noted in section (3.1) the settling column can be divided into four region as described in figure (5.2)

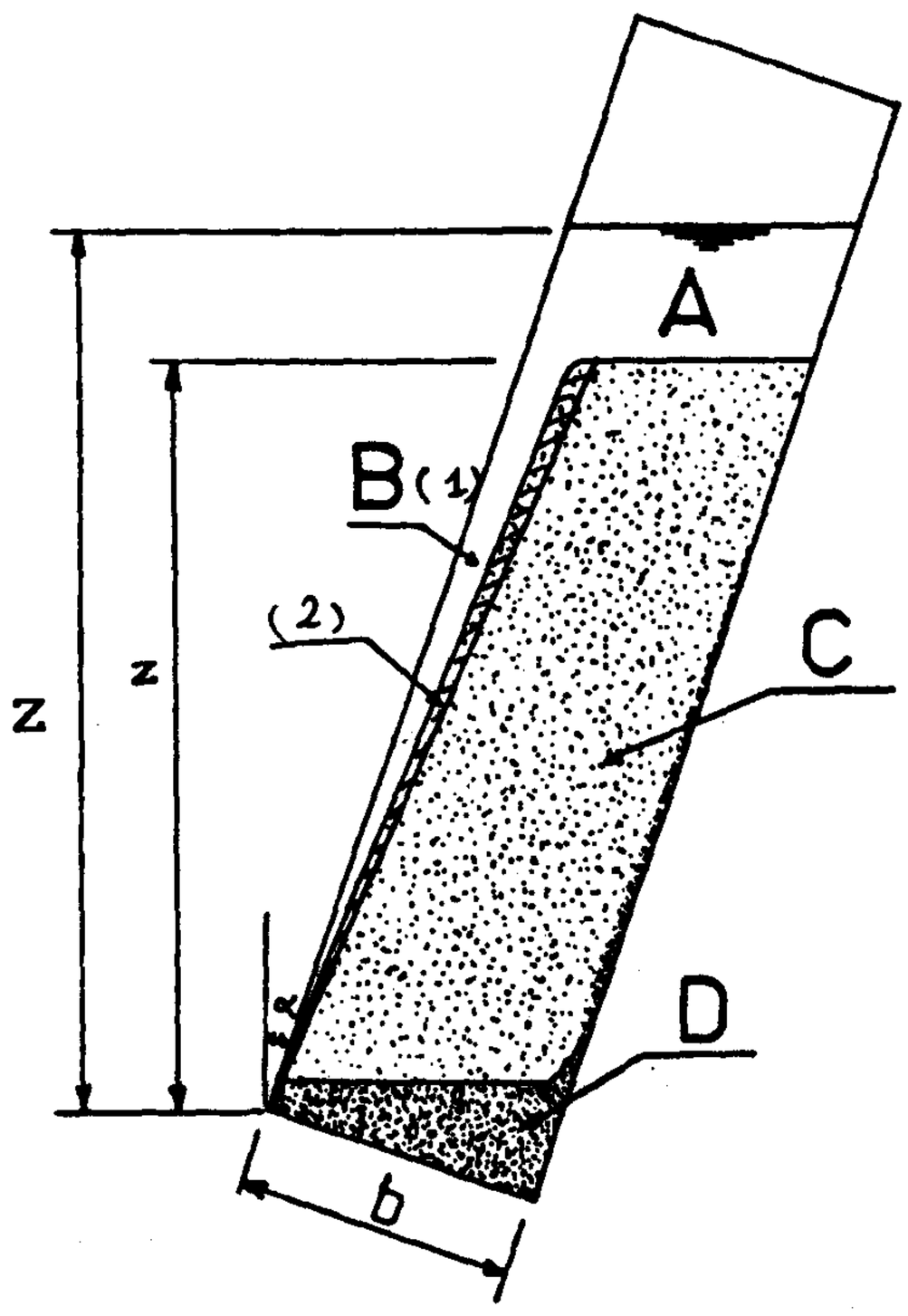

Figur 5.2: Settling column

Of direct concern are: region (1), the clear fluid moving upward by the action of the buoyancy force and region (2), the thin layer of suspension which is driven upward by the friction forces exerted by the clear fluid layer moving upward.

It can be assumed that V_p, the velocity of particles on the interface

between region (1) and region (2) is closely linked to V_r the mean velocity within region (1) and can be represented by a relationship of the form:

$$V_p = V_r . f \qquad \ldots\ldots (5.1)$$

where f is defined by the ratio V_p/V_r.

By measuring the upward velocity of particles within or in contact with region (1), the magnitude of the upward velocity of the clear fluid layer can be, deduced provided f is known.
In these experiments beads with d ≈ 133 μm were used, C_o was 0.2 and 0.1, the initial suspension height (inclined) H_o = 20 cm, the viscosity μ = 0.48 poise and the angle of inclination α = 30°.

The suspension was prepared in the way described in section (4.2.5). The video camera was focussed on the lowest part of the settling column and adjusted to view (on the monitor screen) as large a number as possible of the particles which are moving along the inclined interface (see figure 5.3). This procedure was repeated at 1 cm intervals until the top of the settling column. Measurements were recorded on the video tape.

To reduce the experimental errors a large number of observations were carried out at 1 cm interval over the height of the settling column.

Tables (A18-A32) in appendix A summarises velocity-time data for H = 1 cm to 17 cm for C=0.2 and, tables (A33 to A49) in appendix A shows the corresponding data for C = 0.1.

Figure (5.4) shows examples of the change of upward velocity with time at H = 1, 5, 14 and 17 cm. The approximate trend of the relationship V-T was drawn by eye and as close as possible to the line fitted by least squares fit of polimaral equation of degree five.

Figure (5.5) illustrates the comparison between the trends of the velocity-time relationships at the heights 1, 4, 7, 9, 11 and 15 cm

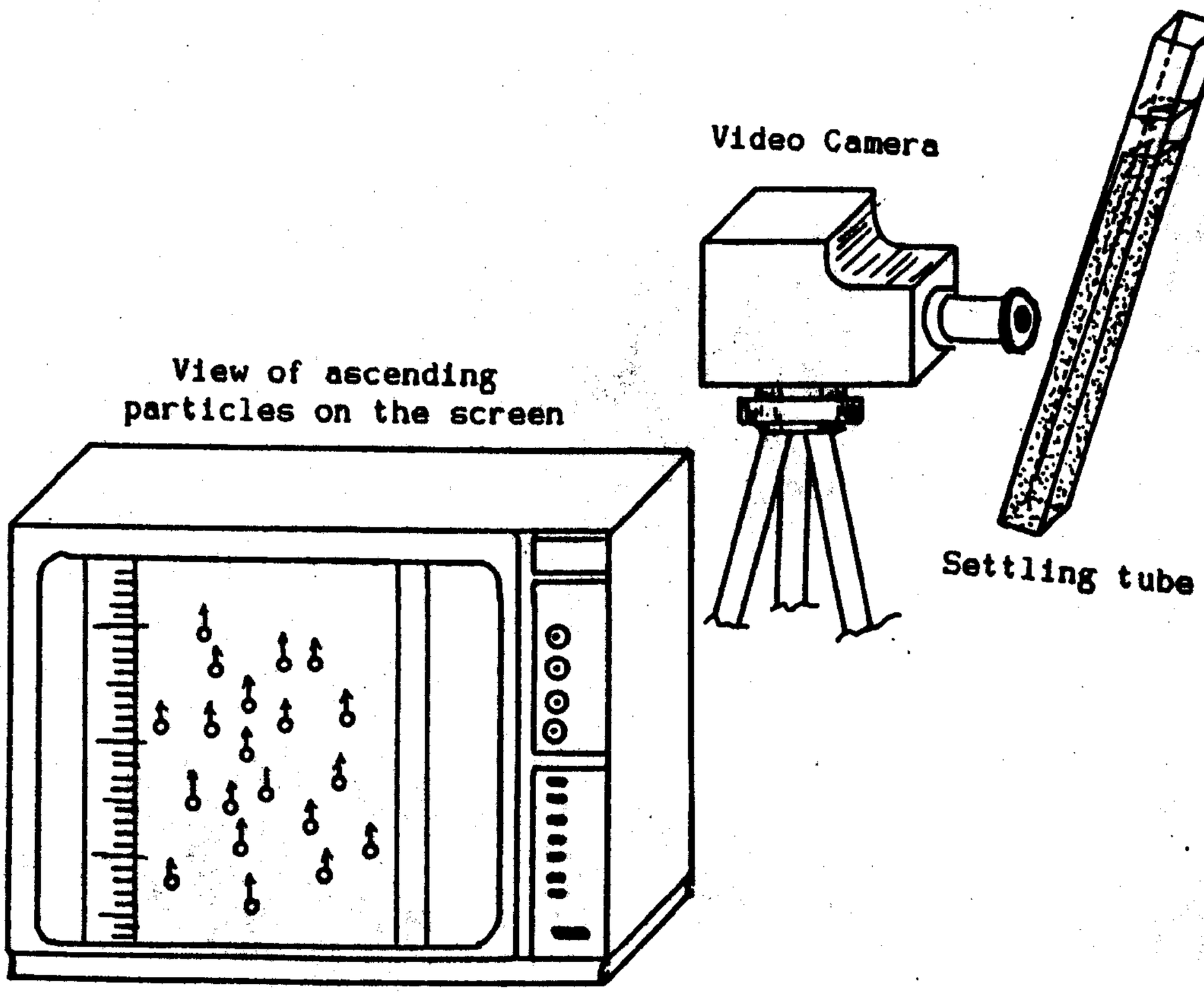

Figure 5.3 the settling tube in recording position

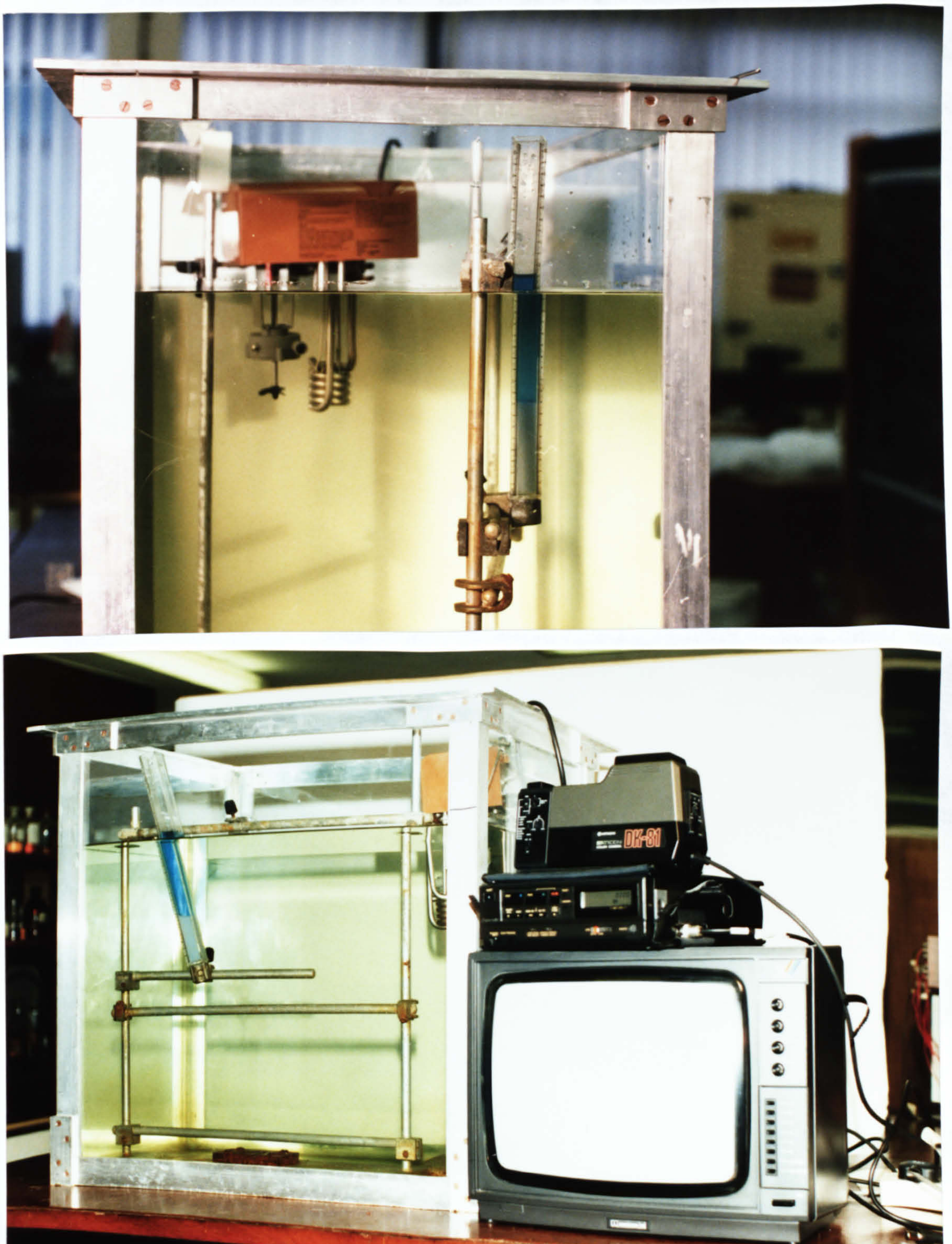

Figure (5.3'): Settling tube and the audio visual equipment

Figure (5.4)

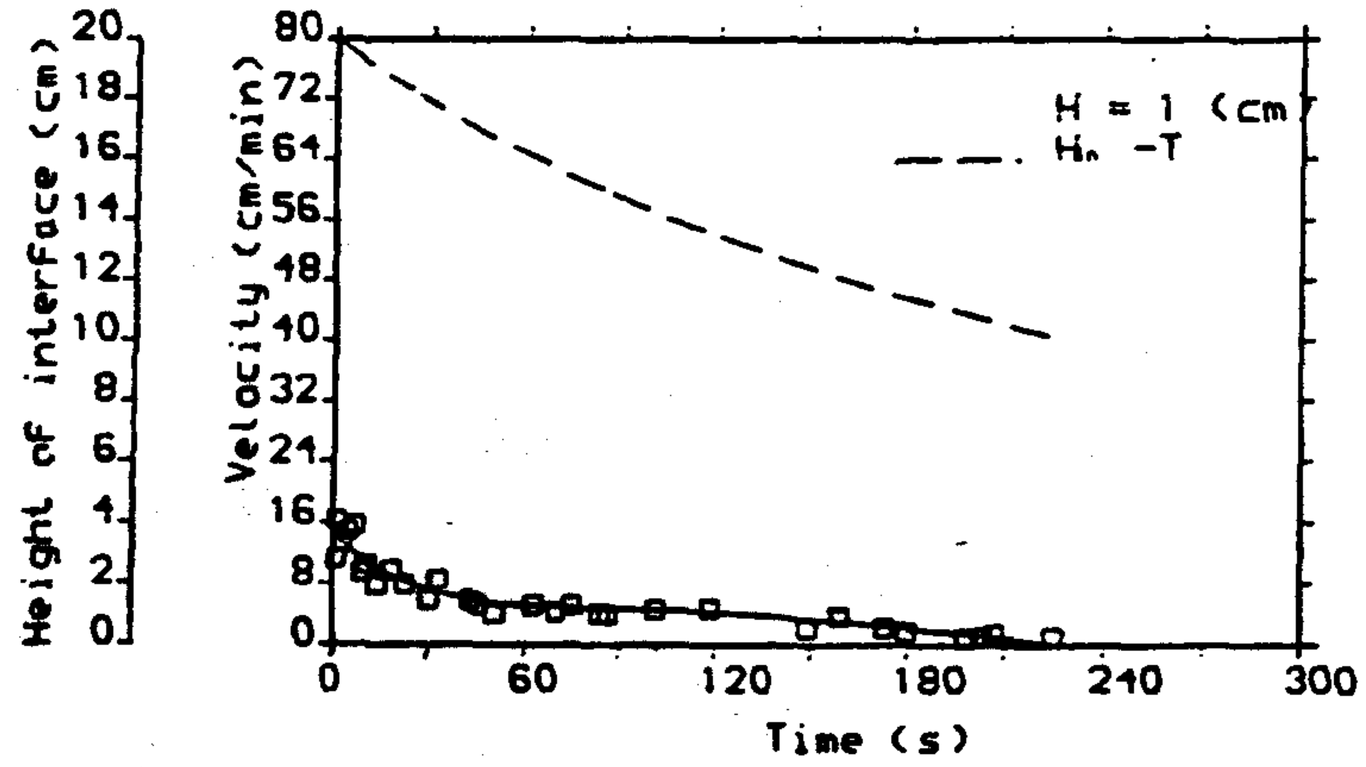

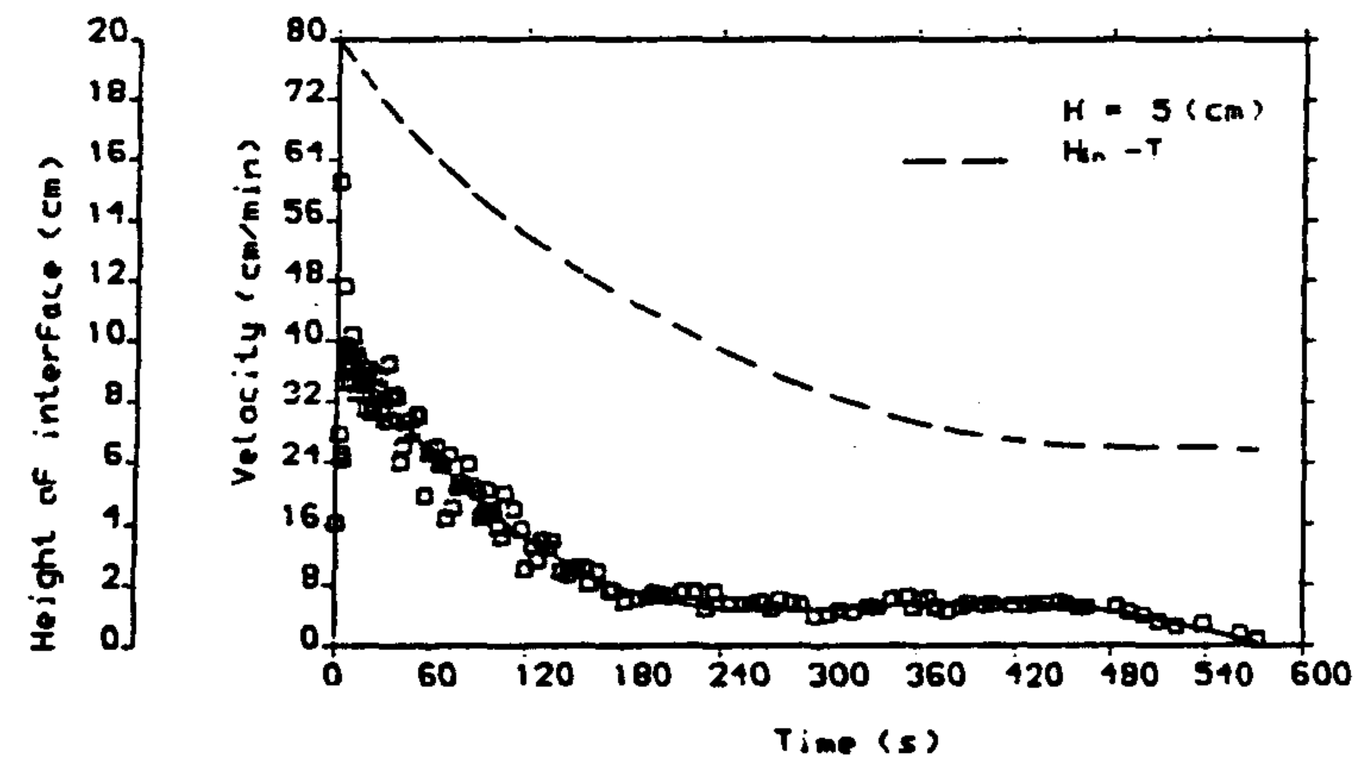

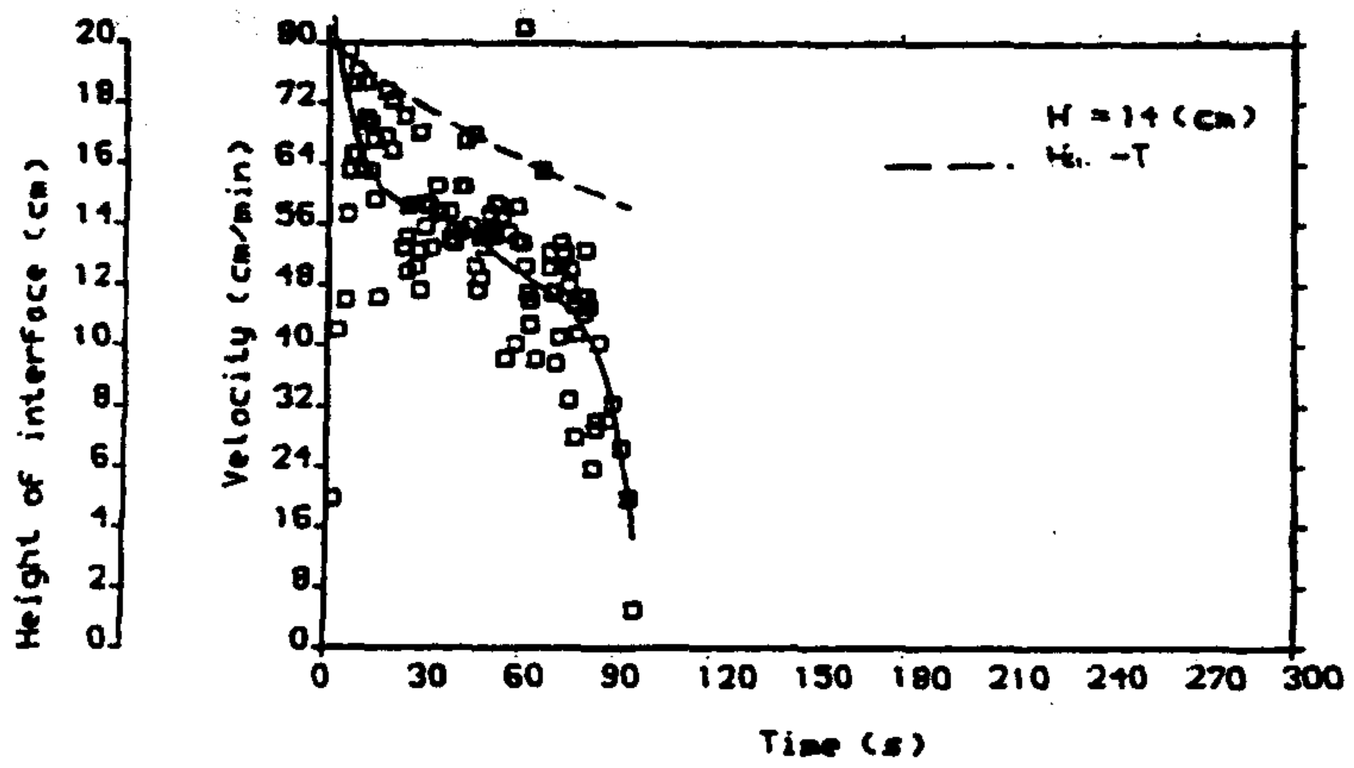

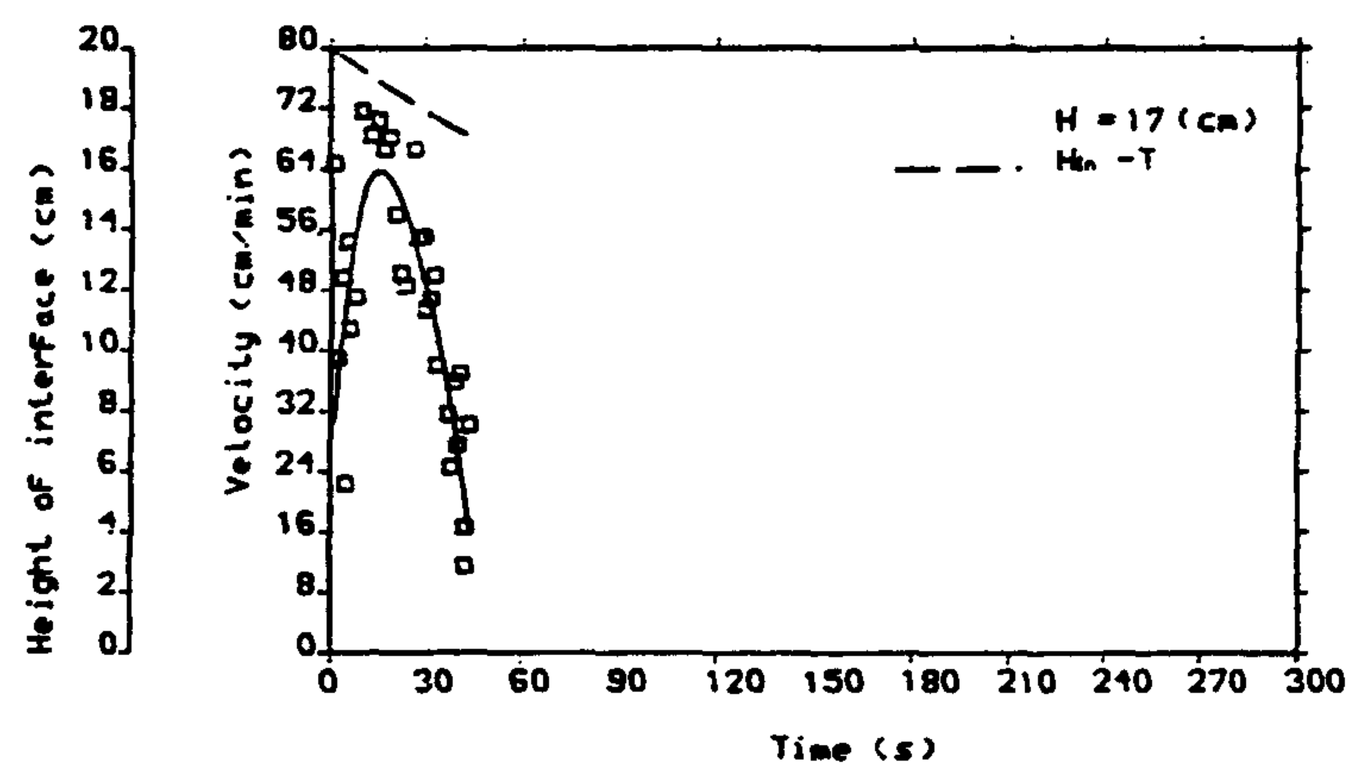

Upward velocity of particles within clear fluid layer

Figure (5.5)

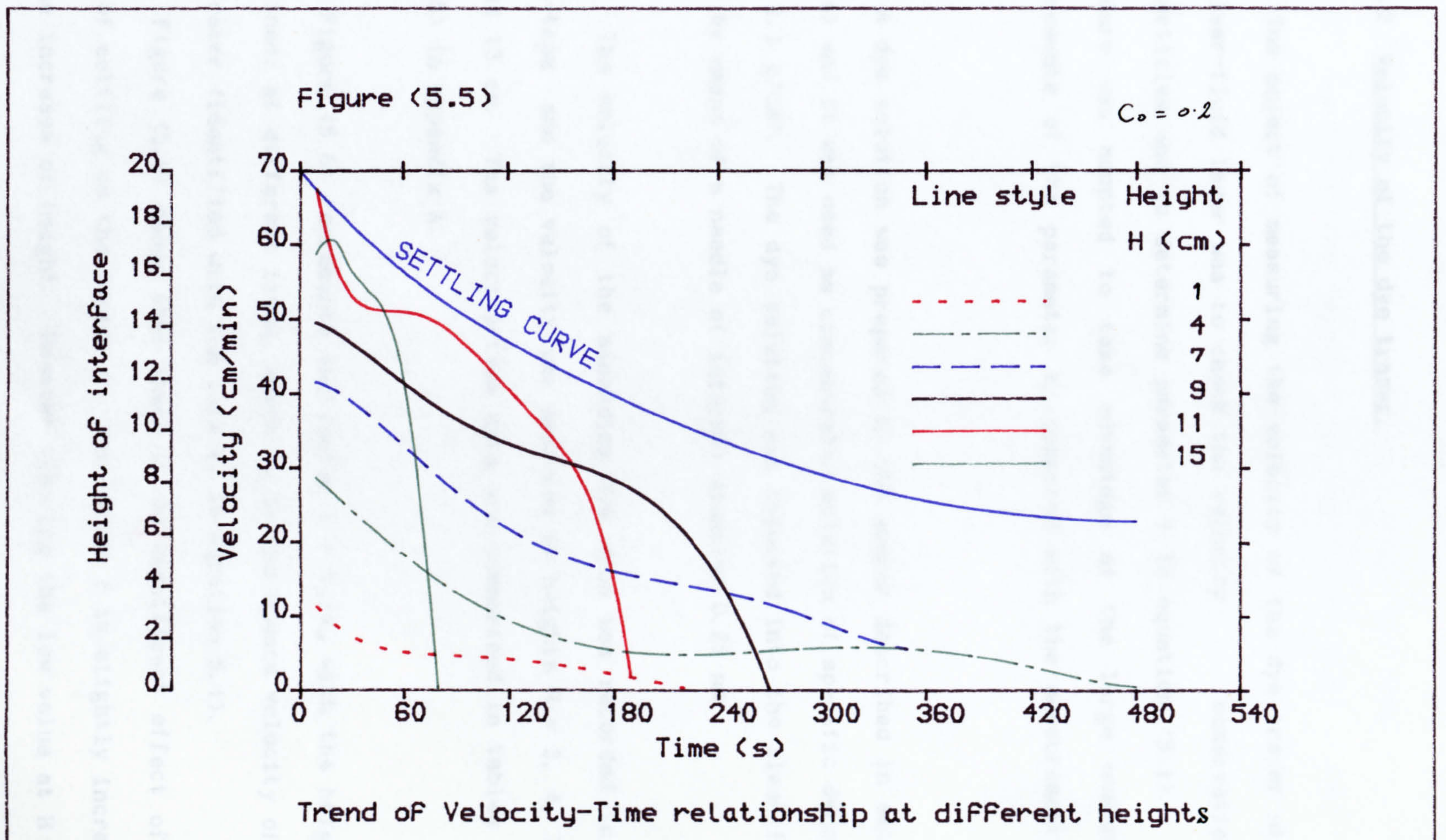

Trend of Velocity-Time relationship at different heights

5.3.1.2 Velocity of the dye tracer.

The object of measuring the velocity of the dye tracer within the clear-fluid layer was to check the velocity observation of the particles and to determine parameter f in equation (5.1). This procedure was adopted to take advantage of the large number of measurements of the parameter V_p compared with the measurements of V_d.

A dye solution was prepared in the manner described in section (4.2.4) and it was used as concentrated solution of specific density ρ_d = 1.1 g/cm^3. The dye solution was injected into the clear-fluid layer by means of a needle of internal diameter 0.25 mm

The velocity of the ascending dye drop was recorded in the video-tape and the velocity was measured at heights H = 3, 4, 7, 8, 12 and 13 cm. The velocity-time data are summarised in tables (A50 to A55) in appendix A.

Figure (5.6) represents the factor $f = V_p/V_d$ with the height H (inclined) at different times, where V_d is the upward velocity of the dye tracer (identified with the term V_r in equation 5.1).

Figure (5.6) shows that there is no significant effect of the time of settling on the factor f. The factor f is slightly increased by the increase of height. However ignoring the low value at H = 13 cm (this point was near the top interface at time 120 s), f can be

taken as the mean value of the whole range H without significant error. The upward velocity of particles within the clear fluid layer can now represent the velocity of the clear fluid layer after multiplying by the factor 1/f where

$$f = 0.85 \pm 0.04$$

Errors refere to 95% confidence limit.

Figure (5.6)

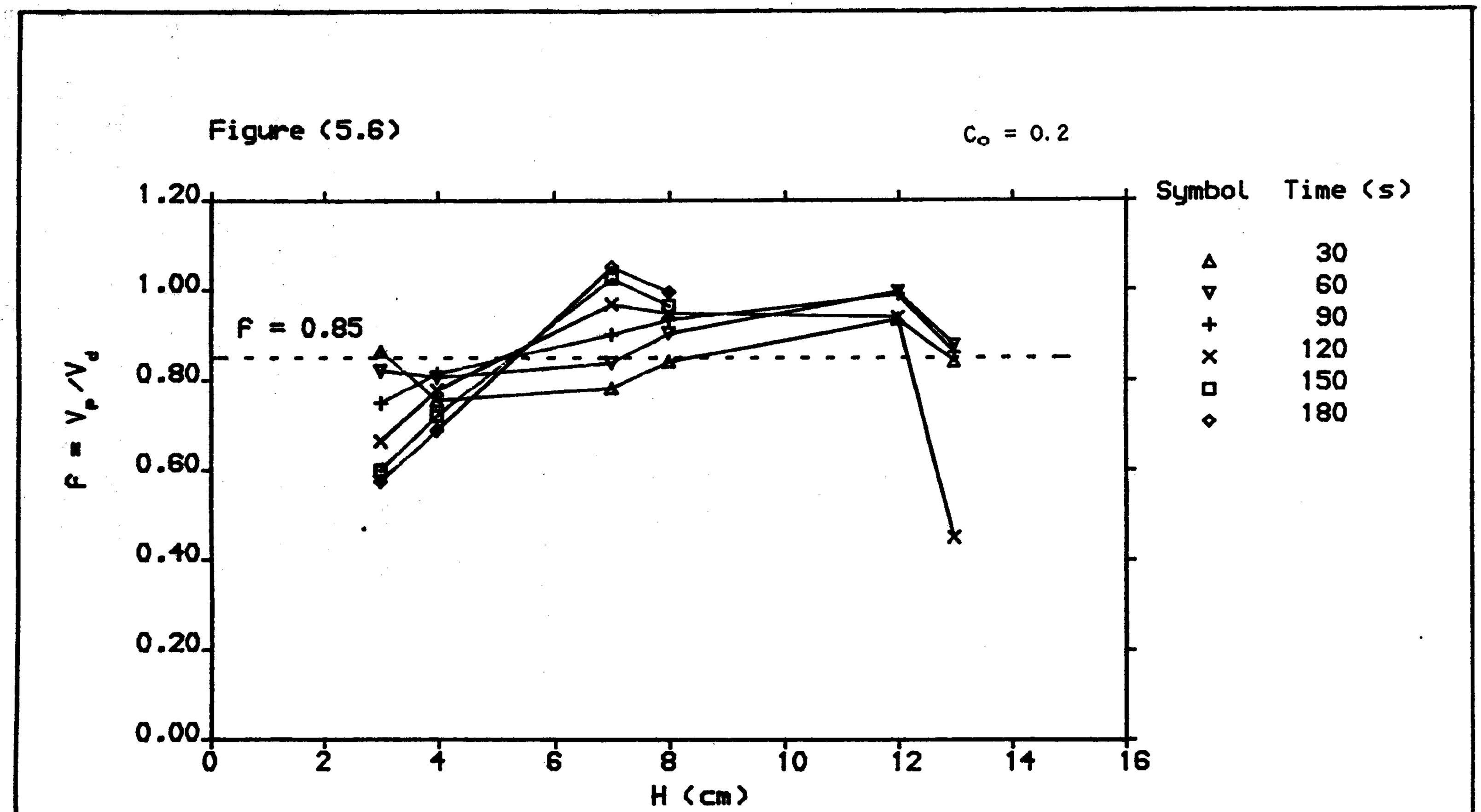

The factor F with height at different times

5.3.3 Dimensions of the clear fluid layer.

There were two objections in this set of tests (1), to observe the change of the dimensions of the clear-fluid layer with time so that the theory described in section (3.3) could be tested and (2), to permit estimates of the flow through the channel given knowledge of the velocity.

In these experiments glass beads with d = 133 μm were used, C_o=0.1 and 0.2 and the initial suspension height H_o = 20 cm (in an inclined position). The viscosity was μ = 0.48 poise.

To reduce the error on the measurements of the channel width, a large magnification was used. The magnification = 10-15 on the audio visual camera was set so as to enlarge the size of the channel, but not to lose view of a 2 cm length of the test tube when displayed on the screen. To eliminate the distortion due to the shape of the monitor-screen, it was ensured that the image being surveyed was in the middle of the monitor screen.

Tests were carried out in the way described in section (5.3.1) and recordings were carried out over the duration of the settlement. Recordings were taken at every 1 cm intervals over the tube height. The ensue data is summarised in table A56 for C = 0.2 and table A57 for C = 0.1 in appendix A.

Figure (5.7) shows the change of the clear-fluid layer width with time. for C = 0.2. The associated analysis of figure (5.7) is persued in section (5.4)

Figure (5.7) C_0 = 0.2

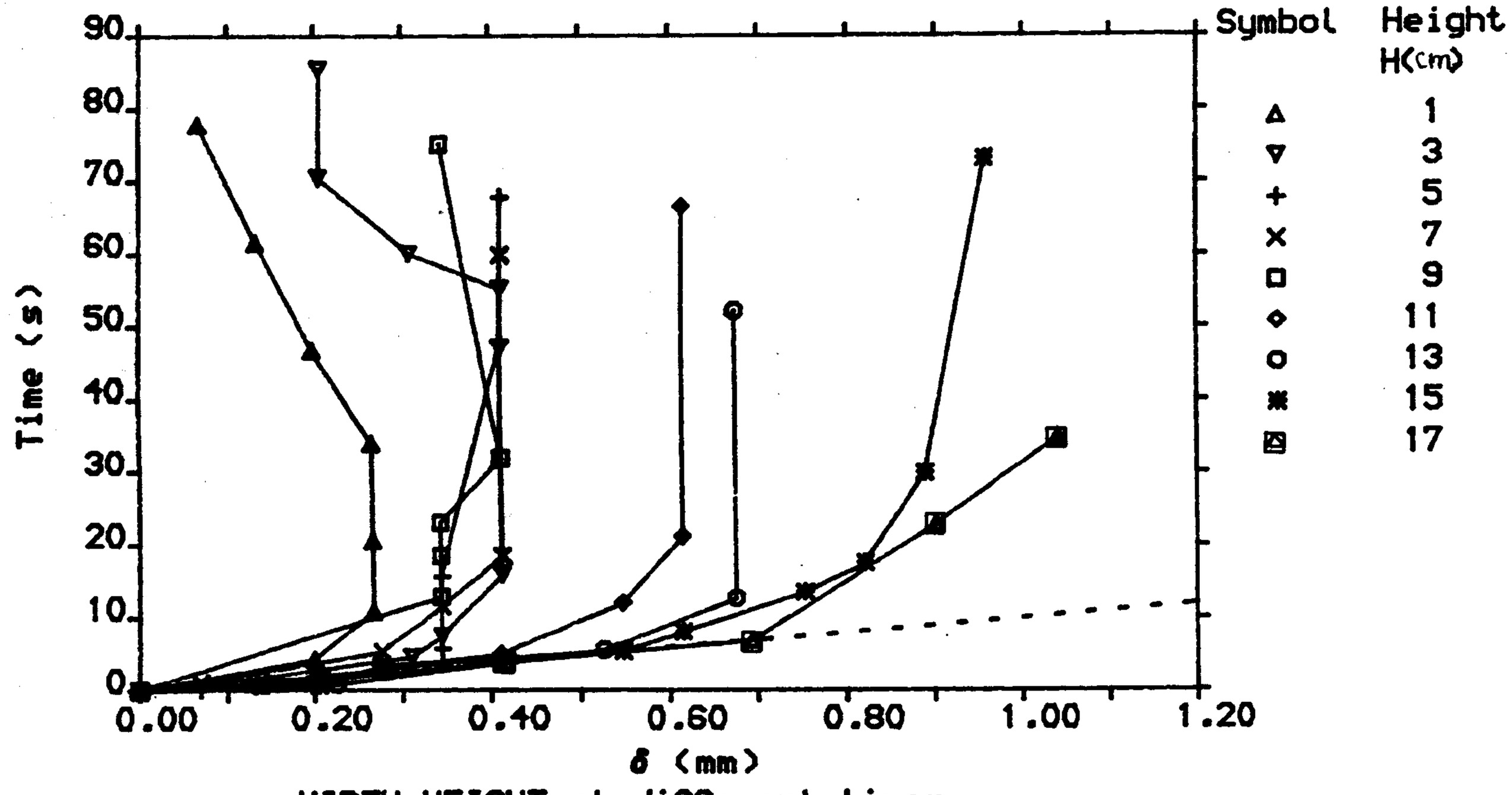

WIDTH-HEIGHT at different times

- - - - Linear increase at early stage of settling

5.3.4 Concentration measurements

Knowledge of the solids concentration distribution at different heights and times within a column of settling particles provides valuable information about the mechanism of settling and the approximations that can be made in theory.

5.3.4.1 Theoretical background

The mode of analysis used in the current study makes use of the approach used in Holdich (1983) and is based on the relationship between electrical conductivity and the solids concentration. Many good relationships between concentration C and the ratio of K_m the conductivity of the mixed phase (solid-liquid) to K_c the conductivity of the continuous phase (liquid) were deduced and tested experimentally

For dilute suspension when C < 0.1 Maxwell (1881), quoted the equation

$$\frac{K_m}{K_c} = \frac{1+ 2\beta C}{1- \beta C} \qquad \ldots.(5.2)$$

where

$$\beta = \frac{K_d - K_c}{K_d - 2K_c} \qquad \ldots.(5.3)$$

and K_d is the conductivity of the particles phase. Maxwell's equation is considered to give an adequate approximation for K_m when $C < 0.1$. When $K_d = 0$

$$\frac{K_m}{K_c} = \frac{1-C}{1+0.5\,C} \qquad \ldots\ldots (5.4)$$

which leads to $$C = \frac{1 - K_m/K_c}{1 + 0.5\,K_m/K_c} \qquad \ldots\ldots (5.5)$$

Maxwell's equation can be expanded as a Taylor series and by restricting analysis to the first two terms, Bruggeman (1935) proposed the following relationship

$$\frac{(K_m/K_c) - (K_d/K_c)}{(K_m/K_c)^{1/3}\,(1-k_d/K_c)} = 1-C \qquad \ldots\ldots (5.6)$$

When $K_d = 0$ this gives $K_m/K_c = (1-C)^{3/2}$ $\qquad \ldots\ldots (5.7)$

Meredith and Tobias (1962) introduced different equation when they calculated the overall conductivity considering the stepwise addition of a dispersed phase to the mixture. In their approach they proposed:

$$\frac{K_m}{K_c} = \frac{2[\frac{K_d}{K_c}] + 2[\frac{K_d}{K_c} - 1]\,C}{2[\frac{K_d}{K_c} + 2] - [\frac{K_d}{K_c} - 1]\,C} \times \frac{(2-C)[\frac{K_d}{K_c} + 2] + 2[\frac{K_d}{K_c} - 1]\,C}{(2-C)[\frac{K_d}{K_c} + 2] - [\frac{K_d}{K_c} - 1]\,C} \qquad (5.8)$$

When $K_d = 0$ the equation is reduced to

$$\frac{K_m}{K_c} = \frac{8(2-C)\,(1-C)}{(4+C)\,(4-C)} \qquad \ldots\ldots (5.9)$$

Holdich (1983) tested the above equation experimentally using ballotini of mean diameter 55 μm, his results are included in figure (5.8).

5.3.4.2 <u>Calibration of the resistance pins</u>

Since the liquid used as settling media is a non-conductor (glycerol-water) a little salt (NaCl) was added to the settling media to bring the conductivity to a level within the range of an AC digital universal resistance bridge.

Each pair of the pins were sequentially joined to the electrodes of the universal bridge. Noting that

$$K_m = 1/R_m, \qquad \text{and} \qquad K_c = 1/R_c$$

where R, is the resistance between the two electrodes, equation (5.9) transform to

$$\frac{R_c}{R_m} = \frac{8(2-C)(1-C)}{(4+C)(4-C)} \qquad \ldots\ldots (5.10)$$

Equation (5.10) can be rearranged to give the concentration as a function of R_c/R_m i.e.

$$C = \frac{12 - \sqrt{12^2 - 16(1-R_c/R_m)(8+R_c/R_m)}}{8 + R_c/R_m} \qquad \ldots\ldots (5.11)$$

R_c differs in practice from one pair of resistance pins to another, and can also change with the original concentration due to the possible dissolution of electrolytes. During any individual experiment, R_c was taken as the resistance associated with pairs of pins within the supernatent zone.

5.3.4.3 Experimental procedure

A set of settling tests were undertaken in a vertical tube for initial volume concentrations in the range 0.05 to 0.45 at intervals of 0.05. The object of these tests was to calibrate the resistance pins and to compare the data with equations (5.4), (5.7) and (5.9). A suspension of the glass beads with diameter d = 133 μm in a fluid of viscosity 0.48 poise was used.

Table (5.1) contains the mean values of R_c/R_m for each value of original concentration C. Errors represent the 95% confidence limits. The mean values were taken for the 8 pairs of the resistance pins along the settling tube.

Table (5.1): R_c/R_m for each pair of resistance pins at different concentrations. Errors are 95% confidence limits

NO.	H(cm)	C=0.05	C=0.10	C=0.15	C=0.20	C=0.25	C=0.30	C=0.35	C=0.40
1	19.5	0.84	0.85	0.75	0.63	0.63	0.59	0.53	0.46
2	17.5	0.83	0.84	0.75	0.74	0.67	0.59	0.55	0.49
3	15.5	0.84	0.85	0.80	0.71	0.64	0.61	0.57	0.47
4	13.5	0.86	0.83	0.74	0.69	0.67	0.58	0.59	0.49
5	11.5	0.81	0.80	0.75	0.71	0.67	0.52	0.57	0.48
6	9.5	0.81	0.91	0.73	0.71	0.68	0.62	0.58	0.48
7	7.5	0.83	0.85	0.73	0.75	0.73	0.62	0.63	****
8	5.5	0.86	0.85	0.77	0.70	0.69	0.58	0.61	****
Mean Values		0.83	0.85	0.75	0.70	0.67	0.60	0.58	0.47
Errors		0.016	0.025	0.019	0.033	0.025	0.014	0.021	0.020

Figure (5.8) gives the theoretical relationships 5.4, 5.7 and 5.9 plus the experimental results on ballotini taken from Wakeman and Holdich (1982).

In a vertical tube the graded concentration layer above the sediment layer is very thin. Since the distance between two

resistance pins is 2 cm, which is more than the thickness of the graded concentration layer, the change in concentration along a vertical settling tube at specific time does not give the accurate description of the graded concentration layer. Therefore the change in concentration with time at fixed height H was ploted and an idea is gained about the thickness of this layer from the time needed for concentration to change from C_o to C_{max} at this specific height.

Figure (5.9) shows the change of concentration with time at interval 2 cm starting from height H = 5.5 cm until H = 19.5 cm for C_o = 0.2 and α = 0. The top and bottom interfaces were also shown in figure (5.9). From the position of bottom interface with time. The difference in position of bottom interface, from time when C = C_o and the time when C = C_{max} was considered to represent the thickness of the graded concentration layer. Figure (5.9) shows that the thickness of the graded concentration layer is very small ($\simeq$ 0.8 cm at the end of the settling process).

Figure (5.8)

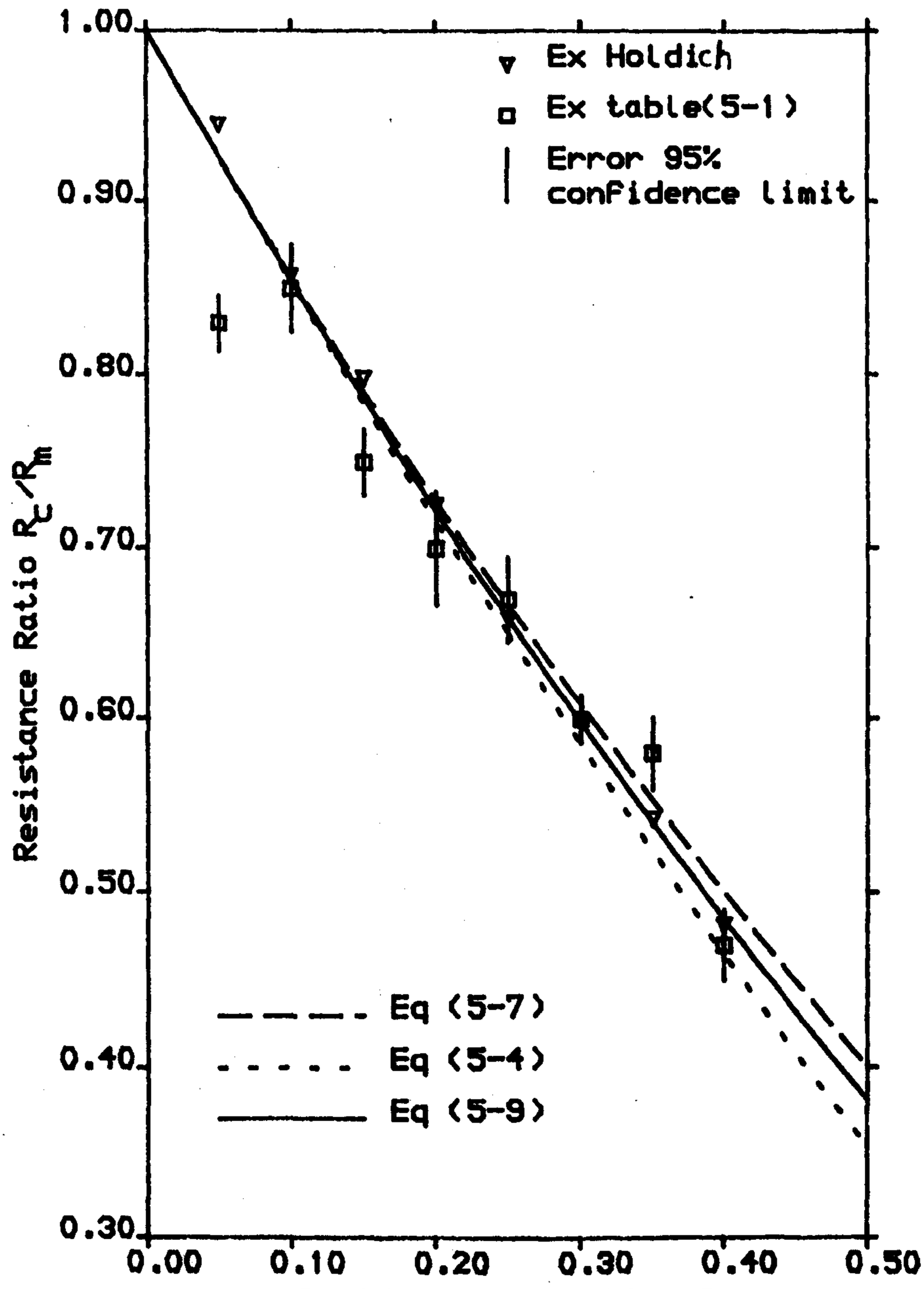

C - R_c/R_m Theoretical relationships and experimental data

Figure (5.9) C= 0.2 α= 0

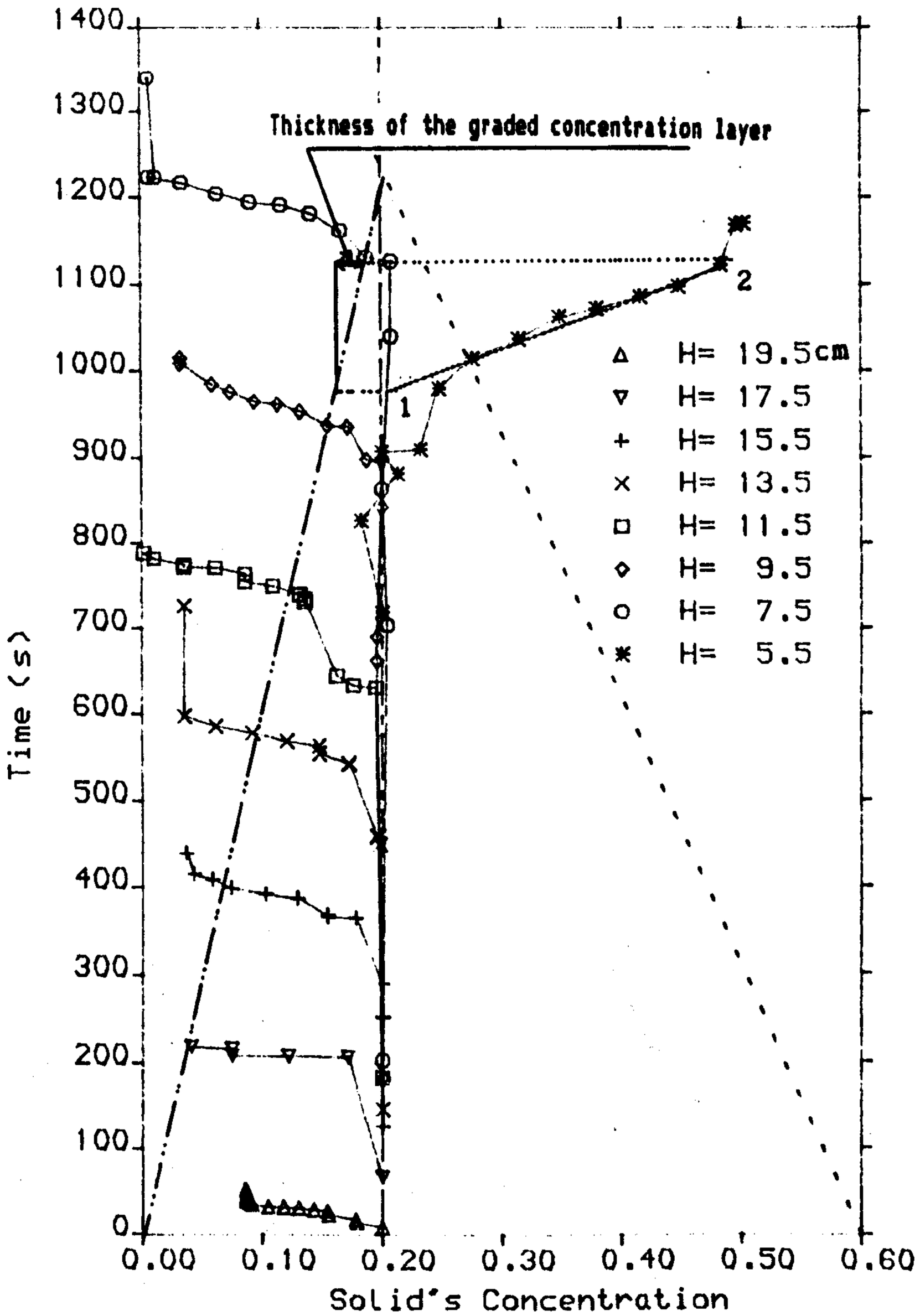

Change in concentration with time
at different heights H

- - - - Position of top interface

——— Initial solids concentration

—·—·— **Position of bottom interface**

Figure (5.10) d = 133 μm μ= 0.48 P

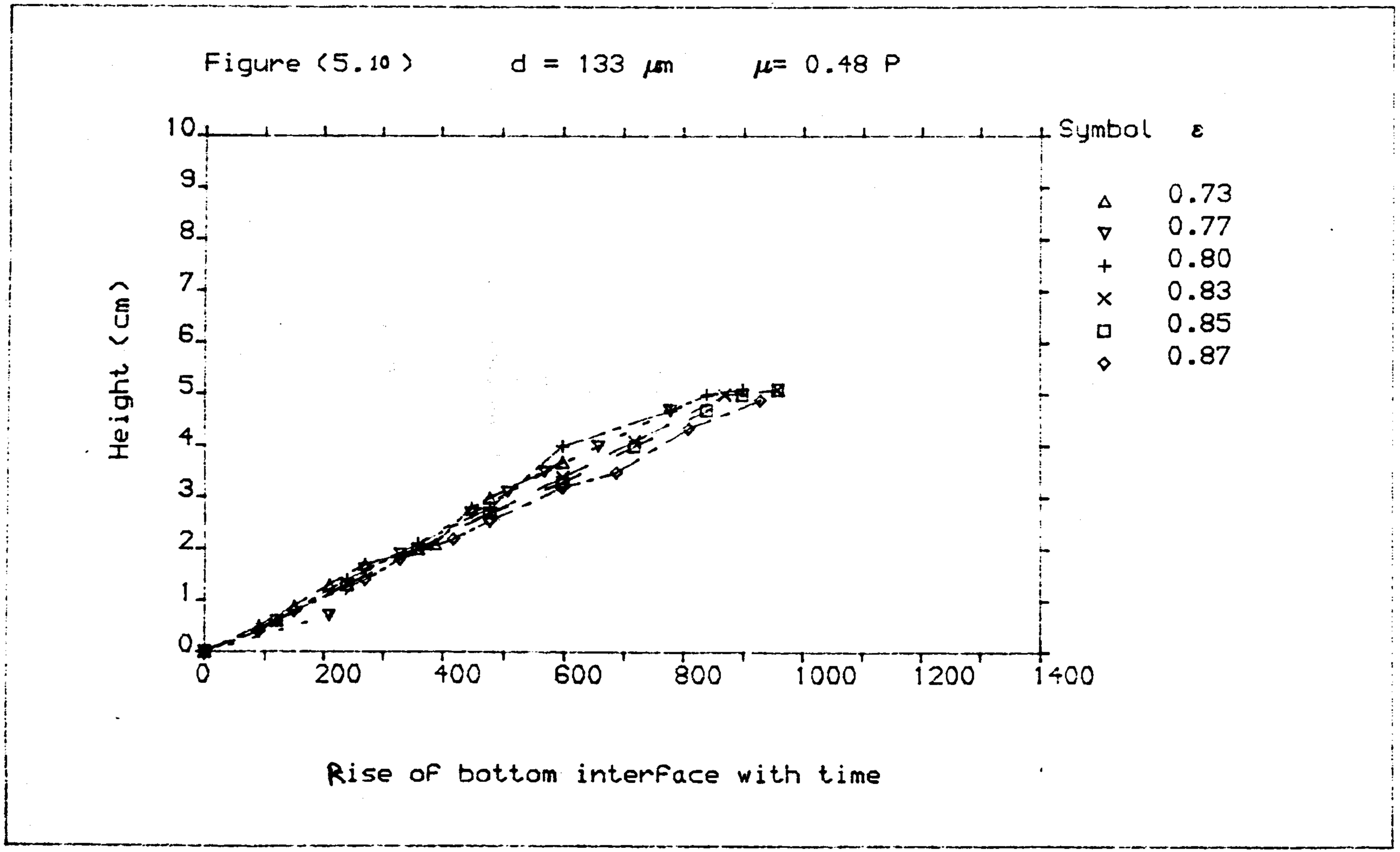

The solids concentration distribution along an inclined settling tube was also measured using the same technique described above.

In the case of an inclined tube, the inclination was such that the resistance pins were kept on the vertical face (see figure 5.1)

Apart from the point at C = 0.05 the data in figure (5.9) gives a reasonable fit of the theoretical curves. It is seen that equation (5.9) by Meredith and Tobias lies in the midrange between equations (5.4) and (5.7). Therefore equation (5.9) can be used as an accepted relationship between the solids concentration and the resistance ratio R_c/R_m. At first scan of the R_m the concentration is already known,

$$C = C_o$$

where C_o is the initial solids concentration.

From equation (5.10) R_c/R_m can be calculated for concentration $C = C_o$. Hence R_c can be deduced for this particular pair of resistance pin

$$A_c = R_c/R_m$$

$$A_c = \frac{8\ (2 - C_o)\ (1 - C_o)}{(4 + C_o)\ (4 - C_o)}$$

$$R_c = A_c \cdot R_m \qquad \ldots\ldots (5.12)$$

One pair of resistance pins was joined to the universal bridge and the change of R_m was scanned all over the settling time. Knowing the value of R_c from equation (5.12) and working via equation (5.11) the solids concentration can be calculated with time at the cross section of the settling column corresponding with the position of the particular resistance pin.

Different run was undertaken for each pair of resistance pins. the above settling test were carried out for C_o = 0.2 and α = 30° and the same suspension (d = 133 μm, μ = 0.48 poise).

The concentration distribution along an inclined settling tube at different times when C_o = 0.2 is shown in Figure (5.11)

Figure (5.11) C_0= 0.2 $\alpha = 30^0$

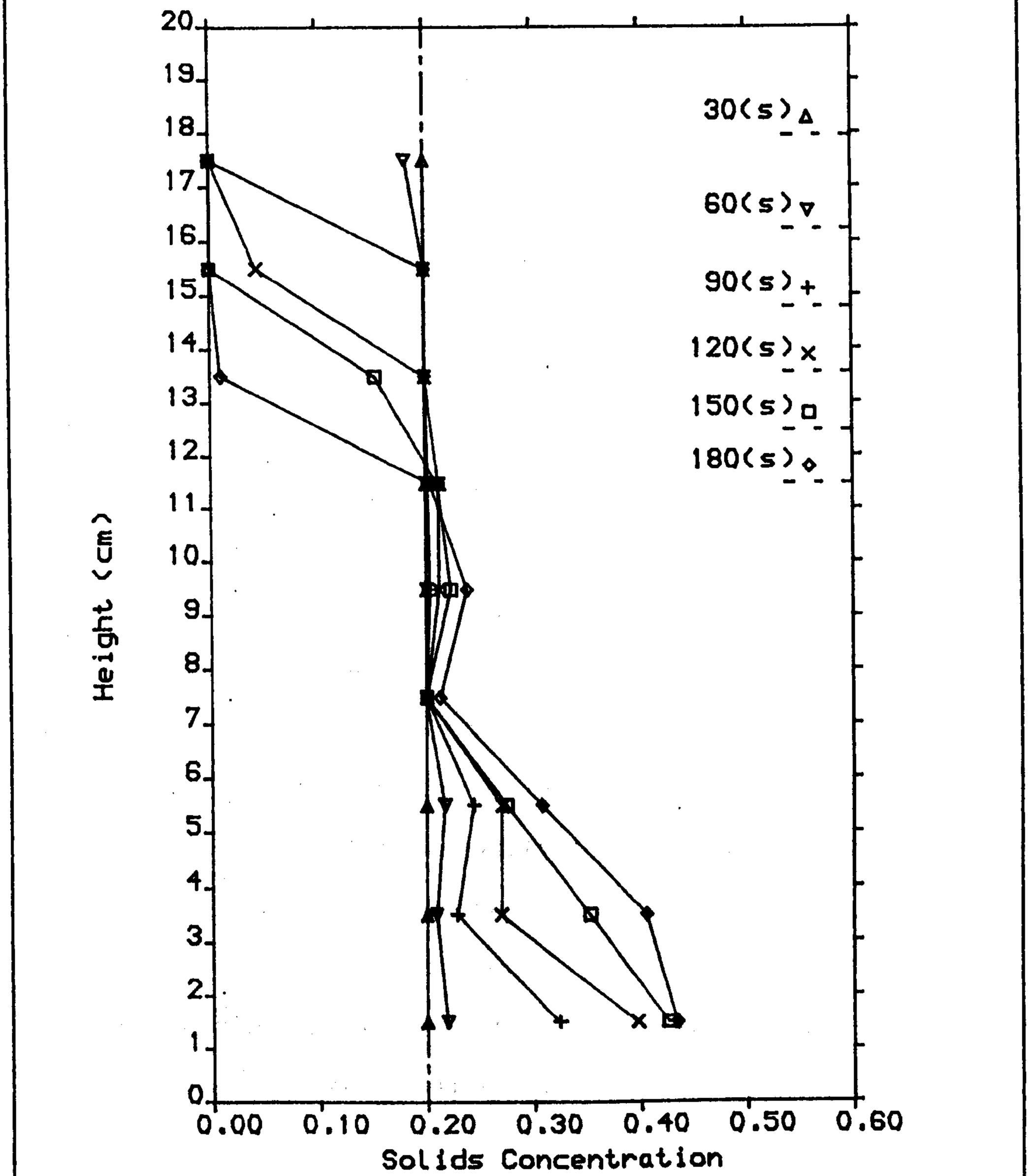

The Concentration distribution along the settling tube at different times

. . . . Position of top interface

____ Initial solids concentration

5.4 Comparison of experimental data with deductions of Acrivos et al (1979)

Acrivos et al (1979) predicted thecharacteristics of the clear fluid layer (see section 3.3). The shape of the layer in its steady state was given by equation (3.16')

$$\delta = (3\ \Gamma^{-1}\ h\ \tan\alpha)^{1/3}\ , \qquad \ldots.(5.13)$$

The time for the clear fluid layer to reach its steady state T was given by equation (3.18)

$$T = \Gamma^{-1/3}(3\ h\ \tan\alpha)^{1/3}/\sin\alpha \qquad \ldots.(5.14)$$

and the upward velocity of the flow within the layer is given by equation (3.20)

$$\underline{v} = 1/2\ \Gamma^{1/3}\ \bar{\delta}^2\ \cos\alpha \qquad \ldots.(5.15)$$

$$\underline{\quad}$$

where $\delta = (3\ h\ \tan\alpha)^{1/3}$

and $\Gamma = 9/2\ .^{\cdot}\ (H_o/a)^2\ .\ C/f(C)$

α the angle of inclination of the inclined interface which is considered constant for simplicity. The term C refers to the original solids concentration and,

$$f(C)=V_c/V_o$$

where $V_c\ /V_o$ refers, to ratio of settling velocity ϕf suspension of concentration C to the settling velocity of discrete particles. The term 'a' is defined by

$$a = d/2 \qquad \ldots.(5.16)$$

in which d is the mean diameter of the settling particles.

H_o is the initial height of the suspension i.e.

$$Z_o = H_o \cos\alpha \qquad \ldots.(5.17)$$

where H_o the initial inclined length of the settling column

Terms δ, T and Γ values are each dimensionless. They are rendered dimensional by the following transformation

$$t = T \cdot H_o/V_o \quad \ldots\ldots (5.18)$$

$$del = \delta \cdot H_o \quad \ldots\ldots (5.19)$$

$$vel = V \cdot V_o \quad \ldots\ldots (5.20)$$

Table (5.2): Parameter of exsisted settling conditions for comparison with Acrivos et al(1979)

Parameters	C_o = 0.2	C_o = 0.1
R	0.53	0.89
Γ	1.6×10^7	4.8×10^7
$\Gamma^{1/3}$	253	169
$\Gamma^{1/6}$	15.9	13.0
$\Gamma^{-1/3}$	2.1×10^{-3}	5.9×10^{-3}
$\bar{U}$	13.8	8.7
$R\Gamma^{-1/3}$	2.1×10^{-3}	5.2×10^{-3}
$\bar{R}$	1.3	2.2
$\bar{R}\Gamma^{-2/3}$	8.3×10^{-6}	3.1×10^{-5}
$\bar{R}\Gamma^{1/3}$	336	377
V_p (cm/s)	0.033	0.033
f(C)	0.374	0.629
Z_o(cm)	17.3	17.3
a (cm)	66.35×10^{-4}	66.35×10^{-4}
ωb	175	117

in which V_o is the settling velocity of the same suspension in the vertical position

and were the particular regime under scruting was characterised by

$\alpha \simeq 30.5^o$, d = 0.0133 cm , Z_o = 17.3 cm and V_o = 0.664 cm/min

The parameters covering the settling conditions are summarised in table (5.2). Figure (5.12) shows the shape of the clear fluid layer at different times. It shows that there are two significant regions along the layer.

region I- from H = 0 to H = 9 cm (the lower half of the settling column) the clear fluid layer has a uniform width which decreases with time .

region II - from H = 9 cm to the top interface the width of the layer widens sharply. At H = 11 cm the layer width is independent of time

Figure (5.13) shows the velocity distribution along the clear fluid layer at different times for initial solid's concentration C = 0.2.

At a fixed height the velocity decreases with time. There is always a layer under the top interface where the velocity starts to decrease until reducing to zero at the top interface. The thickness of this layer is approximately 2 cm and it is constant with time.

Figure (5.12) C_0 = 0.2

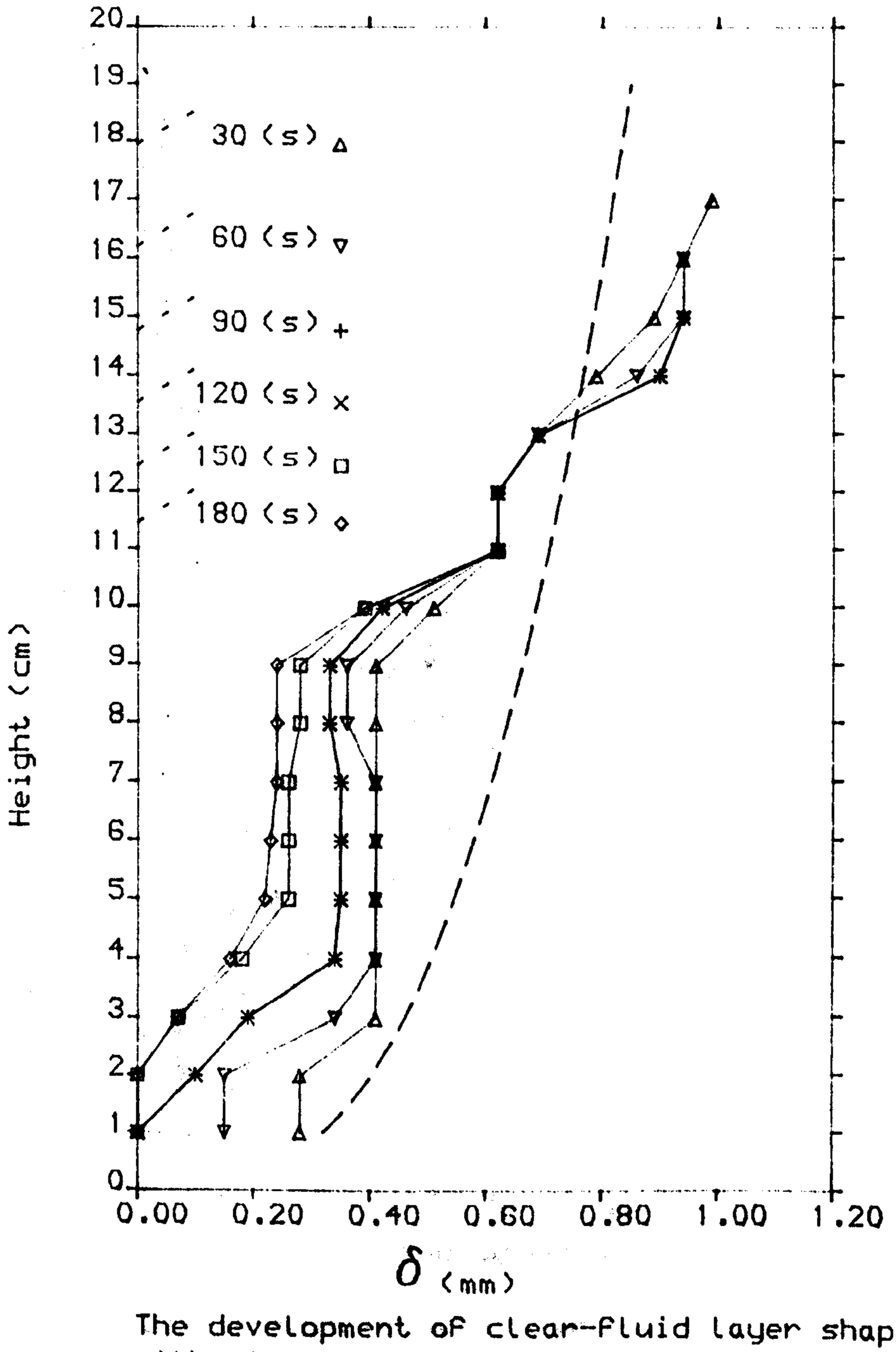

The development of clear-fluid layer shape with time. . . . : Position of interface
— — · : Prediction by Acrivos et al (1979)

Figure (5.13) C_0= 0.2

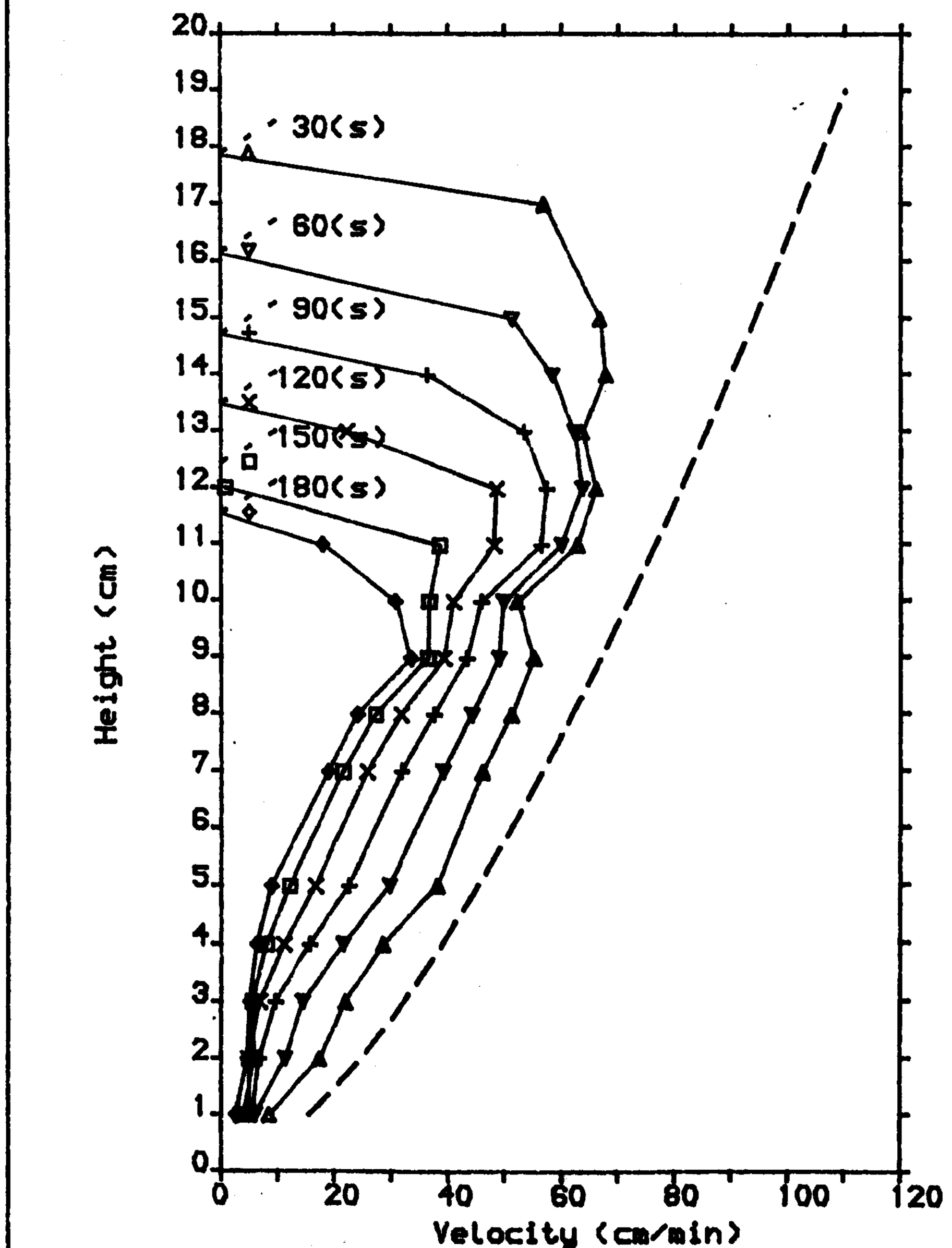

Development of upward velocity with time

- - - :Position of interface

—·—· : prediction of Acrivos et al(1979) eqs. (5.20) and (5.15)

Figure (5.7) shows that the width of the clear fluid layer increases with time until it reaches a maximum width.

Figure (5.7) shows also that the clear fluid layer width increases linearly with time in the early stage of settling test. This linear increase does not continue until the the layer reaches its maximum width as was predicted by Acrivos et al (1979). The time T_2 after which the layer width becomes steady is plotted along the inclined interface. Figure (5.15) shows (i) the time T_1 at which the linear increase ends , (ii) the time T_2 as a function of height H and (iii) the time T (the time to reach the steady state prediction by Acrivos et al (1979). Figure (5.15) shows that T has a midvalue between T_1 and T_2. T_1, T_2 and T are shown schematically in figure (5.14)

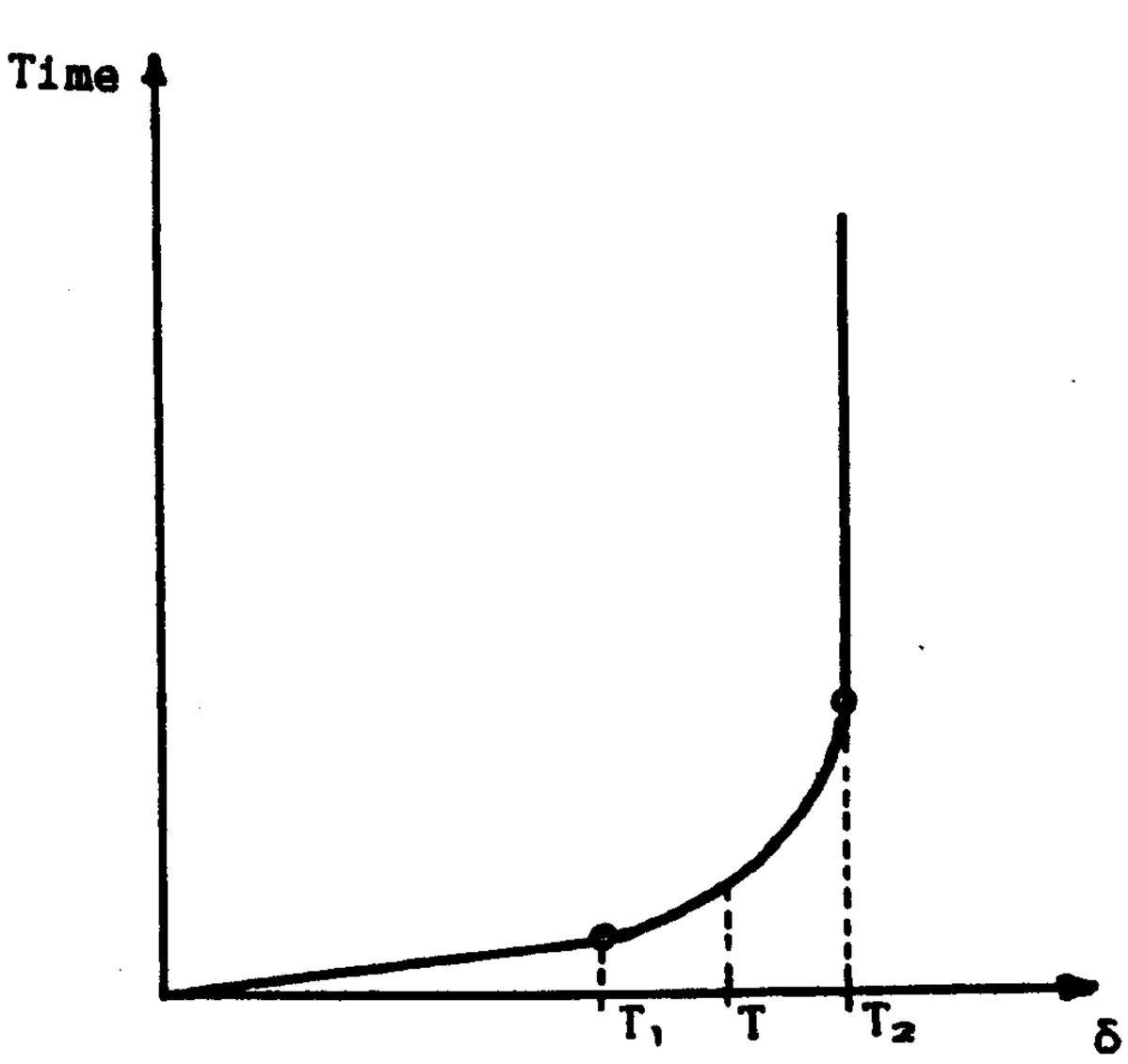

Figure (5.14) Illustrative scheme for the change of δ with time

Figure (5.15)

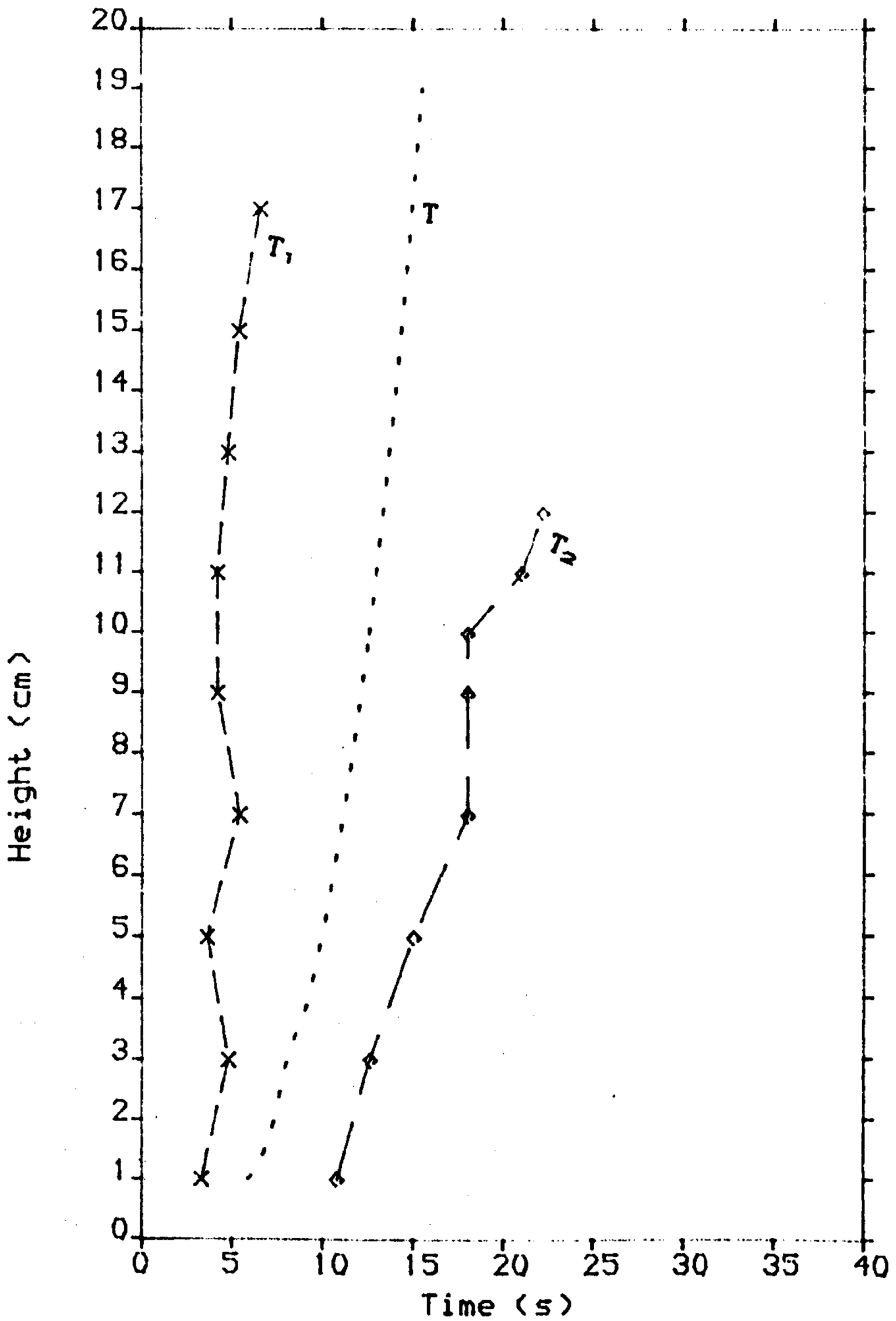

Time during which $\hat{\xi}$ has linear increase with time

Comparison with Acrivos et al's prediction

- - - - : Prediction by Acrivos et al (1979)

Figure (5.16) shows Q along the clear fluid layer at different times for initial solids concentration C_o = 0.2 where

$$Q = \delta \cdot V \qquad \ldots.(5.21)$$

where Q is the volume of supernatent flow within the clear fluid layer measured for the unit depth of the third dimension of the settling column. δ and V are taken from the data shown in figures (5.12) and (5.13) respectively.

From figure (5.16) it is evident that the flow has a maximum value of about 2 cm below the position of the interface. In the top layer there is evidence of decreases in the flow . This suggests that there may be a vortex zone which causes the flow to penetrate the suspension column. (This aspect is thoroughly discussed in section 7.3). Figure (5.16) shows also that the flow predicted by Acrivos et al (1979) is higher than the experimental values.

The gradient of the relationship at any height H represents q the infiltration along the unit area of the inclined interface at this height. The fluid infiltration q at any height H originates from the fluid creeping out of the suspension column at velocity

$$V_v = q/a \qquad \ldots. (5.22)$$

where a is the area of spaces between the solids particles available for fluid to pass through. In a unit area (Voidage ratio).

$$\varepsilon = (1-C)$$

where C is the local solids concentration

$$V_v = q/(1-C) \qquad \ldots.(5.23)$$

To have a close estimation of V_y the concentration C at the inclined interface should be closely predicted.
(Further work on calculating V_y is persuaded in section 6.5).

Figures (5.12), (5.13) and (5.16) show that Acrivos et al (1979) theory gives higher values to δ, and consequently to Q which are according to theory are constant with time. In practice it is evident that this is not the case.

Figures (5.17), (5.18), (5.19), (5.20) and (5.21) show plots corresponding to (5.7), (5.12), (5.13), (5.15) and (5.16) for initial solids concentration C_o = 0.1

For suspension of initial concentration C_o = 0.1 values of δ, V and Q predicted by Acrivos et al (1979) show a good agreement with the experimental data particularly at the beginningof settling process when $t \cong 0$.

Figure (5.16) $C_0 = 0.2$

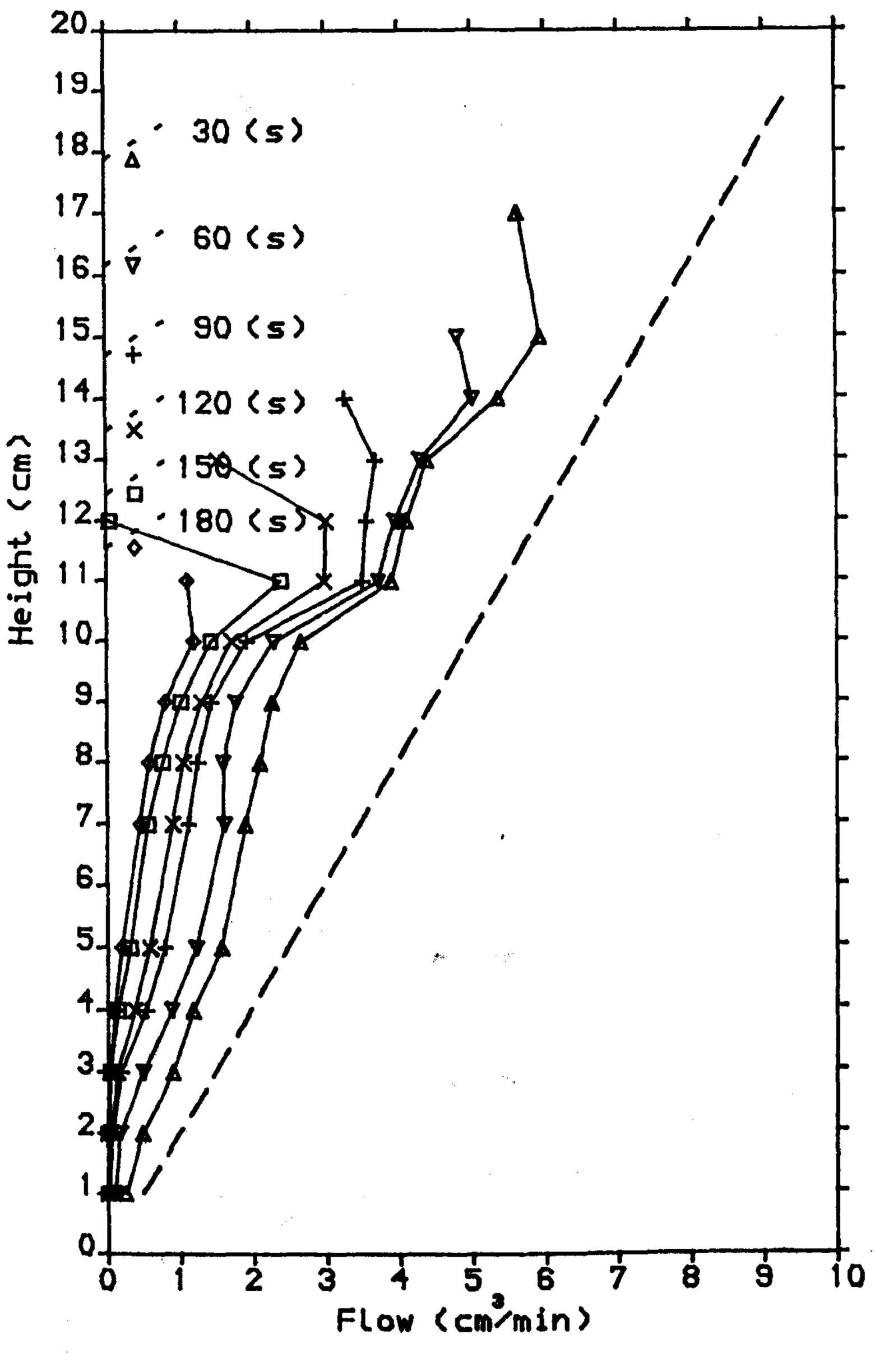

The flow along the clear fluid layer at different times.- - · :position of interface

— — · : Prediction of Acrivos et al (1979)

Figure (5.17)

$C_0 = 0.1$

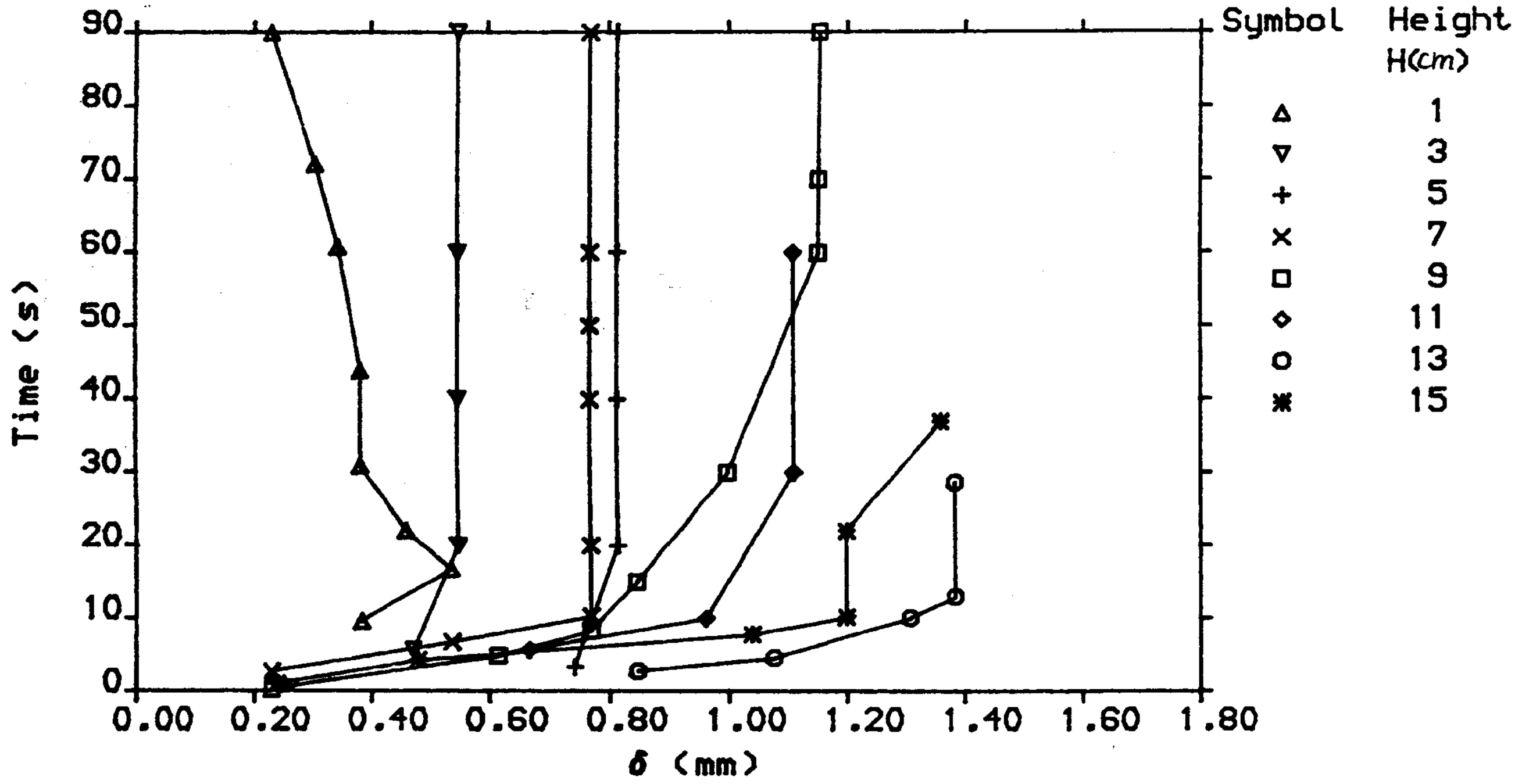

WIDTH-HEIGHT at different times

Figure (5.18) C_0 = 0.1

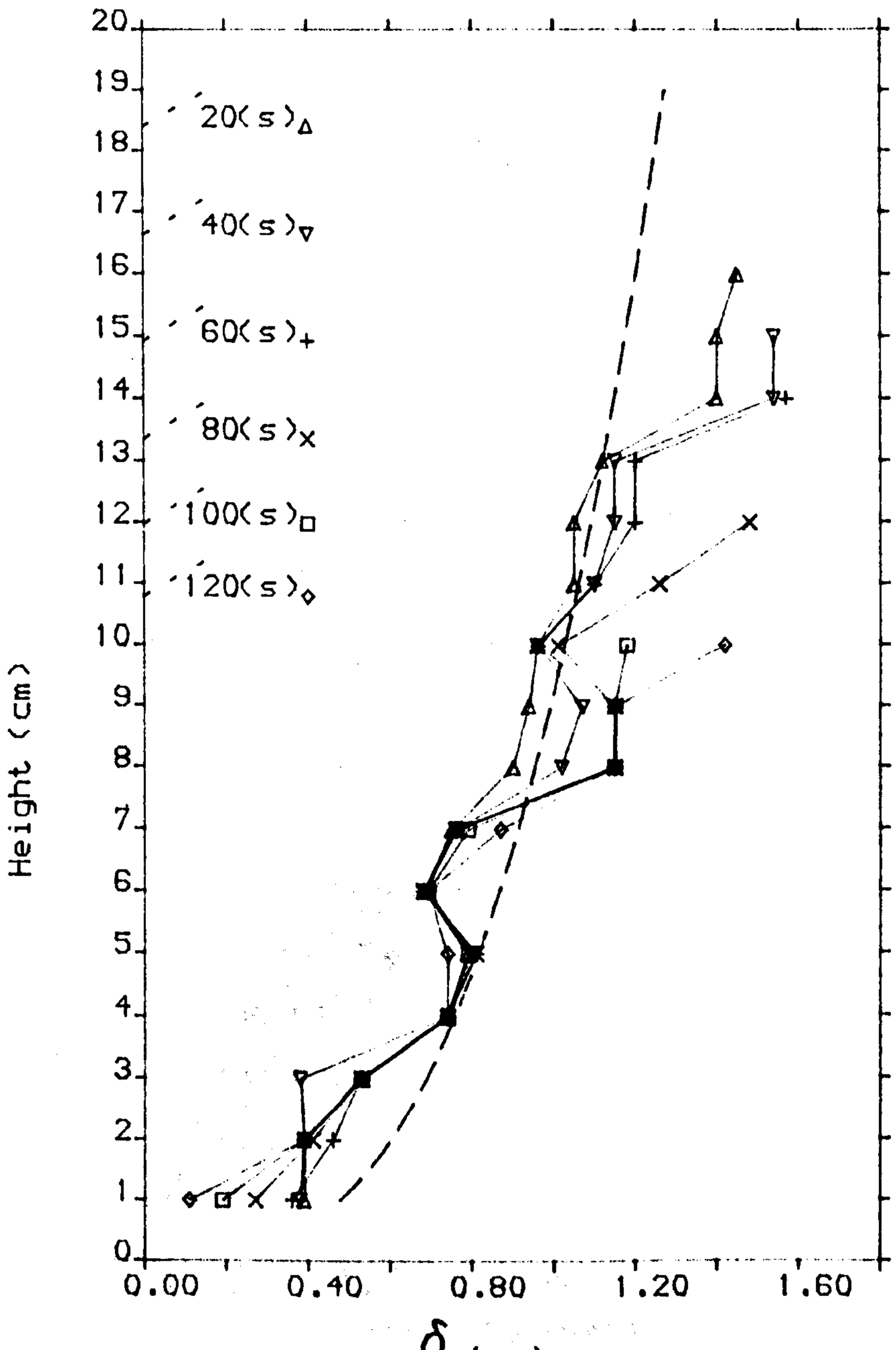

The development of clear-fluid layer shape with time. _ _ _ : Position of interface
— — · : Prediction by Acrivos et al (1979)

Figure (5.19) $C_0 = 0.1$

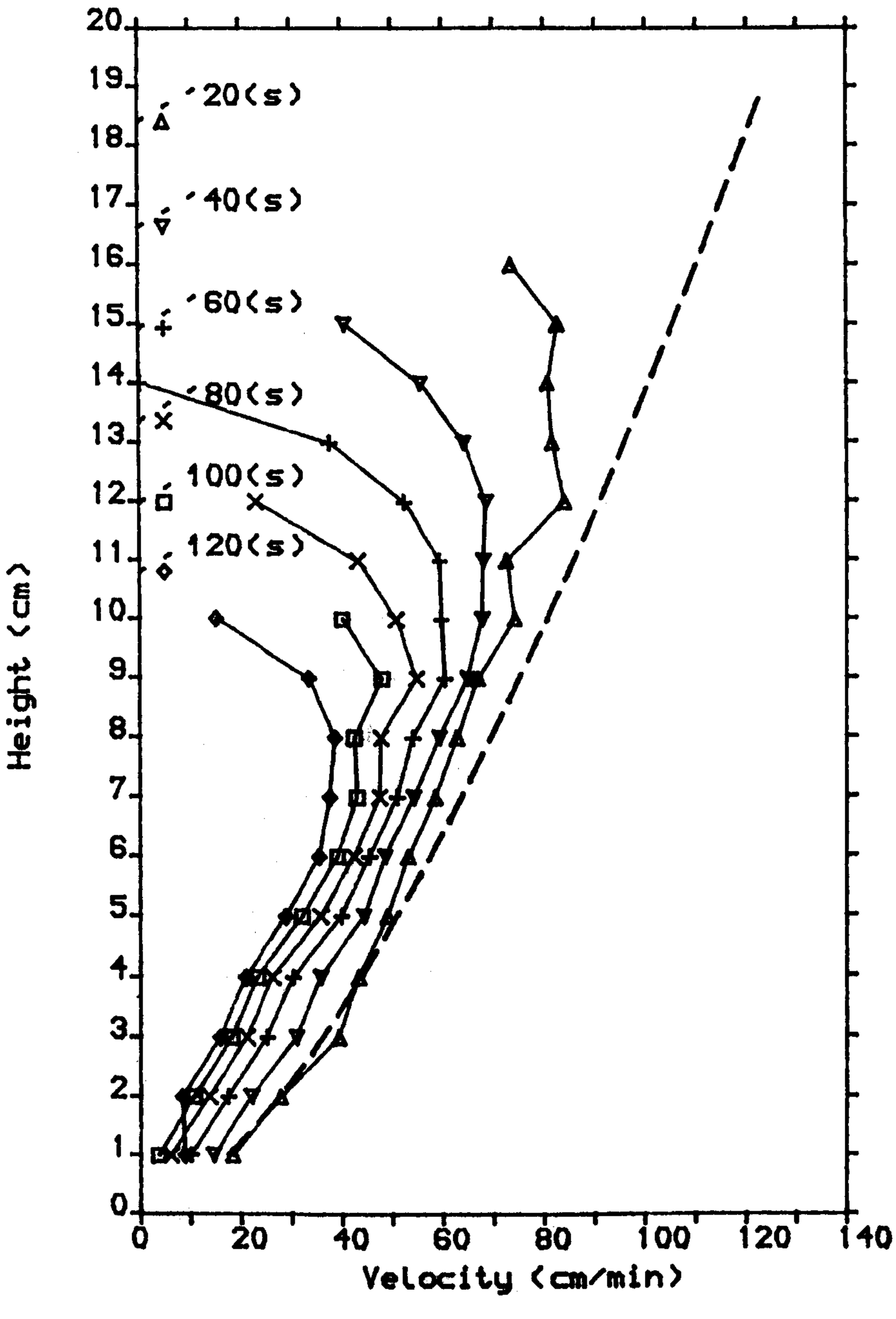

Development of upward velocity with time

- - - :Position of interface

—·— : Prediction of Acrivos et al (1979)

Figure (5.20) $C_0 = 0.1$

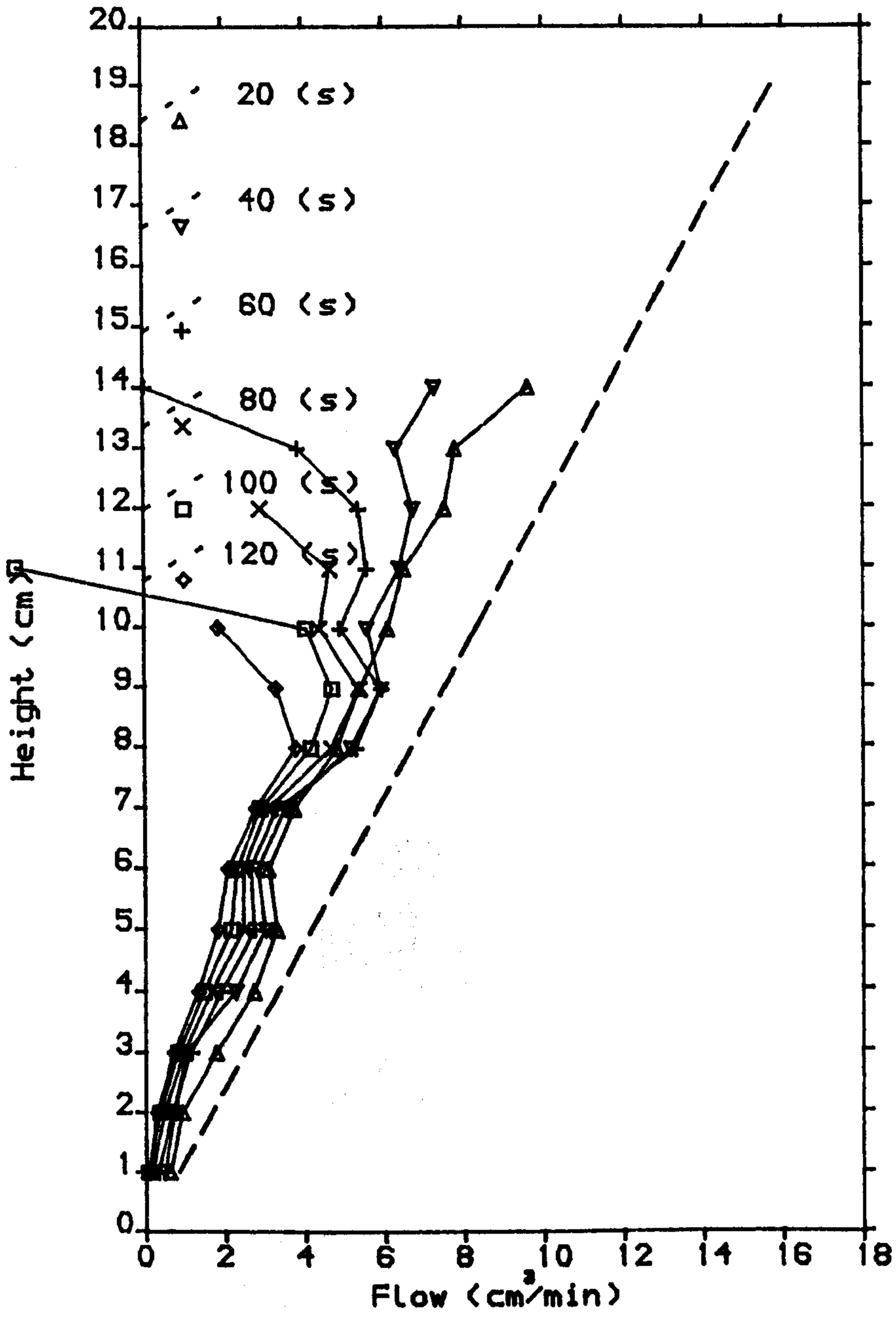

The Flow along the clear fluid layer at different times.- - · :position of interface

— — · : Prediction of Acrivos et al (1979)

5.5 Pathways of fluid release: Macroscopic view

In this section the relative contribution of the clear-fluid layer to the settling process is examined. Assuming that the settling of the top interface is at a velocity v_{in} (cm/min), this settling results in a supernatant volume collected over the top interface during a time interval Δt is V_{tot} givin by

$$V_{tot} = v_{in} \Delta t \; S_a$$

where S_a is the active surface area of the top interface (see figure 5.21)

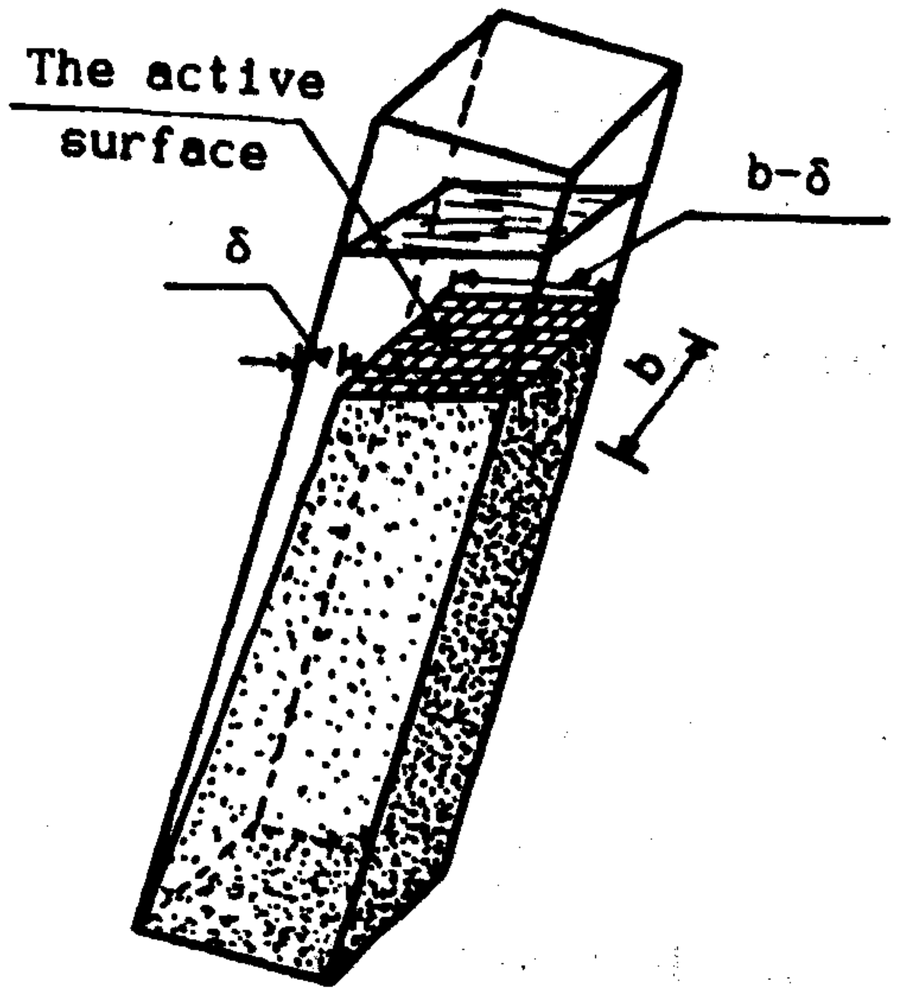

Figure (5.21) : Diagram shows the active suface area of the top interface

This volume V_{tot} is actually a sum of two values :

(i) the volume V_{in} coming from the clear-fluid layer

$$V_{in} = Q_1 . \Delta t \qquad \ldots . (5.24)$$

where Q_1 is the flow coming from the clear-fluid layer and defined by equation (5.21)

(ii) the volume V_{top} coming from the real settling of the particles at top interface. V_{top} can be deduced from the difference

$$V_{top} = V_{tot} - V_{in} \qquad \ldots . (5.25)$$

As a result of the volumes V_{in}, V_{tot} and V_{top} the settling velocity can be divided into two equivalent velocities

(i) The velocity equivalent to the flow Q

$$V_{in}/S_a \qquad \ldots . (5.26)$$

and (ii) the velocity equivalent to setting of the top interface

$$V_{top}/S_a \qquad \ldots . (5.27)$$

RV_{in} is the ratio of V_{in}/S_a to the total settling velocity v_{in} and RV_{top} is the ratio of V_{top}/S_a to the total settling velocity v_{in}.

Calculations and results are summarised in table (5.3) for C_o = 0.2 and table (5.4) for C_o = 0.1 .

Figure (5.22) shows the change of V_{tot}, V_{in} and V_{top} with time for C_o = 0.2 and figure (5.24) shows the corresponding data for C_o = 0.1 .

Figure (5.23) shows the change of RV_{in} and Rv_{tot} with time for C_o = 0.2 and figure (5.25) shows the corresponding data for C_o = 0.1.

To compare between the case of C_o = 0.2 and C_o = 0.1 the share of top interface to the total settling velocity was plotted against the height of the top interface.

Despite the difference in the shape of the curves in figures (5.22) and (5.25), figure (5.26) shows that a common curve can be plotted on the data of C_o = 0.2 and data of C_o = 0.1. This confirms that the height of the settling column has a great effect on the settling behaviour of the top interface.

The equivalent settling velocity of particles at top interface (sv) deduced from the share of the top interface to the total volume Vtot (equation 5.28) providing that the concentration at the top layer of settling column is the initial solids concentration C_o.

$$vs = \frac{V_{top}}{S_a \cdot (1-C_o)} \qquad \ldots\ldots (5.28)$$

Figure (5.27) shows sv changes with time for C_o = 0.2 and for C_o = 0.1. The value of settling velocity of the same suspension in the case of settling in a vertical tube is shown in the same figure. It is evidence that sv is higher than the settling velocity in the case of vertical settling for C_o = 0.2 and for C_o = 0.1 .

Table (5.3):
The share of clear-fluid layer and top interface to settling process in an inclined tube
C_o=0.2 , α = 30°

Time (s)	H_{in} (cm)	v_{in} cm/min	F_{max} cm³/min	v_{in} Mean	F Mean	H_{in} Mean	V_{tot} cm³	V_{in} cm³	V_{top} cm³	Rv_{in}	Rv_{top}	Ve_{top} cm/min	sv cm/min
20	16.1	3.62	11.63										
30	15.5	3.36	11.63	3.49	11.63	15.8	2.548	1.939	0.608	0.761	0.239	0.963	1.20
40	15.0	3.12	10.47	3.24	11.05	15.2	2.362	1.842	0.520	0.780	0.220	0.828	1.03
50	14.5	2.91	8.71	3.01	9.59	14.7	2.198	1.598	0.600	0.727	0.273	0.950	1.19
60	14.0	2.72	8.71	2.81	8.71	14.3	2.052	1.451	0.602	0.707	0.293	0.952	1.19
70	13.6	2.55	8.42	2.64	8.56	13.8	1.924	1.428	0.497	0.742	0.258	0.787	0.98
80	13.2	2.41	8.42	2.48	8.42	13.4	1.812	1.405	0.407	0.775	0.225	0.645	0.81
90	12.8	2.29	7.26	2.35	7.85	13.0	1.713	1.307	0.406	0.763	0.237	0.642	0.82
100	12.4	2.17	6.68	2.22	6.98	12.6	1.626	1.162	0.464	0.715	0.285	0.732	0.91
110	12.0	2.08	6.12	2.12	6.40	12.2	1.551	1.067	0.484	0.688	0.312	0.764	0.95
120	11.7	1.99	5.61	2.03	5.86	11.9	1.484	0.977	0.507	0.658	0.342	0.804	1.00
130	11.4	1.91	5.22	1.96	5.41	11.6	1.426	0.903	0.523	0.633	0.367	0.829	1.04
140	11.1	1.85	4.35	1.88	4.79	11.3	1.374	0.798	0.576	0.581	0.419	0.909	1.14
150	10.7	1.79	3.77	1.82	4.06	10.9	1.327	0.678	0.650	0.510	0.490	1.029	1.29
160	10.5	1.73	4.07	1.76	3.93	10.6	1.286	0.655	0.631	0.509	0.491	0.997	1.25
170	10.2	1.68	3.48	1.71	3.77	10.3	1.247	0.630	0.617	0.505	0.495	0.975	1.22

H_{in} : Height of top interface
V_{in} : settling velocity in the inclined settling tube
F_{max}: the maximum value of the flow Q coming from the clear fluid layer
V_{tot}: the total volume of suspension accumulated over top interface within 10 seconds
V_{in} : volume of supernatent coming from clear fluid layer within 10 seconds
V_{top}: volume of supernatent coming from settling of top interface within 10 seconds
Rv_{in}: the share of inclined interface to the settling velocity
Rv_{top}: the share of top interface to the settling velocity
Ve_{top}: equevelent velocity to Vtop
sv : real settling velocity of particles at top interface providing that the concentration at level (H_{in}-2) cm is the initial concentration C_o

Table (5.4):
The share of clear-fluid layer and top interface to settling process in an inclined tube
C_o=0.1 , α = 30°

Time (s)	H_{in} (cm)	v_{in} cm/min	F_{max} cm³/min	v_{in} Mean	F Mean	H_{in} Mean	V_{tot} cm³	V_{in} cm³	V_{top} cm³	Rv_{in}	Rv_{top}	Ve_{top} cm/min	sv cm/min
20	15,9	4,54	18,53										
				4,57	17,92	15,6	3,07	2,99	0,082	0,973	0,027	0,12	0,14
30	15,2	4,60	17,31										
				4,59	15,45	14,8	3,077	2,575	0,503	0,837	0,163	0,75	0,83
40	14,4	4,57	13,59										
				4,51	12,97	14,0	3,041	2,163	0,879	0,711	0,289	1,30	1,44
50	13,6	4,46	12,36										
				4,37	11,74	13,3	2,954	1,957	0,997	0,662	0,338	1,48	1,64
60	12,9	4,28	11,12										
				4,17	10,50	12,6	2,822	1,750	1,072	0,620	0,380	1,58	1,76
70	12,2	4,07	9,89										
				3,95	9,52	11,9	2,668	1,587	1,082	0,595	0,405	1,60	1,78
80	11,6	3,82	9,15										
				3,70	9,02	11,3	2,505	1,504	1,001	0,600	0,400	1,48	1,64
90	11,0	3,57	8,90										
				3,45	8,65	10,7	2,334	1,442	0,892	0,618	0,382	1,32	1,47
100	10,4	3,32	8,41										
				3,20	8,04	10,1	2,167	1,340	0,827	0,618	0,382	1,22	1,36
110	9,8	3,08	7,67										
				2,97	7,05	9,6	2,009	1,175	0,835	0,585	0,415	1,23	1,37
120	9,4	2,86	6,42										
				2,76	6,18	9,1	1,838	1,030	0,808	0,560	0,440	1,21	1,34
130	8,9	2,66	5,94										
				2,57	5,81	8,68	1,714	0,969	0,745	0,565	0,435	1,12	1,24
140	8,5	2,48	5,68										

H_{in} : Height of top interface
V_{in} : settling velocity in the inclined settling tube
F_{max}: the maximum value of the flow Q coming from the clear fluid layer
V_{tot}: the total volume of suspension accumulated over top interface within 10 seconds
V_{in} : volume of supernatent coming from clear fluid layer within 10 seconds
V_{top}: volume of supernatent coming from settling of top interface within 10 seconds
Rv_{in}: the share of inclined interface to the settling velocity
Rv_{top}: the share of top interface to the settling velocity
Ve_{top}: equevelent velocity to Vtop
sv : equivalent settling velocity of particles at top interface providing that the concentration at level (H_{in}-2) cm is the initial concentration C_o

Figure (5.22) C_0 = 0.2

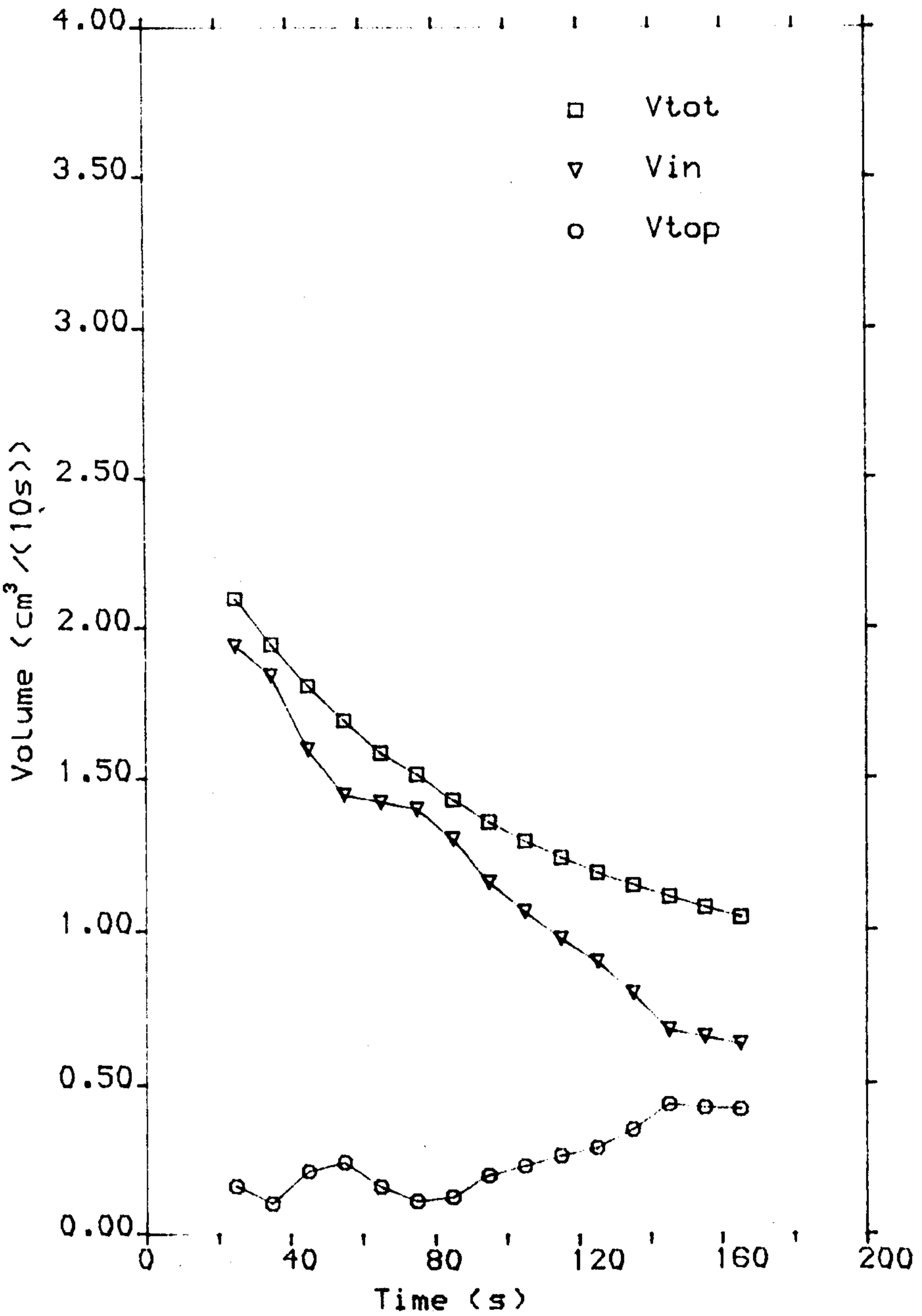

The share of the horizontal interface to

the total volume of supernatent with time

Figure (5.23) C_0 = 0.2

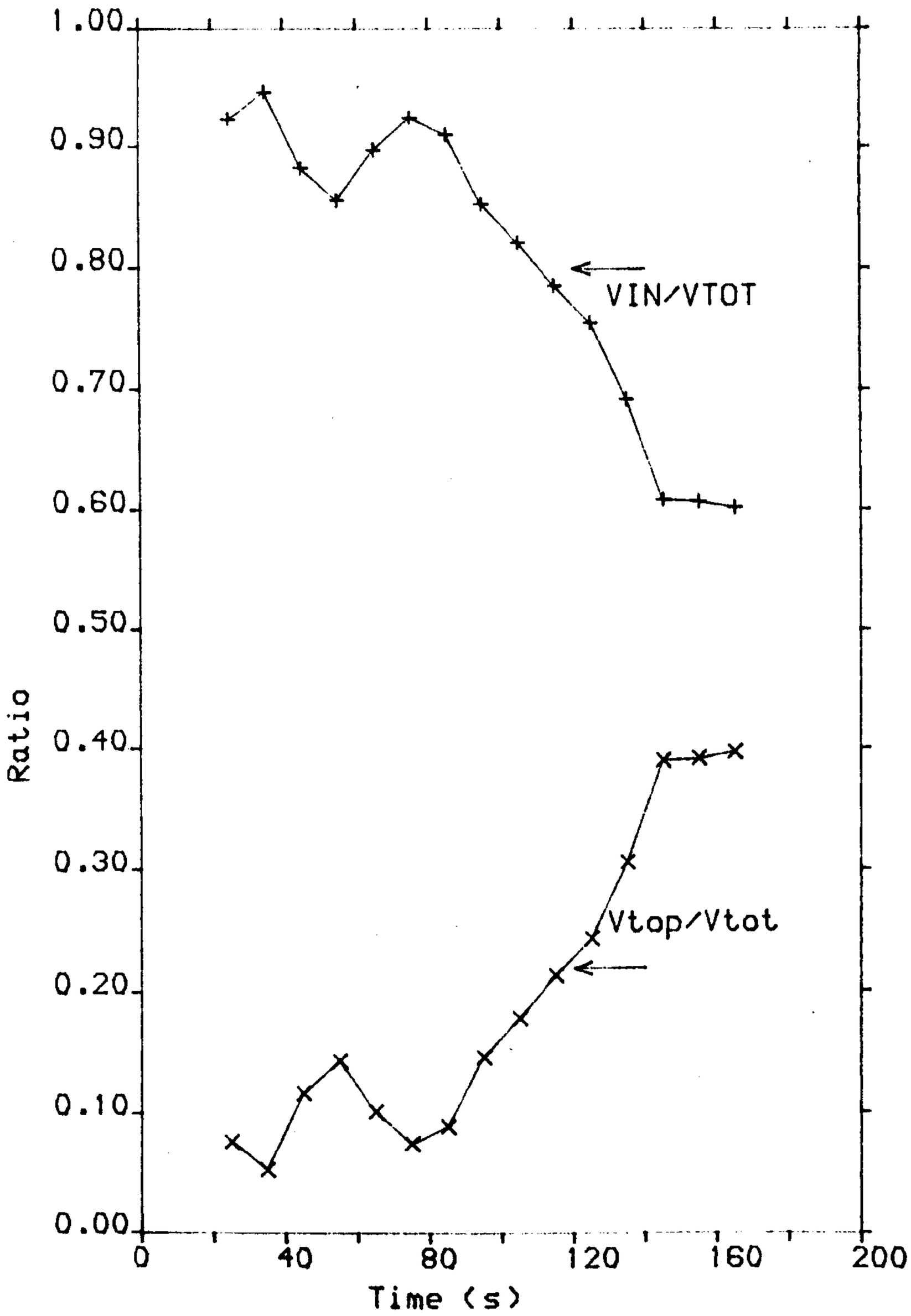

The share of the horizontal interface to

the total settling velocity with time

Figure (5.24) C_0 = 0.1

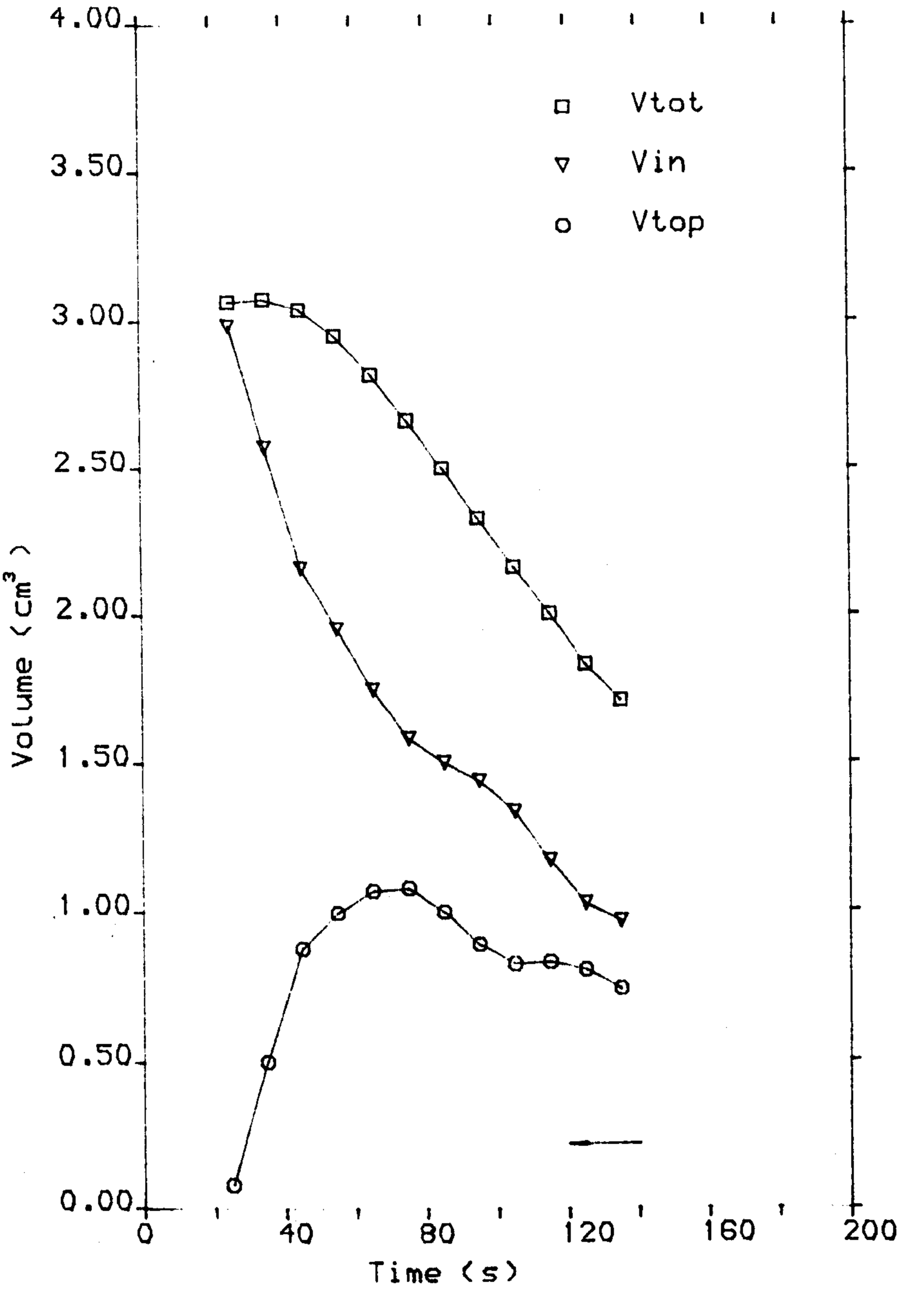

The share of the horizontal interface to the total volume of supernatent with time

Figure (5.25) C_0 = 0.1

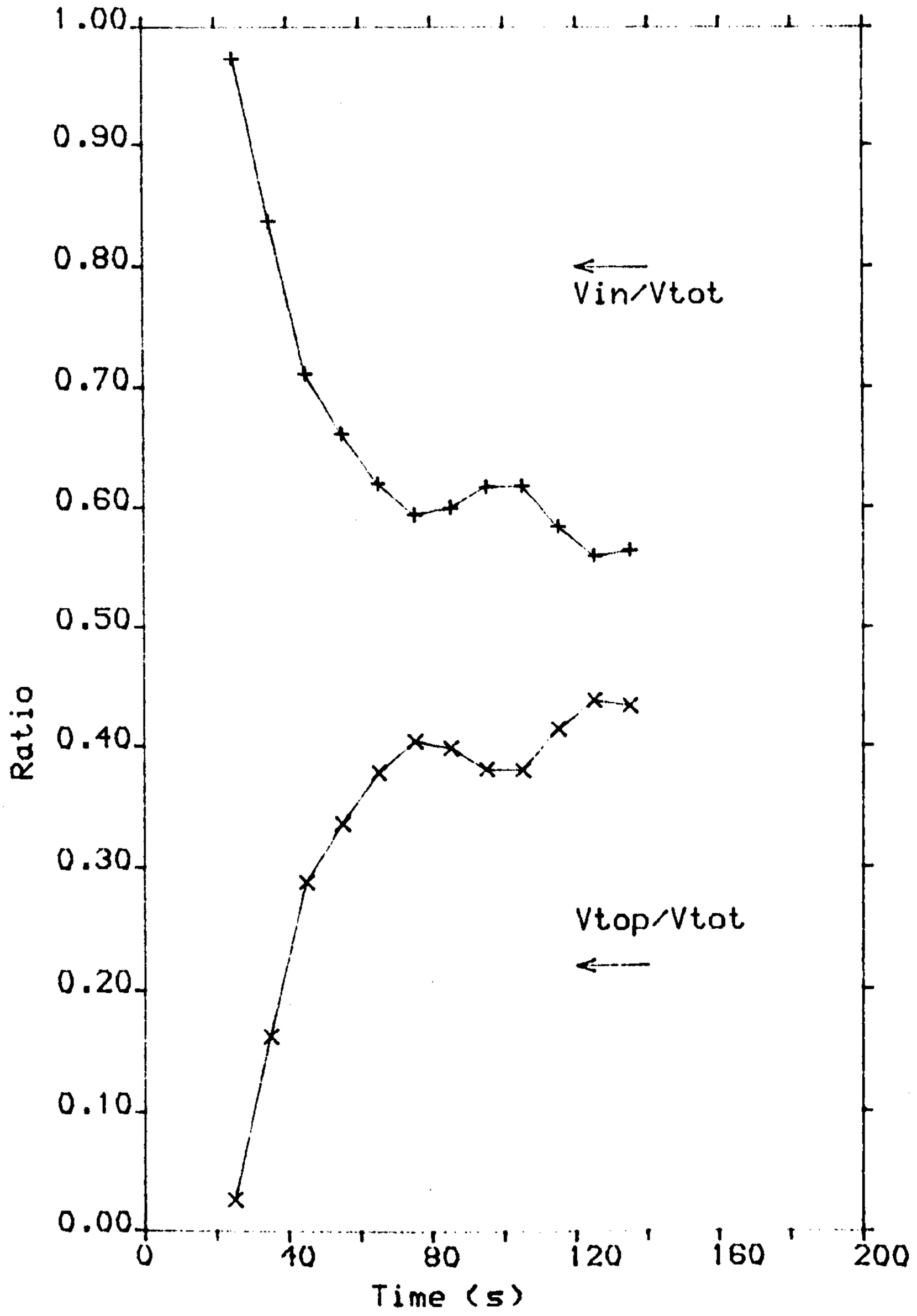

The share of the horizontal interface to the total settling velocity with time

Figure (5.26)

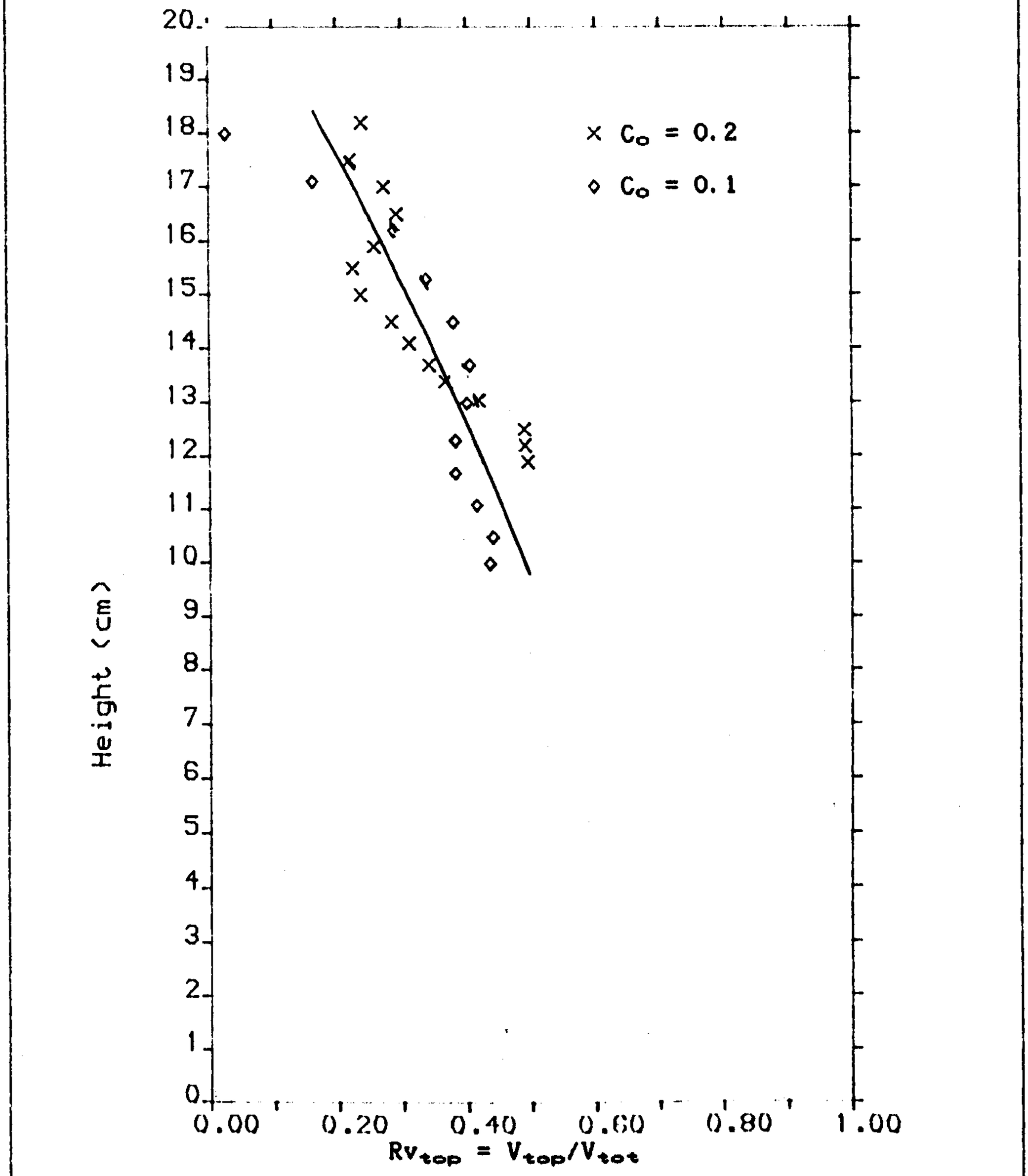

The share of the top interface to the settling process for different values of intial concentration

Figure (5.27)

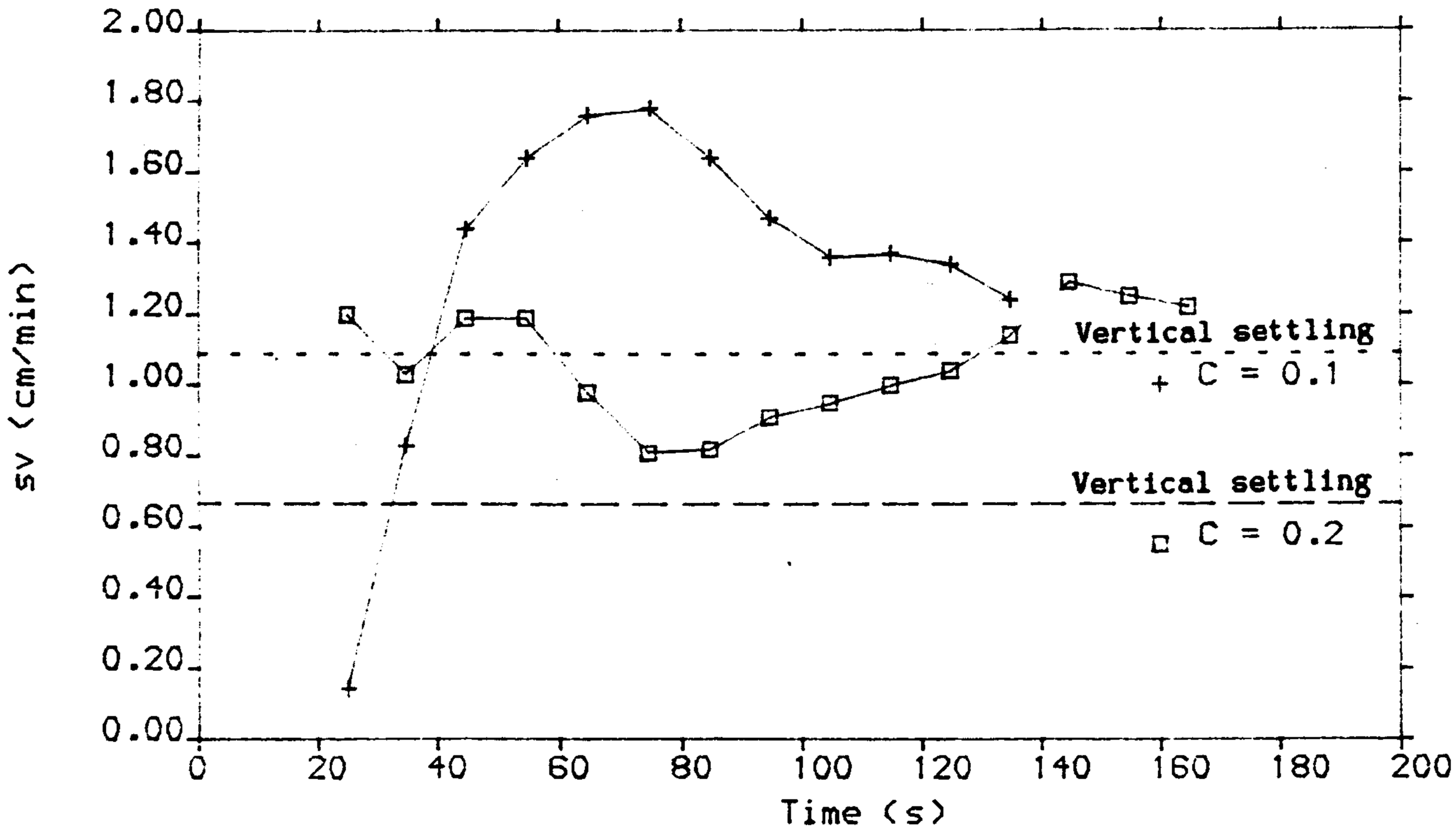

Change of settling velocity of the particles
at top interface with time

CHAPTER SIX

FLOW FIELD WITHIN THE SUSPENSION CORE

CHAPTER SIX

FLOW FIELD WITHIN THE SUSPENSION CORE

6.1 Introduction

This chapter focuses on the flow pattern of the fluid within the suspension core. This was studied experimentally using a dye tracer technique . The aim of the analysis was to gain a clearer idea about the mechanism of the fluid infiltration into the clear fluid layer.

Sections (6.2) and (6.3) describe the experimental set-up together with the methods used to measure the velocity field. In section (6.4) the velocity vectors are examined in terms of their components. Section (6.5) investigates about the velocity components V_y as the feeding velocity of the fluid into the clear-fluid layer. Section (6.6) dwells on the transfer of fluid from the suspension core into the clear- fluid layer. As a consequence of imponderables identified in the previous analysis, a check was carried out on the efficiency of the dye tracer technique, the results being reported in section (6.7) NB. this check was carried out in a vertical settling column. In section (6.8) and (6.9) the continuity equation was checked in the z-x frame and, in sections (6.10) and (6.11) data of velocity vectors were studied and compared with the existed theory . In section (6.12) calculations of the velocity of settling within the suspension based measurements of the concentration distribution along the settling column were compared with the observed velocity

field.

6.2 Experimental set-up

For this set of experiments the apparatus, suspension and suspended fluid are as described in section (4.2). The dye solution mentioned in section (5.3.4) was used as a dye tracer.

The audio visual equipment described in section (5.2.1) was used to observe the movement of the dye drops injected into the settling suspension .

6.3 Experimental procedure

Using the inclined tube the experimental regime is described by

$\alpha = 30^{\circ}$, $C_o = 0.2$, $\mu = 0.48$ P, $H_o = 20$ cm.

The dye mix and the needle described in section (5.3.1.2) were used and, the procedure described in that section was followed to record the movement of ascending dye drops using a video recorder. Due to the time consuming nature of the experiments, observations were restricted to the period of t = 20 s to 70 s from the beginning of the settling test. During this time, dye was injected on 900 occasions at different points within the settling column.

Figure (6.1) shows the velocity vectors within the settling suspension at time intervals 10 seconds for time ranges 25-35, 35-45,

45-55, and 65-75 seconds together with the positions of the top interface.

Figure (6.1) $C_o = 0.2$ $\alpha = 30^\circ$ $\rightarrow$ = 10 cm/min

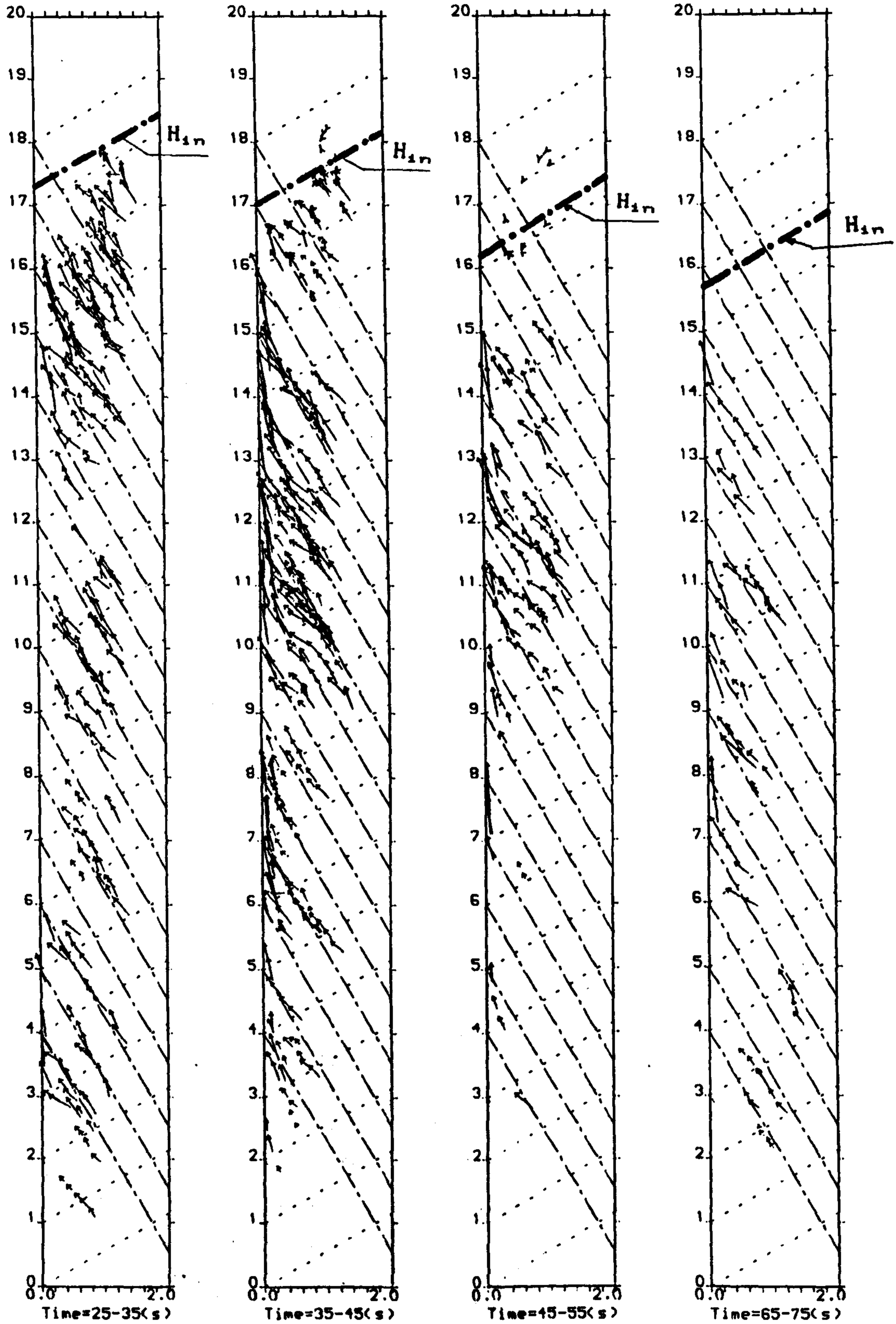

Velocity vectors within the settling column

... Horizontal lines, —·— : Vertical lines

6.4 Velocity components and contours.

Velocity components were deduced from the data plotted in figure (6.1) during the time interval 40 ± 5 seconds. This was selected because of large number of observations carried out during this interval. For convenience the settling tube width was divided into 20 equal slices of width 0.1 cm as a means of collating the data. The velocity components V_h and V_y were plotted along the settling column for y = 0.05 to y = 1.45 cm where y is the distance towards the suspension core starting from the downward facing wall, NB. V_h is the velocity component in the direction H along the inclined wall (see figure 6.2) and V_y is the component perpendicular to the direction H measuring from the upper sloping wall.

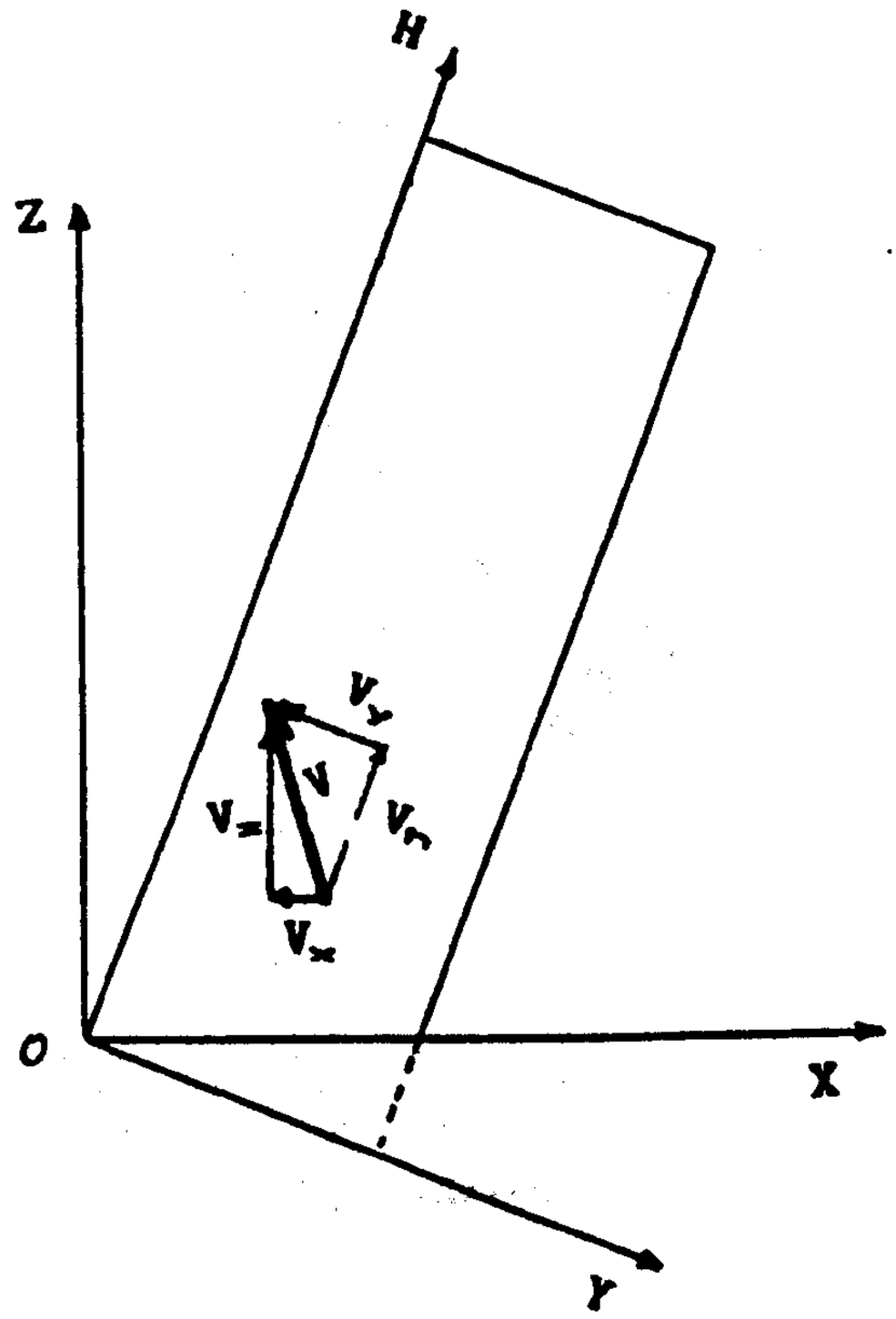

Figure (6.2): Axes for the velocity components.

Figure (6.3)

C_o = 0.2

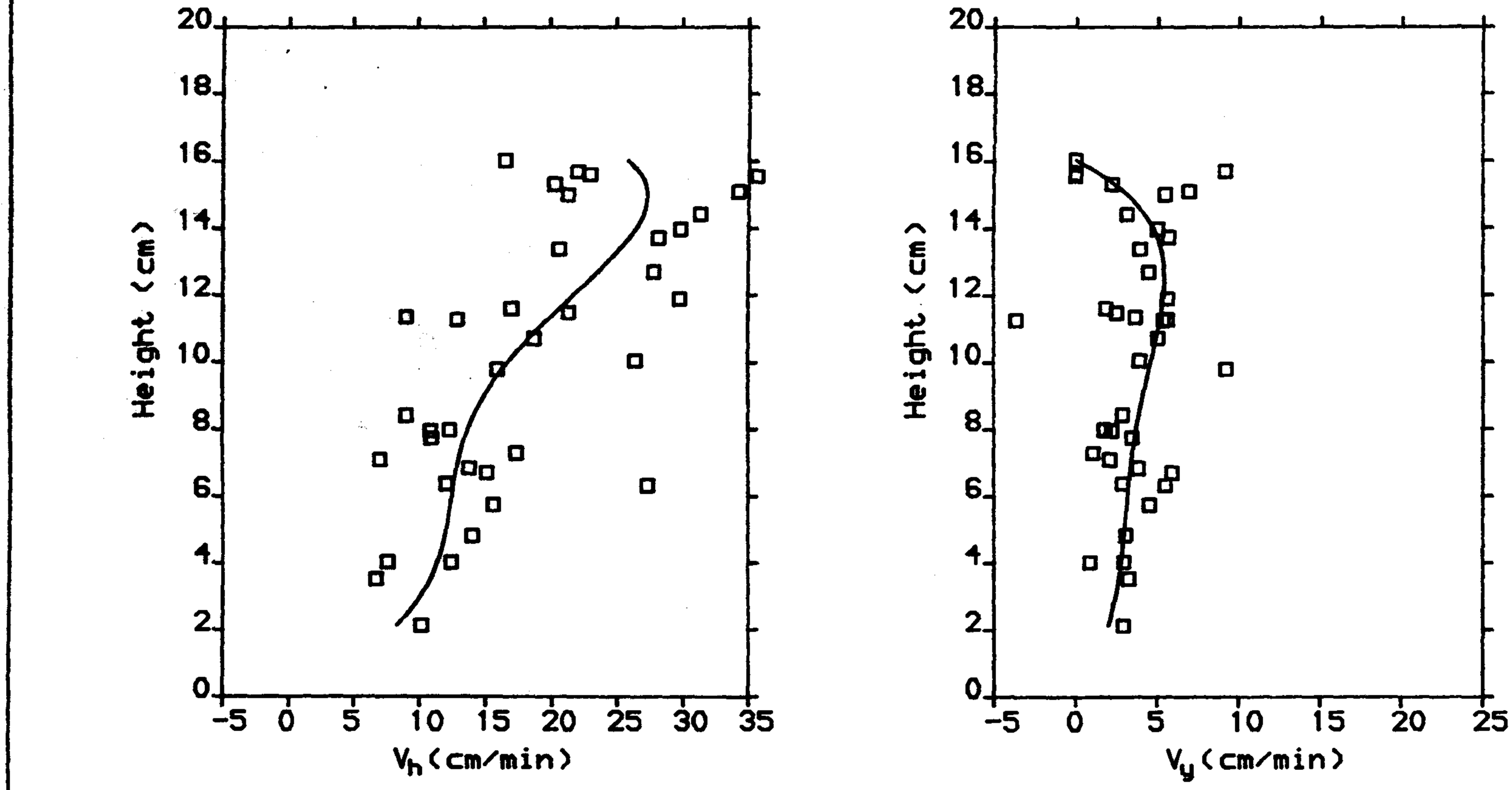

Velocity components at T= 40 (s) and y = 0.15 cm

USER: CHARNS PLOTFILE: FIGURE64 ENTRY NO. 44167 QUEUED ON 27/04/88 AT 08:12 PLOTTED ON 28/04/88 AT 14:11

Velocity components at T= 40 (s) and y = 0.65 cm

C_o = 0.2

Figure (6.4)

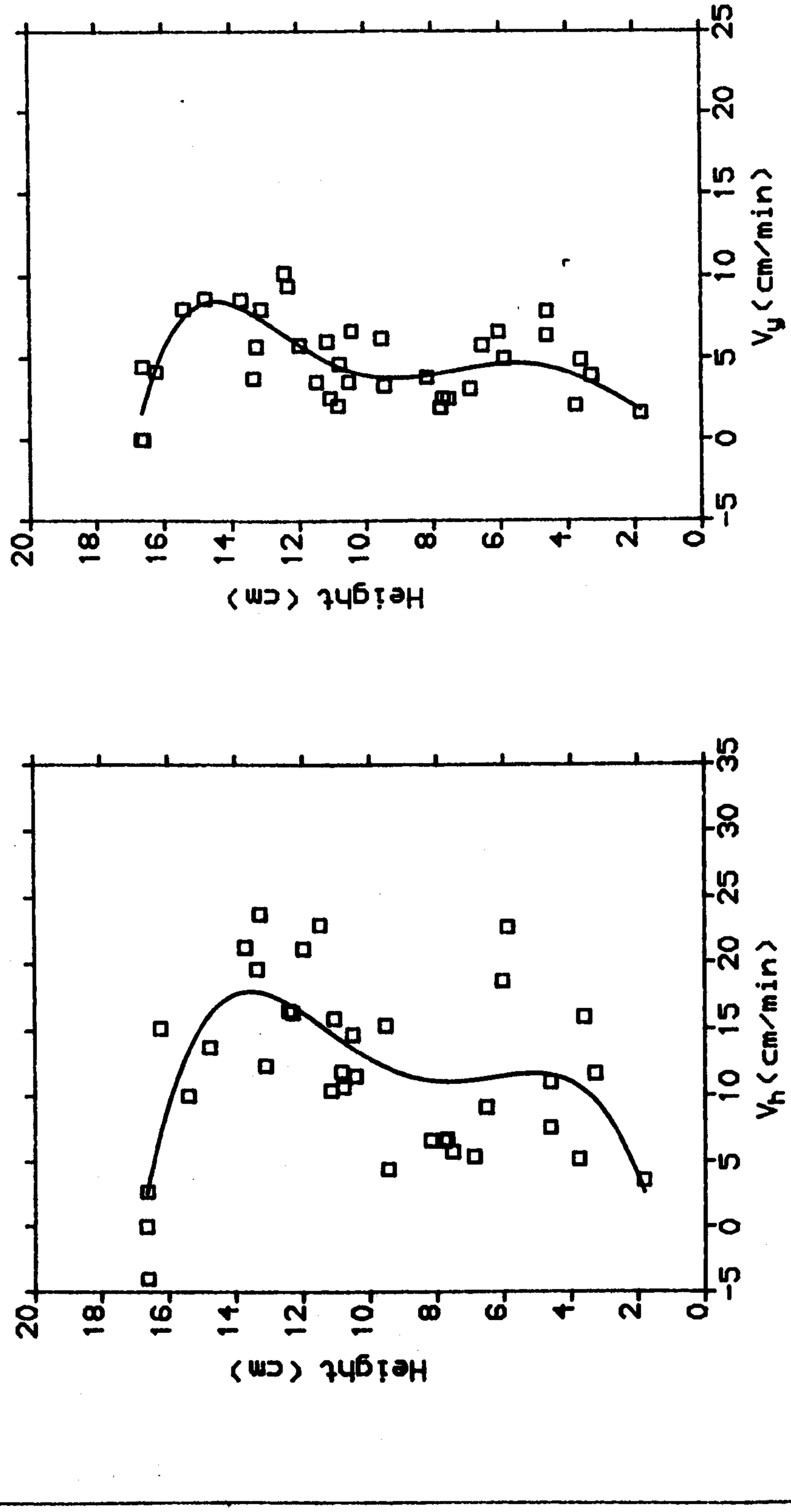

Figure (6.5) T = 40 (s) C_o = 0.2

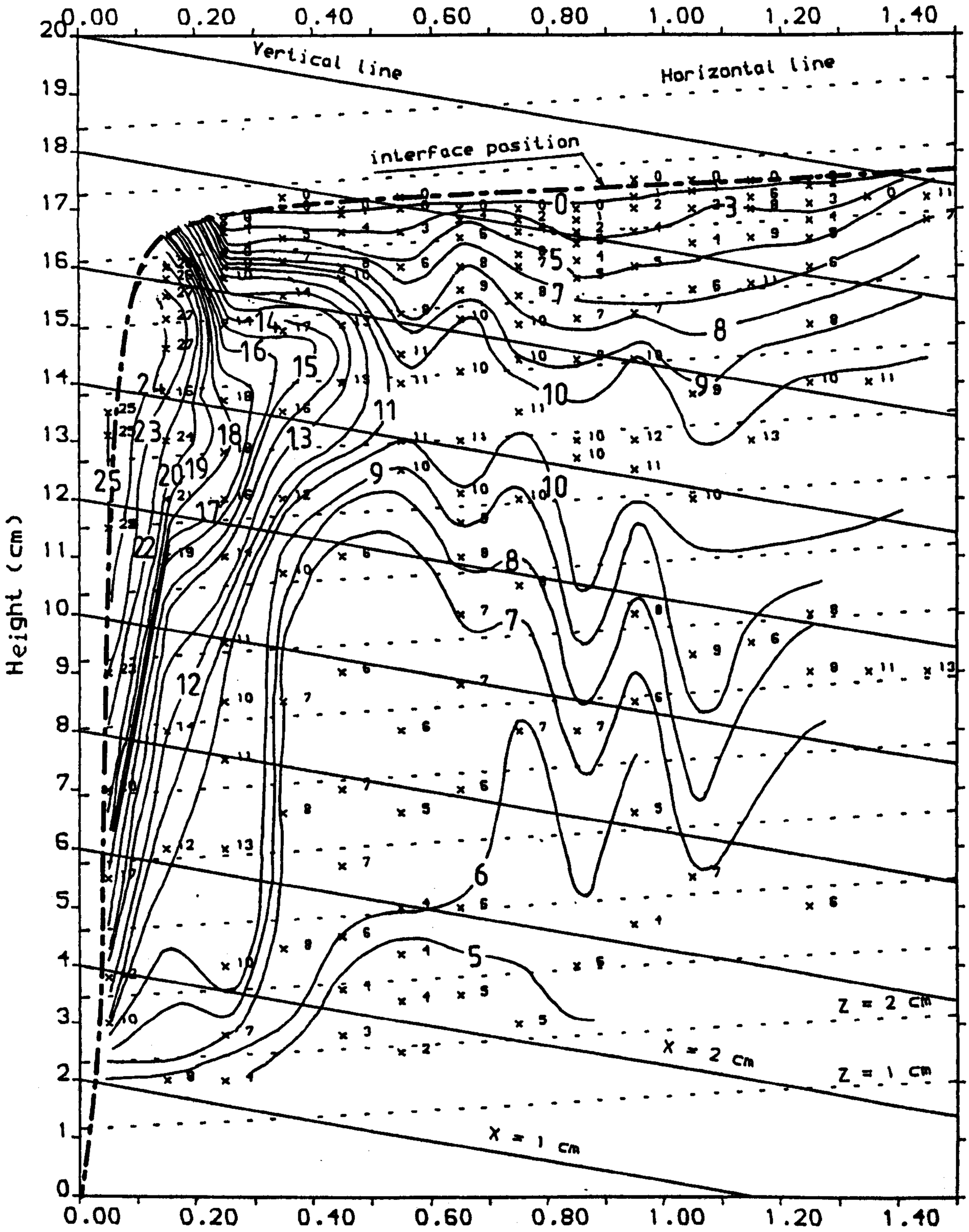

Contours and the velocity components of V_h(cm/min)

Figure (6.6) T = 40 (s) C_o = 0.2

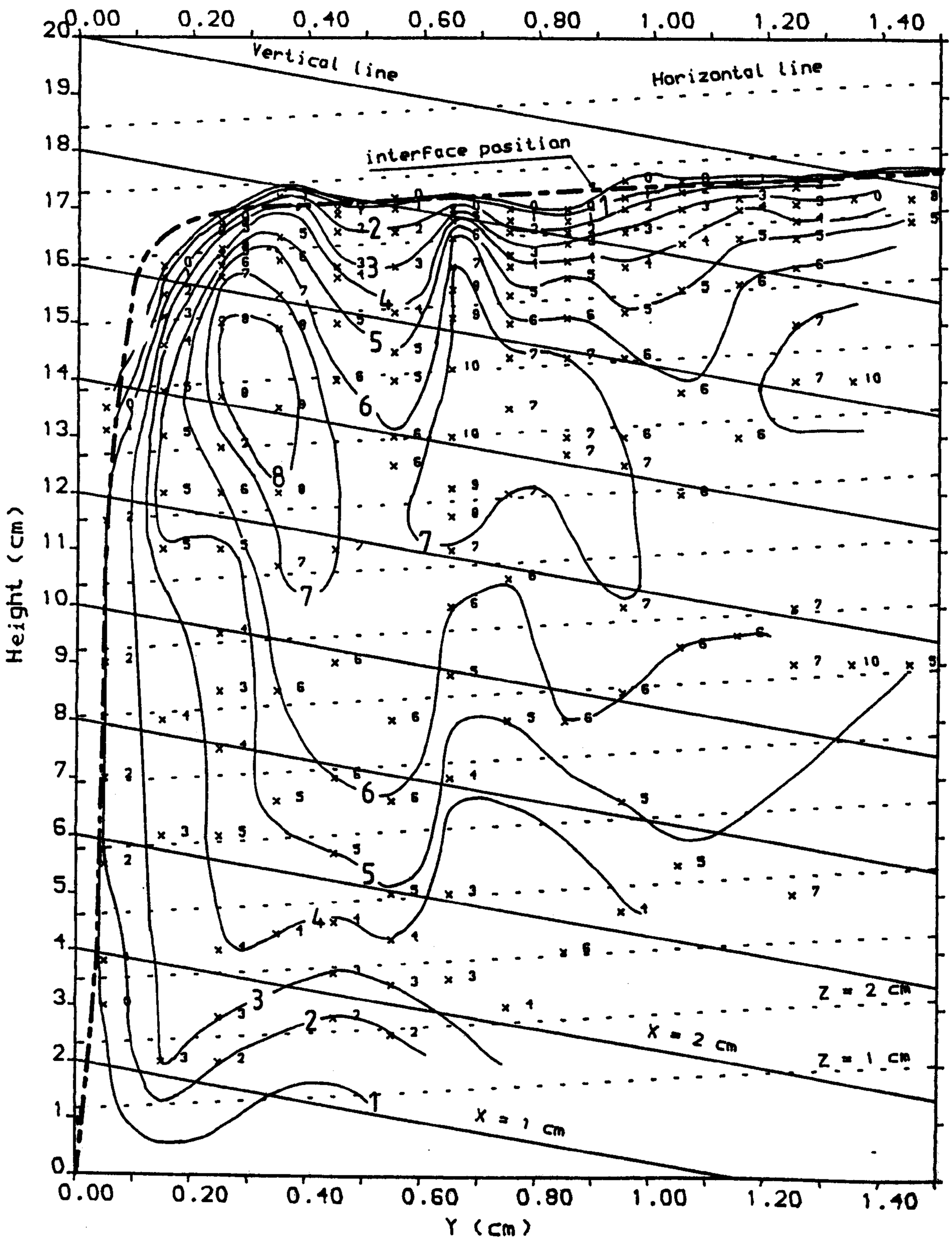

Contours and the velocity components of V_y(cm/min)

Figure (6.7) T = 40 (s) C_o = 0.2

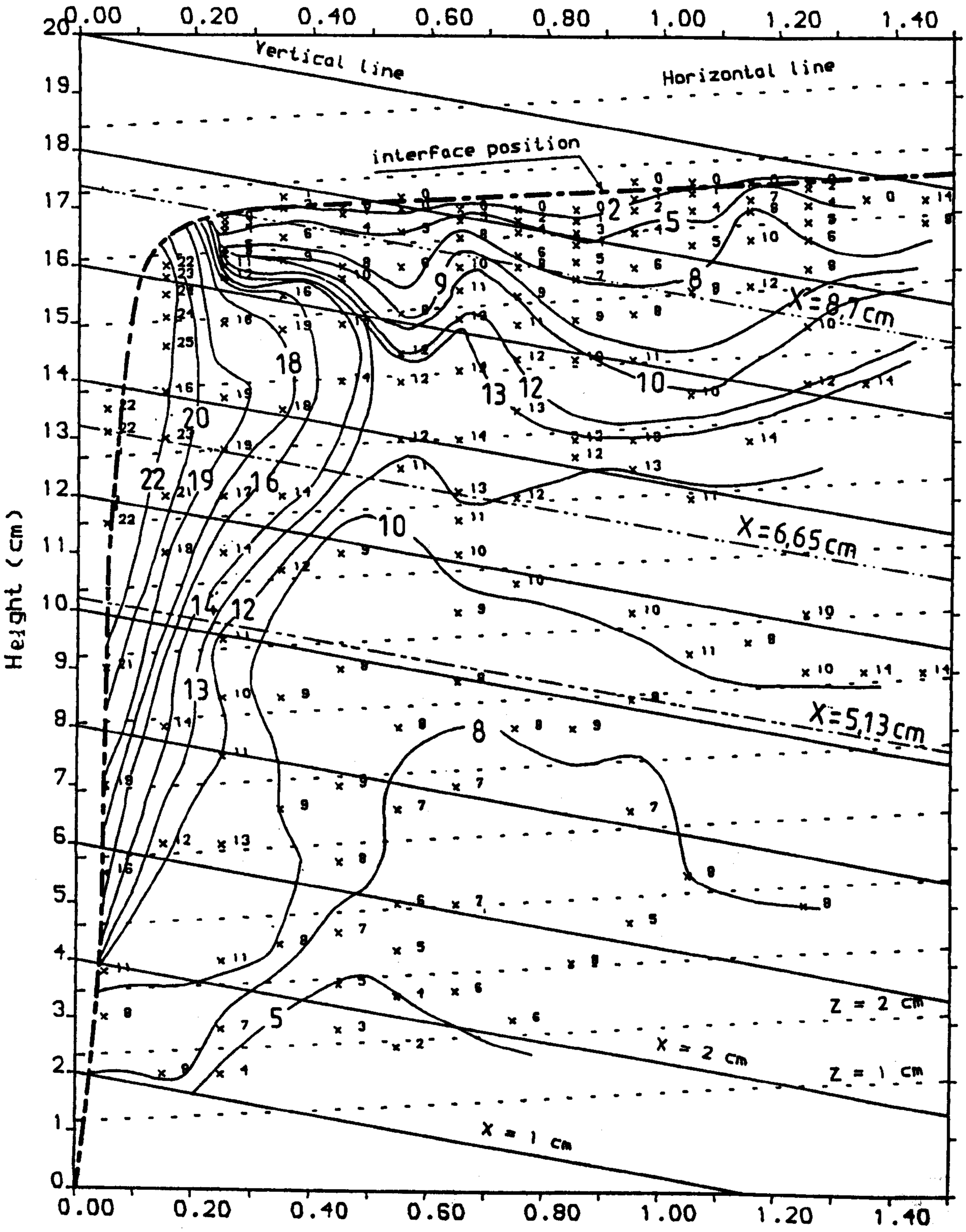

Contours and the velocity components of V_z (cm/min)

Figure (6-8) T = 40 (s) C_o = 0.2

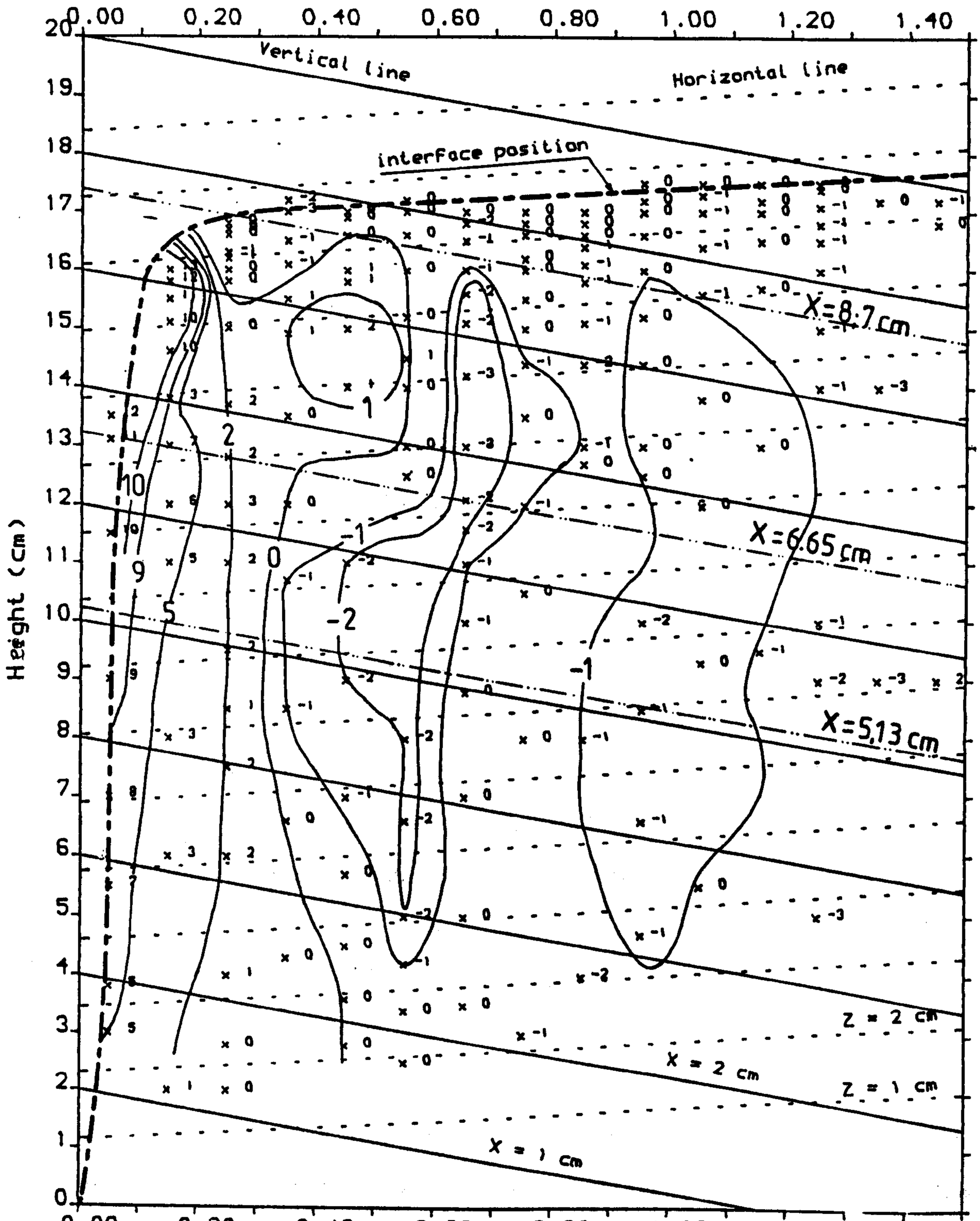

Contours and the velocity components of V_x (cm/min)

Figure (6.3) illustrates the velocity vectors V_h and V_y at y = 0.15 ± 0.05 as an example of the V_h - H and V_y - H plots the smoothed curves in the same figure represent the experimental relationship for V_h and V_y against the suspension height. Figure (6.4) shows the corresponding data at y = 0.65 ± 0.05 cm. Data for the whole range of y values over the settling column for V_h and V_y are presented in figures (6.5) and (6.6) which show the velocity contours for each of the components.

It is also extremely useful to examine the velocity components in the z-x frame. They are V_z and V_x, where V_z is the vertical velocity component (taken as positive as z increases) and V_x is the horizontal component (see figure 6.2 taken as positive from the upper sloping wall). Flow in the z direction coincides with the direction of gravity and is strongly indicative of buoyancy-induced motion. V_z and V_x can be deduced from figures (6.5) and (6.6) as factors of V_h and V_y. From figure (6.2) V_z and V_x can be written

$$V_z = V_h \cos 30 - V_y \sin 30 \qquad \ldots\ldots (6.1)$$

and

$$V_x = V_h \sin 30 + V_y \cos 30 \qquad \ldots\ldots (6.2)$$

Figure (6.7) and (6.8) show the velocity vectors and components for V_z and V_x respectively. Overall figures (6.5) to (6.8) show clearly the flow pattern within the suspension core and suggest that the suspension column can be classified into four zones based on velocity behaviour (see figure 6.9).

Zone I - adjacent to the inclined interface. It has a thickness of 0.2 cm which is about 2 to 3 times the thickness of the clear- fluid layer. Along this layer all the velocity components show an inclination in its values, V_h, V_z tend to increase rapidly towards the clear fluid channel while V_y values tend to decrease. V_y decreases rapidly at the edge of the clear-fluid layer

Zone II - the top interface layer. It has a thickness of about 2 cm. In this layer all the velocity components are reduced to zero at the top interface where $H = H_{in}$

Zone III- the corner at which horizontal interface meets the inclined one. It is a mixing zone where the fluid tend to return back to mix with the suspension.

Zone IV - The suspension core zone. It occupies most of the settling column. Within this zone V_h, V_y and V_z have a horizontal velocity contours which increase in value with the height of the column until it reaches the bottom of the zone II. After that the velocity vectors decreases towards the top interface. For the velocity components V_x the contours are verticals in zone IV.

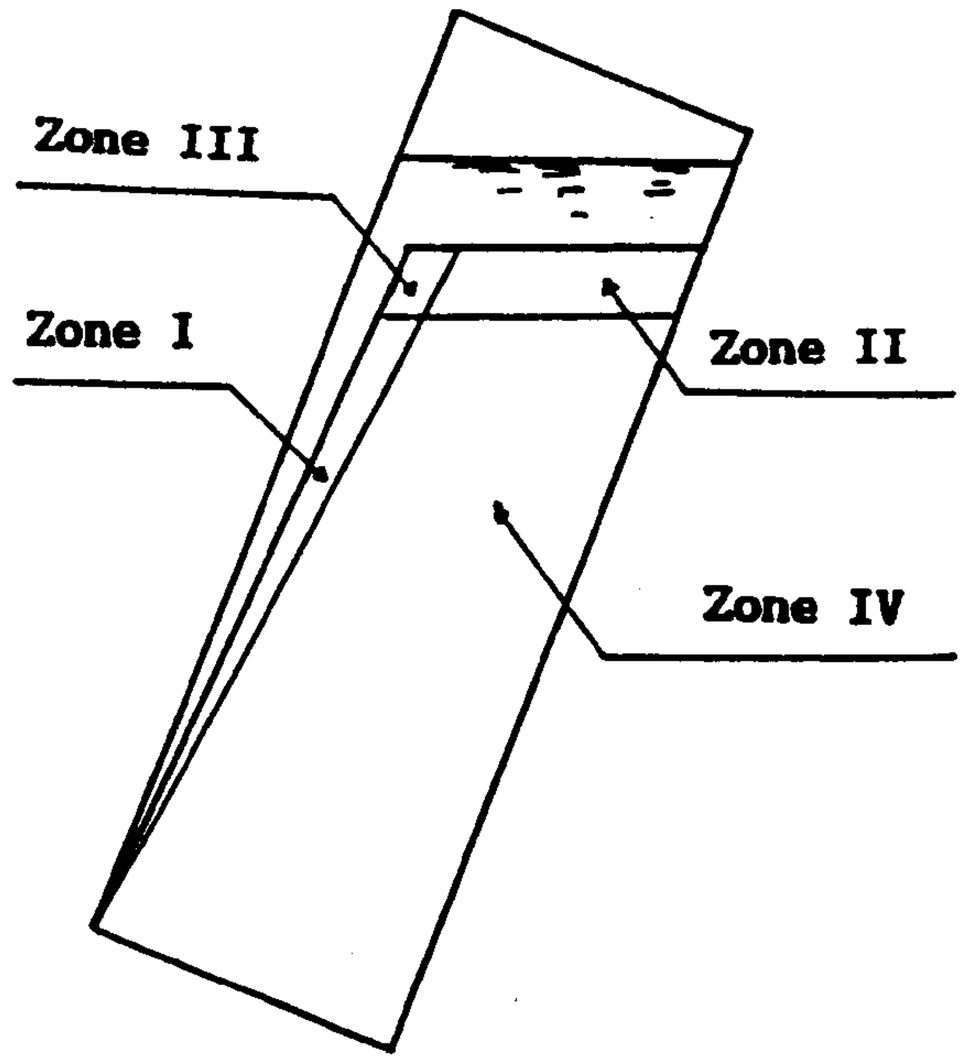

Figure (6.9) Zones of suspension core and the velocity behaviour

Figure (6.10) shows V_y the distribution across the settling column for H = 4, 8, 11 and 13 cm.

Since V_h is virtually parallel to the clear fluid channel, V_y is essentially the only component of the fluid motion which can feed the clear-fluid layer .

Values of velocity components V_y at the inclined interface represents the feeding velocity into the clear-fluid layer.

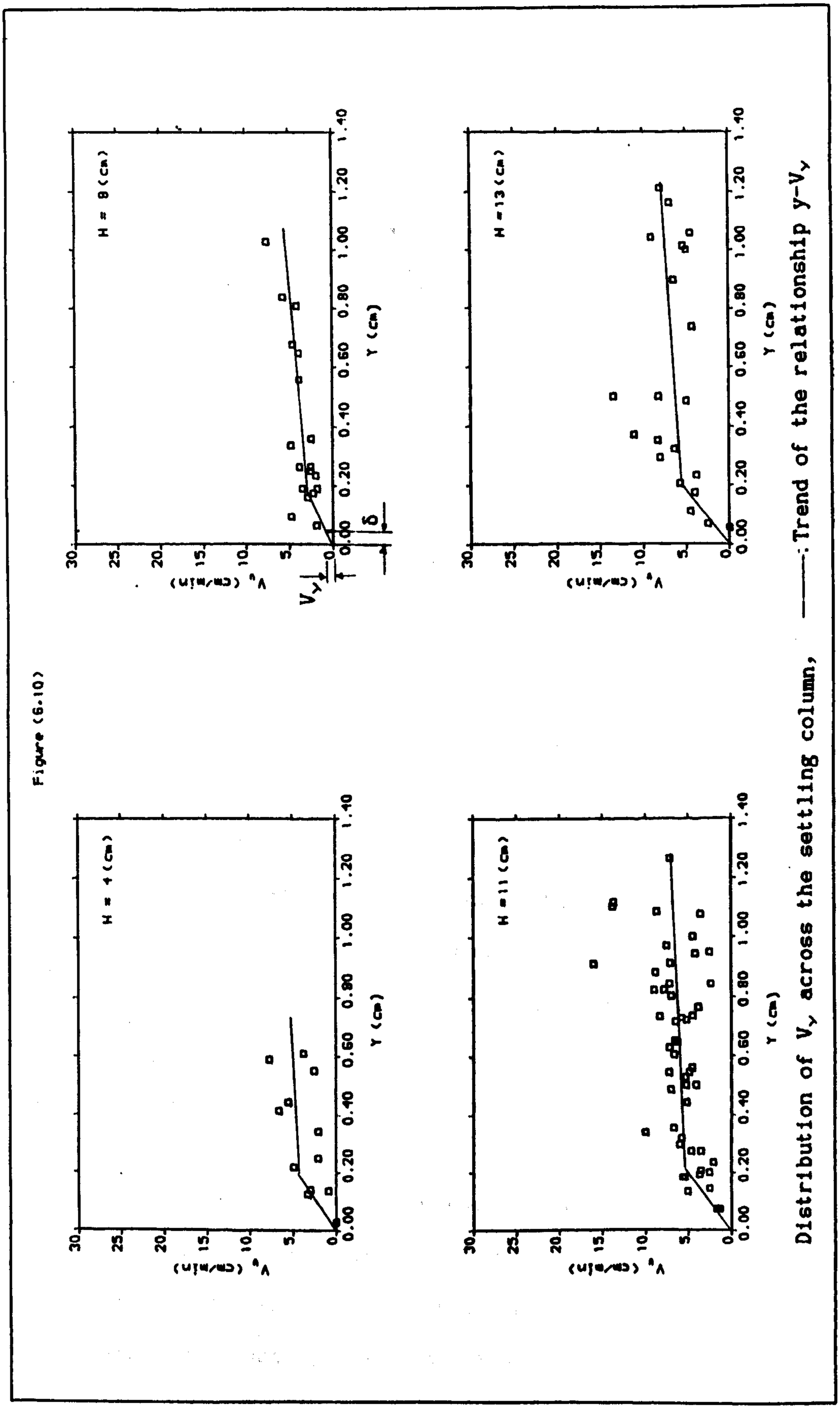

Figure (6.10) Distribution of V_y across the settling column, ——: Trend of the relationship y-V_y

6.5 Investigation of the ' feeding velocity ' ($V_{y,f}$)

In section (5-4) the 'feeding velocity' $V_{y,f}$ was given as a function of the fluid infiltration q through a unit surface of the inclined interface and C, the local solids concentration at the inclined interface

$$V_{y,f} = q / (1-C) \qquad \ldots.(6.3)$$

q can be considered the gradient of the relationship Q - H

$$q = dQ/dH$$

The value of C is very important in calculating V_y. In an inclined settling tube, the solids concentration was shown to increase (with height) along the settling column and this increase becomes more evident with the passage of time (see figure 5.11). At any given level H the concentration must change across zone I (see section 6.4) from the suspension column where the concentration is C to the particle-free fluid (ie C = 0) within the clear-fluid channel. This rapid decrease in the solids concentration is accompanied by a rapid decrease in the velocity components V_y.

Thus it is seen that the feed velocity $V_{y,f}$ lies between the limits

$$q \leq V_{y,f} \leq q/(1-C) \qquad \ldots.(6.4)$$

where C is the solids concentration of settling suspension at level H.

Values of $V_{y,f}$ were compared with the observed values of V_y along the inclined interface in figure (6.10). Figure (6.11) shows a comparison between the velocity component V_y at

$y = \delta$, and the values $V_{y,f}$ deduced via equation (6.4)

From figure 6.11 the fluid infiltration into the clear-fluid layer seems to have two distinct regions along the inclined interface; the bottom region from the tube base to the level H = 9 cm the infitration has a slight increase towards the upper part of the tube and $V_{y,f}$ has a mean value of 0.41 $\left[\frac{cm^3}{cm^2\ min} \right]$. In the region above the level H = 9 cm $V_{y,f}$ values increases very rapidly until the level H = 11 cm, where it has the value 1.2 cm/min. Above the level H = 11 cm the $V_{y,f}$ value remains constant. The value of the velocity component V_y can be considered to be of the same order of magitude as $V_{y,f}$ but it has different behaviour as it increases linearly from the bottom of the settling tube until the elevation H = 12.5 cm at which V_y value starts to fall. It appears to reach zero at H = 14.4 cm. NB the interface is at H = 17.3 cm at the corresponding time.

Figure (6.11) $C_0 = 0.2$

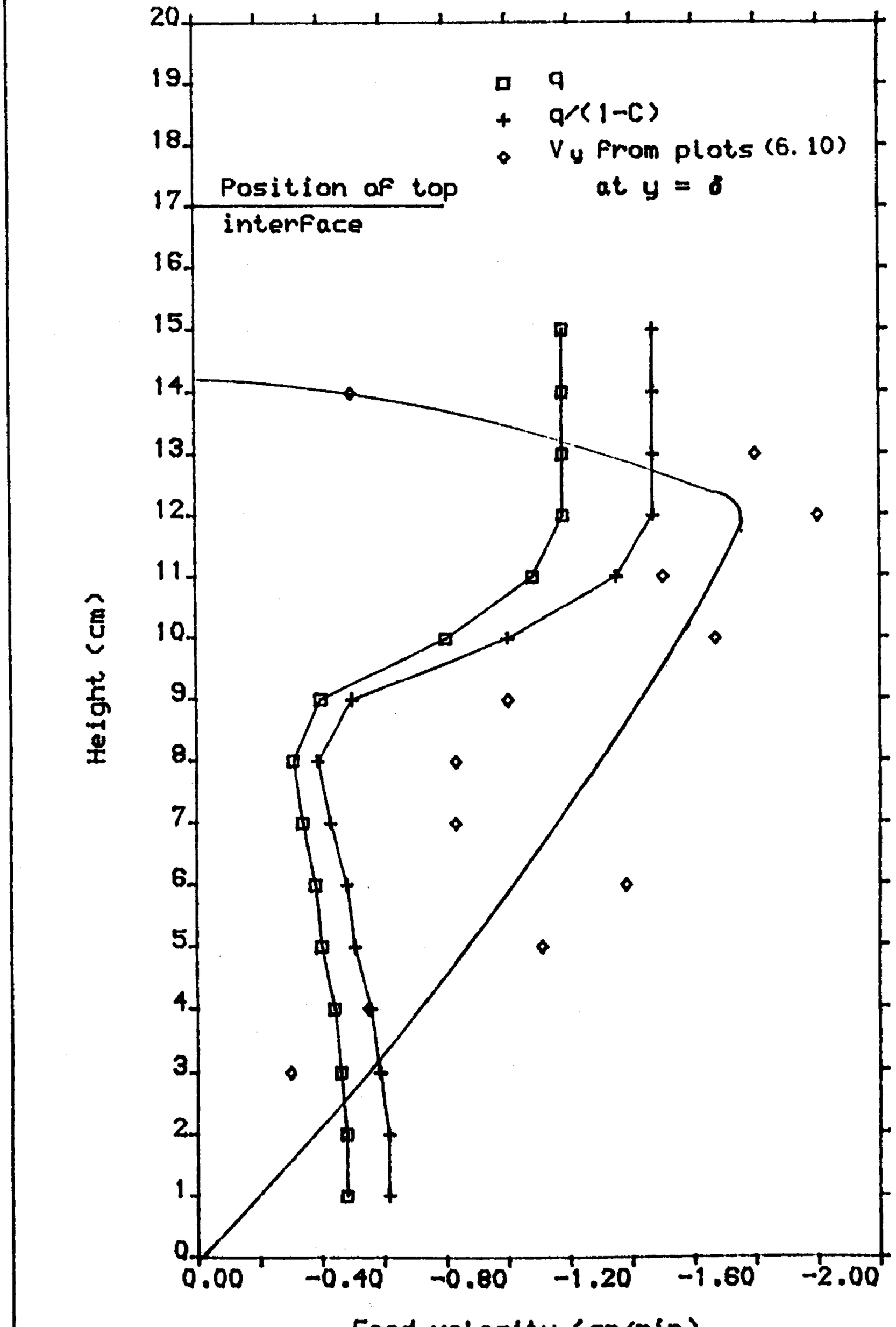

Comparison between V_y and q

6.6 $V_{y,r}$ and the continuity equation within the clear-fluid layer

As further insight into the properties of the $V_{y,r}$, the continuity equation will be examined to try and acertain the effective position of the feed interface compared with the position of channel interface. Within the clear-fluid layer the continuity equation has the form

$$\frac{dV_h}{dh} + \frac{dV_y}{dy} = 0 \qquad \ldots\ldots (6.5)$$

where $V_h \approx V_p$ is the upward velocity along the clear-fluid channel and Vy is the velocity feeding the flow from suspension in the direction y measured from the upper wall. Using the equation (6.5), the distance δy over which the velocity changes by δV_y may be stated as:

$$\delta y = - \frac{\delta V_y}{dV_p/dh} \qquad \ldots\ldots (6.6)$$

The term dV_p/dh can be evaluated from the gradient of the plot V_p-H (see figure 6.5) at time 40 s and δV_y identified with $(V_{y,r} - 0)$ in figure (6.11) ie the distance across which V_y is reduced to zero.

Table (6.1) summarizes the calculation of δy and δV_y and figure (6-12) shows a comparison between δy and δ the width of the clear fluid layer measured directly along the inclined interface (both with origin at the y = 0). The change in behaviour between the upper and lower part of the inclined interface appears again in the comparison between δ and δy as shown in figure (6.12). At the upper part the plane

from which q originates seems to be inside the suspension core. As yet ther is no explanation for this peculiar feature.

Table (6.1)
Calculation of δV_y and δy from the flow within the clear-fluid layer and a comparison with the directly measured values of δ and V_y

H cm	Conc.	q= dq/dh cm^3/min	V_y = -q/(1-C) cm/min	dVy/dy= $-dV_p/dh$ (1/s)	δy (cm)	δ (cm)	V_y cm/min
1	0.220	0.48	-0.615	-6.20	0.077	0.025	****
2	0.220	0.48	-0.615	-5.70	0.084	0.025	****
3	0.215	0.46	-0.585	-5.50	0.084	0.041	0.30
4	0.210	0.44	-0.557	-5.20	0.085	0.041	0.55
5	0.210	0.40	-0.506	-4.70	0.085	0.041	1.11
6	0.210	0.38	-0.481	-4.75	0.080	0.041	1.38
7	0.205	0.34	-0.428	-4.08	0.083	0.041	0.83
8	0.202	0.31	-0.388	-3.75	0.083	0.040	0.83
9	0.200	0.40	-0.500	-3.50	0.114	0.040	1.00
10	0.200	0.80	-1.000	-3.00	0.270	0.050	1.67
11	0.200	1.08	-1.350	-2.70	0.400	0.062	1.50
12	0.200	1.18	-1.470	-2.10	0.560	0.062	2.00
13	0.200	1.18	-1.470	-0.83	1.420	0.069	1.80
14	0.200	1.18	-1.47	*****	*****	*****	0.50
15	0.200	1.18	-1.47	*****	*****	*****	****

Figure (6.12) C_0= 0.2

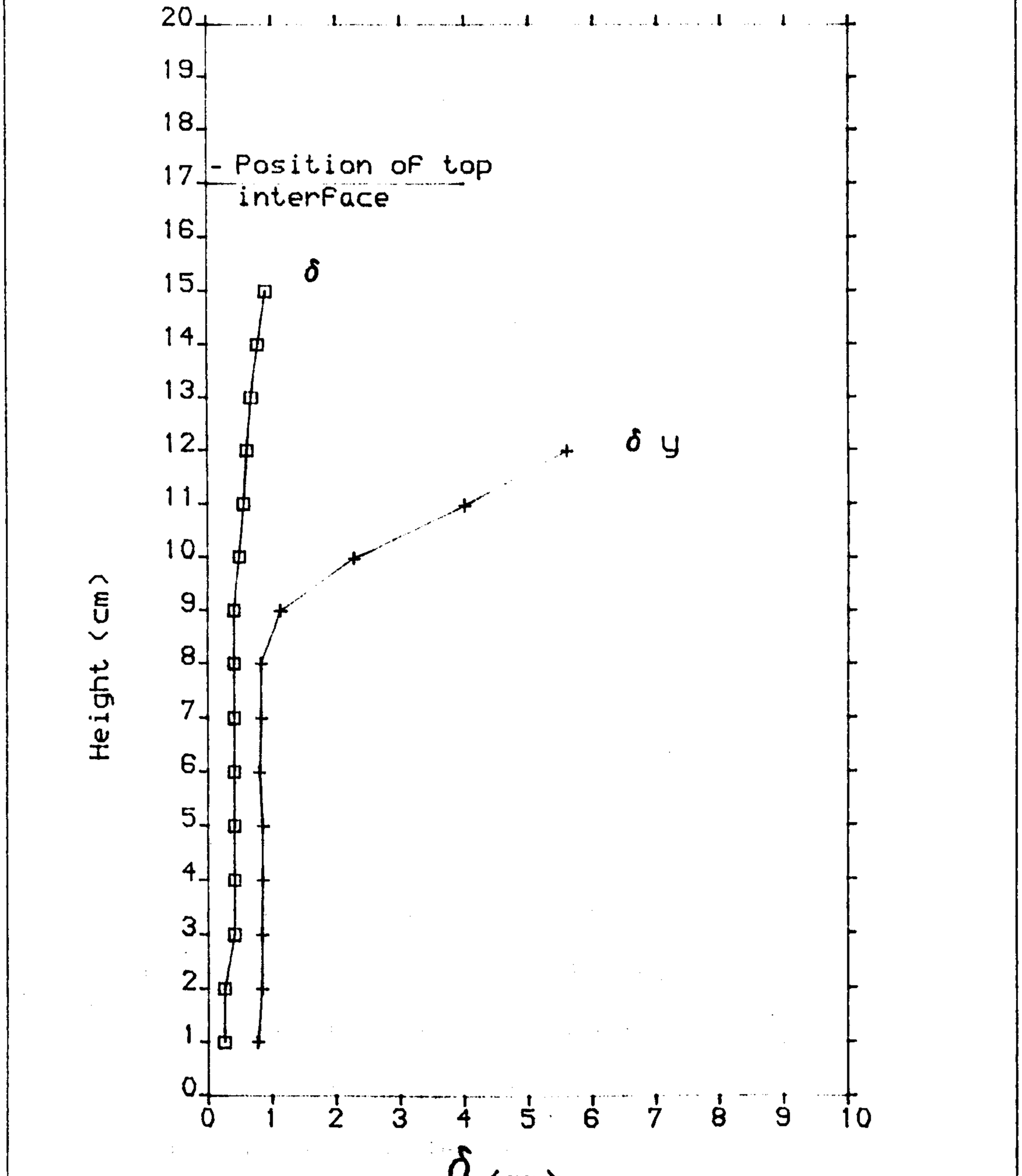

Comparison between δ and δ_Y

6.7 Check on velocity of dye tracer in the case of vertical tube

As a check on the representation of interstitial flow using the dye tracer, it was tested in a media in which the settling velocity is already known. The same settling conditions described in section (6.3) was used to measure the velocity of ascending dye drop in vertical tube. 71 observations were carried out at different point of the settling column. The dye tracer had always an upward velocity of vertical direction and mean value

$$V_d = 5.56 \pm 0.58 \quad \text{(cm/min)}$$

(Errors refer to 95% confidence limit). Assuming that the solids concentration of the suspension is $C_o = 0.2$, the settling velocity of the particles within the suspension V_s is

$$V_s = 5.56/0.8$$

$$V_s = 6.95 \text{ cm/min}$$

From table (4.3) in section (4.3.4) the vertical settling velocity of the same suspension in 0.648 cm/min

Thus there is an adjustment factor f determined by

$$f = 6.95/0.648$$

This suggests that the velocies measured by observing the dye tracer might have to be reduced by a factor shown by (f = 10.7) in order to provide a good estimates of the real fluid velocities within the suspension.

6.8 Check on observed velocity within suspension

Since the velocity components in figures (6.5) to (6.8) show a very high values compared with the vertical settling velocity of a suspension which have the same settling conditions (concentration, particles diameter and fluid viscosity) and since the check on the velocity of dye tracer (in section 6.7) in a vertical tube showed an enhancement of the dye velocity by a factor of 10.7, it was considered that the enhancement might be due to the difference in density between the dye solution and the suspension.

To find out whether the enhancement in the upward velocity of the dye tracer affects only the vertical velocity component or the total velocity vectors, the continuity equation was checked in the directions z-x as distenct from the H - y coordinate systems. The continuity equation has the form

$$\frac{dV_x}{dz} + \frac{dV_z}{dx} = 0 \qquad \ldots\ldots (6.7)$$

Integration of (6.7) at an arbitrary position z at a fixed coordinate x_o yields

$$V_x(x_o, z) - Vz(x_o, z_1) = -\int_{z_1}^{z} \left(\frac{dV_z(x_o, z)}{dx} \right) \cdot dz \qquad \ldots\ldots (6.8)$$

It is convenient to subdivide the integral into a series of discrete steps of interval Δz in which (see figure 6.13)

$\frac{dV_z}{dz}$ is regarded as a constant (the average value $\overline{\frac{dV_z}{dx}}$ within the interval) and leads to

$$Vz(x_o, z) - V_o\ (x_o, z_1) = -\ \Delta z \sum_{i=1}^{n} \overline{\frac{dvx}{dx}}\ (x_o, z) \qquad \ldots\ldots (6.9)$$

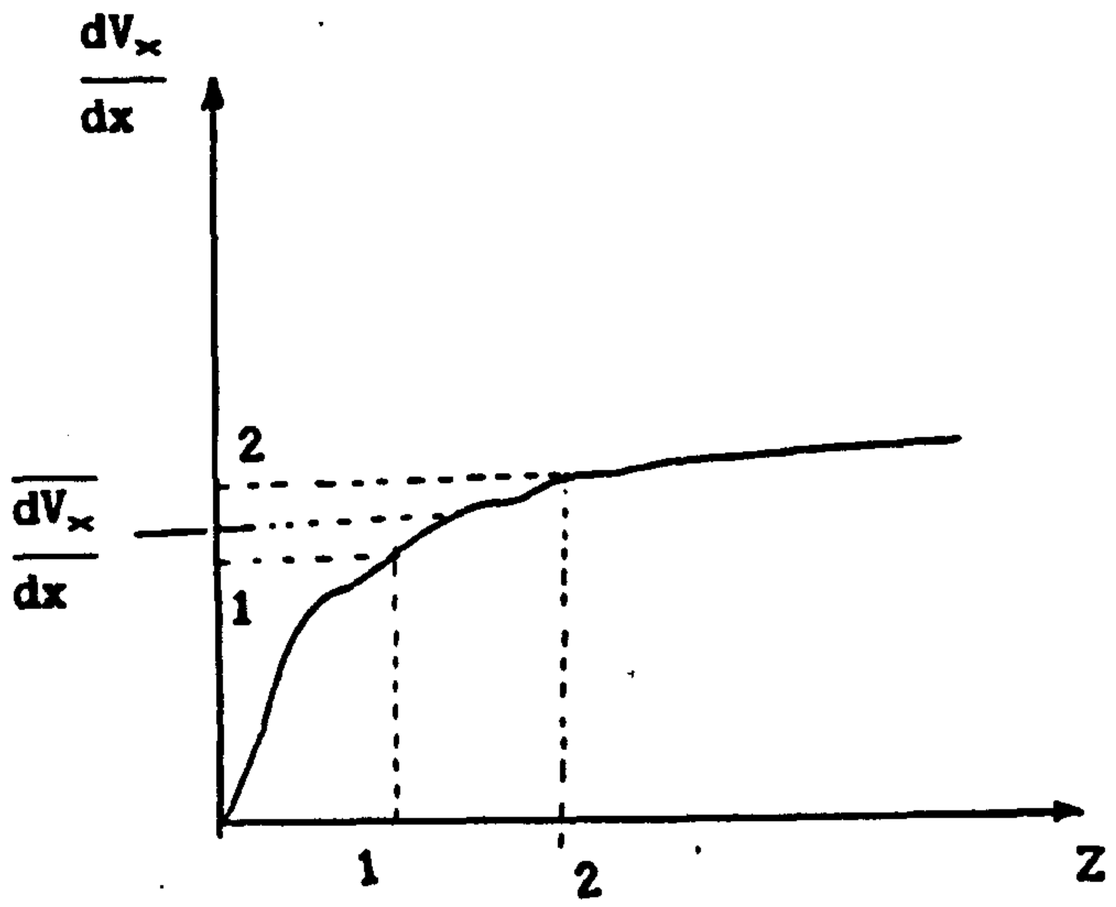

Figure (6.13): Illustrative scheme for the extrapolation

$$V_x(x_o, z_2) - V_o\ (x_o, z_1) = \Delta z \sum_{i=1}^{n} \overline{\frac{dv_x}{dx}}(x_o, z) \qquad \ldots\ldots (6.10)$$

6.9 The co-ordinates Z - X

In the previous section the data were analysed in the H - Y frame (see figure 6.14). To examine the continuity equation in terms of velocity components V_z, V_x a new pair of co-ordinates z-x have to be introduced, the relationship between the h-y and x-z coordinates must be determined by rotation of the coordinate axis shown in figure (6.14)

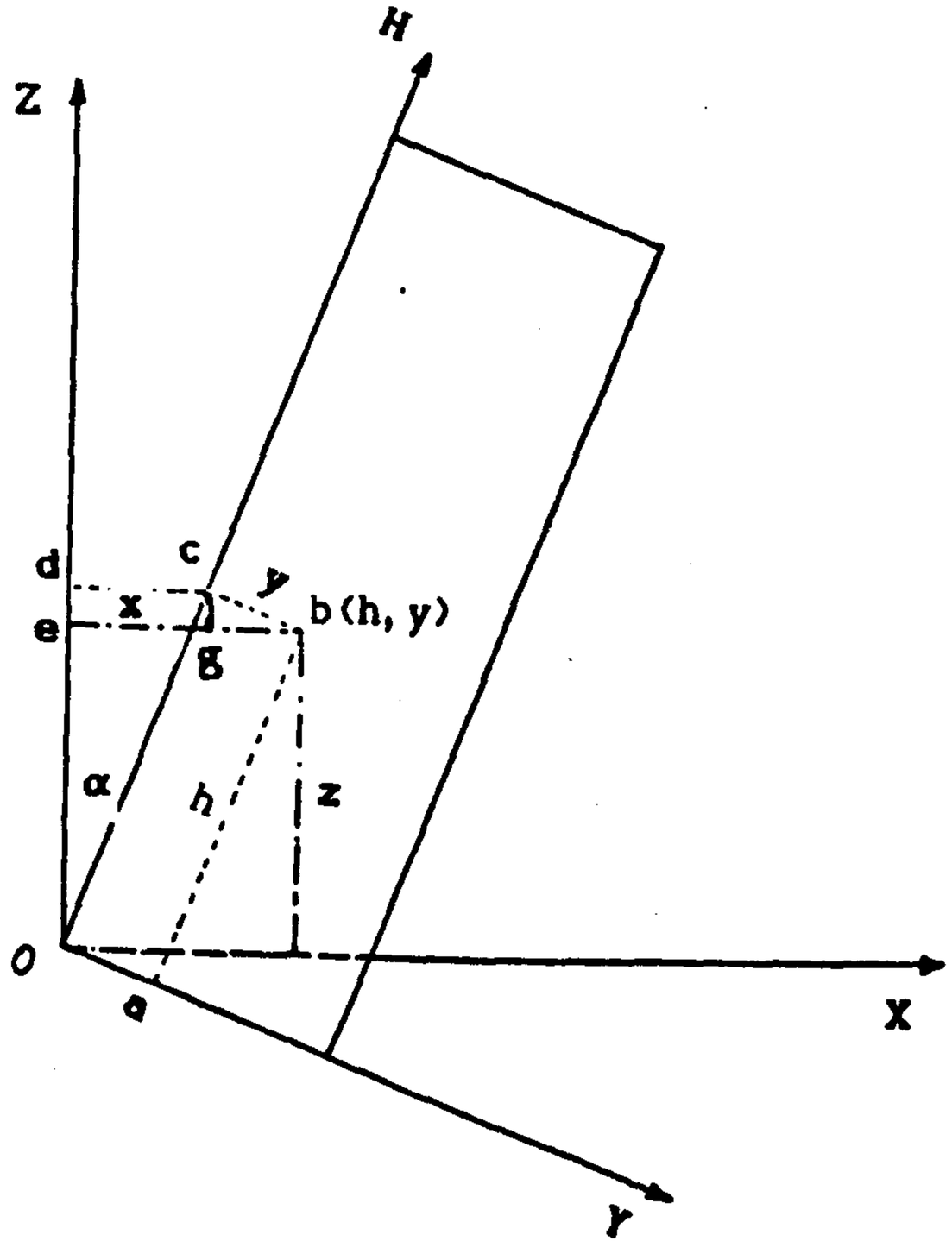

Figure (6.14): Co-ordinates H - Y and Z - X

From figure (6.14) it is seen that

$z = \overline{oe}$ $\qquad\qquad$ $x = \overline{eb}$

$z = \overline{od} - \overline{ed}$ $\qquad\qquad$ $x = \overline{eg} - \overline{gb}$

$z = h\cos\alpha - y\sin\alpha$ $\qquad$ and $\qquad$ $x = h\sin\alpha + y\cos\alpha$ ....(6.11)

Equations (6.11) can be rearranged to give the co-ordinates h - y as a functions of z and x. Thus when $\alpha = 30^{\circ}$ and $x = x_o$

$h = x\sin 30 + z\cos 30$ $\qquad$ and $\qquad$ $y = x\cos 30 - z\sin 30$

To carry out the calculations of V_z, plots (6.7) and (6.8) were used. Calculations were applied on 3 vertical lines where x_o = 5.1, 6.65 and 8.7 cm. x_o values were chosen to represent bottom (as far as data was collected) middle and top area of the settling column. x_o lines are

shown in figures (6.7) and (6.8). Values of V_o was chosen at (x_o , z) corresponding to y = 0.65 cm.

Tables (6.3) to (6.5) summarize the calculations of V_z deduced from the initial value V_o following the continuity equation and the observed values taken from figure (6.7) along the vertical lines at the positions x_o. Figure (6.15) shows the comparison at each x_o value.

It demonstrates that away from the top interface (zone II) the continuity equation appears to hold within the suspension core on the frame z-x

Since the data in tables (6.3) to (6.5) are taken within the range y = 0.25 cm and y = 0.65 cm, the errors on the velocity vectors V_z and V_x are calculated within this range and averages σ_{vz} and σ_{vx} are considered.

σ_{vz} and σ_{vx} were calculated from the values σ_{vv} and σ_{vh}. The distribution of the data differs between the upper part of the column and the lower part. Therefore the errors are calculated twice, for the lower part *of* the settling column, where H = 6-11 cm, and for the upper part where H = 11-16 cm. From equations (6.1) and (6.2)

$$V_z = V_h \cos 30^\circ - V_v \sin 30^\circ$$

$$Vx = V_h \sin 30^\circ + V_v \cos 30^\circ$$

$$(\sigma_{vz})^2 = \left(\frac{\partial_{vz}}{\partial_{vh}}\right)^2 (\sigma_{vh})^2 + \left(\frac{\partial Vz}{\partial_{vv}}\right)^2 (\sigma_{vv})^2$$

$$(\sigma_{vx})^2 = \left(\frac{\delta_{vx}}{\delta_{vh}}\right)^2 (\sigma_{vh})^2 + \left(\frac{\delta Vx}{\delta_{vy}}\right)^2 (\sigma_{vy})^2$$

$$\delta_{vz} = \sqrt{(\cos 30^\circ)^2 (\sigma_{vh})^2 + (\sin 30^\circ)^2 (\sigma_{vy})^2} \quad \ldots\ldots (6.12)$$

$$\delta_{vx} = \sqrt{(\sin 30^\circ)^2 (\sigma_{vh})^2 + (\cos 30^\circ)^2 (\sigma_{vy})^2} \quad \ldots\ldots (6.13)$$

Table (6.2) summarizes the calculations and contains the errors on velocity components V_h, V_y, V_z and V_x at y = 0.25 cm and at y = 0.65 cm

Table (6.2): Errors on the velocity vectors

y cm	H range cm	σ_{vh}	σ_{vy}	σ_{vz}	σ_{vx}
0.25	15.5 - 11.5	3.04	1.42	2.73	1.38
0.65	16.5 - 11.5	2.47	2.20	2.40	1.60
0.25	11.0 - 9.0	1.21	0.61	1.09	0.57
0.65	11.0 - 6.0	1.19	1.43	1.37	0.97

The average values of errors are

σ_{vz} (H = 16,5 - 11,5) (2.73 + 2.4)/2 = 2.56 cm/min

σ_{vx} (H = 16,5 - 11,5) (1.38 + 1.6)/2 = 1.49 cm/min

σ_{vz} (H = 11 -9) (1.09 + 1.37)/2 = 1.17 cm/min

σ_{vx} (H = 11 -9) (0.57 + 0.97)/2 = 0.77 cm/min

Table (6.3): Calculation for continuity equation on the frame z-x at X_o = 5.13 cm

Z cm	$\frac{dV_x}{dx}$	$\overline{\frac{dV_x}{dx}}$	$\overline{\frac{dV_x}{dx}} \cdot \Delta Z$	$V_z (x_o, z)$ from Eq (cm/min)	$V_z (x_o, z)$ measured (cm/min)
7.0	+ 1.0			8.6 ± 0.77	8.6 ± 1.17
7.2	- 6.0	- 2.50	+ 0.50	9.1 ± 1.09	10.2 ± 1.17
7.4	- 3.3	- 4.65	+ 0.93	10.03± 1.09	9.0 ± 1.17
7.6	+ 3.3	0.00	0.00	10.03± 1.33	9.0 ± 1.17
7.8	+ 7.0	+ 5.15	- 1.03	9.0 ± 1.54	8.7 ± 1.17
8.0	- 3.7	+ 1.65	- 0.33	8.7 ± 1.72	8.5 ± 1.17
8.2	-22.5	-13.10	+ 2.62	11.3 ± 1.89	10.0 ± 1.17
8.4	-25.0	-23.75	+ 4.75	16.04± 2.03	12.0 ± 1.17
8.6	-36.5	-30.75	+ 6.15	22.2 ± 2.18	17.0 ± 1.17

Table (6.4): Calculation for continuity equation on the frame z-x at X_o = 6.6 cm

Z cm	$\frac{dV_x}{dx}$	$\overline{\frac{dV_x}{dx}}$	$\overline{\frac{dV_x}{dx}} \cdot \Delta Z$	V_z (x_o, z) from Eq (cm/min)	V_z (x_o, z) measured (cm/min)
9.3	- 3.0			11.90 ± 1.5	11.90 ± 2.6
9.5	+ 2.0	- 0.50	+ 0.10	12.00 ± 2.1	12.00 ± 2.6
9.7	+ 1.7	+ 1.85	- 0.37	11.63 ± 2.1	12.15 ± 2.6
9.9	+ 1.0	+ 1.35	- 0.27	11.43 ± 2.6	12.00 ± 2.6
10.1	+ 1.7	+ 1.35	- 0.27	11.16 ± 3.0	12.70 ± 2.6
10.3	- 2.0	- 0.15	+ 0.03	11.19 ± 3.3	12.50 ± 2.6
10.5	_ 9.3	- 5.65	+ 1.13	12.32 ± 3.6	11.90 ± 2.6
10.7	-17.0	- 13.15	+ 2.63	14.95 ± 3.9	13.95 ± 2.6
10.9	-23.0	-20.00	+ 4.00	18.95 ± 4.2	18.00 ± 2.6
11.1	-38.0	-30.50	+ 6.10	25.00 ± 4.5	20.00 ± 2.6
11.3	-41.0	-39.50	+ 7.90	32.95 ± 4.7	22.50 ± 2.6

Table (6.5) calculation for continuity equation on the frame z-x at X_o = 8.7 cm

Z cm	$\frac{dV_x}{dx}$	$\overline{\frac{dV_x}{dx}}$	$\overline{\frac{dV_x}{dx}} \cdot \Delta Z$	V_z (x_o, z) from Eq (cm/min)	V_z (x_o, z) measured (cm/min)
12.6	- 3.7			10.20 ± 1.5	10.20 ± 2.6
12.8	- 4.0	- 3.85	+ 0.77	10.97 ± 2.1	11.00 ± 2.6
13.0	0.0	- 2.00	+ 0.40	11.37 ± 2.1	9.80 ± 2.6
13.2	+ 4.3	+ 2.15	- 0.43	10.94 ± 2.6	7.20 ± 2.6
13.4	+ 0.7	+ 2.50	- 0.50	10.44 ± 3.0	6.60 ± 2.6
13.6	- 3.3	- 1.30	+ 0.25	10.69 ± 3.3	7.00 ± 2.6
13.8	- 0.7	- 2.00	+ 0.40	11.09 ± 3.6	7.00 ± 2.6
14.0	- 1.0	- 0.85	+ 0.17	11.26 ± 3.9	5.50 ± 2.6
14.2	- 2.7	- 1.85	+ 0.37	11.63 ± 4.2	4.50 ± 2.6
14.4	+ 6.6	+ 1.95	- 0.39	11.24 ± 4.5	4.00 ± 2.6

Figure (6.15)

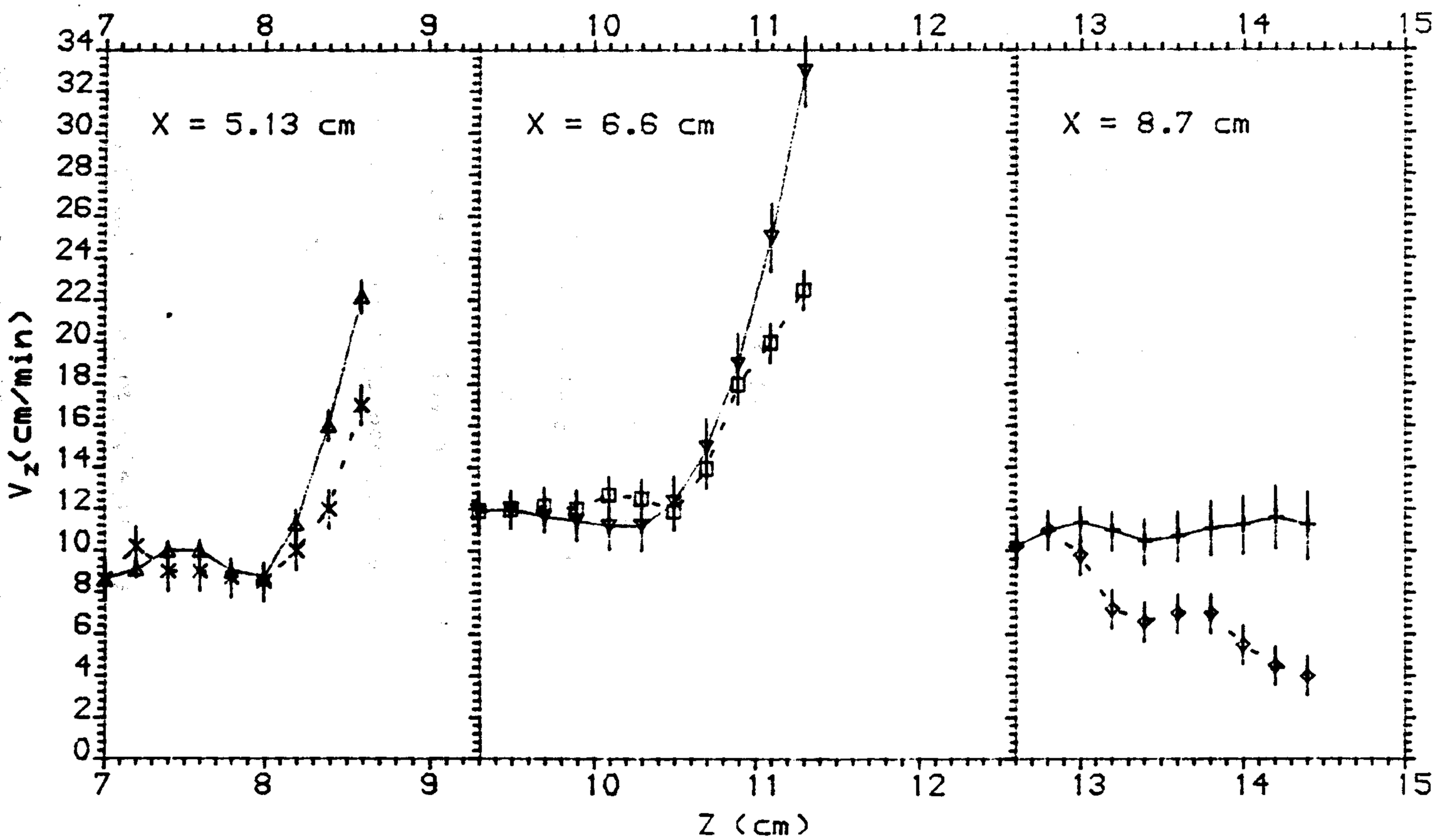

Comparison of V_z deduced from continuity equation and the experimental data
_____ :Continuity equation, ------: data from Figure 6.8)

6.10 Comment on velocity vectors

The continuity equation appears to be valid in the frame z-x in the core suspension zone IV only. This means that there is a velocity enhancement arising from the dye tracer technique, it applies to the total velocity vector and not just to the vertical component alone. If such a factor is considered to exist the question remains at to what is the reduction factor should be used. Table (6.1) suggests a mean value of

$$f = 9.86 \pm 1.56 \quad \text{at } y = 0.25 \text{ cm}$$

(the errors are the 95% confidence limit).

In section (6.7) the dye tracer injected within the same suspension in a vertical settling tube gave an enhancement factor

$$f = 10.72$$

Remembering the upward velocity of fluid within zone I (see section 6.4), a factor of 10 times is accepted as an enhancement factor for the total velocity vector.

6.11 Comparison with Acrivos et al's theory

Acrivos et al (1979) predicted the longitudinal velocity within the bulk suspension to be of the order $(\bar{R}^{-1/2}\Gamma^{1/6})$, (see section 3.3.3).

Using the exerimental data which are listed in table (5.2), the predicted values for U and V when C_o are,

$$V/V_o = 13.8$$

providing that $V_o = 0.664$

and $V = 13.8 \times 0.664$

$$V \simeq 9 \text{ cm/min}$$

In figure (6.5), the velocity vector within the bulk suspension (zone IV) is in the range 6-10 cm/min which is very close to the figure 9 cm/min predicted by Acrivos et al (1979)

6.12 Settling velocity within the suspension core

In section (5.3.4) the concentration distribution was measured along the inclined settling column. In this section, data of the concentration at time 40 s was used to deduce the change in the settling velocity along the suspension column. The relationship between velocity and concentration was taken from table (4.3). For the settling conditions used in this set of experimental work, the relationship is of the form,

$$V_c = 1.73\ (1-C)^{4.4} \qquad \ldots\ldots(6.14)$$

Figure (6.16) shows a comparison between the velocity vectors measured by the dye tracer after reducing them by a factor f = 10 and velocity value deduced from equation (6.12) for the concentration distribution at time 40 s

Figure (6.16) C_0 = 0.2

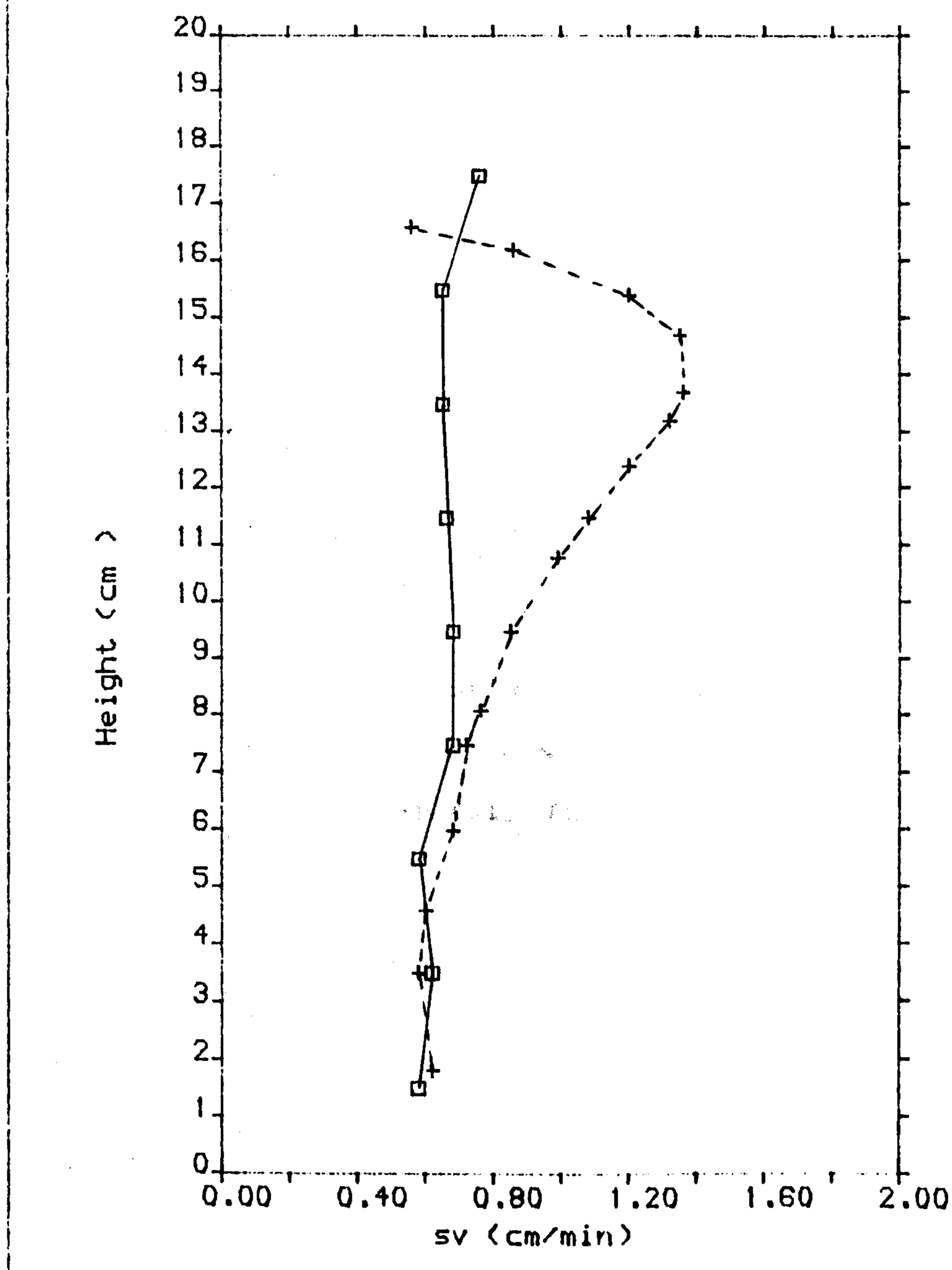

—□— sv From concentration measurements

—+— sv From observation of the Flow Field

Settling velocity within the suspension core

CHAPTER SEVEN

DISCUSSION AND CONCLUSIONS

CHAPTER SEVEN

DISCUSSION AND CONCLUSIONS

7.1 Introduction

In this work the flow field in the clear fluid channel and within the suspension core was studied for suspension under the concentration conditions C_o = 0.1 and C_o = 0.2.

This compares with previous experimental work reported in chapter three which has tended to concentrate on very dilute suspensions ie C_o<<0.1.

NB In some commercial Lamella settlers the slurry can be fairly concentrated. Also the values selected for C_o permited a direct test of the Acrivos et al's theory which was described in section (3.3). All other parameters defining the settling conditions are listed in table (5.2).

Although some preliminary discussion has already been made at the end of individual chapters, the present chapter examines this material more generally.

7.2 Vertical settling

Amongst the many posible relationships between V_c and C the form

$$V_c = A (1 - C)^n \qquad .... (7.1)$$

appears to be the most accurate way of representing the relationship V_c-C (see figure 4.4)

Detailed tests (which have not been found in the literature) show

$$A \alpha d^2 \text{ and } A \alpha 1/\mu$$

Overall the experiments confirm the broadly accepted view that

$$A \equiv V_o \qquad .... (7.2)$$

where V_o is the settling velocity of discrete particles as defined by Stokes' law. NB in the present study $10^{-4} < Re < 10^{-3}$

For fixed particles $\bar{n} = 4.66 \pm 0.11$ (error represents 95% confidence limit) which is in agreement with the value (n = 4.65 when Re <0.2) predicted by equation (3.3) in Richardson and Zaki (1954-b). For a fixed fluid viscosity (μ = 0.48 poise) n increased with increases in d/D according to the relationship

$$n = 3.55 + 189\ d/D \qquad .... (7.3)$$

It should be noted that equation (7.3) is not consistance with Richardson and Zaki's formula which is quoted as n = 4.65 + 19.8 d/D . Nevertheless values of n consistent with (7.3) ie n = 4.4 - 5.4 are around the value n = 5 quoted by Maude et al (1958).

Overall the tests confirm work reported in chapter four and provide support for the techniques which were used in the later

studies.

7.3 The flow field within clear-fluid layer

In chapter five the characteristics of the clear-fluid layer was studied experimentally covering velocity, width and flow.

7.3.1 Velocity

Measurements of velocity of the flow within clear-fluid layer were carried out using two different techniques, (i) by observing the particles of the suspension which are trapped within the clear-fluid layer and, (ii) by injecting a dye solution as a tracer within this layer. The results were in reasonable agreement but both techniques were regarded as not being strectly satisfactory in terms of measuring the average velocity across the clear-fluid channel. Nevertheless they were considered to provide a sufficiently accurate description of the velocity profile along the clear-fluid layer. Measurements relied on the first case (particles velocity) becuase it provides larger number of observation which helps to reduce the experimental errors. The velocity distribution along this layer is shown in figure (5.13) for C_o = 0.2 and in (5.19) for C_o = 0.1. For both cases of initial solids concentration, the velocity changes along the clear fluid layer display the same features. The velocity at the bottom of the clear-fluid layer is zero and increases to

values of about 100 times the settling velocity of the particles within the suspension. The maximum velocity values exist at a level 2 cm below the top interface. Beyond this, the velocity decreases to almost zero at the top interface. The decrease in the velocity at the top interface has not been reported in any previous study. In their analysis of the flow field within the clear-fluid layer Acrivos et al predicted the longitudinal velocity and the width of the channel in the dimensionless form

$$U = O(\Gamma^{1/3}) \quad \text{and} \quad \delta = O(\Gamma^{-1/3}) \qquad \ldots.(7.4)$$

which in the dimensional form equation (7.4) becomes

$$V_h = O(U.V_o) \quad \text{and} \quad \delta = O(\Gamma^{-1/3} . H_o)$$

Using the data shown in table (5.2) shows

$$V_h = O(253 \times 0.648)$$

$$= O(164 \text{ cm/min})$$

and $$\delta = O(0.0021 \times 20)$$

$$= O(0.042 \text{ cm})$$

Thus Acrivos et al's theory seems to give an unrealistically high value of velocity even when compared with the highest velocities (in the upper part of the clear-fluid layer) which were observed to be

$\simeq$ 60 cm/min in the experiments. However apart from the top interface zone, figure (5.13) indicates that the theory provides a fairly good approximation of the velocity field at lower depths when $t \to 0$. NB the nearest comparison to this condition is t = 30 s in figure (5.13) and t = 20 s in figure (5.19)

7.3.2 Width

The development of the clear-fluid channel was observed over the settling time. At the early time of settlement t ≈ 0 the measured shape could be in agreement with Acrivos et al's theory. However, in the experiments, it was seen that the width reduces with time which is in marked in contrast with Acrivos et al' theory; this shows the width to be a constant at any particular height and independent of time. The channel width increased linearly at the very early times of settling. However after a time T_1, the width increased more rapidly until it reached a maximum width at time T_2. The prediction given by eqiuation (5.14) by Acrivos et al (1979) for the period of linear increase until the width reaches its maximum value lies between the observed values of T_1 and T_2 (see figure 5.15). The channel width predicted by Acrivos et al (1979) was very close to the observed value (see figure 5.12) at the beginning of settling tests and in the part of the settling column where the conditions are more stable ie H < 9 cm

7.3.3 Characteristics of top interface

Figures (5.13) and (5.19) show that the maximum values of the upward velocity are not at the top interface as reported by Acrivos et al (1979). Hence an idea about the scale of the channel velocities cannot be gained from observations taken at the top interface such as employed in Ohsasa et al (1982). As noted in the

review by Shiba (1985). Ohsasa et al also used red-coloured polystyrene particles to serve as a tracer. These particles had a diameter of 300 μm, which exceeds the largest dimension of the clear-fluid channel reported in the same paper. This means that the tracer particles occupied the whole width of the clear-fluid channel and indeed, part of the suspension core at the inclined interface. The particles forming the settling suspension are as small as 0.68 μm which means that the tracer particles are 440 times the settling particles in diameter and seems very libely to disturb the flow system of the suspension. Accounting for both of these features means that the comparison between the observed and predicted values of V as carried out by Shiba (1985), is invalid. Another aspect, which was not taken into account when theory was checked experimentally by Ohsasa et al (1982), was in batch settling, that the characteristics of the clear fluid layer were sensitive to time. It is not clear from the review by Shiba (1985) as to what particular time the measurements of velocity and channel width were carried out by Ohsasa et al (1982).

7.4 Flow field within the bulk suspension

A general inspection of the velocity distribution over the settling column is shown in figure (6.1) and provides insight into the flow field - a subject which has not been scrutinised in previous investigations. Velocity vectors show predominantly vertical motion within body of suspension. The fluid velocities (as gauged by a dye

tracer) were exceedingly high, being roughly 10 times the bulk settling velocity of the suspension (see also figures 6.5 and 6.6).

The suspension core can be envisaged as being divided into zones in terms of the velocity vectors (see figure 6.9): (IV) The core suspension over which the velocity seems to have a uniform distribution and is predominantly vertical; (II) the top layer where all the velocity vectors are reduced to zero towards the top interface; (I) The inclined boundary layer where the longitudinal velocity components V_h increased rapidly and, the components perpendicular to V_h (V_v) decreased to zero rapidly and; (III) the most peculiar zone is the 'corner' between the inclined interface and the top interface. It is evident that in this zone the fluid returns into the suspension within a vortex motion (see figure 7.1). This reveals the reason why the upward velocity within the clear fluid layer decreases to zero at the top interface. The vortex motion at this corner was observed on the video monitor during the measurement of the flow field within the suspension core. Where dye was introduced into the suspension and close to the top of the clear-fluid channel, it was observed to move upwards and towards the clear fluid channel. Near the ' corner ' it reversed direction, moving down into the suspension as described in figure (7.1).

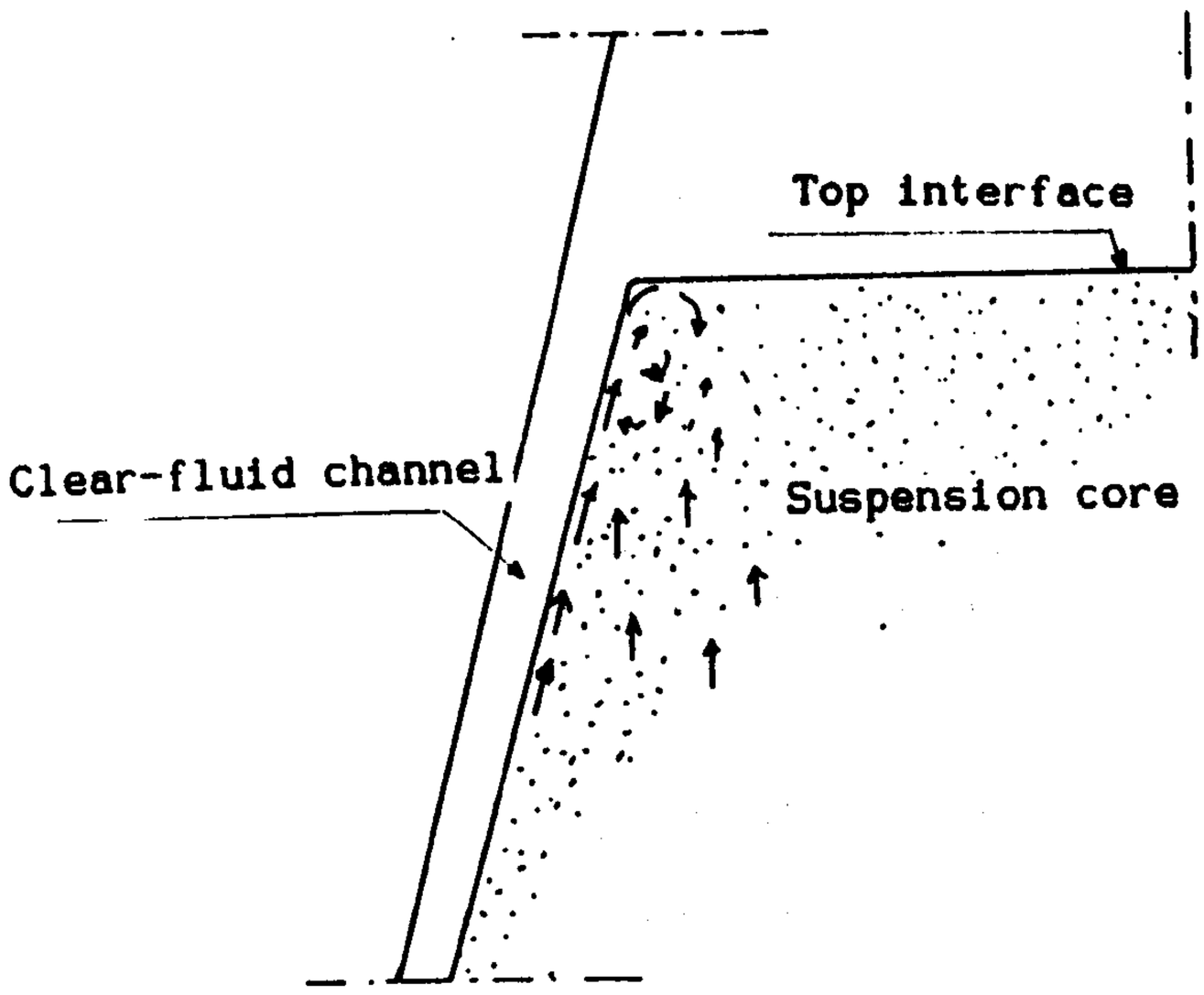

Figure 7.1: The vortex motion within the suspension core

To the author's knowledge, no experimental measurements of flow field within suspension core have been reported previously in the literature. Data on the components velocity V_r and V_y within core suspension zone (IV) are shown in figures (6.5) and (6.6). These are of the same order of magnitude O(6-10 cm/min) and which is in accord with the figure 9 cm/min predicted by Acrivos et al (see section 6.11).

Apart from these aspects, there was concern about the overall accuracy of the flow field measurements stemming from difficulties of explaining the infiltration behaviour (see section 6.5) and from dye tracer work in a vertical column (see section 6.7). Nevertheless tests on continuity equation showed that it was satisfied overall the settling column.

Further investigation on this aspect is needed to clarify the mechanism of fluid infiltration into the clear-fluid channel on the light of the present experimental study.

7.5 Concentration distribution within the settling column

In the vertical position the concentration within the bulk suspension remains constant and equals the initial concentration C_o along the free settling zone until it reaches the sediment layer. This in an agreement with Holdich (1983). The graded concentration layer is very thin ($\simeq$ 0.8 cm) and remains small in thickness as it propagates upwards. This is in contrast to Shanon et al's assumption (see section 2.2.3) who considered that where C_o is in the range 0.15 - 0.45 there are upper and lower interfaces between which exists an expanding layer of graded concentration.

A sliding behaviour of the glass spheres as they attain the maximum packing arrangement was described by Dixon (1977) (see section 2.2.3) and may explain the presence of the very thin layer of graded concentration above the sediment in a vertical tube. However it does not explain Shannon et al's case . In the latter study, the graded concentration layer began from initial concentration as low as 0.15 and was ended at C = 0.45 which is in free settling zone. In this regime Dixon (1977) considered it was impossible for the graded concentration layer to exist.

It should also be noted that the data of Holdich (1983) (using an

electrical-conductivity technique to measure the vertical concentration distribution in a settling column containing micro spheres), showed no evidence of an expanding graded-concentration layer, instead there was a very thin layer of a constant thickness. Holdich results were valid for the range of initial concentration between C = 0.15 and C = 0.45.

In an inclined tube the concentration increased with time towards the bottom of settling column. This could be explained by the thin sediment layer at the upward-facing wall. This layer slides downwards until it reaches the top of the sediment layer at the bottom of the tube. Since the thin sliding layer has a relatively low solids concentration which is less than C_m in the bottom sediment layer (Acrivos et al 1979) it cannot go further than the top of the bottom sediment layer. Thus it 'breaks' up and join a mixing region at the top of the sediment layer. Thus there is a graded concentration layer between the maximum concentration (in the sediment layer) and the concentration (C_o) in the upper region (see figure 5.11) of the bulk suspension .

The mechanism of forming a graded concentration zone within an inclined settling column may explain the reason for the existence of this type of zone observed in Shannon et al (1964). This could have arisen as a result of their experimental technique in that they did not use a container with vertical walls since a conical container was used.

It is the presence of the mixing region which has erroneous Shannon

et al's results and has lead to their questionable explanation . Since their flux plot (see figure 2.8) was deduced from the same confused data, they produced a doubly concave flux plot which satisfies their graded-concentration layer in the range of initial concentration between C = 0.15 and C = 0.45.

Close to the interface, the concentration remains at the initial value C_o. This is in contrast to Zahavi and Rubin (1975), who assumed that the thin sliding sediment layer at the upward-facing surface, collects solids during the settling process and causes a decrease in the concentration values within the bulk suspension (see equation 19 in their analysis).

7.6 The infiltration into the clear-fluid layer

Details of the infiltration process along the inclined interface were reported in chapter six. The infiltration was studied from two viewpoints: (i), the flow along the clear-fluid channel; and (ii), the flow field within the bulk suspension adjacent to the clear fluid channel. Clearly they must be in a state of balance.

From the flow in the clear-fluid channel, the filtration shows two distinct regions along the inclined interface at which the infiltration has a uniform values (see figure 6.11). At the upper part this interface gives twice the infiltration which is given by the lower part.

All the characteristics of the flow field within the clear-fluid channel indicate a change in behaviour between the upper and lower parts of the settling column and take place as if there was a form of rotation above and below a horizontal axis at the level H = 9 cm (when C_o = 0.2) at all times until the interface reaches this level. The corresponding height for C_o = 0.1 is H = 7 cm.

For the second case the infiltration is deduced from the flow field within the bulk suspension (see section 6.5). Figure (6.11) shows that the infiltration increases upwards along the inclined interface until a height at which the infiltration started to decrease in value. At the top interface the infiltration has a negative value which is a strong indication of the presence of a vortex motion at the top interface (zone III).

Figure (6.11) provides evidence that the two estimates of infiltration are of the same order of magnitude. The fact that they are not equal, stems from the difficulty of specifiying the precise position from which the infiltration should be deduced. From the analysis shown in section (6.6). The inclined plane from which the feed velocity was originated has been predicted and compared to the measured channel width. Figure (6.12) demonstrates the comparision between δ and δy. At the lower part of the inclined interface the two values showed a good agreement but deviation started in the upper part (see figure 6.12).

Figure (6.11) also shows that the infiltration is not constant along the inclined interface as predicted by Acrivos et al' theory.

(NB the slope of the curves in the figures 5.16 and 5.20 represent the infiltration rate for the experimental and theory by Acrivos et al 1979).

From the literature it appears that no experimental work has been previously carried out on infiltration. All previous theories including Acrivos et al, (see figures 5.16 and 5.20), have assumed that the infiltration rate is constant along the inclined interface. This is because the settling velocity has been considered solely as a function only of the solids concentration, and that the concentration distibution is uniform taking the initial value C_o. The present study shows clearly that the concentration is not uniform along the suspension column and vertical concentration gradient generally increases with time.

Although in the early phase of settlement the concentration changes along the settling tube can be neglected the data shows that in spite of this, the infiltration increases up the inclined interface; this means that concentration is not the only factor affecting the settling process within the inclined column.

The effect of initial solids concentration on the mean value of infiltration was studied in chapter four. Zahavi and Rubin (1975) considered that the settling velocity in an inclined tube can be divided into two parts (equation 3.6)

$$V_{in} = V_v + V_p$$

where V_p is the share of the inclined interface to the settling

process and V_v is the share of the top interface. Zahavi and Rubin assumed that V_p originates from two effects along the inclined interface (see section 3.2) ie from infiltration due to density difference between fluid and suspension and from settling of particles along the inclined interface. They stated that as concentration increases the effect of filtration increases and the effect of settling velocity decreases. The combination of filtration effect and settling effect was considered to be constant. Therefore they considered V_p at early stage of settling to be independent from initial solids concentration. In this work V_p was found to depend strongly on C_o but the ratio V_p/V_v was found to be independent from C_o (see figures 4.12 and 4.13)

7.7 Pathways of fluid release

The balance between the volume of supernatent accumulated over the top interface and the volume of fluid released from the clear-fluid channel was calculated during a time interval Δt (see section 5.5). This was for two values of solids concentration (C_o = 0.2 and C_o = 0.1). For both values C_o, the ratio of volume released from top interface to the total supernatent volume decreased with time and this decrease was shown (in figure 5.26) to be independent from initial concentration and depend strongly on the position of top interface.

The settling velocity of particles within the bulk suspension which is deduced from the fluid release through top interface indicates a higher settling velocity than that of the same suspension with a vertical settling column. This velocity is fairly constant with time.

7.8 Modified PNK theory

When the origin PNK theory given by equation (3.4) was tested against experimental data of monodisperse suspension good agreement was only obtained in a very diluted suspension (C_o = 0.05, see figure 4.11). For higher values of initial concentration equation (3.4) was found to be deficient. In its modified form, taking account of the height of the sediment layer at the bottom of the tube (see section 4.4.3) it may be expressed by

$$Z - z = \frac{b + Z \sin\alpha}{(1 + \beta) \sin\alpha} \left\{ 1 - \exp \left[\frac{-V_o\, t}{b} \sin\alpha \, (1 + \beta) \right] \right\} \quad .. (7.5)$$

where $$\beta = \frac{C_m}{C_m - C_o}$$

(For the derivation and definitions see section 4.4)

Plot (5.11) shows that the concentration at the sediment layer is about Cm = 0.55.

Although most of the assumption on which PNK theory depends (ie constancy of concentration distribution, filtration rate and settling velocity) are strictly invalid, the modified PNK equation was found to provide an excellent agreement with the experimental batch settling curves over the range of conditions studied ie C_m = 0.55 . This agreement is more evident with the increase of initial concentration or the angle of inclination (see figures 4.10 and 4.11)

It is recommended that equation (7.5) should be used as a means of representing settling phenomena in inclined tubes when using cohesionless suspensions.

7.9 Summary of the main conclusions

Conclusions centred on the flow distribution and comparison with theory

1) - In a vertical tube the settling velocity concentration relationship followed Richardson and Zaki's form

$$V_c = A\ (1-C)^n$$

where A represents the settling velocity of discrete particles and was found proportional to d^2 and $1/\mu$, μ referring to the particle free fluid viscosity . n has values in the range 4.4 to 5.4 depending on particle diameter for Reynolds numbere << 0.1

2) - The velocity within clear-fluid layer was found to change from zero at the bottom of the tube to a maximum value of about 100 times the settling velocity of the suspension. This maximum values exists at a level roughly 2 cm below the top interface initially at H_o = 20 cm. At the top of the channel the velocity reduces to zero. The decrease in the velocity appears to be connected to a local vortex motion within the suspension; this causes components of fluid to enter the suspension and results in a reduced channel velocity.

Apart from the top interface zone, figure (5.13) indicates that theory by Acrivos et al (1979) provides a fairly good approximation of the velocity field at lower depths when $t \rightarrow 0$.

3) - The development of the channel shape with time shows that at a fixed height, the width of the channel reduces as time passes. This is in contrast with Acrivos et al's theory, which shows the width is constant at any particular height and <u>independent</u> of time.

4) - An assessment of the flow field within the bulk suspension showed clearly the vertical nature direction of fluid motion. Velocities within the core of the suspension were shown to be 10 times the settling velocity of the same suspension within a vertical tube.

The suspension core can be envisaged as being divided into zones in terms of the velocity vectors (see figure 6.9): (IV) The core suspension over which the velocity has a uniform distribution and is

predominantly vertical; (II) the top layer where all the velocity vectors are reduced to zero towards the top interface; (I) The inclined boundary layer, where the longitudinal velocity components V_h increased rapidly and, the perpendicular component (V_y) decreased to zero rapidly and; (III) the 'corner' between the inclined interface and the top interface in which a vortex resides (see conclusion 2).

5) - In the case of a vertical tube the solids concentration was independent of height in the free settling zone and equals to the initial value C_o over the settling time. The sediment layer has a maximum concentration C_{max} = 0.6 which is close to the value C_{max} = 0.64 predicted by Shannon et al (1963). Between the free settling zone and the sediment layer exists a very thin layer of graded concentration which does not expand with time as reported by Shannon et al (1964).

In an inclined tube there is a graded concentration layer between the maximum concentration, which occurs in the sediment layer and the concentration C_o in the upper region (see figure 5.11), the later being independent of time.

All the characteristics of the flow field within the clear-fluid channel indicate a change in behaviour between the upper and lower parts of the settling column and take place as if there was a form of rotation above and below a horizontal axis at the level H = 9 cm

(when C_o = 0.2) at all times until the interface reaches this level. The corresponding height for C_o = 0.1 is H = 7 cm.

6) All previous theories, including Acrivos et al (1979), (see figures 5.16 and 5.20), assume that the infiltration rate is constant along the inclined interface. The present study shows that the infiltration increases with height up the inclined interface. At the upper part of the settling tube the infiltration was twice the value in the lower region.

7) - Zahavi and Rubin (1975) considered V_p the share of the clear-fluid layer to the settling velocity at early stage of settling to be independent from initial solids concentration (see section 3.2 and equation 3.6). In this work V_p was found to depend strongly on C_o (see figure 4.12-a and 4.13-a). However the ratio V_p/V_∞ was found to be independent from C_o (see figure 4.12-b and 4.13-b).

8) Acrivos et al's theory (1979) gives reasonable upper limits of the clear-fluid layer characteristics (upward velocity and channel width) away from the top onterface zone . It fails to predict the conditions at top interface and the flow field within the suspension core.

9) - PNK theory in its original form does not provide an appropriate prediction for the settling of interface in an inclined settling column . The modified form shown below provides an excellent agreement with experimental bach settling curves over the range of

conditions studied apart from the final stages when the top interface and the sediment are very close to each other.

$$Z - z = \frac{b + Z \sin\alpha}{(1 + \beta)\sin\alpha}\left\{1 - \exp\left[\frac{-V_o\, t}{b}\sin\alpha\,(1 + \beta)\right]\right\}$$

where $$\beta = \frac{C_m}{C_m - C_o}$$

It is recommended that equation (7.5) should be used as a means of representing settling phenomena in inclined tubes when using cohsionless suspensions.

LITERATURE

REFERENCES

REFERENCES

ACRIVOS, A., and HERBOLZHEIMER, E. 1979. Enhanced sedimentation in settling tanks with inclined walls. J. Fluid Mech. 92: 435-457.

BARNEA, E. and MIZRAHI, J. 1973. A generalized approach to the fluid dynamics of partculate systems: Part 1, General correlation for fluidization and sedimentation in solid multiparticle systems. Chem. Eng. J. 5: 171-189

BATCHELOR, G. K. 1972. Sedimentation in a dilute dispersion of spheres. J. Fluid Mech. 52: 245-268.

BERCZELLER, L. and WASTL, F. H. 1924., The settling of erthrocytes in blood columns of various heights, Biochem. Z. 146: 370.

BOYCOTT, A. E. 1920. Sedimentation of blood corpuscles. Nature 104: 532

BRUGGEMAN, D. A. C., 1935. Ann Phusik, 24: 636.

BURGERS, J. M. 1942. Proc. K. Ned. Acad. Wet., 1942. 45: 126

COE, H. S., DENVER, COLO., and CLEVENGER, G. H. 1916. Methods for determining the capacities of slime-settling tanks. Trans. A. I. M. E. 55: 356-384

DAVIES, L. and DOLLIMORE, D. 1976. Sedimentation of suspension: Implication of theories of hindered settling. Powder Tech. 13: 123-132.

DIXON, D. C., 1977. Momentume-balance aspects of free-settling theory. I: Batch thickening. Sep. Scie. 12: 171-191

DIXON, D. C., SOUTER, P., and BUCHANAN, J. E., 1976. A study of internal effects in sedimentation. Chem. Eng. Sci. 31: 737-740.

FAMULARO, J., 1962. Eng. Sc. D. Thesis, New York University.

FEUILLEBOIS, F. 1984. Sedimentation in a dispersion with vertical inhomogeneities. J. Fluid Mech. 139: 145-172.

FLEMMER, R. L. C. and BANKS, C. L., 1986. On the drag coefficient of a sphere. Powder Tech. 48: 217-221.

GARSIDE, J., Al-DIBOUNI, M. R. 1977. Velocity-voidage relationship for fluidization and sedimentation in solid-liquid systems. Ind. Eng. Chem. proc. Des. Dev. 16: 206-214

References Cont.

GRAHAM, W. and LAMA, R., 1963. Sedimentation in inclined vessels. Can. J. Chem. Eng. 41:31-32

HAWKSLEY, P. G., 1950. Symposium: Some Aspects of fluid flow. Edward Arnold and Co., London.

HERBOLZHEIMER, E. 1980. Enhanced sedimentation in settling vessels having inclined walls. PhD thesis. Stanford University. Stanford, Calif.

HILL, W. D. 1974. Boundary-enhanced sedimentation due to settling convection. PhD thesis. Carnegie-Mellon Univ., Pittsburgh, Pa.

HILL, W. D., Rothfus, R. R. and L$_I$, K. 1977. Boundary-enhanced sedimentation due to settling convection. Int. J. Multiphase Flow 3:561.

HOLDICH, R. G., 1983. A study of the formation of compressible compacts in filtration and thickening process. PhD Thesis. University of Exeter, Exeter.

INOUYE, K., UCHIBORI, T. and KATSURAI, T., 1954. Acceleration of sedimentation in a vessel which consists of two tubes of differing diameter, Kolloid-Zeitschrift, 139: 167-170

KINOSITA, K. 1949. Sedimentation in tilted vessels. J. Colloid Sci. 4:525-535.

KYNCH, G. J. 1952. A theory of sedimentation. Trans. Faraday Soc. 48:166-176.

LEWIS, W. K., GILLILAND, E. H., and BAUER, W. C., 1949. Ind. Eng. Chem. 41:1104.

LUNDGREN, R. 1927. Acta. Med. Scand. 67:63

MAUDE, A. D. and WHITMORE, R. L., 1958. A generalization theory of sedimentation. British J. of Apply. Phys., 9:dec.: 477-482.

MAXWELL, J. C., 1881. A treatise on electricity and magnetism. vol. 1, 2nd ed., Clarendon Press, Oxford, p 435.

McNOWN, J. S., LEE, H. M., McPHERSON, M. B., and S. M., Engez., 1948. Proc. 7th Int. Cong. Apply. Mech., London.

MERDITH, R. E. and TOBIAS, C. W. 1962. in Advances in Electrochemestry and Electrochemical Engineering. vol. 2, Intrescience, New York.

References Cont.

NAKAMURA, N., KURODA. K. 1937. " La cause de l'accleration de la vitesse de sedimentation des suspension dans les recipients inclines". Keijo J. Med. 8:256 (in French)

OHSASA, K., SAMBUICHI, M. NAKAKURA, H. and SHIBUYA, T. 1982. The initial settling rate in a tilted rectangular tubes. Kagaku kogaku ronbunshu. 8: No. 3, May: 291-296. (in Japanese) (English summary)

OLIVER, D. R. and JENSON, V. G. 1964. The inclined settling of dispersed suspension of spherical particles in square-section tubes. Can. J. Chem. Eng., 42: 191-195.

PEARCE, K. W., 1962. Settling in the presence of downward facing surfaces, in, Interaction between fluid and particles. London, Inst. Chem. engrs., pp. 30-39

PONDER, E., 1925. On sedimentation and rouleoux formation, Quart. J. Exp. Physiol. 15:235-252.

PYUN, C. W. and FIXMAN, M. 1964. Frictional coefficient of polymer molecules in solution. J. Chem. Phys., 41:937.

RICHARDSON, J. F., ZAKI, W. N. 1954-a. Sedimentation and fluidization: Part I. Trans. Inst. Chem. Eng. 32:35-53.

RICHARDSON, J. F., and ZAKI, W. N. 1954-b. The sedimentation of a suspension of uniform spheres under conditiions of viscous flow. Chem. Eng. Scie. 3:65-73.

SCHNEIDER, W. 1982. Kinematic-wave theory of sedimentation beneath inclined walls. J. Fluid Mech., 120: 323-346.

SHANNON, P. T., STROUPE, E. and TORY, E., 1963. Batch and continuous thickening. Ind. Eng. Chem., Fundam, 2: No. 3 Aug.: 203-211.

SHANNON, P. T., STROUPE, E., DEHAAS, R. D., and TORY, E., 1964. Batch and continuous thickening. Ind. Eng. Chem., Fundam, 3: Aug.: 250-260.

SHIBA, S. M. 1985. Flow under tilt surface for High Rate settling. J. Environmental Eng. 111: No3, June: 285-303.

STIENOUR, H. H. 1944. Ind. Eng. Chem., 36:618

STOKES, G. G., 1851. Trans. Camb. Phil. Soc., 9:8

References Cont.

WAKEMAN, R. J. and HOLDICH, R. C., 1982. The use of electrical conductivity measurements to elucidate the theory of gravity thickening. Proc. Int. Symp. On Water Filtration , (271 st. event of EFCE), Antwerp, pp 6.47-6.53.

ZAHAVI, E. and RUBIN, E. 1975. Settling of solid suspensions under and between inclined surfaces. Ind. Eng. Chem., Process Des. Dev. 14: 34-41.

APPENDIX

RAW DATA

Table A1: Raw data for initial height and settling velocity (section 4.3.1)

H =18,9cm		H =16,9cm		H =14,8cm		H =12,9cm		H =10,8cm		H = 9,0cm	
t min	h cm	t min	h cm	t min	h cm	t min	h cm	t min	h cm	t min	h cm
0,0	19,0	0,0	17,0	0,0	15,0	0,0	13,0	0,0	11,0	0,0	9,0
2,5	17,9	2,0	16,1	2,0	14,0	1,5	12,3	1,0	10,4	1,0	8,5
4,0	17,3	4,0	15,3	4,0	13,3	4,5	11,1	2,0	10,0	3,0	7,6
6,5	16,3	6,0	14,5	6,0	12,5	6,0	10,6	4,0	9,3	4,0	7,2
8,5	15,6	10,0	13,0	9,5	11,1	8,0	9,8	6,5	8,3	5,0	6,8
11,0	14,6	12,0	12,2	12,0	10,1	10,0	9,0	8,0	7,8	6,0	6,4
14,0	14,6	16,0	10,7	14,0	9,4	11,5	8,4	10,5	6,8	7,0	6,0
18,0	11,9	18,0	9,9	16,0	8,8	14,0	7,4	12,5	6,0	8,0	5,6
21,0	10,8	21,0	8,8	18,0	7,8	16,0	6,7	17,0	4,4	9,5	5,0
24,0	9,6	24,0	7,6	20,0	7,2	18,0	6,0	18,0	4,1	10,0	4,3

Table A2: Raw data for viscosity - settling velocity
(section 4-3-3)

μ = 0.145 poise							
ϵ =0.85		ϵ =0.83		ϵ =0.80		ϵ =0.77	
t min	h cm	t min	h cm	t min	h cm	t min	h cm
0.0	20.0	0.0	18.0	0.0	15.0	0.0	13.5
0.5	18.8	0.5	16.8	0.5	14.2	0.5	12.7
1.5	16.5	2.0	13.6	1.5	12.4	1.0	12.0
2.5	14.0	3.0	11.5	2.5	10.7	1.5	11.2
4.0	10.6	4.0	9.2	3.5	9.0	2.5	9.7
5.0	8.2	5.0	7.2	4.5	7.2	3.5	8.2
6.0	6.0	6.0	5.4	5.5	5.6	4.5	6.7

Table A3: Raw data for viscosity - settling velocity
(section 4-3-3)

μ = 0.200 poise							
ϵ =0.85		ϵ =0.83		ϵ =0.80		ϵ =0.77	
t min	h cm	t min	h cm	t min	h cm	t min	h cm
0.0	20.0	0.0	18.0	0.0	15.0	0.0	13.5
0.5	19.2	0.5	17.3	0.5	14.3	0.5	12.9
2.0	17.0	1.5	16.0	2.0	12.7	2.0	11.5
3.5	14.8	3.5	13.5	3.0	11.6	2.5	11.0
4.5	13.0	5.0	11.5	4.0	10.6	3.5	10.1
7.0	9.5	6.0	10.0	5.0	9.4	4.0	9.6
8.0	8.0	7.0	8.5	6.5	7.7	5.0	8.6
9.0	6.5	8.5	6.4	7.5	6.5	6.0	7.6
9.5	5.2	10.0	5.2	9.0	5.3	7.0	6.6

Table A4: Raw data for viscosity - settling velocity
(section 4-3-3)

μ = 0.305 poise							
ϵ =0.85		ϵ =0.83		ϵ =0.80		ϵ =0.77	
t min	h cm	t min	h cm	t min	h cm	t min	h cm
0.0	20.0	0.0	18.0	0.0	15.0	0.0	13.5
1.0	19.0	1.0	17.0	1.0	14.2	1.0	12.7
2.5	17.5	3.0	15.2	2.5	13.0	2.0	12.1
4.0	16.0	4.5	13.8	4.0	11.9	3.0	11.4
6.0	14.0	7.5	11.0	5.0	11.1	4.0	10.8
8.5	11.5	9.5	9.2	6.0	10.4	5.0	10.2
11.0	9.0	10.0	8.8	7.0	9.7	6.5	8.0
12.5	7.5	12.5	6.5	8.0	8.8	8.1	9.0
14.0	6.0	13.5	5.5	10.0	7.4	9.0	7.5

Table A5: Raw data for viscosity - settling velocity
(section 4-3-3)

μ = 0.480 poise							
ϵ =0.86		ϵ =0.85		ϵ =0.83		ϵ =0.82	
t min	h cm	t min	h cm	t min	h cm	t min	h cm
0.0	21.7	0.0	20.0	0.0	18.0	0.0	16.5
1.0	20.9	1.0	19.2	1.0	17.5	1.5	15.8
3.0	19.7	3.0	18.0	2.5	16.7	3.0	15.0
5.0	18.2	7.5	15.2	5.0	15.3	5.0	14.0
7.5	16.6	10.0	13.4	8.0	13.5	7.0	12.9
9.0	15.5	11.0	12.0	11.5	11.3	9.0	11.8
11.5	13.7	13.5	11.2	15.5	8.9	13.0	9.0
15.5	11.2	16.5	9.1	18.0	7.3	16.5	7.7
17.5	9.5	19.0	7.6	20.0	6.2	18.0	6.8

Table A6: Raw data for viscosity - settling velocity
(section 4-3-3)

μ = 0.870 poise							
ϵ =0.85		ϵ =0.83		ϵ =0.80		ϵ =0.77	
t min	h cm	t min	h cm	t min	h cm	t min	h cm
0.0	20.0	0.0	18.0	0.0	15:0	0.0	13.5
3.0	19.0	2.0	17.4	2.0	14.4	2.0	13.0
7.0	17.8	8.0	15.7	7.0	13.3	4.0	12.6
10.0	16.9	9.0	15.4	9.0	12.8	6.0	12.2
13.0	16.0	12.0	14.5	13.0	11.9	8.0	11.7
16.0	15.0	13.0	14.3	16.0	11.1	11.0	11.1
20.0	13.8	16.0	13.4	18.0	10.8	15.0	10.3
24.0	12.5	21.0	12.0	20.0	10.2	18.0	9.7
29.0	11.0	25.0	10.7	22.0	9.8	20.0	9.3
33.0	9.7	26.0	10.6	24.0	9.3	24.0	9.7
35.0	9.0	29.0	9.8	28.0	8.4	27.0	7.8
36.0	8.8	33.0	8.7	30.0	8.0	32.0	6.9
39.0	7.9	37.0	7.5	33.0	7.2	35.0	6.4
42.0	7.0	38.0	7.4	37.0	6.3	37.0	6.0

Table A7: Raw data for viscosity - settling velocity
(section 4-3-3)

μ = 1.530 poise							
ϵ =0.84		ϵ =0.82		ϵ =0.79		ϵ =0.76	
t min	h cm	t min	h cm	t min	h cm	t min	h cm
0.0	20.0	0.0	18.0	0.0	15.0	0.0	13.5
6.0	18.7	3.0	17.3	3.0	14.4	3.0	13.0
10.0	17.8	8.0	16.3	4.0	14.2	6.0	12.5
14.0	17.0	12.0	15.6	9.0	13.4	9.0	12.1
18.0	16.2	18.0	14.4	14.0	12.6	13.0	11.5
23.0	15.0	22.0	13.6	20.0	11.7	17.0	11.0
30.0	13.4	27.0	12.6	25.0	10.8	21.0	10.5
34.0	12.5	32.0	11.5	30.0	10.0	25.0	9.9
39.0	11.4	36.0	10.8	38.0	8.9	30.0	9.2
43.0	10.5	39.0	10.3	42.0	8.3	34.0	8.6
49.0	9.3	46.0	8.9	48.0	7.3	39.0	8.0
57.0	7.4	52.0	7.6	53.0	6.6	42.0	7.7
60.0	6.8	55.0	7.3	57.0	6.0	46.0	7.1

Table A 8: Raw data for particle size-settling velocity (section 4-3-4)

d =0,0117 cm											
ϵ = 0,86		ϵ = 0,85		ϵ = 0,83		ϵ = 0,82		ϵ = 0,80		ϵ = 0,77	
t min	h cm	t min	h cm	t min	h cm	t min	h cm	t min	h cm	t min	h cm
0,0	21,7	0,0	20,0	0,0	18,0	0,0	16,5	0,0	15,0	0,0	13,5
1,0	20,9	1,0	19,2	1,0	17,5	1,5	15,8	1,0	14,5	1,0	13,0
3,0	19,7	3,0	18,0	2,5	16,7	3,0	15,0	3,0	13,6	2,5	12,4
5,0	18,2	7,5	15,2	5,0	15,3	5,0	14,0	5,0	12,6	4,0	11,8
7,5	16,6	10,0	13,4	8,0	13,5	7,0	12,9	6,0	12,2	5,0	10,4
9,0	15,5	11,0	13,0	11,5	11,3	9,0	11,8	7,5	11,5	7,0	10,5
11,5	13,7	13,5	11,2	15,5	8,9	12,0	10,1	10,0	10,3	10,0	9,3
15,5	11,2	16,5	9,1	18,0	7,3	13,0	9,6	12,0	9,3	13,0	8,0
17,5	9,5	19,0	7,6	20,0	6,2	16,5	7,7	14,0	8,3	15,0	7,2

Table A 9: Raw data for particle size-settling velocity (section 4-3-4)

d =0,0133 cm											
ϵ = 0,86		ϵ = 0,85		ϵ = 0,83		ϵ = 0,80		ϵ = 0,77		ϵ = 0,73	
t min	h cm	t min	h cm	t min	h cm	t min	h cm	t min	h cm	t min	h cm
0,0	21,7	0,0	20,0	0,0	18,0	0,0	15,0	0,0	13,5	0,0	11,2
2,0	19,8	2,0	18,2	1,0	17,1	1,5	14,0	2,0	12,2	1,0	10,6
4,0	18,0	3,5	17,0	2,5	16,0	2,5	13,3	3,5	11,4	2,0	10,2
6,0	16,3	6,0	14,9	3,5	15,3	3,0	13,0	5,0	10,6	3,0	9,8
7,0	15,2	8,0	13,4	5,0	14,2	5,0	11,8	6,0	10,0	4,0	9,4
9,0	8,6	9,0	12,5	6,5	13,0	6,0	11,0	7,5	9,3	5,5	8,7
9,5	13,1	10,0	11,7	9,0	11,1	7,0	10,4	8,5	8,7	7,0	8,1
11,5	11,2	12,0	10,0	11,0	9,6	8,0	9,8	10,0	7,7	8,0	7,7
13,5	9,6	13,0	9,2	13,0	8,0	10,0	8,5	13,0	6,3	10,0	6,9

Table A10; Raw data for particle size-settling velocity (section 4-3-4)

d =0,0168 cm											
ϵ = 0,86		ϵ = 0,85		ϵ = 0,83		ϵ = 0,80		ϵ = 0,77		ϵ = 0,72	
t min	h cm	t min	h cm	t min	h cm	t min	h cm	t min	h cm	t min	h cm
0,0	21,7	0,0	20,0	0,0	18,0	0,0	15,0	0,0	13,5	0,0	11,2
1,0	20,1	1,0	18,6	1,0	16,8	1,0	14,0	1,0	12,6	1,0	10,4
2,5	18,1	2,0	17,4	2,0	15,7	2,0	13,1	2,0	11,9	2,0	9,9
3,0	17,5	3,0	16,2	3,0	14,7	3,0	12,3	3,0	11,1	3,0	9,4
4,0	16,2	4,0	15,2	4,0	13,7	4,0	11,5	4,0	10,3	3,6	9,0
5,0	15,1	5,0	14,0	5,0	12,7	5,0	10,7	4,5	10,0	4,0	8,8
6,5	13,2	6,0	12,8	6,0	11,7	6,0	9,8	5,0	9,6	5,0	8,3
7,0	12,5	7,0	11,6	7,0	10,7	7,0	9,0	6,0	8,9	6,0	7,8
8,0	11,3	8,0	10,4	8,0	9,7	8,0	8,2	7,0	8,2	6,6	7,5
9,0	10,0	9,0	9,1	9,0	8,7	9,0	7,5	8,0	7,5	7,0	7,3
10,0	8,7	9,5	8,8	10,0	7,7	9,5	7,0	9,0	6,8	8,0	6,8

Table A11; Raw data for particle size-settling velocity (section 4-3-4)

d =0,0200 cm											
ϵ = 0,86		ϵ = 0,85		ϵ = 0,83		ϵ = 0,80		ϵ = 0,77		ϵ = 0,72	
t min	h cm	t min	h cm	t min	h cm	t min	h cm	t min	h cm	t min	h cm
0,0	21,7	0,0	20,0	0,0	18,0	0,0	15,0	0,0	13,5	0,0	11,2
1,0	19,4	1,0	18,0	1,0	16,3	1,0	13,6	1,0	12,3	1,0	10,2
2,0	17,4	2,0	16,3	2,0	14,7	2,0	12,4	2,0	11,2	2,0	9,5
3,0	15,5	2,7	15,0	3,0	13,2	3,0	11,1	3,0	10,1	2,6	9,0
4,0	13,6	3,0	14,5	4,0	11,6	4,0	10,0	4,0	9,1	3,0	8,7
5,0	11,5	4,0	12,9	5,0	10,1	5,0	8,9	5,0	8,1	4,0	8,0
6,0	9,9	5,0	11,1	6,0	8,6	6,0	7,6	6,0	7,1	5,0	7,3
7,0	8,0	6,0	9,5	7,0	7,2	7,0	6,5	7,0	6,2	6,0	6,6

Table A12; Raw data for particle size-settling velocity (section 4-3-4)

d =0,0217 cm											
ϵ = 0,86		ϵ = 0,85		ϵ = 0,83		ϵ = 0,79		ϵ = 0,77		ϵ = 0,72	
t min	h cm	t min	h cm	t min	h cm	t min	h cm	t min	h cm	t min	h cm
0,0	21,0	0,0	20,0	0,0	18,0	0,0	15,0	0,0	13,5	0,0	11,0
1,0	19,0	1,0	17,8	1,0	16,0	1,0	13,4	1,0	12,0	1,0	10,1
2,0	17,0	1,4	17,0	2,0	14,2	2,0	12,0	1,5	11,5	2,0	9,3
3,0	15,0	2,0	15,8	2,7	13,0	3,0	10,6	2,0	10,8	2,4	9,0
4,0	13,0	3,0	13,8	3,0	12,3	4,0	9,3	3,0	9,6	3,0	8,5
5,0	11,0	4,0	11,8	4,0	10,4	5,0	8,0	4,0	8,5	4,0	7,6
6,0	9,0	5,0	10,0	5,0	8,6	6,0	6,8	5,0	7,3	5,0	6,8
7,0	7,0	6,0	8,0	6,0	7,0	7,0	5,5	6,0	6,2	6,0	6,0

Table A13: raw data for settling in an inclined tubes
(sections 4.4.3 and 4.4.6)

μ = 0.48 poise		α = 5°						d = 133 μm							
ε = 95%		ε = 90%		ε = 85%		ε = 80%		ε = 75%		ε = 70%		ε = 65%		ε = 60%	
t min	h cm	t min	h cm	t min	h cm	t min	h cm	t min	h cm	t min	h cm	t min	h cm	t min	h cm
0,0	20,0	0,0	20,0	0,0	20,0	0,0	20,0	0,0	20,0	0,0	20,0	0,0	20,0	0,0	20,0
0,5	19,0	1	18,4	1	18,7	1,0	18,9	1	19,2	1,5	19,1	2	19,2	1,5	19,5
1	18,0	2	16,8	2	17,5	2,0	18,0	2	18,5	2	18,9	4	18,5	3	19,2
2	16,0	3	15,2	3	16,3	3,0	17,0	5	16,3	3	18,5	7	17,5	6	18,5
3	14,0	4	13,5	4	15,1	4,0	16,1	7	15,0	4	18,0	11	16,3	9	17,9
4	12,0	5	12,0	5	14,0	5,5	14,8	9	13,8	7	17,0	17	14,8	12	17,3
5	10,0	6	10,5	6	12,9	7,0	13,4	11	12,7	9	16,0	20	14,1	15	16,8
6	8,0	7	9,2	7	11,8	8,5	12,2	13	11,6	11,5	14,9	23	13,5	18	16,2
7	6,5	8	7,7	8	10,7	10,0	11,0	15	10,7	14	14,0	27	12,9	21	15,8
8	5,0	9	6,5	9	9,5	11,5	10,0	17	10,0	17	13,0	30	12,5	24	15,3
9	3,5	10	5,0	10	8,7	13,0	9,0	19	9,5	20	12,1	34	12,0	28	14,8
10	2,4	11	3,9	11	7,8	14,5	8,2	21	9,0	24	11,2	35	12,0	31	14,5
11,1	1,8			12	6,8	16,0	7,6	24	8,5	26	10,9			35,5	14,0
				13	6,0	18,5	7,0	25	8,5	29	10,5			40	13,8
				14	5,5	19,5	6,8			32	10,3				
				15	5,1										

Table A14: raw data for settling in an inclined tubes
(sections 4.4.3 and 4.4.6)

μ = 0.48 poise α = 10° d_s = 133 µm

ε = 95%		ε = 90%		ε = 85%		ε = 80%		ε = 75%		ε = 70%		ε = 65%		ε = 60%	
t min	h cm	t min	h cm	t min	h cm	t min	h cm	t min	h cm	t min	h cm	t min	h cm	t min	h cm
0,0	20,0	0,0	20,0	0,0	20,0	0,0	20,0	0,0	20,0	0,0	20,0	0,0	20,0	0,0	20,0
0,6	18,0	1,0	17,7	1,0	18,2	1,0	18,5	1,0	18,9	1,0	19,5	1,5	19,1	1,5	19,4
1,5	15,3	2,0	15,5	2,0	16,3	2,0	16,9	2,0	17,9	2,0	18,4	3,0	18,5	3,0	18,9
2,0	14,0	3,0	14,5	3,0	14,5	3,0	15,5	3,0	17,0	3,0	17,7	5,0	17,5	6,0	18,0
3,0	11,0	4,0	11,4	4,0	13,0	4,0	14,4	4,0	16,1	5,0	16,4	7,0	16,8	9,0	17,2
4,0	9,0	5,0	9,7	5,0	11,6	5,0	13,3	5,0	15,3	7,0	15,4	10,0	15,7	12,0	16,5
5,0	7,0	6,0	8,0	6,0	10,2	6,0	12,2	7,0	13,9	9,0	14,4	13,0	14,7	15,0	15,9
6,0	4,5	7,0	6,7	7,0	9,2	7,0	11,3	9,0	12,6	11,0	13,5	16,0	14,0	18,0	15,3
7,0	3,0	8,0	5,2	8,0	8,1	8,0	10,5	11,0	11,5	16,0	11,9	20,0	13,1	21,0	14,8
		9,0	4,2	9,0	7,2	9,0	9,8	13,0	10,6	19,0	11,2	24,0	12,5	25,0	14,3
		10,0	3,3	10,0	6,3	10,0	9,0	16,0	9,7	23,0	10,6	28,0	12,0	28,0	13,9
				11,0	5,7	11,0	8,5	18,0	9,2	24,0	10,5	30,0	12,0	29,0	13,8
				12,0	5,4	12,0	8,0	20,0	8,9	25,0	10,4			30,0	13,8
				13,0	5,2	13,0	7,6	22,0	8,6	27,0	10,2				
				14,0	5,0	14,0	7,4	23,0	8,6	29,0	10,2				
				14,5	5,0	15,5	7,1	26,0	8,6						
						16,0	7,0								
						17,5	6,8								
						20,0	6,7								

Table A15: raw data for settling in an inclined tubes
(sections 4.4.3 and 4.4.6)

μ = 0.48 poise		α = 15°		d = 133 µm											
ε = 95%		ε = 90%		ε = 85%		ε = 80%		ε = 75%		ε = 70%		ε = 65%		ε = 60%	
t min	h cm	t min	h cm	t min	h cm	t min	h cm	t min	h cm	t min	h cm	t min	h cm	t min	h cm
0,0	20,0	0,0	20,0	0,0	20,0	0,0	20,0	0,0	20,0	0,0	20,0	0,0	20,0	0,0	20,0
0,5	18,0	0,6	18,0	1,0	17,2	1,0	17,8	1,0	18,4	1,0	18,9	1,0	19,2	1,0	19,5
1,0	16,0	1,0	16,8	2,0	14,9	2,0	16,0	2,0	17,1	2,0	17,9	2,0	18,5	2,0	19,0
2,0	12,0	1,5	15,2	3,0	12,9	3,0	14,3	3,0	15,9	3,0	17,0	4,0	17,3	5,0	17,9
3,0	9,5	2,0	13,8	4,0	11,1	4,0	13,0	4,0	14,9	4,0	16,2	6,0	16,3	8,0	16,9
4,0	6,8	2,5	12,5	5,0	9,7	5,0	11,8	5,0	13,9	6,0	14,9	8,0	15,5	11,0	16,0
5,0	4,7	3,0	11,2	6,0	8,4	6,0	10,8	6,0	13,1	8,0	13,8	10,0	14,8	14,0	15,3
6,0	3,0	4,0	9,3	7,0	7,3	7,0	9,9	7,0	12,4	10,0	12,9	13,0	13,8	17,0	14,7
8,0	3,0	5,0	7,5	8,0	6,4	8,0	9,1	9,0	11,2	12,0	12,2	16,0	13,1	20,0	14,3
		5,5	6,7	9,0	5,7	9,0	8,5	11,0	10,2	15,0	11,3	19,0	12,5	22,0	14,0
		6,0	6,0	10,0	5,5	10,0	8,0	13,0	9,6	17,0	10,9	22,0	12,2	23,0	13,9
		6,5	5,3	11,0	5,2	11,0	7,6	15,0	9,1	19,0	10,5	26,0	12,0	24,0	13,8
		7,0	4,7	12,0	5,1	12,0	7,3	17,0	8,8	20,0	10,5				
		8,0	3,5	13,0	5,0	13,0	7,1	20,0	8,7	24,0	10,4				
		9,0	3,2	13,2	5,0	14,0	7,0								
						15,0	6,8								
						17,0	6,8								

Table A16: raw data for settling in an inclined tubes
(sections 4.4.3 and 4.4.6)

μ = 0.48 poise		α = 20°		d = 133 μm											
ε = 95%		ε = 90%		ε = 85%		ε = 80%		ε = 75%		ε = 70%		ε = 65%		ε = 60%	
t min	h cm	t min	h cm	t min	h cm	t min	h cm	t min	h cm	t min	h cm	t min	h cm	t min	h cm
0,0	20,0	0,0	20,0	0,0	20,0	0,0	20,0	0,0	20,0	0,0	20,0	0,0	20,0	0,0	20,0
0,5	17,6	0,5	17,8	0,5	18,4	0,6	18,2	1	18,0	1,0	18,7	1,5	18,5	2,0	18,8
1,0	15,0	1,0	15,8	1,0	16,7	1,0	17,3	2,0	16,4	2,0	17,5	2,0	18,1	4,0	17,8
1,5	12,6	1,5	14,0	1,5	15,2	1,5	16,2	3,0	15,1	3,0	16,5	3,5	17,1	6,0	17,0
2,0	10,7	2,0	12,3	2,0	13,9	2,0	15,3	4,0	14,0	4,0	15,7	5,0	16,2	8,0	16,3
3,0	7,5	2,5	11,0	2,5	12,7	3,0	13,5	5,5	12,6	6,0	14,2	7,0	15,5	10,0	15,7
3,5	6,0	3,0	9,7	3,0	11,6	4,0	12,1	6,0	12,2	8,0	13,1	9,0	14,4	12,0	15,5
4,0	4,7	4,0	7,5	4,0	9,9	5,0	10,8	7,0	11,5	10,0	12,2	11,0	13,7	14,0	14,8
4,5	3,5	4,0	6,5	5,0	8,4	6,0	9,9	8,0	10,8	12,0	11,5	14,0	12,9	16,0	14,4
5,0	2,8	5,0	5,8	6,0	7,2	7,0	9,0	10,0	9,9	14,0	11,0	17,0	12,3	18,0	14,1
6,5	2,8	5,5	5,0	7,0	6,2	8,0	8,3	12,0	9,3	16,0	10,6	18,0	12,2	20,0	13,8
		6,0	4,3	8,0	5,6	9,0	7,7	14,0	8,9	17,0	10,5	20,0	12,0		
		7,0	3,5	9,0	5,4	10,0	7,4	16,0	8,6	18,0	10,4				
		8,1	3,5	10,0	5,3	11,0	7,2	17	8,5	20	10,3				
				12,0	5,2	13,0	6,8								
						15,0	6,7								

Table A17: raw data for settling in an inclined tubes
(sections 4.4.3 and 4.4.6)

μ = 0.48 poise		α = 30°		d = 133 μm											
ε = 95%		ε = 90%		ε = 85%		ε = 80%		ε = 75%		ε = 70%		ε = 65%		ε = 60%	
t min	h cm	t min	h cm	t min	h cm	t min	h cm	t min	h cm	t min	h cm	t min	h cm	t min	h cm
0,0	20,0	0,0	20,0	0,0	20,0	0,0	20,0	0,0	20,0	0,0	20,0	0,0	20,0	0,0	20,0
0,5	16,8	0,5	17,2	0,5	17,6	1,0	16,5	0,5	18,5	0,5	19,0	1,5	18,1	1,0	19,0
1,0	13,2	1,0	14,2	1,0	15,5	2,0	13,6	1,0	17,2	1,5	17,3	2,0	17,6	2,0	18,3
1,5	10,3	1,5	12,0	1,5	13,6	2,5	12,7	1,5	16,2	2,0	16,6	3,0	16,7	3,0	17,6
2,0	8,0	2,0	10,2	2,0	12,1	3,0	11,8	2,0	15,3	3,0	15,3	4,0	16,0	4,0	17,1
2,5	6,3	3,0	7,4	2,5	10,7	3,5	11,0	3,0	13,7	4,0	14,3	6,0	14,7	7,0	15,6
3,0	4,7	3,5	6,2	3,0	9,8	4,0	10,2	4,0	12,6	6,0	12,8	8,0	13,8	9,0	14,9
3,5	3,3	4,0	5,3	3,5	8,8	4,5	9,7	5,0	11,5	8,5	11,4	10,0	13,0	10,0	14,6
4,0	2,5	4,5	4,5	4,0	8,0	5,0	9,1	6,0	10,7	11,0	10,6	12,0	12,4	11,0	14,3
		5,0	3,8	5,0	6,6	5,5	8,8	7,0	10,1	12,0	10,4	13,5	12,0	12,0	14,1
		6,0	3,3	6,0	5,7	6,0	8,2	8,0	9,6	15,0	10,3			15,0	13,9
				7,0	5,3	7,0	7,6	9,0	9,2						
						8,0	7,2	13,0	8,8						
						9,0	7,0								

Table **A18: Raw** data for velocity of ascending particles within clear-fluid channel at height H = 1 cm , C_o=0.2 (section 5-3-1-1)

N	Time (min)	V (cm/min)	N	Time (min)	V (cm/min)	N	Time (min)	V (cm/min)
1	0.02	11.35	11	0.50	5.85	21	1.70	4.54
2	0.02	16.40	12	0.55	8.56	22	1.98	4.75
3	0.05	13.45	13	0.72	5.81	23	2.49	2.21
4	0.08	15.04	14	0.76	5.18	24	2.65	3.78
5	0.12	15.79	15	0.85	4.05	25	2.89	2.28
6	0.16	9.57	16	1.05	5.13	26	2.99	1.76
7	0.18	10.64	17	1.17	4.21	27	3.30	0.82
8	0.23	7.85	18	1.26	5.22	28	3.44	1.39
9	0.31	9.87	19	1.40	4.05	29	3.38	1.04
10	0.38	7.94	20	1.44	3.95	30	3.74	0.93

Table **A19: Raw** data for velocity of ascending particles within clear-fluid channel at height H = 2 cm , C_o=0.2 (section 5-3-1-1)

N	Time (min)	V (cm/min)	N	Time (min)	V (cm/min)	N	Time (min)	V (cm/min)
1	0.02	30.14	13	0.41	16.92	24	1.17	9.00
2	0.04	19.53	14	0.45	17.54	25	1.79	4.22
3	0.05	21.64	15	0.48	14.80	26	1.78	3.68
4	0.09	22.83	16	0.53	12.30	27	1.91	2.57
5	0.13	21.26	17	0.56	15.24	28	2.18	4.30
6	0.17	21.53	18	0.66	11.48	29	2.30	5.49
7	0.20	20.01	19	0.81	13.63	30	2.45	5.28
8	0.23	18.47	20	0.88	11.41	31	2.49	5.03
9	0.27	21.29	21	0.93	9.36	32	2.57	5.08
10	0.29	16.79	22	0.97	5.03	33	2.70	6.11
11	0.33	14.35	23	1.08	8.53	34	2.78	4.88
12	0.36	15.40						

Table **A20: Raw** data for velocity of ascending particles within clear-fluid channel at height H= 3 cm , C_o=0.2 (section 5-3-1-1)

N	Time (min)	V (cm/min)	N	Time (min)	V (cm/min)	N	Time (min)	V (cm/min)
1	0.02	23.68	28	0.69	15.04	55	3.44	4.25
2	0.03	26.95	29	0.73	15.07	56	3.60	5.37
3	0.05	27.86	30	0.70	18.13	57	3.74	4.66
4	0.07	29.47	31	0.76	16.19	58	3.91	5.29
5	0.09	37.15	32	0.80	10.19	59	3.92	5.21
6	0.10	14.29	33	0.88	12.75	60	4.07	5.05
7	0.13	28.38	34	0.94	12.51	61	4.20	5.15
8	0.15	28.71	35	1.05	13.12	62	4.25	4.95
9	0.16	24.81	36	1.16	9.57	63	4.39	4.32
10	0.17	20.81	37	1.23	11.62	64	4.48	3.67
11	0.19	23.16	38	1.28	10.61	65	4.58	4.50
12	0.22	24.06	39	1.48	4.96	66	4.85	3.43
13	0.23	23.49	40	1.63	2.77	67	5.00	4.09
14	0.23	24.80	41	1.71	6.89	68	5.08	4.48
15	0.24	24.61	42	1.85	6.12	69	5.22	4.05
16	0.26	26.69	43	1.98	6.35	70	5.35	3.67
17	0.28	24.81	44	2.05	5.76	71	5.48	3.10
18	0.32	22.03	45	2.13	6.39	72	5.65	2.65
19	0.34	22.83	46	2.19	5.26	73	5.74	2.55
20	0.35	9.11	47	2.32	3.56	74	5.94	2.31
21	0.39	16.28	48	2.42	4.58	75	5.96	2.21
22	0.41	20.61	49	2.56	3.06	76	6.08	2.37
23	0.44	22.48	50	2.69	5.26	77	6.17	2.02
24	0.50	17.54	51	2.82	4.80	78	6.41	2.27
25	0.52	21.53	52	2.92	4.26	79	6.70	1.81
26	0.61	18.05	53	3.03	5.20	80	7.12	0.53
27	0.66	17.07	54	3.15	4.74			

Table **A21: Raw** data for velocity of ascending particles within clear-fluid channel at height H = 4 cm , C_o=0.2 (section 5-3-1-1)

N	Time (min)	V (cm/min)	N	Time (min)	V (cm/min)	N	Time (min)	V (cm/min)
1	0.02	15.30	33	0.78	19.58	64	3.49	5.51
2	0.05	37.15	34	0.82	22.56	65	3.57	4.82
3	0.06	35.93	35	0.91	19.24	66	3.68	4.29
4	0.10	28.71	36	0.97	18.58	67	3.80	5.34
5	0.13	29.42	37	1.04	18.76	68	4.04	5.66
6	0.14	33.55	38	1.08	16.13	69	4.22	4.50
7	0.17	26.11	39	1.12	15.04	70	4.29	5.61
8	0.20	26.32	40	1.24	9.76	71	4.33	7.16
9	0.23	32.02	41	1.27	15.91	72	4.53	6.46
10	0.26	25.96	42	1.31	18.17	73	4.69	5.26
11	0.28	27.46	43	1.36	12.79	74	4.77	6.05
12	0.32	16.54	44	1.42	17.91	75	4.88	6.24
13	0.35	26.25	45	1.48	10.70	76	5.08	6.73
14	0.37	25.26	46	1.50	13.75	77	5.20	5.94
15	0.38	31.15	47	1.55	20.04	78	5.38	6.63
16	0.37	29.61	48	1.62	10.72	79	5.52	5.92
17	0.39	22.56	49	1.70	8.58	80	5.64	4.59
18	0.41	15.22	50	1.78	8.61	81	5.74	4.98
19	0.43	27.86	51	1.87	12.63	82	5.82	5.50
20	0.47	32.01	52	1.91	10.47	83	6.05	5.69
21	0.48	26.25	53	2.01	11.00	84	6.27	3.82
22	0.50	26.32	54	2.09	8.59	85	6.50	3.60
23	0.53	22.71	55	2.17	7.89	86	6.67	4.01
24	0.56	16.40	56	2.26	8.48	87	6.96	2.56
25	0.58	21.53	57	2.32	8.23	88	7.08	3.45
26	0.62	26.95	58	2.43	6.24	89	7.24	3.72
27	0.64	23.11	59	2.53	5.69	90	7.36	2.24
28	0.66	23.68	60	2.63	6.42	91	7.54	2.12
29	0.68	22.83	61	2.84	2.04	92	7.68	2.56
30	0.70	21.53	62	2.96	1.94	93	7.86	2.29
31	0.72	21.53	63	3.30	6.02	94	8.16	2.01
32	0.75	26.11						

Table **A22: Raw** data for velocity of ascending particles within clear-fluid channel at height H = 5 cm , C_o=0.2 (section 5-3-1-1)

N	Time (min)	V (cm/min)
1	0.01	16.19
2	0.03	27.86
3	0.03	61.12
4	0.05	25.26
5	0.06	24.47
6	0.07	47.37
7	0.09	39.47
8	0.10	36.44
9	0.11	39.04
10	0.13	34.54
11	0.14	37.15
12	0.15	40.87
13	0.17	39.04
14	0.18	34.45
15	0.20	33.18
16	0.22	38.13
17	0.24	34.45
18	0.26	34.17
19	0.27	34.74
20	0.30	31.15
21	0.31	35.33
22	0.34	36.40
23	0.35	30.65
24	0.38	31.58
25	0.40	35.75
26	0.42	32.63
27	0.45	33.55
28	0.46	35.60
29	0.48	30.59
30	0.50	29.61
31	0.54	37.15
32	0.56	29.61
33	0.57	32.57
34	0.60	32.57
35	0.62	33.18
36	0.64	32.57
37	0.67	24.06
38	0.70	26.25
39	0.71	29.61
40	0.73	27.86
41	0.76	29.67
42	0.79	28.47
43	0.83	30.59
44	0.87	30.21
45	0.94	19.74

N	Time (min)	V (cm/min)
46	0.96	25.26
47	1.00	25.96
48	1.06	26.25
49	1.09	24.06
50	1.12	23.68
51	1.16	16.84
52	1.19	25.10
53	1.24	18.13
54	1.28	20.84
55	1.32	21.53
56	1.36	20.83
57	1.39	23.83
58	1.43	21.05
59	1.49	20.18
60	1.52	16.92
61	1.56	17.57
62	1.59	20.54
63	1.62	17.54
64	1.64	18.05
65	1.70	15.63
66	1.73	14.28
67	1.77	20.01
68	1.87	17.96
69	1.94	15.38
70	1.99	10.09
71	2.07	13.16
72	2.11	11.28
73	2.16	13.95
74	2.22	12.81
75	2.26	13.82
76	2.36	9.76
77	2.44	9.37
78	2.52	10.41
79	2.61	10.20
80	2.66	8.27
81	2.74	9.85
82	2.86	7.43
83	2.90	7.27
84	3.02	5.80
85	3.15	6.24
86	3.24	6.40
87	3.31	7.09
88	3.40	6.82
89	3.49	6.51
90	3.62	7.15

N	Time (min)	V (cm/min)
91	3.74	7.15
92	3.85	4.85
93	3.94	7.17
94	4.09	5.58
95	4.22	5.47
96	4.32	5.57
97	4.41	5.97
98	4.52	4.83
99	4.60	6.21
100	4.72	5.81
101	4.82	5.52
102	4.95	3.91
103	5.09	4.11
104	5.20	4.91
105	5.34	4.48
106	5.50	5.26
107	5.58	5.11
108	5.74	6.23
109	5.91	6.53
110	5.96	4.93
111	6.04	6.09
112	6.12	6.42
113	6.20	5.22
114	6.20	4.99
115	6.31	4.57
116	6.46	5.06
117	6.52	5.78
118	6.68	5.34
119	6.76	5.57
120	6.96	5.34
121	7.12	5.41
122	7.19	5.72
123	7.32	5.69
124	7.45	5.88
125	7.53	5.63
126	7.67	5.05
127	7.74	5.13
128	8.06	5.29
129	8.19	4.49
130	8.33	4.09
131	8.49	3.17
132	8.68	2.60
133	8.98	3.00
134	9.36	1.68
135	9.54	0.97

Table A23: **Raw** data for velocity of ascending particles within clear-fluid channel at height H = 7 cm , C_o=0.2 (section 5-3-1-1)

N	Time (min)	V (cm/min)	N	Time (min)	V (cm/min)	N	Time (min)	V (cm/min)
1	0.02	19.87	31	0.66	37.89	61	1.58	28.38
2	0.04	58.95	32	0.69	40.31	62	1.62	27.69
3	0.07	27.46	33	0.72	37.43	63	1.66	23.59
4	0.09	42.11	34	0.75	38.13	64	1.69	25.96
5	0.11	33.37	35	0.78	33.24	65	1.72	20.37
6	0.12	35.47	36	0.80	38.39	66	1.76	25.26
7	0.14	45.28	37	0.83	32.11	67	1.79	19.94
8	0.16	32.11	38	0.85	45.11	68	1.81	23.68
9	0.18	48.80	39	0.88	42.90	69	1.87	25.96
10	0.20	35.75	40	0.91	35.79	70	1.90	21.53
11	0.21	37.89	41	0.95	33.24	71	1.94	28.55
12	0.23	97.89	42	0.99	25.76	72	1.98	27.97
13	0.25	29.61	43	1.05	31.58	73	2.01	21.75
14	0.28	38.54	44	1.08	29.61	74	2.05	19.53
15	0.30	39.47	45	1.14	40.52	75	2.08	21.05
16	0.31	51.82	46	1.17	31.58	76	2.12	16.17
17	0.33	41.45	47	1.19	28.79	77	2.19	18.71
18	0.34	35.75	48	1.22	30.59	78	2.21	20.84
19	0.36	45.93	49	1.24	28.38	79	2.25	21.05
20	0.38	47.37	50	1.27	31.58	80	2.29	23.27
21	0.40	40.19	51	1.29	31.58	81	2.32	19.69
22	0.43	37.89	52	1.32	23.31	82	2.35	17.57
23	0.46	39.96	53	1.36	41.66	83	2.39	22.91
24	0.48	40.87	54	1.38	31.58	84	2.47	21.64
25	0.53	38.67	55	1.41	26.82	85	2.50	19.30
26	0.54	46.05	56	1.44	27.97	86	2.54	21.53
27	0.56	38.39	57	1.47	21.41	87	2.58	21.27
28	0.57	37.02	58	1.50	23.31	88	2.61	17.57
29	0.61	44.50	59	1.53	27.69	89	2.66	18.05
30	0.65	38.67	60	1.55	26.11	90	2.69	20.03

Table **A24: Raw** data for velocity of ascending particles within clear-fluid channel at height H = 8 cm , C_o=0.2 (section 5-3-1-1)

N	Time (min)	V (cm/min)
1	0.01	16.41
2	0.01	50.00
3	0.01	60.00
4	0.02	56.90
5	0.01	58.62
6	0.02	71.74
7	0.05	32.29
8	0.06	44.74
9	0.09	31.82
10	0.10	33.67
11	0.12	36.36
12	0.14	36.25
13	0.16	34.69
14	0.17	38.46
15	0.19	40.54
16	0.22	40.79
17	0.24	36.96
18	0.25	37.50
19	0.27	37.50
20	0.29	39.77
21	0.30	43.14
22	0.32	34.09
23	0.34	34.62
24	0.36	34.38
25	0.38	34.04
26	0.41	34.09
27	0.45	32.05
28	0.47	33.90
29	0.49	34.38
30	0.53	19.05
31	0.55	29.59
32	0.59	25.36
33	0.61	28.33
34	0.65	29.25
35	0.67	30.00
36	0.70	34.69
37	0.73	25.78
38	0.77	28.57
39	0.80	30.43
40	0.81	28.45
41	0.84	31.63
42	0.86	36.17
43	0.90	29.09
44	0.95	25.78
45	1.06	25.83
46	1.07	34.37
47	1.11	25.95
48	1.15	26.61
49	1.18	30.00
50	1.20	35.83
51	1.23	23.91
52	1.25	29.82
53	1.30	26.72
54	1.32	34.31
55	1.34	28.18
56	1.38	28.57
57	1.42	26.56
58	1.45	26.67
59	1.48	26.32
60	1.51	26.98
61	1.54	28.33
62	1.62	24.17
63	1.66	25.45
64	1.68	26.52
65	1.73	18.67
66	1.76	24.53
67	1.82	19.53
68	1.85	23.97
69	1.91	21.43
70	1.94	17.03
71	1.99	16.67
72	2.02	17.14
73	2.09	23.19
74	2.11	20.67
75	2.15	19.87
76	2.17	20.67
77	2.20	17.31
78	2.26	16.48
79	2.33	16.24
80	2.39	11.70
81	2.41	21.74
82	2.44	19.85
83	2.49	20.31
84	2.52	14.67
85	2.55	15.63
86	2.50	1.44
87	2.63	17.61
88	2.65	17.05
89	2.70	18.67
90	2.72	17.05
91	2.80	20.24
92	2.85	21.33
93	2.87	17.09
94	2.93	19.59
95	2.99	14.45
96	3.06	16.02
97	3.14	12.61
98	3.18	15.23
99	3.28	7.56
100	3.33	15.57
101	3.44	15.74
102	3.50	14.60
103	3.57	15.53
104	3.62	12.41
105	3.70	15.23
106	3.78	15.32
107	3.82	14.71
108	3.86	15.47
109	3.93	13.45
110	3.98	12.89
111	4.06	7.24
112	4.11	13.75
113	4.16	10.19
114	4.27	9.36
115	4.32	12.85
116	4.41	13.27
117	4.47	12.40
118	4.52	12.84
119	4.54	13.89
120	4.66	10.22
121	4.71	7.55
122	4.80	9.62
123	4.86	8.22
124	4.91	10.64
125	4.94	4.93
126	4.98	9.79
127	5.03	7.26
128	5.07	7.14
129	5.08	9.09
130	5.12	7.39
131	5.16	3.55
132	5.24	4.55
133	5.29	1.64
134	5.30	5.68
135	5.40	3.52
136	5.42	2.53

Table **A25: Raw** data for velocity of ascending particles within clear-fluid channel at height H = 9 cm , C_o=0.2 (section 5-3-1-1)

N	Time (min)	V (cm/min)	N	Time (min)	V (cm/min)	N	Time (min)	V (cm/min)
1	0.00	21.76	51	1.08	41.68	101	2.42	33.25
2	0.02	47.36	52	1.10	38.30	102	2.45	31.33
3	0.03	25.53	53	1.14	38.56	103	2.47	32.91
4	0.06	63.83	54	1.17	41.68	104	2.49	34.62
5	0.08	58.20	55	1.18	32.42	105	2.52	27.98
6	0.10	51.06	56	1.21	35.83	106	2.55	30.92
7	0.10	61.17	57	1.25	40.03	107	2.58	27.05
8	0.14	49.32	58	1.28	33.97	108	2.60	26.53
9	0.17	49.47	59	1.31	38.80	109	2.62	31.91
10	0.19	45.26	60	1.35	33.66	110	2.64	32.98
11	0.21	49.32	61	1.38	39.89	111	2.67	33.66
12	0.24	49.10	62	1.41	29.01	112	2.69	29.79
13	0.26	44.56	63	1.42	31.92	113	2.71	32.35
14	0.28	46.97	64	1.45	36.32	114	2.74	30.04
15	0.29	47.87	65	1.47	38.80	115	2.77	26.60
16	0.31	47.46	66	1.50	34.04	116	2.80	33.54
17	0.32	47.87	67	1.54	35.67	117	2.82	33.54
18	0.34	45.35	68	1.55	40.38	118	2.86	22.80
19	0.37	47.87	69	1.58	39.46	119	2.89	28.88
20	0.38	46.58	70	1.61	38.54	120	2.92	26.38
21	0.39	54.26	71	1.64	30.92	121	2.95	30.44
22	0.43	42.55	72	1.66	40.24	122	2.99	27.98
23	0.44	45.79	73	1.68	35.83	123	3.02	30.92
24	0.46	40.38	74	1.71	43.52	124	3.05	11.05
25	0.48	44.97	75	1.73	43.52	125	3.08	22.20
26	0.49	46.28	76	1.76	37.42	126	3.13	10.41
27	0.51	44.97	77	1.78	36.32	127	3.15	32.46
28	0.54	41.22	78	1.81	29.92	128	3.19	27.48
29	0.57	50.74	79	1.84	33.26	129	3.23	27.11
30	0.58	44.68	80	1.88	34.04	130	3.26	26.38
31	0.61	56.74	81	1.92	32.46	131	3.29	27.87
32	0.63	41.03	82	1.94	34.82	132	3.32	24.24
33	0.65	41.30	83	1.96	28.37	133	3.42	30.92
34	0.67	47.87	84	2.00	28.68	134	3.45	25.36
35	0.69	38.54	85	2.03	27.80	135	3.47	21.51
36	0.71	46.54	86	2.07	34.73	136	3.50	22.04
37	0.72	46.04	87	2.10	30.92	137	3.53	16.98
38	0.75	60.18	88	2.13	36.82	138	3.58	17.80
39	0.77	40.38	89	2.15	33.54	139	3.63	16.46
40	0.82	31.00	90	2.17	31.91	140	3.65	22.80
41	0.83	43.52	91	2.19	31.91	141	3.67	21.92
42	0.86	36.32	92	2.20	39.08	142	3.70	21.47
43	0.88	45.39	93	2.22	33.59	143	3.73	25.53
44	0.90	53.19	94	2.25	31.91	144	3.75	19.50
45	0.91	43.46	95	2.27	27.23	145	3.78	21.03
46	0.93	47.53	96	2.31	31.92	146	3.81	17.65
47	0.95	37.33	97	2.34	29.79	147	3.82	17.48
48	0.99	54.01	98	2.36	29.10	148	3.86	21.02
49	1.01	31.91	99	2.38	28.68	149	3.88	23.13
50	1.06	42.99	100	2.40	30.04	150	3.90	14.48

Table A25: Raw data for velocity of ascending particles within clear-fluid channel at height H = 9 cm , C_o=0.2 (section 5-3-1-1)

N	Time (min)	V (cm/min)
151	3.93	22.24
152	3.97	17.41
153	3.99	16.72
154	4.03	4.91
155	4.06	12.16
156	4.08	19.95
157	4.09	11.40
158	4.12	16.90
159	4.13	19.43
160	4.15	8.78
161	4.17	14.33
162	4.23	6.20
163	4.25	9.25
164	4.31	11.10
165	4.33	7.45
166	4.37	3.68
167	4.39	5.07
168	4.42	5.80

N	Time (min)	V (cm/min)
169	0.01	46.90
170	0.03	24.02
171	0.07	49.32
172	0.17	50.77
173	0.19	48.20
174	0.28	49.32
175	0.34	49.27
176	0.37	48.74
177	0.48	46.42
178	0.50	51.31
179	0.54	51.86
180	0.91	43.46
181	0.99	53.67
182	1.01	47.03
183	1.65	39.89
184	1.69	34.89
185	1.74	43.67

N	Time (min)	V (cm/min)
186	2.07	35.74
187	2.42	23.01
188	2.82	34.82
189	3.42	30.04
190	3.47	27.98
191	3.53	18.93
192	3.75	19.79
193	3.78	21.76
194	3.82	17.73
195	3.86	17.73
196	3.91	11.75
197	3.97	17.48
198	4.00	10.38
199	4.06	12.89
200	4.12	16.55
201	4.17	13.73
202	4.23	8.74

Table A26: Raw data for velocity of ascending particles within clear-fluid channel at height H = 10 cm , C_o=0.2 (section 5-3-1-1)

N	Time (min)	V (cm/min)	N	Time (min)	V (cm/min)	N	Time (min)	V (cm/min)
1	0.01	30.57	51	1.15	37.50	101	2.50	35.29
2	0.02	36.23	52	1.17	43.64	102	2.52	28.13
3	0.03	37.65	53	1.20	33.96	103	2.54	33.68
4	0.04	37.96	54	1.21	51.43	104	2.57	38.18
5	0.06	55.50	55	1.26	38.82	105	2.59	29.17
6	0.07	61.71	56	1.29	43.64	106	2.62	40.68
7	0.09	49.23	57	1.31	36.25	107	2.66	37.06
8	0.12	40.00	58	1.35	40.91	108	2.68	32.00
9	0.13	36.25	59	1.37	40.91	109	2.72	29.17
10	0.15	48.00	60	1.38	33.96	110	2.75	28.12
11	0.16	41.25	61	1.40	40.91	111	2.77	27.27
12	0.19	61.67	62	1.44	39.66	112	2.81	25.00
13	0.19	45.00	63	1.46	42.27	113	2.86	29.51
14	0.21	35.00	64	1.48	35.79	114	2.89	28.23
15	0.25	38.08	65	1.51	38.18	115	2.92	25.00
16	0.26	43.64	66	1.53	36.47	116	2.95	30.00
17	0.30	36.73	67	1.55	38.18	117	2.98	30.81
18	0.31	58.18	68	1.57	46.15	118	3.00	28.00
19	0.33	34.62	69	1.58	42.86	119	3.05	25.06
20	0.37	53.14	70	1.60	42.27	120	3.09	27.27
21	0.38	45.00	71	1.62	43.20	121	3.15	14.46
22	0.42	45.00	72	1.65	40.00	122	3.19	26.30
23	0.43	48.00	73	1.68	37.65	123	3.21	20.83
24	0.46	54.86	74	1.70	29.03	124	3.24	23.23
25	0.47	38.18	75	1.73	47.37	125	3.29	16.36
26	0.50	45.00	76	1.76	36.84	126	3.31	26.67
27	0.51	54.86	77	1.79	35.77	127	3.34	19.69
28	0.53	47.14	78	1.81	29.03	128	3.36	15.60
29	0.54	40.91	79	1.85	29.17	129	3.39	13.61
30	0.55	47.69	80	1.88	27.00	130	3.41	21.18
31	0.57	36.73	81	1.91	40.68	131	3.44	12.91
32	0.60	37.65	82	1.94	31.94	132	3.47	6.52
33	0.64	41.74	83	1.97	32.83	133	3.49	13.75
34	0.65	48.65	84	1.99	36.00	134	3.51	15.62
35	0.67	39.60	85	2.04	31.00	135	3.56	4.69
36	0.71	40.91	86	2.08	45.00	136	3.61	13.64
37	0.72	40.50	87	2.13	33.06	137	3.62	4.09
38	0.74	48.00	88	2.16	35.51	138	3.65	15.00
39	0.76	41.25	89	2.18	29.51	139	3.67	10.91
40	0.79	50.00	90	2.22	31.48	140	3.70	6.55
41	0.86	32.73	91	2.24	33.96	141	0.03	36.00
42	0.91	35.77	92	2.26	31.53	142	0.02	35.59
43	0.93	58.29	93	2.28	32.00	143	0.01	48.98
44	0.97	30.00	94	2.31	22.41	144	0.05	26.09
45	0.98	51.43	95	2.33	33.96	145	0.11	42.27
46	1.00	53.14	96	2.36	31.53	146	0.13	45.28
47	1.02	33.68	97	2.39	31.53	147	0.16	43.64
48	1.05	36.23	98	2.43	31.23	148	0.19	46.91
49	1.08	39.07	99	2.45	31.23	149	0.23	42.69
50	1.12	45.00	100	2.48	25.81	150	0.26	57.27

Table A26: Raw data for velocity of ascending particles within clear-fluid channel at height H = 10 cm , C_o=0.2 (section 5-3-1-1)

N	Time (min)	V (cm/min)
151	0.41	45.82
152	0.48	38.44
153	0.51	53.18
154	0.82	49.20
155	0.92	35.29
156	0.96	43.64
157	1.23	32.63
158	1.26	36.23
159	1.30	37.50
160	1.35	37.06
161	1.37	40.00
162	1.45	30.75
163	1.73	41.33
164	1.76	29.06
165	1.78	33.96
166	2.04	31.38
167	2.06	33.96
168	2.08	45.82
169	2.24	35.29
170	2.27	29.12
171	2.32	40.00
172	2.34	34.29
173	2.41	34.41
174	2.54	32.90
175	2.80	26.47
176	2.83	32.81
177	3.10	18.75
178	3.12	21.14
179	3.15	24.80
180	3.19	25.00
181	3.32	19.35
182	3.37	28.57
183	3.41	20.45
184	3.44	18.00
185	3.49	9.92
186	3.55	14.63
187	3.59	21.82

Table A27: Raw data for velocity of ascending particles within clear-fluid channel at height H = 11 cm , C_o=0.2 (section 5-3-1-1)

N	Time (min)	V (cm/min)	N	Time (min)	V (cm/min)	N	Time (min)	V (cm/min)
1	0.00	55.26	51	1.07	50.53	101	2.48	37.47
2	0.02	63.16	52	1.09	44.21	102	2.51	36.94
3	0.04	57.42	53	1.11	47.37	103	2.54	29.72
4	0.05	74.30	54	1.12	48.80	104	2.59	20.56
5	0.06	55.26	55	1.14	48.80	105	2.64	34.54
6	0.09	73.68	56	1.16	53.68	106	2.66	26.32
7	0.11	65.34	57	1.18	46.62	107	2.73	28.07
8	0.13	74.85	58	1.20	49.12	108	2.78	25.08
9	0.14	65.79	59	1.21	51.88	109	2.81	20.10
10	0.15	75.30	60	1.24	50.24	110	2.85	18.53
11	0.17	68.90	61	1.26	51.67	111	2.93	23.68
12	0.19	63.16	62	1.29	50.24	112	2.97	20.71
13	0.22	68.90	63	1.32	51.67	113	3.00	15.79
14	0.24	63.16	64	1.35	41.63	114	3.01	22.56
15	0.27	50.09	65	1.41	50.24	115	3.02	15.79
16	0.30	53.05	66	1.45	48.80	116	3.04	15.57
17	0.32	53.44	67	1.48	40.46	117	3.07	20.37
18	0.33	54.45	68	1.50	46.86	118	3.08	24.29
19	0.35	35.53	69	1.52	52.33	119	3.09	23.39
20	0.37	65.20	70	1.54	56.39	120	3.10	16.19
21	0.38	54.55	71	1.54	52.63	121	3.11	19.85
22	0.41	65.34	72	1.56	50.53	122	3.13	11.08
23	0.42	53.68	73	1.58	36.94	123	3.14	4.80
24	0.45	54.14	74	1.62	47.37	124	0.00	53.59
25	0.49	49.62	75	1.65	60.73	125	0.03	54.62
26	0.51	54.14	76	1.68	40.19	126	0.06	57.42
27	0.54	70.38	77	1.70	53.44	127	0.08	64.96
28	0.56	51.67	78	1.72	43.42	128	0.11	68.57
29	0.58	41.63	79	1.76	41.63	129	0.13	15.67
30	0.60	45.93	80	1.79	43.06	130	0.33	55.26
31	0.62	61.12	81	1.84	40.19	131	0.37	59.92
32	0.64	53.68	82	1.87	43.82	132	0.42	54.14
33	0.68	56.84	83	1.89	43.06	133	0.82	49.62
34	0.71	55.26	84	1.91	45.34	134	1.13	61.50
35	0.73	54.14	85	1.94	37.89	135	1.21	51.82
36	0.75	45.93	86	1.97	44.96	136	1.25	55.26
37	0.78	43.94	87	2.00	37.89	137	1.29	50.20
38	0.80	47.37	88	2.02	47.37	138	1.32	57.89
39	0.81	50.24	89	2.04	40.87	139	1.33	51.21
40	0.83	52.63	90	2.11	30.59	140	1.35	43.34
41	0.85	47.37	91	2.16	47.37	141	1.66	41.45
42	0.87	49.29	92	2.19	43.06	142	1.68	41.45
43	0.87	49.29	93	2.21	36.94	143	2.07	31.58
44	0.88	54.13	94	2.27	41.68	144	2.12	33.55
45	0.92	47.37	95	2.30	40.00	145	2.16	38.78
46	0.94	51.21	96	2.31	43.64	146	2.19	43.42
47	0.96	53.68	97	2.34	39.16	147	2.21	38.71
48	0.98	50.20	98	2.38	28.81	148	2.27	47.67
49	1.05	46.78	99	2.41	30.14	149	2.30	41.68
50	1.06	47.37	100	2.46	35.60	150	2.36	32.57

Table A27: Raw data for velocity of ascending particles within clear-fluid channel at height H = 11 cm , C_o=0.2 (section 5-3-1-1)

N	Time (min)	V (cm/min)
151	2.41	37.15
152	2.51	36.56
153	2.55	27.46
154	2.59	20.18
155	2.64	34.26

N	Time (min)	V (cm/min)
156	2.77	18.76
157	2.81	19.74
158	2.86	18.13
159	2.93	16.92

N	Time (min)	V (cm/min)
160	2.97	16.62
161	3.00	14.80
162	3.05	27.46
163	3.10	9.57

Table A28: Raw data for velocity of ascending particles within clear-fluid channel at height H = 12 cm , C_o=0.2 (section 5-3-1-1)

N	Time (min)	V (cm/min)
1	0.06	27.63
2	0.08	43.42
3	0.10	55.26
4	0.12	63.16
5	0.13	84.21
6	0.14	66.48
7	0.16	59.65
8	0.17	58.95
9	0.18	71.58
10	0.22	51.46
11	0.26	66.32
12	0.28	53.44
13	0.31	47.85
14	0.33	75.79
15	0.33	54.14
16	0.35	66.32
17	0.36	54.74
18	0.39	63.16
19	0.41	72.63
20	0.43	63.16
21	0.46	40.60
22	0.49	61.12
23	0.50	61.12
24	0.51	47.91
25	0.53	45.39
26	0.54	63.16
27	0.56	54.13
28	0.58	57.90
29	0.62	48.58
30	0.65	56.14
31	0.67	57.89
32	0.68	63.16
33	0.70	53.59
34	0.72	45.93
35	0.73	52.33
36	0.76	57.74
37	0.78	48.80
38	0.79	70.18
39	0.83	69.47
40	0.84	48.42
41	0.86	50.93
42	0.87	48.72
43	0.89	45.93
44	0.93	65.07
45	0.95	47.37
46	0.97	60.15
47	1.02	51.88
48	1.03	60.29
49	1.05	43.31
50	1.06	42.72
51	1.08	56.39
52	1.10	49.62
53	1.12	55.26
54	1.13	52.27
55	1.16	54.13
56	1.18	79.63
57	1.20	50.09
58	1.24	52.63
59	1.27	49.50
60	1.36	58.30
61	1.37	52.63
62	1.38	50.09
63	1.41	52.27
64	1.44	47.37
65	1.46	50.53
66	1.48	50.53
67	1.50	42.63
68	1.51	47.85
69	1.53	41.55
70	1.55	54.45
71	1.57	43.86
72	1.59	50.53
73	1.64	43.06
74	1.65	48.12
75	1.67	46.54
76	1.70	41.05
77	1.72	54.45
78	1.73	54.45
79	1.76	40.97
80	1.79	44.02
81	1.80	60.73
82	1.83	42.63
83	1.84	47.37
84	1.88	44.02
85	1.90	47.85
86	1.93	42.63
87	1.98	40.87
88	2.00	33.76
89	2.02	36.56
90	2.06	39.47
91	2.07	43.72
92	2.08	29.92
93	2.11	40.87
94	2.15	35.09
95	2.17	28.71
96	2.20	42.10
97	2.22	29.61
98	2.24	35.75
99	2.25	34.68
100	2.28	21.05
101	0.01	54.14
102	0.05	74.85
103	0.07	22.97
104	0.08	72.18
105	0.10	57.74
106	0.12	61.24
107	0.13	42.11
108	0.16	67.67
109	0.17	82.38
110	0.19	65.34
111	0.21	69.47
112	0.25	69.93
113	0.28	39.96
114	0.29	63.16
115	0.31	58.17
116	0.33	73.34
117	0.39	59.74
118	0.42	35.75
119	0.47	43.06
120	0.50	58.42
121	0.54	69.27
122	0.67	54.14
123	0.97	53.11
124	1.03	56.14
125	1.19	48.12
126	1.20	54.13
127	1.27	50.83
128	1.36	54.13
129	1.38	56.84
130	1.44	48.80
131	1.51	68.57
132	1.60	47.95
133	1.61	51.67
134	1.72	48.58
135	1.79	42.45
136	1.81	57.42
137	1.95	37.89
138	2.07	40.46
139	2.17	29.61
140	2.23	26.69
141	2.25	32.04
142	2.31	29.72
143	2.42	5.85
144	2.45	10.77
145	2.49	11.70

Table **A29: Raw** data for velocity of ascending particles within clear-fluid channel at height H = 13 cm , C_o=0.2 (section 5-3-1-1)

N	Time (min)	V (cm/min)
1	0.02	37.32
2	0.05	37.32
3	0.08	37.55
4	0.10	44.74
5	0.12	71.58
6	0.13	63.16
7	0.14	56.39
8	0.15	66.32
9	0.16	74.30
10	0.18	55.58
11	0.21	58.11
12	0.22	54.45
13	0.23	54.74
14	0.26	69.81
15	0.26	58.65
16	0.29	55.01
17	0.30	51.67
18	0.32	63.16
19	0.34	49.76
20	0.36	57.90
21	0.38	51.88
22	0.41	47.85
23	0.42	47.91
24	0.45	44.82
25	0.47	33.08
26	0.49	50.93
27	0.51	53.80
28	0.52	51.88
29	0.54	51.88
30	0.56	50.88
31	0.61	53.44
32	0.66	58.30
33	0.67	54.45
34	0.68	55.26
35	0.70	54.45
36	0.71	57.89
37	0.73	60.53
38	0.75	41.50
39	0.75	43.56
40	0.79	48.20
41	0.80	55.01
42	0.82	53.59
43	0.83	45.93
44	0.85	33.08

N	Time (min)	V (cm/min)
45	0.89	63.16
46	0.90	54.13
47	0.95	52.97
48	0.96	56.33
49	0.98	47.91
50	1.00	56.62
51	1.02	49.76
52	1.04	57.04
53	1.04	57.90
54	1.07	56.39
55	1.09	51.88
56	1.09	55.01
57	1.12	50.53
58	1.14	45.79
59	1.16	76.32
60	1.17	65.79
61	1.19	47.85
62	1.23	47.91
63	1.26	52.27
64	1.27	55.01
65	1.30	49.76
66	1.32	50.09
67	1.33	36.09
68	1.35	53.05
69	1.37	38.87
70	1.40	45.93
71	1.43	46.09
72	1.45	44.38
73	1.47	41.55
74	1.48	45.79
75	1.50	42.63
76	1.52	46.92
77	1.55	41.63
78	1.59	53.44
79	1.62	42.11
80	1.63	38.87
81	1.66	42.78
82	1.67	47.37
83	1.70	37.89
84	1.72	40.19
85	1.74	37.32
86	1.75	35.89
87	1.76	34.45

N	Time (min)	V (cm/min)
88	1.77	37.89
89	1.79	31.58
90	1.80	26.41
91	1.84	32.22
92	1.86	28.71
93	0.01	32.10
94	0.02	36.44
95	0.04	44.50
96	0.05	35.75
97	0.10	45.93
98	0.14	53.44
99	0.16	78.95
100	0.23	57.74
101	0.26	61.24
102	0.31	56.33
103	0.39	54.14
104	0.44	47.91
105	0.53	55.26
106	0.54	50.24
107	0.68	53.19
108	0.77	65.20
109	0.83	46.62
110	0.86	52.63
111	0.96	54.14
112	0.98	52.63
113	1.16	59.55
114	1.20	57.42
115	1.22	55.26
116	1.28	48.95
117	1.30	53.11
118	1.37	45.11
119	1.43	45.93
120	1.49	44.50
121	1.52	44.50
122	1.68	44.50
123	1.70	35.93
124	1.74	35.75
125	1.77	40.08
126	1.81	35.53
127	1.85	33.76
128	1.87	25.26
129	1.96	17.54
130	2.06	20.37

Table A30: Raw data for velocity of ascending particles within clear-fluid channel at height H = 14 cm , C_o=0.2 (section 5-3-1-1)

N	Time (min)	V (cm/min)	N	Time (min)	V (cm/min)	N	Time (min)	V (cm/min)
1	0.06	42.11	38	0.85	54.45	74	0.24	59.33
2	0.06	45.73	39	0.87	58.80	75	0.30	67.67
3	0.09	66.32	40	0.88	58.65	76	0.33	72.51
4	0.10	46.09	41	0.90	57.05	77	0.39	53.11
5	0.12	63.16	42	0.94	54.85	78	0.41	49.86
6	0.13	74.64	43	0.98	40.19	79	0.46	50.53
7	0.15	74.64	44	0.99	53.80	80	0.48	47.37
8	0.16	76.32	45	1.01	53.59	81	0.51	55.73
9	0.18	63.16	46	1.02	82.11	82	0.57	57.74
10	0.20	74.85	47	1.04	46.96	83	0.63	57.74
11	0.21	69.47	48	1.05	45.93	84	0.66	55.26
12	0.22	69.47	49	1.08	38.16	85	0.69	61.24
13	0.24	67.23	50	1.15	52.33	86	0.71	61.24
14	0.26	46.44	51	1.17	46.92	87	0.77	50.53
15	0.30	73.68	52	1.19	37.59	88	0.79	48.98
16	0.33	65.79	53	1.21	41.05	89	0.81	53.19
17	0.40	70.45	54	1.22	53.59	90	0.84	54.85
18	0.41	54.45	55	1.23	52.33	91	0.88	58.42
19	0.42	58.48	56	1.26	47.80	92	0.92	38.28
20	0.48	52.63	57	1.27	50.09	93	0.98	58.30
21	0.48	68.21	58	1.29	45.34	94	1.02	50.53
22	0.51	58.80	59	1.30	41.55	95	1.05	42.82
23	0.52	58.48	60	1.33	44.21	96	1.12	63.16
24	0.54	52.97	61	1.34	52.63	97	1.16	50.24
25	0.57	61.12	62	1.36	45.11	98	1.18	47.08
26	0.58	57.42	63	1.39	23.83	99	1.21	50.53
27	0.63	54.13	64	1.40	30.14	100	1.26	32.91
28	0.65	53.59	65	0.03	19.74	101	1.30	27.89
29	0.69	55.01	66	0.06	38.28	102	1.32	46.54
30	0.71	67.23	67	0.09	65.34	103	1.34	46.40
31	0.74	55.87	68	0.10	57.42	104	1.40	28.95
32	0.76	68.02	69	0.11	78.95	105	1.41	40.31
33	0.78	47.37	70	0.13	65.34	106	1.45	30.07
34	0.79	54.39	71	0.15	65.34	107	1.49	32.39
35	0.81	54.85	72	0.20	70.18	108	1.58	19.74
36	0.83	55.01	73	0.22	63.16	109	1.63	13.16
37	0.84	57.42						

Table **A31: Raw** data for velocity of ascending particles within clear-fluid channel at height H = 15 cm , C_o=0.2 (section 5-3-1-1)

N	Time (min)	V (cm/min)	N	Time (min)	V (cm/min)	N	Time (min)	V (cm/min)
1	0.02	34.14	13	0.49	42.11	24	1.04	40.79
2	0.07	40.42	14	0.52	64.74	25	1.05	67.23
3	0.10	59.55	15	0.56	63.16	26	1.08	52.11
4	0.14	61.24	16	0.61	52.43	27	1.09	43.06
5	0.17	61.35	17	0.64	64.23	28	1.12	37.15
6	0.21	54.14	18	0.74	40.81	29	1.15	17.30
7	0.23	50.00	19	0.81	49.80	30	1.16	33.59
8	0.25	50.80	20	0.88	60.58	31	1.19	37.25
9	0.28	66.48	21	0.96	45.93	32	1.23	31.58
10	0.33	64.59	22	0.99	33.68	33	1.24	20.72
11	0.37	64.96	23	1.02	27.07	34	1.28	24.81
12	0.43	66.77						

Table **A32: Raw** data for velocity of ascending particles within clear-fluid channel at height H = 17 cm , C_o=0.2 (section 5-3-1-1)

N	Time (min)	V (cm/min)	N	Time (min)	V (cm/min)	N	Time (min)	V (cm/min)
1	0.02	64.71	11	0.28	66.67	20	0.53	46.97
2	0.04	38.99	12	0.31	68.25	21	0.54	50.00
3	0.06	49.70	13	0.34	57.97	22	0.56	38.10
4	0.08	22.47	14	0.36	50.29	23	0.62	31.75
5	0.09	54.42	15	0.39	48.61	24	0.63	24.69
6	0.10	42.94	16	0.43	66.67	25	0.65	35.90
7	0.13	47.13	17	0.45	54.90	26	0.67	27.59
8	0.16	71.67	18	0.48	55.00	27	0.70	16.67
9	0.21	68.57	19	0.49	45.45	28	0.72	30.30
10	0.25	70.71						

Table **A33: Raw** data for velocity of ascending particles within clear-fluid channel at height H = 1 cm , C_o=0.1 (section 5-3-1-1)

N	Time (min)	V (cm/min)	N	Time (min)	V (cm/min)	N	Time (min)	V (cm/min)
1	0.03	11.43	12	0.34	16.00	22	0.74	11.54
2	0.05	11.69	13	0.38	15.00	23	0.83	9.06
3	0.08	13.60	14	0.41	14.81	24	0.90	6.62
4	0.12	14.75	15	0.46	13.24	25	0.96	10.08
5	0.14	20.34	16	0.49	14.75	26	1.02	9.76
6	0.16	15.25	17	0.51	15.00	27	1.07	8.91
7	0.17	17.65	18	0.54	12.86	28	1.12	8.85
8	0.19	16.36	19	0.58	15.00	29	1.26	5.36
9	0.21	15.25	20	0.65	14.29	30	1.43	4.94

Table **A34: Raw** data for velocity of ascending particles within clear-fluid channel at height H = 2 cm , C_o=0.1 (section 5-3-1-1)

N	Time (min)	V (cm/min)	N	Time (min)	V (cm/min)	N	Time (min)	V (cm/min)
1	0.02	18.75	23	0.44	23.75	44	0.98	15.19
2	0.04	21.43	24	0.46	22.17	45	0.99	8.00
3	0.05	22.50	25	0.50	25.50	46	1.05	14.12
4	0.07	23.16	26	0.51	18.11	47	1.08	14.46
5	0.09	20.34	27	0.55	22.64	48	1.10	15.43
6	0.12	30.00	28	0.57	21.36	49	1.15	14.32
7	0.13	27.69	29	0.59	21.05	50	1.17	16.19
8	0.16	27.39	30	0.62	21.05	51	1.20	13.24
9	0.19	26.25	31	0.65	18.37	52	1.23	11.74
10	0.20	25.00	32	0.66	15.79	53	1.27	12.99
11	0.22	25.50	33	0.68	17.65	54	1.34	8.51
12	0.25	25.53	34	0.71	19.57	55	1.39	10.97
13	0.27	23.53	35	0.74	20.00	56	1.42	12.37
14	0.29	19.35	36	0.77	16.98	57	1.47	9.90
15	0.30	23.53	37	0.79	14.06	58	1.59	11.74
16	0.32	22.64	38	0.80	18.75	59	1.62	9.90
17	0.34	22.50	39	0.83	13.24	60	1.66	8.69
18	0.36	24.55	40	0.85	15.00	61	1.73	9.81
19	0.37	19.57	41	0.87	18.11	62	1.76	10.30
20	0.38	25.50	42	0.93	20.00	63	1.90	9.70
21	0.40	23.18	43	0.96	14.29	64	1.97	6.21
22	0.41	23.75						

Table **A35: Raw** data for velocity of ascending particles within clear-fluid channel at height H = 3 cm , C_o=0.1 (section 5-3-1-1)

N	Time (min)	V (cm/min)
1	0.01	25.25
2	0.02	16.53
3	0.03	24.24
4	0.05	29.38
5	0.06	19.44
6	0.07	24.24
7	0.09	30.30
8	0.10	51.04
9	0.11	34.63
10	0.12	31.35
11	0.13	38.38
12	0.14	39.63
13	0.16	31.22
14	0.18	38.10
15	0.19	36.36
16	0.20	32.47
17	0.21	39.63
18	0.24	39.10
19	0.24	32.63
20	0.25	33.33
21	0.27	34.19
22	0.30	28.71
23	0.31	35.19
24	0.32	31.68
25	0.37	32.76
26	0.39	31.68
27	0.41	31.08
28	0.42	33.67
29	0.43	27.55
30	0.46	25.97
31	0.48	27.55
32	0.50	23.77
33	0.53	26.42
34	0.55	28.93
35	0.58	31.04
36	0.64	23.57
37	0.68	27.27
38	0.69	25.25
39	0.70	23.42
40	0.71	27.55
41	0.73	31.17
42	0.76	24.74
43	0.78	24.24

N	Time (min)	V (cm/min)
44	0.81	22.04
45	0.84	22.87
46	0.89	23.77
47	0.92	17.68
48	0.94	21.27
49	0.96	22.60
50	0.98	24.74
51	1.00	14.20
52	1.01	17.76
53	1.02	20.66
54	1.05	20.20
55	1.06	18.94
56	1.10	20.94
57	1.11	23.99
58	4.13	0.03
59	1.18	22.26
60	1.23	13.61
61	1.26	12.63
62	1.31	13.04
63	1.35	16.10
64	1.37	22.73
65	1.40	17.93
66	1.42	11.54
67	1.45	16.97
68	1.48	18.88
69	1.50	17.57
70	1.55	15.74
71	1.58	8.95
72	1.60	18.94
73	1.62	16.53
74	1.66	16.45
75	1.68	17.20
76	1.70	19.32
77	1.72	10.10
78	1.76	20.20
79	3.28	0.07
80	1.81	15.62
81	1.83	13.81
82	1.85	11.48
83	1.87	16.38
84	1.90	15.15
85	1.97	11.71

N	Time (min)	V (cm/min)
86	1.99	11.44
87	2.03	16.44
88	2.18	10.01
89	2.20	14.46
90	2.26	9.85
91	2.30	11.07
92	2.41	11.20
93	2.47	12.00
94	2.50	11.16
95	2.56	10.29
96	2.59	12.54
97	2.62	9.54
98	2.66	12.24
99	2.74	10.58
100	2.77	11.51
101	2.81	5.36
102	2.85	8.48
103	2.88	10.96
104	2.93	8.59
105	2.98	10.49
106	3.03	9.32
107	3.07	4.83
108	3.12	7.91
109	3.15	8.81
110	3.31	6.89
111	3.36	4.78
112	3.42	8.35
113	3.48	6.49
114	3.55	5.92
115	3.59	7.49
116	3.68	5.43
117	3.74	7.58
118	3.80	6.60
119	3.97	5.59
120	4.03	3.31
121	4.09	4.62
122	4.19	7.05
123	4.26	5.37
124	4.67	5.86
125	4.75	3.70
126	4.88	4.02
127	5.01	5.14

Table **A36: Raw** data for velocity of ascending particles within clear-fluid channel at height H = 4 cm , C_o=0.1 (section 5-3-1-1)

N	Time (min)	V (cm/min)
1	0.03	19.13
2	0.05	43.73
3	0.07	12.81
4	0.08	24.26
5	0.09	38.27
6	0.09	32.41
7	0.11	38.27
8	0.14	40.82
9	0.14	34.99
10	0.15	36.73
11	0.17	42.67
12	0.18	40.82
13	0.18	33.24
14	0.19	38.00
15	0.71	0.18
16	0.23	37.11
17	0.26	40.82
18	0.28	26.02
19	0.29	38.27
20	0.30	38.48
21	0.31	34.99
22	0.32	40.82
23	0.36	33.09
24	0.38	37.17
25	0.41	34.21
26	0.42	31.40
27	0.44	30.61
28	0.49	36.73
29	0.50	33.09
30	0.51	30.61
31	0.52	32.14
32	0.53	33.40
33	0.55	34.99
34	0.57	33.40
35	0.58	23.55
36	0.59	30.61
37	0.60	28.06
38	0.61	33.09
39	0.62	31.54
40	0.62	29.22
41	0.65	32.97
42	0.67	29.00
43	0.69	34.99
44	0.72	30.61
45	0.75	27.83
46	0.76	24.99
47	0.78	33.24
48	0.80	24.49
49	0.83	34.99
50	0.84	29.15

N	Time (min)	V (cm/min)
51	0.87	23.10
52	0.88	29.22
53	0.90	29.34
54	0.92	29.22
55	0.93	24.49
56	0.93	25.51
57	0.95	30.61
58	0.97	24.49
59	0.99	22.56
60	0.99	34.37
61	1.01	29.06
62	1.02	27.21
63	1.05	19.33
64	1.09	21.24
65	1.11	27.83
66	1.12	23.65
67	1.13	26.02
68	1.14	21.68
69	1.16	26.44
70	1.17	20.41
71	1.19	23.10
72	1.20	25.05
73	1.21	17.81
74	1.22	23.13
75	1.24	26.05
76	1.25	22.26
77	1.26	24.49
78	1.28	26.79
79	1.30	23.65
80	1.30	22.96
81	1.32	26.44
82	1.34	24.01
83	1.35	23.10
85	1.42	23.38
86	1.44	19.44
87	1.46	19.13
88	1.48	24.73
89	1.50	22.63
90	1.51	15.31
91	1.52	25.97
92	1.53	19.13
93	1.55	20.06
94	1.57	16.26
95	1.58	23.92
96	1.60	17.49
97	1.63	18.01
98	1.65	22.00
99	1.68	22.26
100	1.69	15.08

N	Time (min)	V (cm/min)
101	3.22	0.08
102	1.74	23.85
103	1.76	20.97
104	1.78	21.68
105	1.81	20.97
106	1.83	19.39
107	1.84	16.26
108	3.36	-0.05
109	1.88	17.35
110	1.91	22.00
111	1.92	16.26
112	1.95	15.50
113	1.96	16.27
114	1.99	16.26
115	2.01	18.18
116	2.04	20.41
117	2.07	16.21
118	2.11	16.57
119	2.14	19.44
120	2.15	15.31
121	2.19	20.41
122	2.22	15.50
123	2.25	12.76
124	2.28	15.31
125	2.33	16.33
126	2.37	21.43
127	2.41	17.14
128	2.45	14.26
129	2.48	17.64
130	2.51	13.17
131	2.53	17.60
132	2.56	18.18
133	2.58	17.64
134	2.60	18.55
135	2.62	14.19
136	2.66	18.01
137	2.67	14.45
138	2.70	17.01
139	2.73	10.77
140	2.76	12.37
141	2.78	8.50
142	2.81	15.50
143	2.84	16.77
144	2.89	16.77
145	2.91	11.34
146	2.93	13.91
147	2.95	13.61
148	2.97	9.98
149	2.98	15.68
150	3.00	15.11

Table **A36: Raw** data for velocity of ascending particles within clear-fluid channel at height H = 4 cm , C_o=0.1 (section 5-3-1-1)

N	Time (min)	V (cm/min)
151	3.02	18.60
152	3.05	13.89
153	3.08	15.31
154	3.09	16.21
155	3.15	6.17
156	3.19	14.82
157	3.25	13.46
158	3.26	17.01
159	3.29	16.17
160	3.31	14.58
161	3.33	8.39
162	3.36	15.68
163	3.39	11.13
164	3.41	8.50
165	3.45	13.61

N	Time (min)	V (cm/min)
166	3.47	13.04
167	3.49	13.31
168	3.30	0.40
169	3.56	11.75
170	3.61	15.31
171	3.64	14.18
172	3.68	11.85
173	3.71	13.17
174	3.74	6.80
175	3.77	13.91
176	3.82	10.70
177	3.84	13.17
178	3.88	10.52
179	3.93	7.05

N	Time (min)	V (cm/min)
180	3.98	7.41
181	4.01	9.28
182	4.06	11.48
183	4.09	7.70
184	4.12	10.80
185	4.18	6.25
186	4.21	5.19
187	4.29	7.48
188	4.34	11.85
189	4.36	7.52
190	4.42	10.86
191	4.48	6.49
192	4.52	4.91
193	4.69	4.43

Table A37: Raw data for velocity of ascending particles within clear-fluid channel at height H = 5 cm , C_o=0.1 (section 5-3-1-1)

N	Time (min)	V (cm/min)	N	Time (min)	V (cm/min)	N	Time (min)	V (cm/min)
1	0.02	10.40	51	0.68	37.49	101	1.36	30.93
2	0.04	31.72	52	0.69	29.52	102	1.38	26.51
3	0.05	37.11	53	0.73	40.53	103	1.40	27.77
4	0.08	46.39	54	0.77	34.36	104	1.41	26.71
5	0.10	39.91	55	0.79	35.35	105	1.42	28.12
6	0.11	43.53	56	0.79	35.35	106	1.43	21.91
7	0.12	42.66	57	0.80	36.08	107	1.45	37.49
8	0.13	41.24	58	0.81	29.45	108	1.46	30.93
9	0.15	41.24	59	0.82	32.33	109	1.48	20.30
10	0.19	39.36	60	0.83	30.93	110	1.49	28.12
11	0.20	41.24	61	0.85	29.52	111	1.51	29.52
12	0.21	44.79	62	0.87	35.61	112	1.52	25.55
13	0.23	41.24	63	0.88	37.11	113	1.53	23.34
14	0.25	41.97	64	0.89	30.93	114	1.55	30.93
15	0.25	45.89	65	0.91	26.89	115	1.58	28.12
16	0.27	39.91	66	0.92	39.91	116	1.60	30.93
17	0.28	44.54	67	0.93	26.71	117	1.63	26.32
18	0.29	44.79	68	0.96	31.72	118	1.64	25.77
19	0.29	44.18	69	0.97	34.36	119	1.66	22.91
20	0.30	37.49	70	0.98	34.36	120	1.67	27.49
21	0.31	47.58	71	0.99	32.56	121	1.69	30.93
22	0.32	33.74	72	1.00	30.93	122	1.70	28.24
23	0.33	37.11	73	1.01	34.18	123	1.71	28.12
24	0.35	39.36	74	1.02	33.31	124	1.72	23.34
25	0.36	37.49	75	1.03	29.52	125	1.74	28.12
26	0.36	44.18	76	1.04	24.42	126	1.75	28.87
27	0.37	43.90	77	1.05	38.88	127	1.76	28.12
28	0.38	45.20	78	1.06	33.58	128	1.79	26.32
29	0.39	39.36	79	1.08	35.61	129	1.80	29.52
30	0.41	39.36	80	1.09	32.47	130	1.81	28.24
31	0.42	43.90	81	1.09	33.74	131	1.82	26.32
32	0.44	37.49	82	1.12	32.33	132	1.85	35.35
33	0.45	39.91	83	1.13	28.12	133	1.87	26.17
34	0.46	47.58	84	1.14	33.58	134	1.89	26.89
35	0.46	39.36	85	1.15	32.47	135	1.91	23.51
36	0.48	41.90	86	1.16	27.84	136	1.92	23.34
37	0.50	37.49	87	1.18	35.11	137	1.93	29.46
38	0.51	37.11	88	1.19	32.47	138	1.95	30.13
39	0.52	45.36	89	1.21	28.35	139	1.96	26.51
40	0.53	35.35	90	1.22	30.93	140	1.97	14.39
41	0.55	37.49	91	1.23	34.89	141	1.98	20.97
42	0.56	33.74	92	1.25	26.51	142	2.01	19.92
43	0.57	38.88	93	1.26	28.12	143	2.03	21.65
44	0.58	37.49	94	1.28	32.40	144	2.04	25.25
45	0.60	26.32	95	1.28	34.36	145	2.07	23.87
46	0.61	37.80	96	1.30	32.65	146	2.08	23.34
47	0.62	39.91	97	1.30	31.72	147	2.09	26.89
48	0.64	36.78	98	1.31	35.57	148	2.11	22.49
49	0.65	39.91	99	1.32	26.51	149	2.12	25.77
50	0.67	36.08	100	1.34	34.36	150	2.13	25.47

Table A37: **Raw** data for velocity of ascending particles within clear-fluid channel at height H = 5 cm , C_o=0.1 (section 5-3-1-1)

N	Time (min)	V (cm/min)
151	2.14	25.38
152	2.16	25.77
153	2.18	20.28
154	2.19	22.72
155	2.21	28.12
156	2.23	22.40
157	2.25	28.12
158	2.26	23.90
159	2.30	29.46
160	2.31	24.51
161	2.33	25.25
162	2.35	15.27
163	2.37	19.33
164	2.38	19.95
165	2.40	20.97
166	2.42	23.62
167	2.44	20.62
168	2.47	23.34
169	2.49	22.49
170	2.50	24.51
171	2.51	8.38
172	2.53	17.67
173	2.55	24.74
174	2.56	19.33

N	Time (min)	V (cm/min)
177	2.67	19.33
178	2.69	22.49
179	2.72	22.79
180	2.72	19.92
181	2.75	14.90
182	2.77	20.28
183	2.78	24.26
184	2.80	17.03
185	2.83	23.34
186	2.84	22.49
187	2.86	20.62
188	2.88	17.42
189	2.91	18.19
190	2.94	22.02
191	2.97	21.70
192	2.98	14.73
193	3.01	18.74
194	3.02	17.67
195	3.04	21.70
196	3.07	12.71
197	3.10	20.62
198	3.12	8.17
199	3.13	20.62

N	Time (min)	V (cm/min)
202	3.21	15.46
203	3.22	16.37
204	3.24	13.75
205	3.25	20.34
206	3.27	7.73
207	3.31	18.19
208	3.33	20.62
209	3.34	20.97
210	3.36	15.46
211	3.40	8.16
212	3.45	16.49
213	3.55	18.87
214	3.58	15.82
215	3.61	16.40
216	3.63	13.31
217	3.65	14.40
218	3.68	6.92
219	3.72	15.46
220	3.77	5.75
221	3.85	13.30
222	3.89	14.95
223	3.91	10.64
224	3.95	4.91

Table **A38: Raw** data for velocity of ascending particles within clear-fluid channel at height H = 6 cm , C_o=0.1 (section 5-3-1-1)

N	Time (min)	V (cm/min)	N	Time (min)	V (cm/min)	N	Time (min)	V (cm/min)
1	0.04	11.60	51	0.74	45.20	101	1.42	35.35
2	0.05	28.12	52	0.74	39.36	102	1.44	22.20
3	0.05	24.98	53	0.75	36.26	103	1.45	37.49
4	0.08	32.47	54	0.76	41.90	104	1.45	41.24
5	0.09	29.52	55	0.77	29.93	105	1.47	42.66
6	0.10	42.66	56	0.78	43.11	106	1.48	33.74
7	0.12	41.24	57	0.80	44.18	107	1.49	32.65
8	0.12	44.54	58	0.82	37.49	108	1.50	35.35
9	0.13	45.20	59	0.84	41.90	109	1.51	37.11
10	0.14	41.97	60	0.85	41.24	110	1.55	35.61
11	0.16	49.06	61	0.85	31.81	111	1.56	35.35
12	0.17	45.36	62	0.87	32.40	112	1.57	36.48
13	0.18	50.40	63	0.90	41.90	113	1.58	37.49
14	0.19	46.92	64	0.91	36.78	114	1.59	35.35
15	0.21	42.66	65	0.94	36.26	115	1.61	23.20
16	0.22	42.66	66	0.95	41.24	116	1.62	35.35
17	0.23	44.18	67	0.97	43.82	117	1.63	32.47
18	0.24	45.89	68	0.98	35.35	118	1.64	28.12
19	0.25	50.61	69	0.99	33.44	119	2.61	9.99
20	0.27	41.24	70	1.00	38.21	120	2.66	8.10
21	0.29	50.81	71	1.00	39.36	121	1.69	37.11
22	0.32	44.79	72	1.02	39.36	122	1.70	35.35
23	0.33	38.20	73	1.03	26.51	123	1.71	32.56
24	0.34	46.39	74	1.05	37.11	124	1.73	32.56
25	0.35	35.57	75	1.07	43.30	125	1.74	27.49
26	0.37	44.79	76	1.09	39.36	126	1.75	28.55
27	0.39	35.35	77	1.11	38.88	127	1.76	37.80
28	0.44	42.42	78	1.12	31.62	128	1.78	33.74
29	0.45	48.11	79	1.12	36.08	129	1.80	33.31
30	0.46	40.53	80	1.14	37.49	130	1.81	30.93
31	0.47	43.11	81	1.15	31.87	131	1.83	35.35
32	0.49	39.91	82	1.15	37.49	132	1.85	19.33
33	0.50	47.58	83	1.18	38.39	133	1.86	35.35
34	0.51	35.35	84	1.19	36.39	134	1.87	30.93
35	0.53	41.24	85	1.20	31.72	135	1.89	27.84
36	0.54	42.82	86	1.23	33.58	136	1.90	36.08
37	0.38	30.93	87	1.24	36.78	137	1.91	37.11
38	0.40	35.01	88	1.25	37.56	138	1.95	34.02
39	0.55	37.91	89	1.27	34.36	139	1.97	33.58
40	0.56	39.36	90	1.28	35.35	140	1.99	29.52
41	0.57	45.89	91	1.29	37.49	141	2.00	29.46
42	0.58	49.96	92	1.30	39.91	142	2.02	30.93
43	0.60	38.88	93	1.31	37.11	143	2.04	29.46
44	0.61	42.66	94	1.33	39.18	144	2.04	29.52
45	0.63	39.91	95	1.36	25.25	145	2.06	28.12
46	0.66	44.34	96	1.37	41.90	146	2.08	24.74
47	0.68	39.91	97	1.38	36.26	147	2.08	25.77
48	0.70	31.99	98	1.39	42.66	148	2.10	28.12
49	0.71	51.55	99	1.40	34.36	149	2.11	29.52
50	0.73	42.66	100	1.41	30.93	150	2.13	21.21

Table **A38: Raw** data for velocity of ascending particles within clear-fluid channel at height H = 6 cm , C_o=0.1 (section 5-3-1-1)

N	Time (min)	V (cm/min)
151	2.14	28.12
152	2.16	30.13
153	2.17	24.51
154	2.18	30.93
155	2.19	26.71
156	2.20	29.52
157	2.22	19.20
158	2.25	29.00
159	2.27	27.29
160	2.28	31.49
161	2.29	24.30
162	2.32	22.31
163	2.33	25.60
164	2.35	26.94
165	2.37	29.00
166	2.38	26.84
167	2.40	27.06
168	2.43	22.49
169	2.44	18.19
170	2.46	28.12
171	2.48	27.06
172	2.53	53.33
173	2.54	27.93
174	2.58	25.42

N	Time (min)	V (cm/min)
175	2.59	24.53
176	2.61	22.23
177	2.64	23.62
178	2.65	18.83
179	2.66	16.80
180	7.12	5.30
181	7.19	5.61
182	2.72	22.49
183	2.73	23.94
184	2.75	23.34
185	2.78	16.00
186	2.80	15.73
187	2.82	19.49
188	2.84	25.98
189	2.86	18.19
190	2.88	22.68
191	2.89	15.24
192	2.92	24.16
193	2.94	23.06
194	2.95	11.25
195	2.97	28.12
196	3.02	21.37
197	3.07	24.74

N	Time (min)	V (cm/min)
198	3.09	16.34
199	3.13	11.65
200	3.14	19.76
201	3.16	10.54
202	3.19	15.82
203	3.21	7.40
204	3.26	6.95
205	3.29	19.68
206	3.36	15.66
207	3.44	13.20
208	3.53	11.97
209	3.54	15.73
210	3.59	4.03
211	3.69	7.50
212	3.71	9.10
213	3.77	4.45
214	3.81	4.69
215	1.65	35.35
216	1.67	32.47
217	1.68	34.18
218	2.67	18.19
219	2.68	17.67
220	2.70	23.43

Table **A39: Raw** data for velocity of ascending particles within clear-fluid channel at height H= 7 cm , C_o=0.1 (section 5-3-1-1)

N	Time (min)	V (cm/min)	N	Time (min)	V (cm/min)	N	Time (min)	V (cm/min)
1	0.01	32.39	51	0.44	40.75	101	1.01	38.60
2	0.02	36.09	52	0.45	38.28	102	1.03	42.11
3	0.03	34.90	53	0.46	49.12	103	1.03	42.95
4	0.04	42.11	54	0.47	45.93	104	1.05	42.78
5	0.05	28.95	55	0.48	49.62	105	1.06	42.86
6	0.06	40.19	56	0.49	47.37	106	1.07	37.15
7	0.07	27.27	57	0.50	51.46	107	1.09	40.75
8	0.08	40.35	58	0.51	48.00	108	1.11	44.82
9	0.10	51.88	59	0.53	52.63	109	1.12	40.75
10	0.10	65.59	60	0.53	39.77	110	1.13	35.29
11	0.11	57.42	61	0.55	47.37	111	1.14	36.84
12	0.12	45.47	62	0.55	45.93	112	1.16	44.21
13	0.13	50.09	63	0.56	41.38	113	1.16	41.38
14	0.13	52.63	64	0.57	45.93	114	1.18	32.84
15	0.14	38.71	65	0.58	44.82	115	1.19	40.19
16	0.15	47.37	66	0.59	39.70	116	1.19	43.56
17	0.15	52.63	67	0.60	45.93	117	1.20	38.28
18	0.16	52.63	68	0.61	47.37	118	1.21	41.38
19	0.17	45.74	69	0.62	57.67	119	1.23	34.14
20	0.17	45.73	70	0.63	47.37	120	1.25	39.70
21	0.18	53.05	71	0.64	40.75	121	1.26	35.63
22	0.19	50.53	72	0.65	43.56	122	1.26	42.86
23	0.20	52.63	73	0.65	47.37	123	1.28	37.02
24	0.22	56.84	74	0.66	38.28	124	1.30	45.11
25	0.22	63.16	75	0.67	40.75	125	1.31	37.55
26	0.23	21.05	76	0.68	38.28	126	1.32	38.28
27	0.24	55.87	77	0.68	51.01	127	1.33	37.90
28	0.25	46.94	78	0.69	48.58	128	1.35	42.11
29	0.26	50.00	79	0.70	47.37	129	1.36	47.37
30	0.27	50.09	80	0.71	46.78	130	1.37	38.28
31	0.28	52.63	81	0.71	51.01	131	1.38	39.70
32	0.29	42.78	82	0.72	30.68	132	1.39	42.11
33	0.30	46.78	83	0.73	42.86	133	1.40	42.11
34	0.31	51.46	84	0.74	40.75	134	1.41	38.28
35	0.31	47.91	85	0.75	39.70	135	1.42	38.28
36	0.33	52.63	86	0.76	52.63	136	1.42	36.09
37	0.33	47.37	87	0.88	40.75	137	1.44	36.57
38	0.34	50.09	88	0.77	51.01	138	1.45	37.89
39	0.34	52.63	89	0.90	44.82	139	1.46	40.75
40	0.35	51.01	90	0.91	43.72	140	1.50	48.58
41	0.36	50.53	91	0.91	42.78	141	1.51	41.50
42	0.37	50.00	92	0.92	45.73	142	1.52	38.28
43	0.38	47.91	93	0.93	46.78	143	1.53	34.14
44	0.39	49.62	94	0.94	42.86	144	1.53	40.75
45	0.39	48.00	95	0.95	36.09	145	1.54	43.72
46	0.40	47.91	96	0.96	34.14	146	1.55	36.36
47	0.41	39.47	97	0.97	33.16	147	1.56	46.15
48	0.41	43.56	98	0.98	39.70	148	1.57	42.11
49	0.42	49.62	99	0.99	46.78	149	1.58	41.38
50	0.43	40.19	100	1.00	52.63	150	1.59	36.09

Table **A39: Raw** data for velocity of ascending particles within clear-fluid channel at height H= 7 cm , C_o=0.1 (section 5-3-1-1)

N	Time (min)	V (cm/min)	N	Time (min)	V (cm/min)	N	Time (min)	V (cm/min)
151	1.59	34.90	183	1.99	31.58	214	2.45	19.74
152	1.60	39.70	184	2.00	33.33	215	2.48	15.04
153	1.62	37.55	185	2.01	32.48	216	2.50	25.26
154	1.62	33.16	186	2.02	28.71	217	2.51	18.31
155	1.65	36.09	187	2.04	38.60	218	2.53	20.71
156	1.66	42.11	188	2.05	25.78	219	2.54	23.68
157	1.67	35.09	189	2.06	34.14	220	2.57	22.07
158	1.68	35.85	190	2.07	25.26	221	2.59	18.36
159	1.69	23.11	191	2.09	35.09	222	2.60	18.31
160	1.69	40.75	192	2.11	22.11	223	2.62	27.83
161	1.70	35.09	193	2.13	18.95	224	2.64	26.64
162	1.71	31.58	194	2.13	28.71	225	2.65	28.42
163	1.73	34.45	195	2.15	25.78	226	2.67	23.27
164	1.74	35.09	196	2.17	30.14	227	2.69	18.62
165	1.75	36.57	197	2.18	30.26	228	2.71	16.06
166	1.76	31.58	198	2.19	31.58	229	2.72	14.76
167	1.77	31.58	199	2.20	34.74	230	2.76	16.00
168	1.79	33.16	200	2.23	25.00	231	2.77	20.72
169	1.80	31.58	201	2.25	31.58	232	2.79	16.51
170	1.82	36.09	202	2.26	22.56	233	2.80	18.75
171	1.83	40.19	203	2.27	26.53	234	2.83	13.59
172	1.84	28.71	204	2.29	17.54	235	2.85	14.65
173	1.86	28.71	205	2.30	25.78	236	2.86	18.51
174	1.87	24.77	206	2.32	26.88	237	2.89	11.40
175	1.89	34.59	207	2.33	31.58	238	2.92	21.36
176	1.91	34.45	208	2.35	26.88	239	2.93	20.53
177	1.93	36.09	209	2.36	33.16	240	2.96	17.68
178	1.94	33.16	210	2.37	31.58	241	2.99	18.34
179	1.94	34.90	211	2.38	17.68	242	3.02	19.90
180	1.95	27.07	212	2.40	27.27	243	3.06	8.61
181	1.97	37.89	213	2.43	14.69	244	3.14	9.34
182	1.98	28.71						

Table **A40: Raw** data for velocity of ascending particles within clear-fluid channel at height H = 8 cm , C_o=0.1 (section 5-3-1-1)

N	Time (min)	V (cm/min)	N	Time (min)	V (cm/min)	N	Time (min)	V (cm/min)
1	0.00	21.91	51	0.58	57.42	101	1.20	52.63
2	0.07	-2.46	52	0.59	40.75	102	1.20	41.50
3	0.03	26.32	53	0.63	50.53	103	1.22	51.21
4	0.04	34.14	54	0.65	44.74	104	1.23	47.37
5	0.04	28.25	55	0.66	47.91	105	1.24	34.14
6	0.05	37.89	56	0.68	44.44	106	1.26	28.31
7	0.06	43.56	57	0.68	52.17	107	1.27	40.75
8	0.07	43.72	58	0.69	26.32	108	1.27	66.48
9	0.07	23.68	59	0.70	40.75	109	1.29	40.75
10	0.09	34.14	60	0.71	48.58	110	1.32	46.32
11	0.09	45.74	61	0.71	39.20	111	1.33	40.75
12	0.10	43.56	62	0.72	43.56	112	1.35	44.44
13	0.11	52.63	63	0.75	45.11	113	1.36	43.56
14	0.13	50.53	64	0.75	50.09	114	1.38	47.91
15	0.15	63.16	65	0.77	40.75	115	1.39	43.56
16	0.16	55.26	66	0.78	53.44	116	1.40	42.78
17	0.16	47.91	67	0.78	52.63	117	1.41	40.19
18	0.18	47.37	68	0.79	40.75	118	1.42	37.89
19	0.19	52.63	69	0.81	36.84	119	1.45	36.09
20	0.19	55.26	70	0.83	47.91	120	1.45	44.82
21	0.20	40.19	71	0.86	70.17	121	1.46	35.09
22	0.21	52.63	72	0.87	50.00	122	1.47	47.91
23	0.21	53.05	73	0.89	40.75	123	1.48	30.14
24	0.22	52.63	74	0.90	52.63	124	1.50	37.89
25	0.23	53.05	75	0.92	28.07	125	1.51	42.10
26	0.24	52.63	76	0.92	41.50	126	1.52	43.56
27	0.24	57.89	77	0.93	34.90	127	1.54	17.79
28	0.25	60.29	78	0.94	46.86	128	1.56	31.58
29	0.26	56.14	79	0.95	42.78	129	1.58	36.09
30	0.27	60.29	80	0.97	38.28	130	1.64	48.90
31	0.28	55.26	81	0.98	43.56	131	1.66	36.56
32	0.29	50.09	82	0.98	46.78	132	1.66	38.28
33	0.30	50.09	83	1.00	51.88	133	1.68	35.85
34	0.32	55.26	84	1.00	42.10	134	1.69	36.36
35	0.34	63.16	85	1.02	50.00	135	1.71	37.59
36	0.37	52.63	86	1.03	45.11	136	1.72	31.58
37	0.40	54.14	87	1.04	45.73	137	1.73	28.22
38	0.40	50.53	88	1.05	47.91	138	1.42	0.31
39	0.41	63.16	89	1.08	43.56	139	1.76	43.73
40	0.42	55.26	90	1.08	42.11	140	1.78	28.71
41	0.44	52.63	91	1.09	51.01	141	1.79	32.39
42	0.44	31.58	92	1.11	40.75	142	1.80	21.05
43	0.46	56.84	93	1.11	46.86	143	1.81	28.71
44	0.47	53.68	94	1.12	44.02	144	1.82	40.75
45	0.49	63.16	95	1.13	37.90	145	1.83	38.28
46	0.51	55.26	96	1.14	36.84	146	1.84	43.56
47	0.52	52.63	97	1.15	28.71	147	1.85	31.58
48	0.53	45.11	98	1.16	40.19	148	1.86	34.90
49	0.54	53.80	99	1.18	42.10	149	1.89	30.14
50	0.57	45.74	100	1.19	31.58	150	1.91	30.08

Table **A40: Raw** data for velocity of ascending particles within clear-fluid channel at height H = 8 cm , C_o=0.1 (section 5-3-1-1)

N	Time (min)	V (cm/min)
151	1.92	24.11
152	1.93	24.77
153	1.94	36.09
154	1.95	34.01
155	1.96	25.78
156	1.97	38.28
157	1.99	22.16
158	2.00	25.78
159	2.01	34.01
160	2.02	35.09
161	2.03	32.25
162	2.06	27.46
163	2.07	21.05
164	2.09	34.01
165	2.10	20.67
166	2.11	34.01
167	2.12	28.95

N	Time (min)	V (cm/min)
168	2.13	31.58
169	2.15	34.74
170	2.16	28.42
171	2.17	28.42
172	2.19	27.25
173	2.22	22.97
174	2.24	23.68
175	2.26	27.63
176	2.27	32.54
177	2.30	38.87
178	2.31	20.72
179	2.34	26.53
180	2.35	26.32
181	2.37	31.58
182	2.39	23.68
183	2.41	30.77

N	Time (min)	V (cm/min)
184	2.42	26.32
185	2.44	23.16
186	2.45	27.27
187	2.47	14.18
188	2.49	25.05
189	2.50	16.62
190	2.51	15.79
191	2.53	21.05
192	2.55	21.78
193	2.56	12.92
194	2.60	10.85
195	2.64	12.76
196	2.66	21.05
197	2.69	4.51
198	2.73	4.56
199	2.78	11.78

Table **A41: Raw** data for velocity of ascending particles within clear-fluid channel at height H= 9 cm , C_o=0.1 (section 5-3-1-1)

N	Time (min)	V (cm/min)	N	Time (min)	V (cm/min)	N	Time (min)	V (cm/min)
1	0.02	15.42	51	0.55	89.29	101	1.04	44.64
2	0.04	23.58	52	0.55	56.25	102	1.05	51.72
3	0.07	25.94	53	0.57	62.50	103	1.07	31.25
4	0.08	37.88	54	0.57	48.61	104	1.08	62.50
5	0.08	45.26	55	0.59	48.08	105	1.09	53.57
6	0.09	32.09	56	0.60	46.88	106	1.10	49.57
7	0.09	52.08	57	0.62	51.14	107	1.11	45.26
8	0.10	54.69	58	0.63	54.69	108	1.12	51.34
9	0.11	49.57	59	0.63	49.57	109	1.12	56.82
10	0.12	52.50	60	0.64	45.26	110	1.14	55.00
11	0.13	45.26	61	0.66	42.28	111	1.14	50.00
12	0.14	57.29	62	0.67	52.88	112	1.17	45.26
13	0.15	56.25	63	0.69	57.87	113	1.18	49.11
14	0.16	52.08	64	0.70	53.24	114	1.20	35.47
15	0.17	43.10	65	0.71	45.26	115	1.21	48.08
16	0.18	52.08	66	0.72	52.08	116	1.22	54.69
17	0.19	47.41	67	0.74	45.67	117	1.23	29.83
18	0.20	57.29	68	0.74	52.08	118	1.24	46.88
19	0.21	50.00	69	0.75	49.57	119	1.25	47.41
20	0.23	51.72	70	0.76	34.38	120	1.25	48.08
21	0.24	57.29	71	0.77	52.08	121	1.27	43.10
22	0.25	52.50	72	0.78	46.30	122	1.30	40.32
23	0.26	62.50	73	0.79	50.00	123	1.31	56.82
24	0.26	53.12	74	0.80	46.87	124	1.31	46.30
25	0.27	54.35	75	0.81	53.57	125	1.33	39.77
26	0.29	52.08	76	0.82	51.34	126	1.34	45.26
27	0.29	47.41	77	0.83	57.50	127	1.34	42.41
28	0.30	69.08	78	0.84	53.13	128	1.35	50.93
29	0.31	56.25	79	0.85	51.72	129	1.37	32.81
30	0.32	59.90	80	0.86	54.69	130	1.38	52.08
31	0.34	62.50	81	0.86	11.03	131	1.39	46.37
32	0.35	54.69	82	0.87	56.82	132	1.40	48.08
33	0.36	51.34	83	0.88	49.57	133	1.41	45.26
34	0.37	59.37	84	0.89	39.29	134	1.45	41.67
35	0.38	50.00	85	0.90	52.08	135	1.50	44.64
36	0.39	55.56	86	0.91	47.41	136	1.51	42.34
37	0.40	71.02	87	0.92	62.50	137	1.52	41.07
38	0.42	57.69	88	0.93	52.08	138	1.53	43.10
39	0.43	54.69	89	0.94	47.50	139	1.53	40.32
40	0.44	52.08	90	0.94	56.82	140	1.55	48.08
41	0.44	54.69	91	0.95	56.82	141	1.56	41.67
42	0.45	34.23	92	0.95	54.69	142	1.57	35.26
43	0.46	59.90	93	0.97	52.08	143	1.57	44.64
44	0.48	43.10	94	0.98	48.08	144	1.58	28.27
45	0.50	40.32	95	0.99	53.57	145	1.59	31.25
46	0.50	59.90	96	1.00	47.41	146	1.61	28.13
47	0.51	50.00	97	1.01	41.67	147	1.62	21.74
48	0.52	56.82	98	1.02	62.50	148	1.63	37.50
49	0.53	43.10	99	1.03	45.26	149	1.65	39.77
50	0.54	52.08	100	1.04	50.93	150	1.66	37.50

Table **A41: Raw** data for velocity of ascending particles within clear-fluid channel at height H= 9 cm , C_o=0.1 (section 5-3-1-1)

N	Time (min)	V (cm/min)
151	1.67	48.08
152	1.68	39.29
153	1.69	25.51
154	1.71	46.30
155	1.73	29.76
156	1.76	37.88
157	1.77	31.25
158	1.79	33.78
159	1.80	33.78
160	1.81	32.05
161	1.82	35.98
162	1.84	37.50
163	1.86	21.19
164	1.87	35.71

N	Time (min)	V (cm/min)
165	1.88	37.88
166	1.89	35.47
167	1.90	28.27
168	1.91	28.27
169	1.92	34.72
170	1.93	37.50
171	1.96	31.25
172	1.97	37.88
173	2.00	12.75
174	2.04	28.69
175	2.05	24.12
176	2.07	30.70
177	2.08	24.19

N	Time (min)	V (cm/min)
178	2.10	28.30
179	2.13	18.49
180	2.13	24.65
181	2.14	19.17
182	2.16	17.97
183	2.17	25.22
184	2.20	11.72
185	2.21	21.59
186	2.22	23.57
187	2.25	11.13
188	2.27	12.50
189	2.29	11.68
190	2.31	12.31

Table A42: Raw data for velocity of ascending particles within clear-fluid channel at height H= 10 cm , C_o=0.1 (section 5-3-1-1)

N	Time (min)	V (cm/min)	N	Time (min)	V (cm/min)	N	Time (min)	V (cm/min)
1	0.01	8.79	51	0.55	52.27	101	1.09	51.46
2	0.02	11.92	52	0.56	50.53	102	1.11	50.53
3	0.08	24.29	53	0.57	63.16	103	1.12	50.53
4	0.09	48.58	54	0.58	53.80	104	1.12	54.14
5	0.10	33.33	55	0.59	63.16	105	1.14	44.82
6	0.11	35.09	56	0.60	53.05	106	1.15	56.84
7	0.12	43.56	57	0.61	54.55	107	1.16	36.84
8	0.13	57.89	58	0.62	60.53	108	1.18	51.01
9	0.14	60.53	59	0.63	55.26	109	1.18	38.23
10	0.15	69.47	60	0.64	58.11	110	1.19	45.73
11	0.15	72.63	61	0.65	57.89	111	1.20	42.78
12	0.17	65.79	62	0.67	31.58	112	1.21	46.86
13	0.18	50.00	63	0.68	50.00	113	1.22	53.44
14	0.18	63.16	64	0.69	52.63	114	1.23	46.78
15	0.19	69.47	65	0.71	50.00	115	1.24	51.01
16	0.19	68.42	66	0.72	55.26	116	1.25	36.56
17	0.20	65.68	67	0.73	57.89	117	1.26	50.53
18	0.21	65.79	68	0.73	42.72	118	1.27	46.78
19	0.21	74.64	69	0.74	53.05	119	1.30	37.89
20	0.22	69.47	70	0.76	57.89	120	1.30	42.11
21	0.23	60.53	71	0.78	55.26	121	1.31	49.12
22	0.24	57.42	72	0.80	50.53	122	1.33	36.09
23	0.25	65.50	73	0.80	60.53	123	1.34	42.10
24	0.25	72.63	74	0.82	53.05	124	1.35	35.09
25	0.26	55.58	75	0.83	50.09	125	1.37	27.63
26	0.27	63.16	76	0.84	52.63	126	1.38	50.09
27	0.27	63.16	77	0.85	55.26	127	1.40	49.12
28	0.28	71.77	78	0.85	56.84	128	1.41	39.70
29	0.31	63.16	79	0.86	55.87	129	1.42	24.77
30	0.31	57.42	80	0.87	52.63	130	1.43	42.11
31	0.32	66.48	81	0.89	52.27	131	1.44	50.00
32	0.33	42.11	82	0.89	50.53	132	1.45	33.24
33	0.34	66.32	83	0.90	50.53	133	1.47	34.74
34	0.36	63.16	84	0.92	43.56	134	1.48	42.10
35	0.36	60.53	85	0.94	63.16	135	1.51	31.58
36	0.37	63.16	86	0.96	51.46	136	1.52	42.78
37	0.39	56.39	87	0.96	43.56	137	1.53	30.14
38	0.39	65.79	88	0.97	63.16	138	1.54	38.28
39	0.41	57.42	89	0.99	52.63	139	1.55	24.45
40	0.42	63.16	90	1.00	51.01	140	1.57	30.14
41	0.44	63.16	91	1.00	39.20	141	1.58	30.14
42	0.46	63.16	92	1.01	50.09	142	1.60	21.41
43	0.47	50.09	93	1.01	51.46	143	1.61	40.75
44	0.48	57.42	94	1.02	45.11	144	1.62	37.89
45	0.49	66.03	95	1.04	54.14	145	1.63	17.07
46	0.51	57.89	96	1.05	51.01	146	1.66	22.37
47	0.51	63.16	97	1.07	40.75	147	1.69	29.86
48	0.52	55.58	98	1.08	43.56	148	1.71	26.41
49	0.53	57.90	99	1.08	51.67	149	1.73	27.07
50	0.54	52.63	100	1.09	50.53	150	1.73	41.19

Table **A42: Raw** data for velocity of ascending particles within clear-fluid channel at height H= 10 cm , C_o=0.1 (section 5-3-1-1)

N	Time (min)	V (cm/min)
151	1.75	34.56
152	1.77	22.97
153	1.78	26.49
154	1.80	27.56
155	1.81	35.75
156	1.83	25.09

N	Time (min)	V (cm/min)
157	1.84	26.22
158	1.85	32.48
159	1.87	15.79
160	1.90	20.53
161	1.91	20.53

N	Time (min)	V (cm/min)
162	1.92	27.79
163	1.94	15.79
164	1.98	23.83
165	1.99	21.53
166	2.02	10.53

Table **A43: Raw** data for velocity of ascending particles within clear-fluid channel at height H = 11 cm , C_o=0.1 (section 5-3-1-1)

N	Time (min)	V (cm/min)	N	Time (min)	V (cm/min)	N	Time (min)	V (cm/min)
1	0.03	9.49	48	0.52	41.62	94	1.02	46.72
2	0.05	40.55	49	0.53	64.52	95	1.03	58.65
3	0.06	34.74	50	0.54	73.31	96	1.04	48.94
4	0.07	33.87	51	0.55	64.52	97	1.06	43.01
5	0.08	41.06	52	0.55	59.14	98	1.08	98.92
6	0.09	35.84	53	0.56	53.39	99	1.09	44.49
7	0.10	56.45	54	0.58	30.86	100	1.11	56.10
8	0.10	41.06	55	0.61	59.14	101	1.12	43.01
9	0.11	44.49	56	0.61	53.76	102	1.13	43.01
10	0.12	44.49	57	0.62	51.61	103	1.15	43.70
11	0.13	53.76	58	0.63	53.76	104	1.16	39.10
12	0.14	53.76	59	0.63	46.72	105	1.17	53.76
13	0.15	55.30	60	0.64	54.19	106	1.18	48.94
14	0.15	53.76	61	0.65	67.91	107	1.19	33.96
15	0.17	52.57	62	0.66	64.52	108	1.20	32.26
16	0.19	61.94	63	0.68	56.45	109	1.21	47.87
17	0.19	70.97	64	0.69	56.45	110	1.22	44.49
18	0.20	56.45	65	0.70	55.30	111	1.23	41.06
19	0.20	59.14	66	0.71	43.70	112	1.24	19.35
20	0.21	64.52	67	0.73	53.76	113	1.26	52.57
21	0.22	70.97	68	0.84	1.27	114	1.27	47.87
22	0.23	64.52	69	0.77	38.36	115	1.28	36.62
23	0.24	61.83	70	0.78	56.45	116	1.29	43.01
24	0.25	61.83	71	0.79	56.45	117	1.30	41.62
25	0.26	82.11	72	0.80	51.61	118	1.32	32.26
26	0.27	64.52	73	0.82	56.45	119	1.33	33.09
27	0.28	64.52	74	0.83	51.17	120	1.35	27.65
28	0.29	51.61	75	0.84	53.76	121	1.37	23.36
29	0.30	64.52	76	0.85	54.19	122	1.38	29.33
30	0.31	61.94	77	0.87	59.14	123	1.39	20.87
31	0.32	56.77	78	0.88	67.91	124	1.41	29.33
32	0.32	80.64	79	0.88	59.14	125	1.42	39.10
33	0.33	53.00	80	0.90	61.83	126	1.44	35.84
34	0.34	61.83	81	0.91	64.52	127	1.46	16.13
35	0.35	73.31	82	0.92	56.45	128	1.48	37.02
36	0.36	64.52	83	0.93	59.14	129	1.50	29.03
37	0.37	67.74	84	0.93	48.94	130	1.51	37.95
38	0.38	64.52	85	0.95	33.96	131	1.53	33.87
39	0.39	51.61	86	0.96	50.18	132	1.54	17.60
40	0.41	61.58	87	0.97	43.70	133	1.56	17.80
41	0.42	64.52	88	0.98	41.62	134	1.59	24.19
42	0.43	67.74	89	0.98	41.06	135	1.60	19.59
43	0.45	44.49	90	0.99	56.77	136	1.61	24.06
44	0.48	53.76	91	1.00	50.18	137	1.62	13.26
45	0.50	52.79	92	1.01	45.16	138	1.64	29.33
46	0.50	55.30	93	1.01	41.06	139	1.66	7.68
47	0.51	53.76						

Table **A44: Raw** data for velocity of ascending particles within clear-fluid channel at height H= 12 cm , C_o=0.1 (section 5-3-1-1)

N	Time (min)	V (cm/min)	N	Time (min)	V (cm/min)	N	Time (min)	V (cm/min)
1	0.04	14.57	33	0.43	70.97	64	0.95	40.55
2	0.06	39.10	34	0.45	70.13	65	0.96	27.42
3	0.07	21.51	35	0.47	61.83	66	0.98	46.08
4	0.08	82.44	36	0.50	70.97	67	0.98	45.79
5	0.10	29.49	37	0.50	64.52	68	0.99	50.69
6	0.11	33.87	38	0.51	64.52	69	1.01	43.70
7	0.13	67.74	39	0.52	64.52	70	1.02	19.26
8	0.13	56.45	40	0.58	53.76	71	1.04	49.63
9	0.14	87.10	41	0.61	67.20	72	1.05	33.87
10	0.15	80.65	42	0.62	64.52	73	1.06	41.62
11	0.16	77.42	43	0.63	60.07	74	1.07	49.95
12	0.16	70.97	44	0.64	64.52	75	1.08	32.26
13	0.17	59.14	45	0.59	1.51	76	1.09	36.87
14	0.19	75.27	46	0.69	35.48	77	1.11	47.79
15	0.20	80.65	47	0.71	59.35	78	1.12	48.94
16	0.22	77.42	48	0.72	39.10	79	1.14	41.62
17	0.22	73.12	49	0.77	59.35	80	1.16	49.63
18	0.24	80.64	50	0.78	52.79	81	1.17	35.84
19	0.25	80.65	51	0.80	45.79	82	1.17	44.49
20	0.26	51.17	52	0.81	43.70	83	1.18	39.10
21	0.27	80.65	53	0.82	56.77	84	1.20	19.06
22	0.27	70.97	54	0.83	41.62	85	1.21	30.79
23	0.28	80.65	55	0.84	47.87	86	1.22	25.81
24	0.29	74.19	56	0.86	56.45	87	1.24	36.62
25	0.30	67.74	57	0.86	61.83	88	1.25	48.39
26	0.32	67.20	58	0.87	35.38	89	1.27	27.42
27	0.32	67.91	59	0.89	46.72	90	1.28	26.57
28	0.34	70.97	60	0.91	50.18	91	1.29	33.87
29	0.34	58.06	61	0.92	49.63	92	1.33	27.30
30	0.39	77.42	62	0.93	53.76	93	1.38	16.54
31	0.40	75.27	63	0.94	34.87	94	1.40	8.27
32	0.42	64.52						

Table A45: Raw data for velocity of ascending particles within clear-fluid channel at height H= 13 cm , C_o=0.1 (section 5-3-1-1)

N	Time (min)	V (cm/min)
1	0.03	29.33
2	0.04	33.96
3	0.05	51.61
4	0.06	37.35
5	0.07	33.79
6	0.08	43.01
7	0.09	46.08
8	0.10	44.49
9	0.12	61.83
10	0.15	66.91
11	0.16	74.19
12	0.17	70.97
13	0.18	70.97
14	0.20	64.52
15	0.21	64.52
16	0.22	70.97
17	0.24	64.52
18	0.25	64.52
19	0.25	64.52
20	0.26	52.79
21	0.27	54.19
22	0.29	67.74
23	0.31	71.31
24	0.35	53.00
25	0.36	64.52
26	0.36	53.00
27	0.37	64.52
28	0.38	67.74
29	0.43	74.19
30	0.46	7.33
31	0.45	64.52
32	0.46	81.49
33	0.47	77.42
34	0.49	48.94
35	0.50	61.83
36	0.51	74.19
37	0.52	53.76
38	0.53	78.10
39	0.54	51.61
40	0.56	70.97
41	0.57	53.39
42	0.57	70.38
43	0.59	70.38
44	0.61	59.14
45	0.62	40.04
46	0.63	53.76
47	0.65	59.14
48	0.66	71.69
49	0.67	46.72
50	0.70	53.39
51	0.72	48.88
52	0.74	44.49
53	0.74	45.79
54	0.76	46.72
55	0.77	53.00
56	0.78	53.00
57	0.80	48.94
58	0.83	33.60
59	0.85	59.55
60	0.87	40.10
61	0.89	53.76
62	0.90	38.71
63	0.92	54.84
64	0.93	46.08
65	0.94	29.33
66	0.95	32.26
67	0.96	41.62
68	0.97	17.44
69	0.99	36.87
70	1.01	41.62
71	1.02	29.03
72	1.04	30.79
73	1.08	27.83
74	1.11	29.33
75	1.12	32.26
76	1.15	14.66

Table **A46: Raw** data for velocity of ascending particles within clear-fluid channel at height H = 14 cm , C_o=0.1 (section 5-3-1-1)

N	Time (min)	V (cm/min)
1	0.01	39.70
2	0.03	62.13
3	0.04	59.91
4	0.06	67.74
5	0.07	61.83
6	0.09	80.65
7	0.09	84.68
8	0.10	80.65
9	0.11	80.65
10	0.12	83.49
11	0.13	74.19
12	0.15	81.49
13	0.20	72.58
14	0.22	56.45
15	0.23	74.70
16	0.25	64.52
17	0.26	49.63
18	0.29	76.25
19	0.30	70.97
20	0.32	49.63
21	0.33	80.65
22	0.34	71.31
23	0.35	67.91
24	0.36	36.05
25	0.37	64.52

N	Time (min)	V (cm/min)
26	0.39	48.94
27	0.40	53.76
28	0.42	64.52
29	0.43	80.65
30	0.44	64.52
31	0.44	64.52
32	0.45	70.97
33	0.47	70.97
34	0.49	67.74
35	0.51	59.35
36	0.52	51.17
37	0.53	59.14
38	0.55	52.03
39	0.56	61.83
40	0.57	46.72
41	0.59	39.10
42	0.61	38.71
43	0.61	67.74
44	0.63	43.01
45	0.64	56.45
46	0.65	53.76
47	0.66	37.63
48	0.66	44.49
49	0.67	50.18

N	Time (min)	V (cm/min)
50	0.68	51.17
51	0.69	58.65
52	0.70	47.79
53	0.73	35.84
54	0.75	24.35
55	0.76	51.17
56	0.77	47.79
57	0.78	29.33
58	0.79	25.30
59	0.81	29.33
60	0.82	32.26
61	0.83	39.10
62	0.83	9.22
63	0.85	32.26
64	0.85	30.79
65	0.86	12.17
66	0.87	8.60
67	0.89	32.26
68	0.90	37.95
69	0.92	24.35
70	0.93	7.33
71	0.95	13.17
72	0.99	7.68
73	1.02	3.33

Table **A47: Raw** data for velocity of ascending particles within clear-fluid channel at height H = 15 cm , C_o=0.1 (section 5-3-1-1)

N	Time (min)	V (cm/min)	N	Time (min)	V (cm/min)	N	Time (min)	V (cm/min)
1	0.02	21.51	18	0.32	50.83	34	0.55	50.69
2	0.04	23.77	19	0.34	39.10	35	0.57	20.42
3	0.04	25.81	20	0.36	32.26	36	0.59	38.71
4	0.06	36.87	21	0.38	53.76	37	0.61	57.84
5	0.07	40.55	22	0.38	77.42	38	0.62	56.45
6	0.10	40.55	23	0.41	64.52	39	0.63	51.17
7	0.10	53.76	24	0.42	27.86	40	0.65	27.65
8	0.13	43.01	25	0.43	67.10	41	0.66	41.22
9	0.15	64.52	26	0.43	67.74	42	0.68	45.79
10	0.16	67.74	27	0.44	70.97	43	0.69	43.01
11	0.17	61.58	28	0.48	64.52	44	0.71	17.68
12	0.18	77.42	29	0.49	67.45	45	0.73	37.63
13	0.18	80.65	30	0.50	46.72	46	0.76	28.83
14	0.22	80.65	31	0.53	33.08	47	0.78	16.33
15	0.25	80.65	32	0.53	59.35	48	0.79	20.16
16	0.25	70.97	33	0.54	44.49	49	0.67	-0.41
17	0.29	74.70						

Table **A48: Raw** data for velocity of ascending particles within clear-fluid channel at height H = 16 cm , C_o=0.1 (section 5-3-1-1)

N	Time (min)	V (cm/min)	N	Time (min)	V (cm/min)	N	Time (min)	V (cm/min)
1	0.01	27.17	16	0.23	78.26	30	0.40	57.07
2	0.03	38.04	17	0.24	78.26	31	0.41	35.87
3	0.05	43.48	18	0.26	57.07	32	0.42	59.78
4	0.06	31.88	19	0.27	68.48	33	0.43	57.39
5	0.07	31.13	20	0.29	52.17	34	0.45	35.25
6	0.08	32.61	21	0.30	37.27	35	0.46	54.35
7	0.11	52.68	22	0.30	43.48	36	0.47	42.08
8	0.11	55.18	23	0.34	54.35	37	0.49	57.39
9	0.14	62.50	24	0.34	65.22	38	0.50	20.60
10	0.14	62.25	25	0.35	71.74	39	0.52	29.64
11	0.15	62.25	26	0.36	55.90	40	0.55	27.17
12	0.17	81.52	27	0.37	51.72	41	0.56	24.61
13	0.18	81.52	28	0.38	57.69	42	0.59	11.86
14	0.19	81.52	29	0.39	71.74	43	0.60	23.72
15	0.20	75.00						

Table **A49: Raw** data for velocity of ascending particles within clear-fluid channel at height H = 17 cm , C_o=0.1 (section 5-3-1-1)

N	Time (min)	V (cm/min)
1	0.04	35.48
2	0.05	36.39
3	0.06	41.62
4	0.08	35.48
5	0.10	33.96
6	0.11	43.70
7	0.12	45.79
8	0.14	51.61
9	0.15	50.69
10.	0.17	86.02
11	0.19	70.97
12	0.20	70.97
13	0.22	41.62
14	0.23	70.97
15	0.24	64.52
16	0.28	64.52

N	Time (min)	V (cm/min)
17	0.31	66.05
18	0.28	67.91
19	0.03	39.85
20	0.04	64.52
21	0.05	33.72
22	0.07	38.71
23	0.08	46.08
24	0.09	49.63
25	0.11	50.69
26	0.11	52.79
27	0.12	51.17
28	0.13	54.19
29	0.15	58.65
30	0.17	54.96
31	0.19	80.65

N	Time (min)	V (cm/min)
32	0.20	74.19
33	0.21	74.19
34	0.23	51.61
35	0.24	64.52
36	0.24	70.97
37	0.25	58.06
38	0.26	77.42
39	0.27	70.97
40	0.28	70.97
41	0.29	51.61
42	0.31	22.89
43	0.32	18.98
44	0.34	39.17
45	0.35	33.24
46	0.37	28.05

Table A50: Raw data for velocity of dye tracer within clear-fluid channel at height H = 3 cm , C_o=0.2 (section 5-3-1-2)

N	Time (min)	V (cm/min)	N	Time (min)	V (cm/min)	N	Time (min)	V (cm/min)
1	0.59	19.57	7	3.14	1.56	13	2.20	8.46
2	0.62	19.57	8	3.35	9.33	14	3.71	13.81
3	0.67	18.68	9	0.69	29.89	15	5.37	6.55
4	0.92	14.68	10	0.89	19.11	16	0.76	9.90
5	1.32	14.29	11	1.54	10.81	17	2.60	6.32
6	2.64	5.30	12	1.58	10.40	18	4.44	7.61
						19	5.01	5.01

Table A51: Raw data for velocity of dye tracer within clear-fluid channel at height H = 4 cm , C_o=0.2 (section 5-3-1-2)

N	Time (min)	V (cm/min)	N	Time (min)	V (cm/min)	N	Time (min)	V (cm/min)
1	0.63	25.68	9	4.79	5.93	17	1.41	15.96
2	0.66	29.25	10	5.09	5.46	18	1.61	15.41
3	0.82	23.64	11	5.39	7.23	19	3.22	6.85
4	0.96	23.48	12	5.69	7.15	20	3.43	12.84
5	1.39	18.68	13	0.72	39.23	21	0.81	12.09
6	2.55	35.96	14	0.96	27.86	22	2.74	4.78
7	3.21	8.02	15	1.10	18.06	23	4.54	3.90
8	3.86	6.74	16	1.20	21.92	24	5.12	3.86
						25	0.60	10.16

Table A52: Raw data for velocity of dye tracer within clear-fluid channel at height H = 7 cm , C_o=0.2 (section 5-3-1-2)

N	Time (min)	V (cm/min)	N	Time (min)	V (cm/min)	N	Time (min)	V (cm/min)
1	0.53	56.68	19	3.70	8.89	37	1.27	31.02
2	0.55	37.67	20	4.04	17.61	38	1.29	26.95
3	0.66	49.81	21	4.44	14.68	39	1.39	37.36
4	0.79	34.25	22	4.53	12.82	40	1.46	41.10
5	0.84	28.34	23	4.78	11.66	41	1.57	33.55
6	1.01	35.96	24	5.16	11.74	42	1.79	35.23
7	1.03	35.96	25	5.60	8.84	43	1.81	32.57
8	1.17	33.19	26	6.03	8.06	44	2.29	19.81
9	1.36	35.67	27	6.36	8.93	45	2.31	24.91
10	1.41	28.84	28	6.38	7.61	46	2.38	17.30
11	1.66	29.89	29	0.47	34.61	47	3.51	19.61
12	1.70	28.84	30	0.49	37.36	48	3.74	12.94
13	1.95	25.38	31	0.91	37.67	49	0.57	19.34
14	2.32	22.42	32	0.92	34.52	50	1.62	16.04
15	2.71	16.60	33	1.07	42.05	51	2.38	0.22
16	3.16	17.79	34	1.10	32.88	52	1.98	12.71
17	3.56	23.33	35	1.22	34.12	53	2.39	11.21
18	3.61	13.81	36	1.25	46.97	54	2.72	10.34
						55	3.71	8.39

Table A53: Raw data for velocity of dye tracer within clear-fluid channel at height H = 8 cm , C_o=0.2 (section 5-3-1-2)

N	Time (min)	V (cm/min)	N	Time (min)	V (cm/min)	N	Time (min)	V (cm/min)
1	0.54	54.79	20	3.28	17.87	39	1.81	34.12
2	0.56	42.96	21	3.33	15.96	40	1.84	29.89
3	0.68	59.78	22	3.67	18.17	41	1.87	26.51
4	0.82	53.03	23	3.69	21.35	42	2.51	49.81
5	0.88	37.36	24	3.79	17.87	43	2.68	24.91
6	1.04	24.11	25	4.09	18.76	44	2.87	22.52
7	1.06	44.26	26	4.85	14.68	45	3.04	21.35
8	1.20	39.45	27	4.90	11.66	46	3.08	19.18
9	1.25	33.55	28	0.50	39.23	47	3.25	21.79
10	1.39	37.36	29	1.10	33.19	48	3.40	19.61
11	1.43	35.96	30	1.13	35.96	49	3.44	17.09
12	1.69	34.25	31	1.24	39.23	50	3.57	21.85
13	1.73	35.74	32	1.28	41.10	51	3.60	16.60
14	1.99	30.28	33	1.30	29.89	52	2.38	0.22
15	1.86	0.30	34	1.32	34.25	53	1.98	12.71
16	2.38	27.40	35	1.41	34.12	54	2.39	11.21
17	2.74	24.17	36	1.48	42.15	55	2.72	10.34
18	2.78	20.81	37	1.50	35.96	56	3.71	8.39
19	3.22	16.28	38	1.74	29.89			

Table A54: Raw data for velocity of dye tracer within clear-fluid channel at height H = 12 cm , C_o=0.2 (section 5-3-1-2)

N	Time (min)	V (cm/min)	N	Time (min)	V (cm/min)	N	Time (min)	V (cm/min)
1	0.88	32.88	11	1.94	49.31	21	0.60	58.71
2	0.94	56.51	12	2.02	46.36	22	0.76	56.68
3	0.98	46.97	13	2.17	39.23	23	0.88	58.71
4	0.99	54.79	14	2.19	39.23	24	0.90	43.26
5	1.01	44.26	15	2.39	42.15	25	1.04	51.66
6	1.19	52.30	16	2.43	37.36	26	1.29	58.33
7	1.21	63.22	17	2.54	20.55	27	1.31	41.10
8	1.23	56.68	18	0.40	58.71	28	1.90	44.26
9	1.66	53.03	19	0.44	66.39	29	2.11	37.67
10	1.68	37.52	20	0.47	86.52	30	2.14	39.23
						31	2.35	41.10

Table A55: Raw data for velocity of dye tracer within clear-fluid channel at height H = 13 cm , C_o=0.2 (section 5-3-1-2)

N	Time (min)	V (cm/min)	N	Time (min)	V (cm/min)	N	Time (min)	V (cm/min)
1	0.91	34.12	11	2.04	54.80	21	1.15	61.64
2	0.95	62.35	12	0.42	56.68	22	1.16	60.88
3	1.01	54.79	13	0.46	59.52	23	1.31	57.28
4	1.03	59.08	14	0.49	75.34	24	1.34	58.71
5	1.20	67.51	15	0.62	55.68	25	1.35	57.53
6	1.23	71.92	16	0.67	46.97	26	1.93	35.49
7	1.25	61.64	17	0.78	54.07	27	2.11	37.67
8	1.68	37.52	18	0.80	63.22	28	2.14	39.23
9	1.70	51.66	19	0.91	59.52	29	2.35	41.10
10	1.96	44.43	20	1.07	71.92			

Table A56: Raw data for the width δ (mm) of the clear-fluid layer measured at time t (s) and height H (cm) C_o = 0,2 (section 5,3,3)

H \ t	30 s	40 s	50 s	60 s	70 s	80 s	90 s	100 s	110 s	130 s	140 s	150 s	160 s	170 s	180 s	190 s
1	0,28	0,25	,020	0,15	0,07											
2	0,28	0,25	,020	0,15	0,07											
3	0,41	0,41	,041	0,34	0,21	0,21	0,19	0,16	0,12	0,07	0,07	0,07	0,07	0,07	0,07	0,07
4	0,41	0,41	,041	0,41	0,41	0,40	0,34	0,31	0,28	0,21	0,19	0,18	0,17	0,17	0,16	0,16
5	0,41	0,41	,041	0,41	0,41	0,38	0,35	0,33	0,32	0,29	0,27	0,26	0,25	0,24	0,22	0,21
7	0,41	0,41	,041	0,41	0,39	0,37	0,35	0,33	0,30	0,27	0,27	0,26	0,25	0,25	0,24	0,23
8	0,41	0,40	,039	0,36	0,34	0,34	0,33	0,32	0,31	0,29	0,29	0,28	0,27	0,25	0,24	0,22
9	0,41	0,40	,039	0,36	0,34	0,34	0,33	0,32	0,31	0,29	0,29	0,28	0,27	0,25	0,24	0,22
10	0,51	0,50	,047	0,46	0,45	0,44	0,42	0,41	0,40	0,39	0,39	0,39	0,39	0,39	0,39	0,39
11	0,62	0,62	,062	0,62	0,62	0,62	0,62	0,62	0,62	0,62	0,62	0,62	0,62	0,62		
12	0,62	0,62	,062	0,62	0,62	0,62	0,62	0,62	0,62	0,62						
13	0,69	0,69	,069	0,69	0,69	0,69	0,69	0,69	0,62							
14	0,79	0,83	,084	0,86	0,88	0,90	0,90									
15	0,89	0,91	,092	0,94	0,95											
17	0,99															

Table A57: Raw data for the width δ (mm) of the clear-fluid layer measured at time t(s) and height H(cm)
C_o = 0.1 (section 5.3.3)

H \ t	10 s	30 s	50 s	70 s	90 s	110 s	130 s	140 s
1	0.18	0.40	0.38	0.32	0.24	0.16	0.08	0.08
2	0.20	0.40	0.42	0.40	0.40	0.40	0.36	0.30
3	0.36	0.54	0.54	0.54	0.54	0.54	0.52	0.48
4	0.72	0.72	0.74	0.74	0.74	0.74	0.76	0.76
5	0.76	0.80	0.80	0.80	0.80	0.76	0.76	0.76
6		0.76	0.76	0.76	0.76	0.76	0.76	0.76
7		0.84	0.84	0.84	0.84	0.90	0.96	1.04
8		1.10	1.16	1.22	1.22	1.22	1.22	1.66
9		1.00	1.20	1.22	1.22	1.22	1.30	1.40
10		0.96	0.96	0.98	1.10	0.13		
11		1.08	1.08	1.16	1.52			
12		1.14	1.16	1.30				
13		1.40	1.52	1.60				
14		1.40	1.56					